# Denatonium, torasemide and their transformation products as emerging contaminants in the aquatic environment

**Dissertation**

der Mathematisch-Naturwissenschaftlichen Fakultät

der Eberhard Karls Universität Tübingen

zur Erlangung des Grades eines

Doktors der Naturwissenschaften

(Dr. rer. nat.)

vorgelegt von

Sascha Lege

aus Dorsten

Tübingen

2020

The research described in this thesis was conducted between January 1st, 2014 and June 30th, 2016 in the Environmental Analytical Chemistry group, University of Tübingen, under the supervision of Prof. Dr. Christian Zwiener.

Gedruckt mit Genehmigung der Mathematisch-Naturwissenschaftlichen Fakultät der Eberhard Karls Universität Tübingen.

| | |
|---|---|
| Tag der mündlichen Qualifikation: | 26.05.2020 |
| Dekan: | Prof. Dr. Wolfgang Rosenstiel |
| 1. Berichterstatter: | Prof. Dr. Christian Zwiener |
| 2. Berichterstatter: | Prof. Dr. Stefan B. Haderlein |

*„Be excellent to each other" and "party on, dudes!"*

Bill and Ted's Excellent Adventure

## Table of Contents

# I Summary

Several thousand organic chemicals are used on a daily basis, e.g. as biocides, pharmaceuticals, or in household and personal care products. The majority of these compounds is disposed into sewer systems and reaches surface waters through the release of (un-) treated wastewater. Environmental concentrations of these organic micropollutants are often in the ng $L^{-1}$ to µg $L^{-1}$ range and therefore far below most levels of acute toxicity. However, an impact on the development and behavior of aquatic species was already proven for such low concentrations. Furthermore, increased adverse effects were observed when evaluating mixtures of chemicals rather than single substances. The complexity of the topic about organic micropollutants in the environment increases even more considering abiotic and biotic degradation processes. Multiple transformation products (TPs) can be formed from a single parent molecule and the TPs, as well as their (toxicological) properties, are usually unknown.

The work conducted for this thesis closes knowledge gaps in the context of previously unknown environmental pollutants. Denatonium and torasemide were chosen as study compounds and their concentrations in wastewater treatment plants (WWTPs) and in surface waters were initially measured applying sensitive targeted methods. Various degradation experiments were performed to identify TPs of potential environmental relevance and their occurrence in the environment was finally investigated.

As denatonium is one of the bitterest compounds known today, it is applied in numerous products to prevent an accidental or intentional consumption. Denatonium can be even present in personal care products, without being declared as ingredient, because it is an important additive for the denaturation of alcohol. Despite its wide application, this is the first study reporting denatonium itself as environmental pollutant. Generally, all water samples taken from WWTP effluents in Italy, Switzerland and from 22 plants in the federal state of Baden-Württemberg, Germany, contained denatonium with a maximum concentration of 341 ng $L^{-1}$. Denatonium is not significantly removed during conventional wastewater treatment and the data have shown that this compound is released via (un-) treated wastewater to the environment. Concentrations up to almost 200 ng $L^{-1}$ were detected in wastewater-impacted surface waters. When ozonation is applied as advanced treatment technique, up to 74% of an initial denatonium load could be removed from wastewater. However, removal of denatonium was associated by the formation of at least two polar transformation products (TPs).

This study was actually the first time that these compounds were ever reported and they possess therefore unknown toxicological properties. Denatonium can undergo indirect photodegradation and seven TPs were identified. They formed via amide hydrolysis, hydroxylation, N-dealkylation, and N-dearylation. Lidocaine was however the only TP of denatonium detected after conventional wastewater treatment and in surface waters, but the occurrence of this compound was associated with its application as local anesthetic rather than being a degradation product of denatonium. Generally, data presented previously in literature and the results obtained in this study point towards a persistent nature of denatonium and therefore an accumulation of this compound in the environment.

Torasemide is an important loop diuretic and it was 2017 one of the ten most prescribed drugs in Germany. Maximum concentrations of this drug measured in this study for WWTPs and surface waters were about 350 ng $L^{-1}$ and 70 ng $L^{-1}$, respectively. Despite an already known occurrence of torasemide throughout the urban water cycle, including very low concentrations in drinking water, no studies were performed related to its fate in the environment and an occurrence of TPs so far. Abiotic and biotic degradation experiments were therefore performed and overall sixteen products were identified. The following reaction mechanisms were involved in TP formation: aromatic and aliphatic hydroxylation, including further oxidation to carboxylic acids and quinone imines, amide cleavage, N-dealkylation, N-dearylation, and sulfonamide hydrolysis to sulfonic acids. The formation of quinone imines was in principle of great interest due to their highly reactive nature, but they were not detected in any environmental sample. While both major human metabolites hydroxytorasemide (TP 364a) and carboxytorasemide (TP 378a) were observed in WWTP influents, hydroxytorasemide seems to be removed during wastewater treatment and was most likely transformed into carboxytorasemide. Carboxytorasemide however was detected in all investigated WWTP effluents and surface waters, with an estimated maximum concentration of 1 µg $L^{-1}$.

# II Zusammenfassung

Tausende organische Chemikalien finden, u.a. als Biozid, Arzneimittel, aber auch in Haushalts- und Pflegeprodukten, eine regelmäßige Anwendung in unserem Alltag. Ein Großteil dieser Verbindungen gelangt zunächst in die Kanalisation und schlussendlich über (un-) behandelte Abwässer in Oberflächengewässer. Die Konzentrationen dieser sogenannten Mikroverunreinigungen liegen in der Umwelt üblicherweise im ng $L^{-1}$ bis µg $L^{-1}$ Bereich und somit typischerweise deutlich unter den Dosen für akute Toxizität. Nicht-letale Effekte, wie z.B. Entwicklungsstörungen und Verhaltensänderungen, konnten aber bereits für aquatische Spezies beobachtet werden, welche umweltrelevanten Konzentrationen ausgewählter Verbindungen ausgesetzt wurden. Weiterhin können für Stoffgemische toxische Effekte auftreten, obwohl die Einzelverbindungen in Konzentrationen vorliegen, bei denen sie alleine unwirksam sind. Die Risikoabschätzung bezüglich organischer Mikroverunreinigungen in der Umwelt ist aufgrund der Fülle an anthropogenen Chemikalien bereits sehr schwierig und die Komplexität der Thematik nimmt unter Berücksichtigung von abiotischen und biotischen Transformationsprozessen weiter zu. Zahlreiche Abbauprodukte (TPs) können aus einer einzelnen Ausgangsverbindung hervorgehen, wobei die TPs und deren (toxikologischen) Eigenschaften häufig unbekannt sind.

Das Ziel der vorliegenden Arbeit war es Wissenslücken im Zusammenhang mit bislang unbekannten Spurenstoffen in der Umwelt zu schließen. Aus diesem Grund wurden Denatonium und Torasemid für weitergehende Studien ausgewählt und zunächst wurden die Konzentrationen dieser Verbindungen in Kläranlagen und Oberflächengewässern bestimmt. Zusätzlich wurden verschiedene Abbauexperimente durchgeführt, um mögliche umweltrelevante TPs zu identifizieren, und das Vorkommen dieser TPs in der Umwelt wurde abschließend evaluiert.

Denatonium ist die derzeit bitterste bekannte Substanz und wird daher zahlreichen Produkten (wie z.B. Putzmitteln) beigefügt, um ein unabsichtliches oder absichtliches Verschlucken zu verhindern. Denatonium wird außerdem häufig als Vergällungsmittel für Alkohol eingesetzt und die Verbindung gelangt über denaturierten Alkohol somit auch in Produkte ohne als Inhaltsstoff deklariert zu sein. Trotz einer breiten Anwendung wurde Denatonium in dieser Arbeit zum ersten Mal als Mikroverunreinigung in der Umwelt beschrieben worden.

Grundsätzlich konnte die Substanz in allen untersuchten Abläufen von Kläranlagen aus Italien, der Schweiz und 22 Anlagen aus Baden-Württemberg (Deutschland) nachgewiesen werden und die maximale Konzentration belief sich auf 341 ng $L^{-1}$. Denatonium wird nicht durch konventionelle Abwasseraufbereitung entfernt und gelangt somit über (un-) geklärtes Abwasser in die Umwelt. In Flüssen, welche als Vorfluter dienen, konnten bis zu 200 ng $L^{-1}$ Denatonium detektiert werden. Untersuchungen im Pilotmaßstab haben gezeigt, dass die Freisetzung von Denatonium in die Umwelt um 74% reduziert werden kann, wenn Ozonung als erweiterte Oxidationsmaßnahme mit konventioneller Abwasserbehandlung kombiniert wird. Die Elimination von Denatonium geht unter diesen Bedingungen jedoch mit der Bildung von mindestens zwei polaren TPs einher. Beide Abbauprodukte sind im Rahmen dieser Arbeit zum ersten Mal beschrieben worden und ihre (toxikologischen) Eigenschaften sind bis heute unbekannt. Laborversuche haben außerdem gezeigt, dass Denatonium durch indirekte Photoprozesse abgebaut werden kann und die Amidhydrolyse, Hydroxylierung, N-Dealkylierung und N-Dearylierung wurden als Mechanismen für die Bildung von sieben Abbauprodukten identifiziert. Grundsätzlich weisen die bisherigen Daten in der Literatur und die Ergebnisse dieser Arbeit aber auf eine Persistenz von Denatonium und eine mögliche Akkumulierung der Verbindung in der Umwelt hin. Daher wurde das Vorkommen von Lidocain, dem einzigen Abbauprodukt von Denatonium, welches in konventionellen Kläranlagen und Oberflächengewässern nachgewiesen werden konnte, auch eher dem Einsatz als Lokalanästhetikum zugeordnet.

Torasemid ist ein wichtiges Schleifendiuretikum und war 2017 eines der zehn meist verschriebenen Arzneimittel Deutschlands. Die maximalen Konzentrationen, welche im Rahmen dieser Studie für Kläranlagen und Oberflächengewässer nachgewiesen werden konnten, beliefen sich jeweils auf 350 ng $L^{-1}$ und 70 ng $L^{-1}$. Obwohl das Vorkommen der Substanz im urbanen Wasserkreislauf bereits beschrieben wurde, und geringe Spuren schon im Trinkwasser nachgewiesen wurden, gab es zu Beginn dieser Arbeit wenige Informationen zum Verbleib von Torasemid in der Umwelt und der Bildung von Abbauprodukten. Abiotische und biotische Abbaustudien wurden daher durchgeführt und insgesamt 16 TPs konnten identifiziert werden. Bei den beteiligten Reaktionsmechanismen handelte es sich um aromatische und aliphatische Hydroxylierung, eine weitergehende Oxidation zu Carbonsäuren und Chinoniminen, Amidspaltung, N-Dealkylierung, N-Dearylierung, und der Hydrolyse von Sulfonamiden zu Sulfonsäuren.

Insbesondere die Bildung von Chinoniminen ist zwar aufgrund ihrer hohen Reaktivität von besonderer toxikologischer Bedeutung, aber keines dieser Produkte konnte in der Umwelt nachgewiesen werden. Generell waren nur die beiden bereits bekannten Humanmetabolite Hydroxytorasemid (TP 364a) und Carboxytorasemid (TP 378a) von höherer Relevanz und beide Verbindungen wurden in dem Zulauf einer untersuchten Kläranlage nachgewiesen. Über den Verlauf der konventionellen Abwasserbehandlung schien TP 364a jedoch in TP 378a transformiert zu werden und nur TP 378a konnte neben Torasemid selber in allen untersuchten Kläranlagenabläufen und Oberflächengewässern nachgewiesen werden. Aufgrund der Detektionshäufigkeit und einer abgeschätzten Maximalkonzentration von 1 $\mu g\ L^{-1}$ ist Carboxytorasemid ein umweltrelevantes Abbauprodukt.

# III List of publications and author contributions

**Publication I**

Lege, S., Guillet, G., Merel, S., Yanez Heras, J. E., Zwiener, C., 2017. Denatonium - A so far unrecognized but ubiquitous water contaminant? Water Research 112, 254–260. DOI: 10.1016/j.watres.2017.01.056

*Author contributions*

Sascha Lege planned the study, developed the analytical methods, performed sample analysis, and evaluated the data. All authors participated in the interpretation of the results and Gaëlle Guillet was additionally responsible for the sampling campaigns in Baden-Württemberg, Germany. Sascha Lege wrote the manuscript draft and all additional authors provided critical feedback to shape the manuscript.

**Publication II**

Lege, S., Eisenhofer, A., Yanez Heras, J. E., Zwiener, C., 2019. Identification of transformation products of denatonium – Occurrence in wastewater treatment plants and surface waters. Science of The Total Environment 686, 140–150. DOI: 10.1016/j.scitotenv.2019.05.423

*Author contributions*

Sascha Lege planned the study and shaped the research. He performed most of the experimental work, except for the chemical synthesis of the TP222 and the related characterization (e.g. by NMR), which was done by Anna Eisenhofer. The field experiment for exposure of denatonium to natural sunlight was performed by Julian Sorwat (see acknowledgments of the manuscript). Sascha Lege had the primary role in data evaluation and interpretation, as well as manuscript writing. All additional authors, especially Christian Zwiener, provided helpful feedback to shape the manuscript.

**Publication III**

Lege, S., Sorwat, J., Yanez Heras, J. E., Zwiener, C., 2020. Abiotic and biotic transformation of torasemide - Occurrence of degradation products in the aquatic environment. Submitted to Water Research.

*Author contributions*

Sascha Lege planned the study and shaped the research. He performed all analytical work, including sample analysis, as well as data evaluation and interpretation. Photodegradation and biodegradation experiments were performed by Julian Sorwat and Marius Majewsky (see acknowledgements of this manuscript), respectively. Jorge E.Y. Heras supported the electrochemical degradation experiments. Sascha Lege had the primary role in manuscript writing and all additional authors, especially Christian Zwiener, provided helpful feedback on the data interpretation and the structure of the manuscript.

**Additional manuscripts published during the research for this thesis, but which are not included in it:**

Weigold, P., Ruecker, A., Jochmann, M., Osorio Barajas, X L, Lege, S., Zwiener, C., Kappler, A., Behrens, S., 2015. Formation of chloroform and tetrachloroethene by Sinorhizobium meliloti strain 1021. Letters in applied microbiology 61 (4), 346–353. DOI: 10.1111/lam.12462

Merel, S., Lege, S., Yanez Heras, J. E, Zwiener, C., 2017. Assessment of N-Oxide Formation during Wastewater Ozonation. Environmental Science & Technology 51 (1), 410–417. DOI: 10.1021/acs.est.6b02373

Yanez Heras, J. E, Wang, Z., Lege, S., Obst, M., Roehler, S., Burkhardt, C.J., Zwiener, C., 2017. Application and characterization of electroactive membranes based on carbon nanotubes and zerovalent iron nanoparticles. Water research 108, 78–85. DOI: 10.1016/j.watres.2016.10.055

# IV Oral & poster presentations

Lege, S., Merel, S., Yanez Heras, J. E., Zwiener, C., 2015. “Denatonium- A new surface water contaminant and a potential source of lidocaine in the environment”. Poster presentation at the annual conference of the Water Chemistry Society in Schwerin (11. - 13.05.2015).

Lege, S., Zwiener, C., 2015. “Towards a complete automatisation of non-target screening approaches with high resolution mass spectrometry”. Poster presentation at the ICCE in Leipzig (20. - 24.09.2015).

Lege, S., Zwiener, C., 2016. „Evaluating 2D-LC and ion mobility separation in combination with high-resolution mass spectrometry for non-target screening approaches”. Oral presentation at the annual conference of the German Society of Mass Spectrometry in Hamburg (28.02 - 02.03.2016).

Lege, S., Merel, S., Yanez Heras, J. E., Zwiener, C., 2016. “Vorteile und Limitierungen der All-Ions-Technik für die Untersuchung von anthropogenen Spurenstoffen in wässrigen Matrices”. Poster presentation at the annual conference of the Water Chemistry Society in Bamberg (02. - 04.05.2016).

Lege, S., Yanez Heras, J. E., Zwiener, C., 2016. „ Fast screening for transformation products of water pollutants using electrochemistry and automated non-target screening”. Poster presentation at the Non-target screening of organic chemicals for a comprehensive environmental risk assessment in Ascona (29.05 – 03.06.2016).

Lege, S., Yanez Heras, J. E., Zwiener, C., 2016. „Advantages and limitations of electrochemistry to elucidate micropollutants transformation”. Short oral presentation at the Non-target screening of organic chemicals for a comprehensive environmental risk assessment in Ascona (29.05 – 03.06.2016).

# 1 General introduction

Approximately 300 million tons of synthetic organic compounds are produced globally each year (Schwarzenbach et al., 2006), including compound classes like pharmaceuticals, personal care and household products, as well as industrial chemicals. The contamination of vital aquatic compartments, i.e. surface water, groundwater, and drinking water, with anthropogenic substances was an increasing focus of analytical work in recent years (Richardson, 2003; Richardson and Kimura, 2016; Richardson and Ternes, 2005, 2011, 2014, 2018). Most compounds used on a regular basis are disposed via the sewer system and the highest concentrations are therefore generally detected in the influent of wastewater treatment plants (WWTPs). Although conventional wastewater treatment is applied mainly for the removal of solids, the biological oxygen demand, and nutrients (Ternes et al., 2004), micropollutants can be removed here to varying degrees as well (Margot et al., 2015). Typical WWTP effluent concentrations are in the low to medium ng $L^{-1}$ range (Ratola et al., 2012,Loos et al., 2013,Luo et al., 2014), but maximum concentrations can reach up to almost 1 mg $L^{-1}$, as was recently reported for the antidepressant citalopram (Cunha et al., 2017). The discharge of (un-) treated wastewater into surface waters is considered as the main entry route of organic micropollutants in the environment. Depending on the degree of wastewater dilution, concentration ranges observed for surface waters are generally in the same order of magnitude compared to those measured for WWTP effluents (i.e. in the ng $L^{-1}$ range, Loos et al., 2009). In summary, research has shown that organic micropollutants are present in various aqueous compartments around the world (Luo et al., 2014), including the most remote areas (Loos et al., 2009), and can be detected even in groundwater (Lapworth et al., 2012) and drinking water (Tröger et al., 2018).

Median lethal concentrations required for acute toxicity are typically in the mg $L^{-1}$ range (Fent et al., 2006), which is often more than an order of magnitude higher than environmental concentrations. However, more subtle, non-lethal adverse effects on aquatic life were already correlated to low levels of micropollutant exposure. For example, less than 1 ng $L^{-1}$ of the synthetic sex hormone ethinylestradiol (EE2) were already sufficient to reduce egg fertilization and induce feminization of fathead minnows (Parrott and Blunt, 2005). When wild fish populations are chronically exposed to low doses of EE2, the decreased reproductive success can even lead to their near extinction (Kidd et al., 2007). But not only hormones can influence the functions of the endocrine system.

Several industrial compounds, including plasticizers (Mathieu-Denoncourt et al., 2015), personal care products (Brausch and Rand, 2011), and flame retardants (Legler, 2008) were already proven as endocrine-disruptors. Some of these compounds tend to accumulate in biota and can therefore occur over different trophic levels in the food web (Ruhí et al., 2016). The uptake via the diet can be an important exposure route to anthropogenic pollutants and a positive feedback loop might even occur for compounds that increase the feeding rate (Brodin et al., 2014). Significant impact on the behavioral traits of fish, such as activity, aggression, boldness, and sociality were already reported and linked especially to the presence of psychoactive drugs (Brodin et al., 2014). Even those subtle effects in behavior might impact whole ecosystems, as fish for example influence the structure of aquatic communities (Johansson and Brodin, 2003). The multitude of potential adverse effects and complex ecological interdependencies make the risk-assessment of anthropogenic contaminants already a demanding task. However, it becomes even more challenging as mixture toxicity has to be taken into account for the environment. Micropollutants do not occur here as single compounds and adverse, additive effects were shown for complex mixtures at such low concentrations, where no response is expected for the single substances alone (Orton et al., 2014).

Assessing the entirety of organic micropollutants in the environment and potentially related risks requires also the consideration of products formed via the degradation of anthropogenic substances themselves. Pharmaceuticals for example can already undergo a variety of biochemical reactions once administered to the human body and they are typically excreted as a mixture of the original drug and metabolites. In some cases, transformation products are even the dominating species excreted via urine or feces. For example, the analgesic drug metamizole hydrolyses spontaneously in the human body into 4-methylaminoantipyrine, which undergoes further transformation generating 4-aminoantipyrine, 4-N-acetylaminoantipyrine, and 4-N-formylaminoantipyrine (Levy et al., 1995). Only these metabolites can be detected in WWTPs effluents and surface waters, reaching concentrations in the $\mu g\ L^{-1}$ range (Gómez et al., 2008), and are therefore the only evidence for a metamizole consumption. Once pharmaceuticals, their metabolites, but also other anthropogenic chemicals enter the sewer system, transformation might occur already in-sewer via abiotic hydrolysis, as well as anaerobic or aerobic microbial degradation (Ramin et al., 2016).

The same processes occur also in conventional wastewater treatment and especially the WWTP effluent loads of easily biodegradable compounds like selected surfactants, plastic additives and household chemicals can be significantly reduced (Margot et al., 2015). However, biotransformation can lead here also to an accumulation of degradation products and the compound spectrum released from WWTPs might be therefore shifted towards less biodegradable, i.e. more persistent, compounds. Once micropollutants and their TPs reach surface waters, photodegradation can occur in addition to hydrolysis and biodegradation. Generally, two different mechanisms can be distinguished. In case of a direct photolysis, the micropollutant itself absorbs light in the wavelength range > 290 nm, which can subsequently lead to bond breaking. Diclofenac is an example for a micropollutant that follows this transformation pathway (Salgado et al., 2013). In contrast, the indirect photodegradation process usually involves reactive oxygen species (ROS), e.g. hydroxyl radicals, which were generated for example from excited photosensitizers such as nitrate or nitrite in aquatic environments (Gligorovski et al., 2015) and interact with the micropollutants.

## References


Brausch, J.M., Rand, G.M., 2011. A review of personal care products in the aquatic environment: environmental concentrations and toxicity. Chemosphere 82 (11), 1518–1532.

Brodin, T., Piovano, S., Fick, J., Klaminder, J., Heynen, M., Jonsson, M., 2014. Ecological effects of pharmaceuticals in aquatic systems--impacts through behavioural alterations. Philosophical transactions of the Royal Society of London. Series B, Biological sciences 369 (1656).

Cunha, D.L., de Araujo, Frederico Goytacazes, Marques, M., 2017. Psychoactive drugs: occurrence in aquatic environment, analytical methods, and ecotoxicity-a review. Environmental science and pollution research international 24 (31), 24076–24091.

Fent, K., Weston, A.A., Caminada, D., 2006. Ecotoxicology of human pharmaceuticals. Aquatic toxicology (Amsterdam, Netherlands) 76 (2), 122–159.

Gligorovski, S., Strekowski, R., Barbati, S., Vione, D., 2015. Environmental Implications of Hydroxyl Radicals ((•)OH). Chemical reviews 115 (24), 13051–13092.

Gómez, M.J., Sirtori, C., Mezcua, M., Fernández-Alba, A.R., Agüera, A., 2008. Photodegradation study of three dipyrone metabolites in various water systems: identification and toxicity of their photodegradation products. Water research 42 (10-11), 2698–2706.

Johansson, F., Brodin, T., 2003. Effects of Fish Predators and Abiotic Factors on Dragonfly Community Structure. Journal of Freshwater Ecology 18 (3), 415–423.

Kidd, K.A., Blanchfield, P.J., Mills, K.H., Palace, V.P., Evans, R.E., Lazorchak, J.M., Flick, R.W., 2007. Collapse of a fish population after exposure to a synthetic estrogen. Proceedings of the National Academy of Sciences of the United States of America 104 (21), 8897–8901.

Lapworth, D.J., Baran, N., Stuart, M.E., Ward, R.S., 2012. Emerging organic contaminants in groundwater: A review of sources, fate and occurrence. Environmental pollution (Barking, Essex : 1987) 163, 287–303.
Legler, J., 2008. New insights into the endocrine disrupting effects of brominated flame retardants. Chemosphere 73 (2), 216–222.
Levy, M., Zylber-Katz, E., Rosenkranz, B., 1995. Clinical pharmacokinetics of dipyrone and its metabolites. Clinical pharmacokinetics 28 (3), 216–234.
Loos, R., Carvalho, R., António, D.C., Comero, S., Locoro, G., Tavazzi, S., Paracchini, B., Ghiani, M., Lettieri, T., Blaha, L., Jarosova, B., Voorspoels, S., Servaes, K., Haglund, P., Fick, J., Lindberg, R.H., Schwesig, D., Gawlik, B.M., 2013. EU-wide monitoring survey on emerging polar organic contaminants in wastewater treatment plant effluents. Water research 47 (17), 6475–6487.
Loos, R., Gawlik, B.M., Locoro, G., Rimaviciute, E., Contini, S., Bidoglio, G., 2009. EU-wide survey of polar organic persistent pollutants in European river waters. Environmental pollution (Barking, Essex : 1987) 157 (2), 561–568.
Luo, Y., Guo, W., Ngo, H.H., Nghiem, L.D., Hai, F.I., Zhang, J., Liang, S., Wang, X.C., 2014. A review on the occurrence of micropollutants in the aquatic environment and their fate and removal during wastewater treatment. The Science of the total environment 473-474, 619–641.
Margot, J., Rossi, L., Barry, D.A., Holliger, C., 2015. A review of the fate of micropollutants in wastewater treatment plants. WIREs Water 2 (5), 457–487.
Mathieu-Denoncourt, J., Wallace, S.J., de Solla, Shane R, Langlois, V.S., 2015. Plasticizer endocrine disruption: Highlighting developmental and reproductive effects in mammals and non-mammalian aquatic species. General and comparative endocrinology 219, 74–88.
Orton, F., Ermler, S., Kugathas, S., Rosivatz, E., Scholze, M., Kortenkamp, A., 2014. Mixture effects at very low doses with combinations of anti-androgenic pesticides, antioxidants, industrial pollutant and chemicals used in personal care products. Toxicology and applied pharmacology 278 (3), 201–208.
Parrott, J.L., Blunt, B.R., 2005. Life-cycle exposure of fathead minnows (Pimephales promelas) to an ethinylestradiol concentration below 1 ng/L reduces egg fertilization success and demasculinizes males. Environmental toxicology 20 (2), 131–141.
Ramin, P., Libonati Brock, A., Polesel, F., Causanilles, A., Emke, E., Voogt, P. de, Plósz, B.G., 2016. Transformation and Sorption of Illicit Drug Biomarkers in Sewer Systems: Understanding the Role of Suspended Solids in Raw Wastewater. Environmental science & technology 50 (24), 13397–13408.
Ratola, N., Cincinelli, A., Alves, A., Katsoyiannis, A., 2012. Occurrence of organic microcontaminants in the wastewater treatment process. A mini review. Journal of hazardous materials 239-240, 1–18.
Richardson, S.D., 2003. Water Analysis: Emerging Contaminants and Current Issues. Anal. Chem. 75 (12), 2831–2857.
Richardson, S.D., Kimura, S.Y., 2016. Water Analysis: Emerging Contaminants and Current Issues. Analytical chemistry 88 (1), 546–582.
Richardson, S.D., Ternes, T.A., 2005. Water analysis: emerging contaminants and current issues. Analytical chemistry 77 (12), 3807–3838.
Richardson, S.D., Ternes, T.A., 2011. Water analysis: emerging contaminants and current issues. Analytical chemistry 83 (12), 4614–4648.
Richardson, S.D., Ternes, T.A., 2014. Water analysis: emerging contaminants and current issues. Analytical chemistry 86 (6), 2813–2848.
Richardson, S.D., Ternes, T.A., 2018. Water Analysis: Emerging Contaminants and Current Issues. Analytical chemistry 90 (1), 398–428.

Ruhí, A., Acuña, V., Barceló, D., Huerta, B., Mor, J.-R., Rodríguez-Mozaz, S., Sabater, S., 2016. Bioaccumulation and trophic magnification of pharmaceuticals and endocrine disruptors in a Mediterranean river food web. The Science of the total environment 540, 250–259.

Salgado, R., Pereira, V.J., Carvalho, G., Soeiro, R., Gaffney, V., Almeida, C., Vale Cardoso, V., Ferreira, E., Benoliel, M.J., Ternes, T.A., Oehmen, A., Reis, M A M, Noronha, J.P., 2013. Photodegradation kinetics and transformation products of ketoprofen, diclofenac and atenolol in pure water and treated wastewater. Journal of hazardous materials 244-245, 516–527.

Schwarzenbach, R.P., Escher, B.I., Fenner, K., Hofstetter, T.B., Johnson, C.A., Gunten, U. von, Wehrli, B., 2006. The challenge of micropollutants in aquatic systems. Science (New York, N.Y.) 313 (5790), 1072–1077.

Ternes, T.A., Joss, A., Siegrist, H., 2004. Scrutinizing pharmaceuticals and personal care products in wastewater treatment. Environmental science & technology 38 (20), 392A-399A.

Tröger, R., Klöckner, P., Ahrens, L., Wiberg, K., 2018. Micropollutants in drinking water from source to tap - Method development and application of a multiresidue screening method. The Science of the total environment 627, 1404–1432.

## 2 Screening of water matrices and selection of study compounds

Surface water samples impacted by effluent of wastewater treatment plants were screened at the beginning of this study in 2014 with the aim to identify so far overlooked organic micropollutants in the environment. The data-independent All Ion MS/MS technique was applied to record information for parent molecules and product ions in the same measurement by simply alternating between low and high energies in the collision cell. The obtained data were compared to spectral libraries for a tentative identification of analytes. If available, reference standards were used to verify or reject putative compound identities. The results of a screening approach are exemplarily visualized in Figure 2.1 for a solid phase extract of Ammer river water taken in the federal state of Baden-Württemberg, Germany.

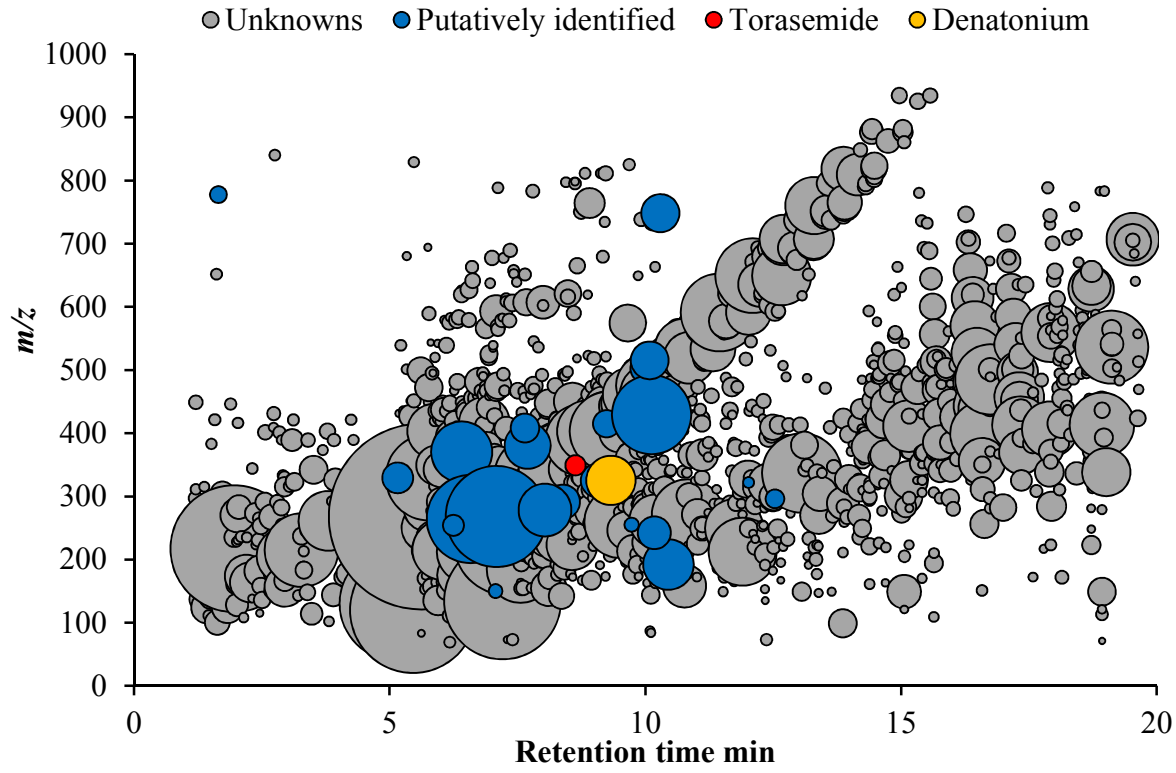


**Figure 2.1:** Overview of unknown (grey), putatively identified (blue) and unequivocally identified (red:torasemide, orange:denatonium) analytes in a solid phase extract of a wastewater impacted surface water sample. Putative identification was performed by comparing All Ion spectra to a spectral library and at least two fragments from the library had to be present for identification. The bubble size represents the analytes peak area.

Applying a non-targeted data evaluation approach based on the molecular feature extraction algorithm in the MassHunter Qualitative Analysis software (Agilent Technologies), almost 1800 analytes were detected.

The structural information recorded for this sample (i.e. All Ion MS/MS data) were compared in addition to the MassHunter Forensic and Toxicology PCDL (Agilent Technologies, version 4.2), which contains MS/MS spectra for about 3000 compounds, including pharmaceuticals and personal care products.

This suspect screening approach enabled the putative identification of 29 out of the 1783 unknown compounds. Most of these substances were already reported as environmental pollutants before and their transformation was often investigated as well. However, a thorough literature study revealed denatonium and torasemide as interesting candidates for further investigations. Reference standards were therefore purchased to unequivocally verify their identity. Being one of the bitterest substances, denatonium is added to a wide range of (household) products to prevent accidental consumption especially by children. Furthermore, the addition of denatonium is the recommended denaturing procedure for alcohol in the European Union. Despite its widespread application, denatonium was however never reported as environmental pollutant before. The pharmaceutical torasemide is generally applied as loop diuretic for the treatment of hypertension and edema. Prescriptions of this compound are increasing annually in Germany and torasemide was 2014 the twelfth most prescribed drug in Germany. Torasemide was already detected in the aqueous environment, but the fate of this compound during wastewater treatment and in surface waters was not yet investigated.

# 3 Research objectives and thesis content

The overall goal of this thesis was to close knowledge gaps about the occurrence and fate of denatonium and torasemide in the environment and therefore generally expanding the picture about compounds of emerging concern. Initially, quantification of these contaminants themselves should be performed with LC-ESI-QqQ mass spectrometry, e.g. for samples from surface waters and wastewater treatment plants (WWTPs). In addition, a comprehensive overview of transformation products (TPs) should be gained applying different abiotic (i.e. photolysis and electrochemical degradation), as well as biotic (i.e. microbial degradation and exposure to human liver microsomes) degradation experiments. Subsequent prioritization of these TPs as environmentally relevant should be performed based on suspect screening of water samples using high-resolution mass spectrometry (HRMS). All MS/MS information of denatonium, torasemide and relevant TPs should be finally made publicly available (e.g. in the MassBank repository) to facilitate their identification by other analysts in samples from all over the world.

The results from this doctoral thesis are presented as three research articles, which were published in peer-reviewed journals:

- **Chapter 4** deals with the development of a sensitive targeted method, which was applied to quantify denatonium in WWTP and surface water samples, as well as in consumer products, from Germany. Exposure to denatonium and entry routes into the environment were discussed. HRMS measurements based on LC-ESI-QTOF MS were applied to WWTP samples of additional European countries to investigate a more widespread occurrence of denatonium.
- In **chapter 5**, the goal was to identify putative environmentally relevant TPs of denatonium and to discuss this compounds´ fate during (advanced) wastewater treatment and in the environment. Anodic oxidation and photodegradation were applied for TP synthesis. WWTP and surface water samples were screened for their presence applying HRMS. In addition, samples from pilot-scale wastewater ozonation were investigated for denatonium removal and TP formation.

- **Chapter 6** focuses on the transformation of torasemide. Microbial degradation, treatment with human liver microsomes, photolysis, and electrochemical degradation were applied for TP synthesis. Torasemide concentrations in aqueous samples were determined with LC-ESI-QqQ MS, while the occurrence of the identified TPs in WWTP and river water samples was investigated with HRMS using LC-ESI-QTOF MS.

A general summary and conclusions are presented in **chapter 7**, while an outlook and ideas for further research and improvements are summarized in **chapter 8**.

# 4 Denatonium – a so far unrecognized but ubiquitous water contaminant?

**Authors**

Sascha Lege[a], Gaëlle Guillet[b], Sylvain Merel[a], Jorge Eduardo Yanez Heras[a], Christian Zwiener[a]

[a] University of Tübingen, Environmental Analytical Chemistry, Hölderlinstraße 12, 72074 Tübingen, Germany

[b] University of Tübingen, Hydrogeochemistry / Applied Geology, Hölderlinstraße 12, 72074 Tübingen, Germany

**Highlights**

- A LC-ESI-QqQ method was developed for denatonium and other anthropogenic pollutants.
- Denatonium was detected in all waters affected by wastewater.
- Maximum denatonium concentration of 341 ng $L^{-1}$ was found in WWTP effluent.

Published 2017 in the Elsevier journal *Water Research*, vol. 112, pp. 254-260, DOI: 10.1016/j.watres.2017.01.056. 

## 4.1 Abstract

Denatonium is one of the bitterest substances known to man and therefore applied in numerous consumer products to prevent an accidental or intentional consumption. So far no information was available on the occurrence of this compound in the environment. A sensitive targeted method was developed and applied to water samples taken in the federal state of Baden-Württemberg, Germany. Denatonium was detected in 100% of the investigated 22 wastewater treatment plant (WWTP) effluents with a maximum concentration of 341 ng $L^{-1}$. Additionally, water samples were taken from the Ammer river over a period of one week and all wastewater impacted samples showed denatonium at concentrations up to 195 ng $L^{-1}$. Retrospective analysis of high-resolution mass spectrometric measurements of WWTP effluents from Italy and Switzerland confirmed and therefore point to an international occurrence of denatonium as anthropogenic contaminant.

## 4.2 Introduction

Denatonium benzoate (trade name Bitrex®) is one of the bitterest substances known to man with recognition thresholds in the range of 3 - 23 µg $L^{-1}$ (Schiffman et al., 1994) and an unpleasant bitterness at elevated concentrations of 10 mg $L^{-1}$ (Cosmetic Ingredient Review Expert Panel, 2008). Volunteer studies from the 1980s and 1990s indicated its usefulness for poisoning prevention, because a reduced ingestion rate of denatonium benzoate-containing formulations was observed for children and non-target animals (Berning et al., 1982; Kleinkauf et al., 1999; Sibert and Frude, 1991). However, no effects on the frequency or severity of pediatric fluid consumption of antifreeze and windshield washer were identified, when poisoning data were compared before and after bittering was required in selected states of the USA (Mullins and Zane Horowitz, 2004; White et al., 2009). Nevertheless, Bitrex® is added nowadays to a wide range of products (e.g. finger paints, household products, and pesticides) and it is used for the denaturation of alcohol. Depending on its application, concentrations between 200 – 300 mg $L^{-1}$ [a)] or 20 - 100 mg $L^{-1}$ are often used in animal repellants or to prevent accidental ingestion by humans (Cosmetic Ingredient Review Expert Panel, 2008; Kleinkauf et al., 1999), while the common denaturing procedure for alcohol in the European Union (EU) requires 10 mg $L^{-1}$ denatonium benzoate (European Commission, 2013).

a) Denatonium concentrations are often reported in [ppm]. For consistent units, a constant density of 1 kg $L^{-1}$ was assumed for aqueous solutions of denatonium and [ppm] were directly converted to [mg $L^{-1}$].

This aversive agent is generally considered as a very safe compound, because animal studies indicate that it is neither carcinogenic, genotoxic (Cosmetic Ingredient Review Expert Panel, 2008), nor mutagenic (Consumer Product Safety Commission United States of America, 1992). It shows a moderate acute oral toxicity for different mammalian species with median lethal doses in the range of 593 - 865 mg $kg^{-1}$ (Consumer Product Safety Commission United States of America, 1992). Due to its unpleasant bitterness it is however very unlikely that humans ingest it in appreciable amounts. Available information about the acute inhalation toxicity and chronic toxicity are not conclusive. While no inhalation hazard was observed for rats exposed to a 0.1% w/v (i.e. 1 g $L^{-1}$) denatonium benzoate solution (Klein-Schwartz, 1991), the European Food Safety Authority (EFSA) reported a median lethal inhalation concentration of 0.2 mg $L^{-1}$ (European Food Safety Authority, 2012). Monkeys showed an increased mortality when orally dosed with 8 or 16 mg denatonium benzoate $kg^{-1}$ $day^{-1}$ over one year, but no compound related effects were observed during a two year study with rats (Cosmetic Ingredient Review Expert Panel, 2008). A single case of Bitrex® related asthma and allergic skin reactions was reported in the 1980s, where adverse effects, i.e. erythema, were still observed at concentrations as low as 2 ng $L^{-1}$ (Björkner, 1980). In contrast, neither skin sensitizing nor irritating properties were observed during several studies with overall more than 1100 humans, which were exposed to denatured alcohol containing denatonium benzoate (Cosmetic Ingredient Review Expert Panel, 2008).

Animal studies with aquatic species point towards a moderate acute toxicity with median lethal concentrations higher than 1000 mg $L^{-1}$ for rainbow trout and $\geq$ 400 mg $L^{-1}$ for selected invertebrates (European Food Safety Authority, 2012). However, lower concentrations in the range of 5 - 10 mg $L^{-1}$ influenced the reproduction of Daphnia magna and reduced the biomass of the freshwater algae Nitzschia palea (European Food Safety Authority, 2012). Generally, the ecotoxicological risk for non-target animals was ranked as low by the EFSA, because only a negligible release of denatonium benzoate into the environment is expected when it is applied as repellant in forestry. However, they concluded that "if other uses resulting in higher exposure were intended in the future, a considerable amount of data would be needed to finalise the environmental exposure assessment" (European Food Safety Authority, 2012) and more studies are required for a comprehensive ecotoxicological risk assessment. Information about the use pattern and annual global production of this aversive agent is however not available, but approximately 10 – 100 tons are manufactured and/or imported each year in the European Economic Area (ECHA, 2016).

Denatonium was not considered so far as a suspect compound for the investigation of surface waters and wastewater, although other chemicals present in industrial products were already extensively studied, e.g. surfactants (Cowan-Ellsberry et al., 2014). Furthermore, non-target screening approaches are not suited for the identification of this compound, because protonation of the analyte is typically expected during electrospray ionization in the positive mode (Velpandian et al., 2012). Wrong molecular formulas are therefore assigned to permanently charged analytes, which was demonstrated recently for triphenylphosphonium compounds (Schlüsener et al., 2015).

We tentatively identified denatonium based on a commercially available, high-resolution spectral library and the main goal of this study was to provide first data on the occurrence of denatonium in the environment and to assess wastewater as a possible source. Therefore, a sensitive multi-analyte targeted method was developed and applied to samples from rivers and wastewater treatment plant (WWTP) effluents in the federal state of Baden-Württemberg, Germany. In the EU there are usually no regulatory thresholds for denatonium in industrial products, except for denatured alcohol. Therefore, 22 consumer products were bought from local supermarkets and analyzed to evaluate the range of denatonium concentrations in personal care products (PCPs), detergents, and antifreeze.

## 4.3 Material and methods

### 4.3.1 Chemicals

Optima™ LC/MS grade acetonitrile (ACN), methanol (MeOH), isopropanol (IPA), formic acid (FA), acetic acid (HAc), ammonium acetate ($NH_4Ac$) and water were purchased from Fisher Chemical (Belgium). The targeted analysis method was generally developed for 72 analytes, but results are presented in this study only for the following six compounds. Benzotriazole (≥ 98%.), denatonium benzoate (≥ 98%), diatrizoic acid (≥ 98%), paracetamol (≥ 99%) and sulfamethoxazole (≥ 98%) were obtained from Sigma-Aldrich (Germany), while lamotrigine (≥ 98%) was purchased from TCI (Belgium). Analytes other than denatonium were used for quality control purposes and to compare the observations for the bittering agent to already known water pollutants. Individual stock solutions with analyte concentrations of 1 g $L^{-1}$ were usually prepared with ACN, except for lamotrigine and diatrizoic acid which were dissolved in MeOH.

A working solution containing all analytes was prepared in ACN with final concentrations of 10 mg $L^{-1}$ and subsequent dilutions in tap water were used for external calibration. Stock and working solutions were stored in the freezer at -18 °C, while dilutions for the calibration were freshly prepared on a daily basis.

### 4.3.2 Sampling and sample preparation

In 2015, 22 consumer products (15 detergents, 6 personal care products (PCPs) and 1antifreeze) were bought from local supermarkets and analyzed for their denatonium content. In order to assess the sources and the distribution of this bittering agent and other organic contaminants in the environment, two sampling campaigns were performed in the federal state of Baden-Württemberg, Germany, in summer 2014 and spring 2015. Surface water and WWTP effluent samples were collected from 13 different locations along six tributaries of the river Neckar and from 22 treatment plants, respectively. Time trends of pollutant concentrations were investigated for one of the surface waters, the river Ammer, by collecting 2 h composite samples over seven consecutive days. All other samples from these two campaigns were grab samples. Additionally, a total of five WWTP effluent samples from two plants in Switzerland and one from Italy were analyzed to investigate the occurrence of denatonium as water contaminant outside of Germany.

Environmental samples were transported to the laboratory on ice. Particles were removed either by centrifugation or filtration and the samples were stored in the dark at 4 °C for a maximum of 48 h until analysis. Consumer products were diluted prior to analysis by a factor of $10^5$ without any further treatment and the dilutions were immediately analyzed after preparation. Further details about the sampling locations, consumer products, and sample processing are provided in the supporting information (section 4.8.1).

### 4.3.3 LC-ESI-QqQ analysis

Target analysis was performed using a 1260 Infinity HPLC system (Agilent Technologies, Germany), consisting of a degasser, a binary pump, an autosampler, a thermostat, and a column oven. Samples were kept in the autosampler at 10 °C and the injection volume was either 10 µl for the diluted consumer products or 100 µl for surface water and WWTP samples, respectively. Analytes were separated on a Poroshell EC-C18 column (2.1 x 100 mm, 2.7 µm, Agilent Technologies, Germany) coupled to a Poroshell EC-C18 guard column (2.1 x 5 mm, 2.7 µm, Agilent Technologies, Germany).

In case of environmental samples, the mobile phases were (A) water + 0.1% HAc + 0.1 mM $NH_4Ac$ and (B) ACN + 0.1% HAc. The following gradient program was used for separation: at 0 min 98% A, at 17 min 20% A, at 17.1 min 0% A, at 23 min 0% A, at 23.1 min 98% A, and at 32 min 98% A.

Diluted consumer products were analyzed with (A) water + 0.1% FA and (B) ACN + 0.1% FA and the following gradient: at 0 min 95% A, at 17 min 10% A, at 17.1 min 0% A, at 22 min 0% A, at 22.1 min 95% A, at 29 min 95% A. The flowrate was always kept constant at 0.4 ml $min^{-1}$ and the column was held at 40 °C.

Determination of analytes was achieved after LC separation with a 6490 triple quadrupole mass spectrometer (Agilent Technologies, Germany) using either the positive ionization mode (consumer products) or fast polarity switching (environmental samples). The ESI source was operated under the following conditions: drying gas temperature 150 °C, drying gas flow 16 L $min^{-1}$, sheath gas temperature 400 °C, sheath gas flow 12 L $min^{-1}$, and a nebulizer pressure of 35 psi. In the positive ionization mode, the capillary and nozzle voltages were kept at 2500 V and 300 V, respectively, while they were increased to 3000 V and 1500 V for the negative ionization mode. Nitrogen, produced on-site with a nitrogen generator from Peak Scientific (Germany), was used as drying, sheath and nebulizing gas, while the collision cell was supplied with ultra-pure nitrogen (≥ 99.999%) from Westfalen AG (Germany).

Two MRM transitions were monitored for each analyte in the dynamic MRM mode, i.e. the response of the quantifier and qualifier ion was measured in a predefined window of ± 0.6 min around the retention time of the compound. Details about the transitions, applied collision energies, intensity ratios, and retention times of the compounds are listed in Table 4.1. Dwell times were automatically adjusted by the acquisition software at a constant scan rate of 3 Hz for each transition and were always ≥ 10 ms.

### 4.3.4 Method validation and analytical quality control for targeted analysis

Matrix effects were the only factors influencing analyte quantification due to direct aqueous injection analysis. Signal enhancement or suppression was estimated for selected river water samples, WWTP effluents, and consumer products either by post column infusion, a dilution approach or by standard addition, respectively. Details about the evaluation of matrix effects are given in section 4.8.1 of the supporting information.

Intra- and interday variations of the quantifier response were investigated at three concentration levels over three consecutive days and expressed as relative standard deviation. External calibration was typically performed between 1-1000 ng $L^{-1}$ and at least 10 concentration levels were considered for calibration. The lowest limits of quantification (LLOQs) were defined as the lowest concentration of the calibration curve with a signal-to-noise ratio (S/N) of ≥ 10 for the quantifier.

Measurements were only considered for further interpretation, when the intensity ratios of the quantifier and qualifier, as well as the retention time, deviated by less than 20% and 0.1 min from the values of reference compounds (Table 4.1), respectively. Furthermore, the peak area had to be greater than the average blank response plus three times the standard deviation.

**Table 4.1:** Details of the MRM method for targeted analysis. Transitions used for quantification are highlighted in bold. Response ratios of both transitions are given as the average ± standard deviation (n=133) obtained from calibration solutions.

| Compound | Retention time [min] | Parent species | MRM transitions | Collision energy [V] | Response ratio (Qualifier/ Quantifier) |
|---|---|---|---|---|---|
| Benzotriazole | 6.03 | $[M+H]^+$ | **120.1 → 64.8**<br>120.1 → 39.1 | **24**<br>48 | 0.72 ± 0.03 |
| Denatonium | 10.18<br>9.16[a] | $[M]^+$ | **325.2 → 86.0**<br>325.2 → 91.1 | **20**<br>46 | 1.11 ± 0.04 |
| Diatrizoic acid | 2.05 | $[M+NH_4]^+$ | **631.8 → 361.0**<br>631.8 → 233.1 | **24**<br>48 | 0.85 ± 0.05 |
| Lamotrigine | 7.22 | $[M+H]^+$ | **256.0 → 211.1**<br>256.0 → 58.2 | **28**<br>36 | 0.80 ± 0.04 |
| Paracetamol | 3.77 | $[M+H]^+$ | **152.1 → 110.0**<br>152.1 → 65.0 | **16**<br>32 | 0.45 ± 0.04 |
| Sulfamethoxazole | 8.01 | $[M+H]^+$ | **254.1 → 92.1**<br>254.1 → 156.0 | **28**<br>16 | 0.87 ± 0.05 |

[a] Evaluation of consumer products with a different gradient.

## 4.4 Results and discussion

### 4.4.1 Method validation for targeted analysis

Response ratios of qualifier and quantifier transitions were important criteria for analyte identification and deviated generally by less than 10% for all analytes. The reproducibility of targeted analysis was expressed as intra- and interday variation of the quantifier response and the results are summarized in the supporting information (Table S4.1 and Table S4.2).

The observed intraday variation was usually ≤ 3% for all sample types, while the interday variation was only investigated for environmental matrices and varied here between 6 and 17%. In case of denatonium, LLOQs were as low as 1 ng $L^{-1}$ for environmental samples (Table S4.1) and 0.1 mg $kg^{-1}$ for consumer products (Table S4.2), respectively. The other analytes were quantified at concentrations ≤ 7.5 ng $L^{-1}$, except for diatrizoic acid were the LLOQ was 25 ng $L^{-1}$. No significant matrix effects were observed at the retention times of the analytes for any of the investigated matrices (supporting information section 4.8.2).

### 4.4.2 Denatonium in consumer products

Denatonium was declared as ingredient in 20 of the 22 investigated consumer products from Germany, i.e. in 4 personal care products (PCP´s), 1 antifreeze windshield washer fluid and 15 detergents. The measured concentrations were in the range of 3.7 – 58 mg $kg^{-1}$ (Figure 4.1). Fourteen out of 20 samples showed concentrations above the unpleasant bitterness level of 10 mg $L^{-1}$ and all measured denatonium concentrations were at least 1000 times higher than the average recognition threshold for young people (Schiffman et al., 1994). Generally, no relation was observed between the content of the bittering agent and the application of the product. Furthermore, high intra-class deviations were observed (up to 61% in case of the detergents), which can be explained by the absence of a regulatory denatonium threshold for most products in the European Union.

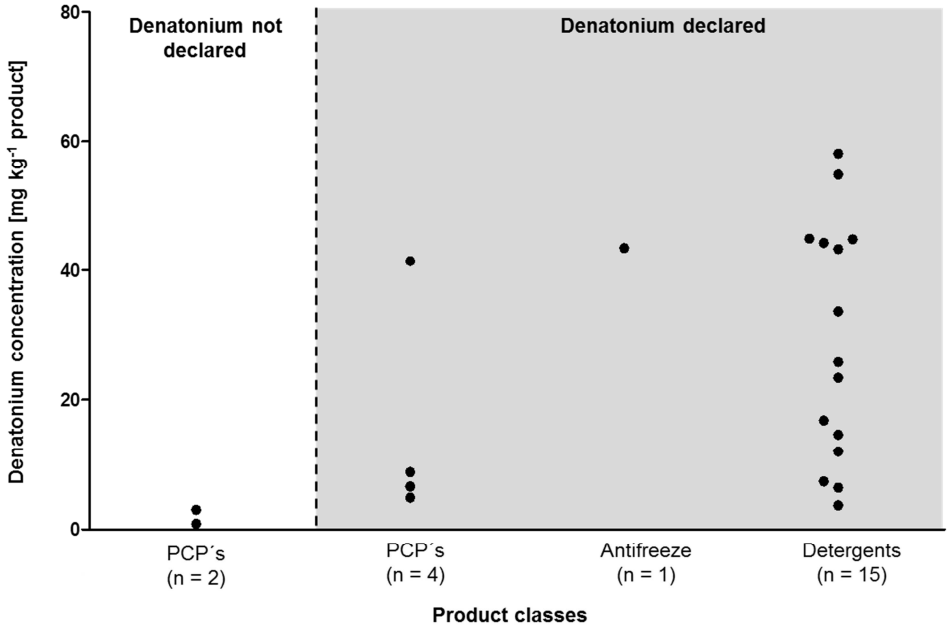


**Figure 4.1**: Denatonium concentrations in 22 consumer products from three different product classes. Denatonium was declared as ingredient in 20 of the investigated formulations (PCP personal care product).

A denatonium concentration of 0.9 mg $kg^{-1}$ was measured in a skin cleansing product and 3.0 mg $kg^{-1}$ in a nail polish remover, although the aversive agent was not declared as an ingredient. However, both products contained denatured alcohol and the common denaturing procedure for all member states of the EU requires 1 g denatonium benzoate per 100 L absolute ethanol (European Commission, 2013). Data collected from the cosmetics industry in the US (Cosmetic Ingredient Review Expert Panel, 2008) revealed that 585 out of 17075 (≈ 3.4%) considered formulations contained specially denatured alcohol with denatonium benzoate (i.e. SD Alcohol 40-B).

The fractions of denatured alcohol ranged from 0.003% in eyeliner to 99% in deodorants. Considering the denaturing procedure for alcohol in the EU, these fractions would correspond to denatonium concentrations between 300 ng $L^{-1}$ and almost 10 mg $L^{-1}$ in the consumer products. Unfortunately, no information is available about sales and application volumes of cosmetics and other household products containing denatonium benzoate. Therefore, it is not possible to estimate the amount of this aversive agent, which could end up in the environment from the use of these products.

### 4.4.3 Sources and distribution of denatonium in a German river

The occurrence of anthropogenic contaminants in the Ammer river, a tributary of the river Neckar, was studied over seven consecutive days in 2014. The sampling campaign included base flow conditions, as well as heavy rainfall events (Figure 4.2B). For dry weather periods, the observed denatonium concentrations downstream of the WWTP were typically in the range between 58 and 128 ng $L^{-1}$. An average concentration of 98 ng $L^{-1}$ was observed for the base flow conditions between Monday and Wednesday (Figure 4.2A), which is similar to the average concentration of 92 ng $L^{-1}$ observed for sulfamethoxazole (Figure S4.4A). Concentrations of most other micropollutants, measured during base flow conditions, were significantly higher and ranged from 283 ng $L^{-1}$ for lamotrigine to 1357 ng $L^{-1}$ for benzotriazole. The average diatrizoic acid concentration for this sampling period was about 842 ng $L^{-1}$, while paracetamol was not detected (Figure 4.2A, Figure S4.4A).

Generally, all investigated analytes showed similar concentration trends as denatonium during the sampling campaign (Figure 4.2A) and the best correlations with the denatonium concentration were observed for sulfamethoxazole ($R^2$= 0.87) and lamotrigine ($R^2$= 0.91).

The here observed weak correlations for benzotriazole ($R^2$= 0.37) and diatrizoic acid ($R^2$= 0.39) (Figure S4.4B) were reported also for the wastewater marker oxypurinol (Funke et al., 2015). The authors explained the weak correlations by an irregular application of diatrizoic acid as x-ray contrast medium and the unknown fate of benzotriazole. A correlation coefficient could not be estimated for paracetamol due to the low number of measurements above the limit of quantification.

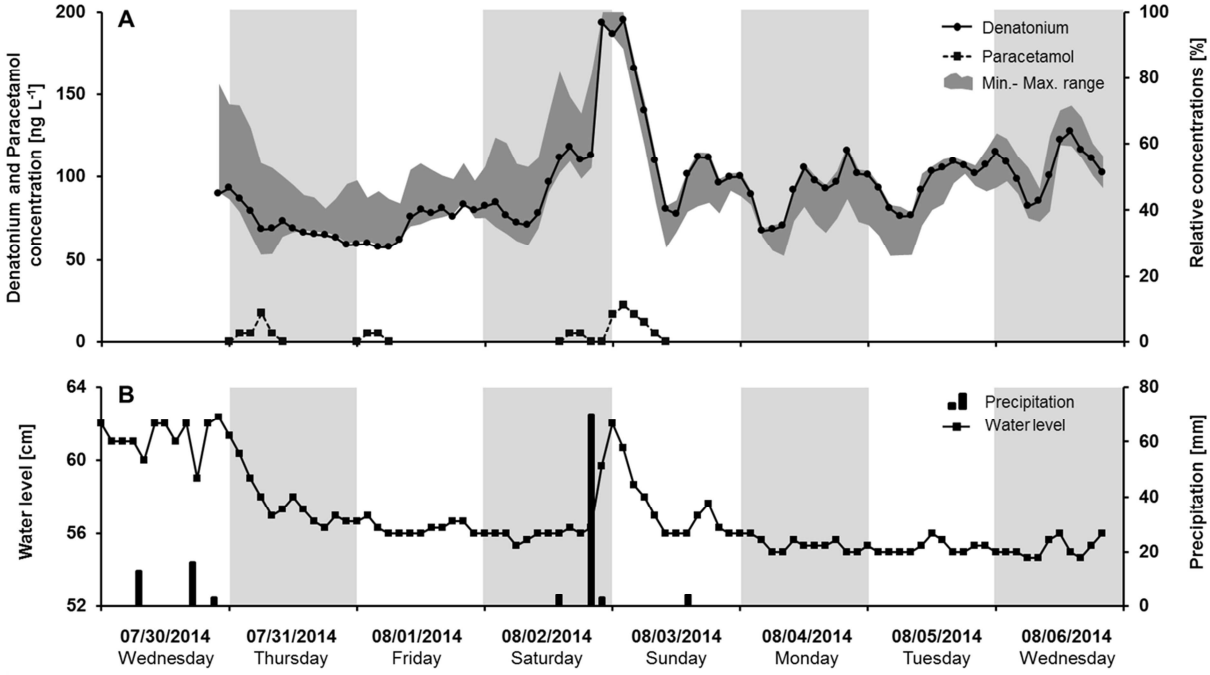


**Figure 4.2**: Absolute concentrations (denatonium and paracetamol) and relative concentration ranges (all six analytes except paracetamol; min. – max. range) measured in the Ammer river downstream of the WWTP (A). Rainfall data and water level measurements from the Ammer river were averaged over two hours and indicate changing weather conditions during the sampling campaign (B).

Maximum contaminant concentrations were detected on Saturday night, after heavy rainfall in the Ammer catchment. Denatonium concentrations up to 195 ng $L^{-1}$ were observed at that time (Figure 4.2A), which is comparable to the observed sulfamethoxazole level of 208 ng $L^{-1}$ (Figure S4.4). Paracetamol was measured during the flood event with a maximum concentration of 23 ng $L^{-1}$ and lamotrigine levels were almost 3 times higher than those of denatonium (i.e. 540 ng $L^{-1}$). However, the highest concentrations were observed for benzotriazole and diatrizoic acid with more than 2.5 µg $L^{-1}$ and about 1.9 µg $L^{-1}$, respectively (Figure S4.4). Generally, the elevated contaminant levels suggested reduced removal efficiencies for anthropogenic pollutants during wastewater treatment, which is confirmed by the occurrence of paracetamol.

This is a marker for untreated or insufficiently treated wastewater input (Tran et al., 2014), since paracetamol is completely eliminated in modern WWTPs under normal conditions (Gao et al., 2012). Median denatonium concentrations of 8 ng $L^{-1}$ were measured in the Ammer upstream and 92 ng $L^{-1}$ downstream of a WWTP. Denatonium was not detected in any of the small creeks discharging into this river (Figure 4.3). The same trend was observed for the other contaminants. This is shown exemplarily for benzotriazole (Figure 4.3), a corrosion inhibitor frequently detected in European rivers and WWTPs (Loos et al., 2009; Loos et al., 2013) and the concentrations of the other compounds are presented in the supporting information (Figure S4.5). The observed denatonium concentrations were generally about 11-15 times lower compared to those of benzotriazole, but still significantly higher than concentrations reported for other compounds frequently used in personal care products. For example, Jonkers et al. investigated the occurrence of parabens, a group of preservatives, in a Swiss river, which received a relative amount of 10 – 20% treated wastewater from a cumulative amount of 160000 inhabitants (Jonkers et al., 2009). These conditions are comparable to the Ammer river, which received a relative amount of 10% treated wastewater from 80000 inhabitants. The median observed concentrations for the parabens in the Swiss river were usually below 1 ng $L^{-1}$ and a maximum concentration of 17 ng $L^{-1}$ was detected for methylparaben (Jonkers et al., 2009). One reason for the concentration differences between denatonium and the parabens might be related to the fate of the compounds during wastewater treatment. While almost complete removal of parabens is usually observed in WWTPs (Kasprzyk-Hordern et al., 2009; González-Mariño et al., 2011), neither considerable sorption nor biodegradation occurred for denatonium during semi-continuous experiments with activated sludge (Corby et al., 1993).

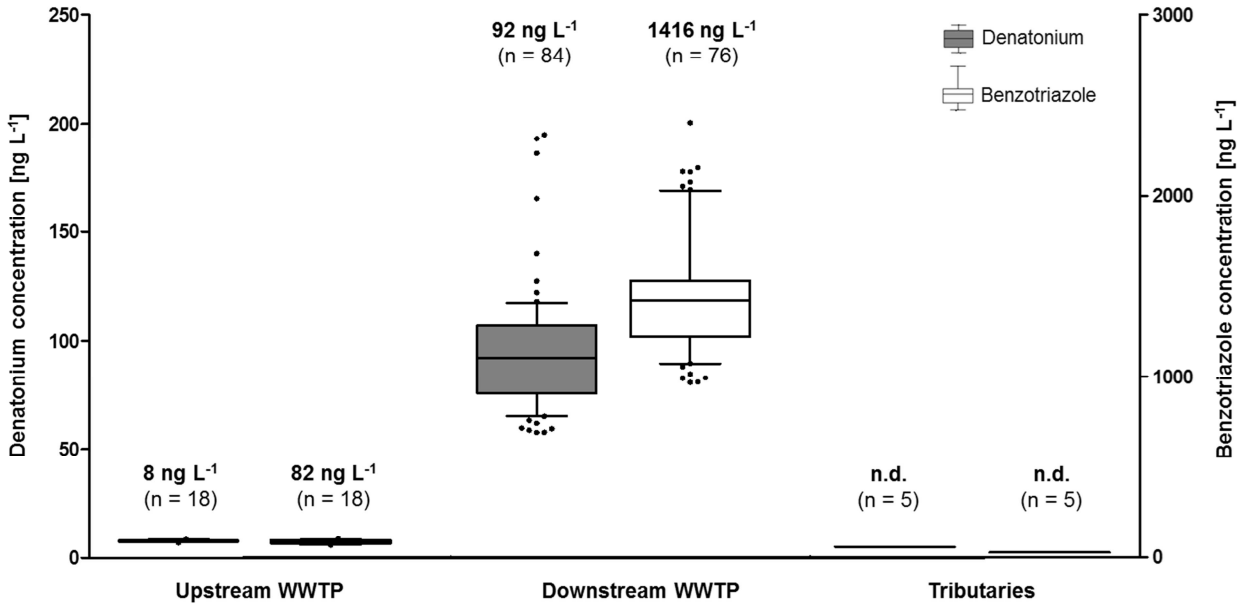


**Figure 4.3**: Denatonium (grey filled, left) and benzotriazole (not filled, right) concentrations measured in the Ammer river up- and downstream of a WWTP and in five small creeks discharging into this river. Median analyte concentrations are indicated above the boxplots (n.d. not detected).

The presence of anthropogenic contaminants upstream of the WWTP (Figure 4.3, Figure S4.5) was most likely related to untreated wastewater input. Leaky pipes of the sewer system of a nearby city were already discussed for this area (Selle et al., 2013) representing a steady source of micropollutants also during base flow conditions. The fact that paracetamol was however only detected in the upstream samples (data not shown) after the heavy rainfall event on Saturday night (Figure 4.2B), points towards combined sewer overflows (CSOs). The influence of these dynamic events on the concentration of polycyclic aromatic hydrocarbons and synthetic musk fragrances was already reported for the Ammer river (Schwientek et al., 2013, Lange et al., 2015). Untreated wastewater and effluents of WWTPs can be therefore considered as main sources of denatonium in the environment. This is in agreement with the application of Bitrex® in consumer products like cleaning products and shower gels, which usually are discharged to wastewater. Diffuse entry routes of this compound into the environment from applications other than household products, e.g. for the prevention of cannibalism in livestock farming, cannot be completely ruled out as detailed information about application volumes are missing. However, when denatonium benzoate is used for example as animal repellant in forestry, the maximum application rate is here only about 0.7 g per 1000 trees. Therefore, the European Food Safety Authority concluded that an environmental exposure from this application is negligible (European Food Safety Authority, 2012).

### 4.4.4 Screening of WWTP effluents in Baden-Württemberg, Germany

In a second campaign effluents of 22 WWTPs and 3 rivers were sampled in Baden-Württemberg, Germany. The data also reveal WWTPs as main sources of the investigated micropollutants, because they were only detected in rivers, which were receiving treated wastewater. The observed median concentrations in these rivers ranged from 34 ng $L^{-1}$ for denatonium to 856 ng $L^{-1}$ in case of benzotriazole (Figure 4.4). Paracetamol was not detected in any of the investigated surface waters (data not shown). Denatonium concentrations in effluents of WWTPs ranged from 16 ng $L^{-1}$ to 341 ng $L^{-1}$ with a median concentration of 156 ng $L^{-1}$. Except for paracetamol, all median concentrations of the other investigated contaminants were at least 2 times higher and ranged from 312 ng $L^{-1}$ for sulfamethoxazole (Figure S4.6) to 3323 ng $L^{-1}$ in case of benzotriazole (Figure 4.4).

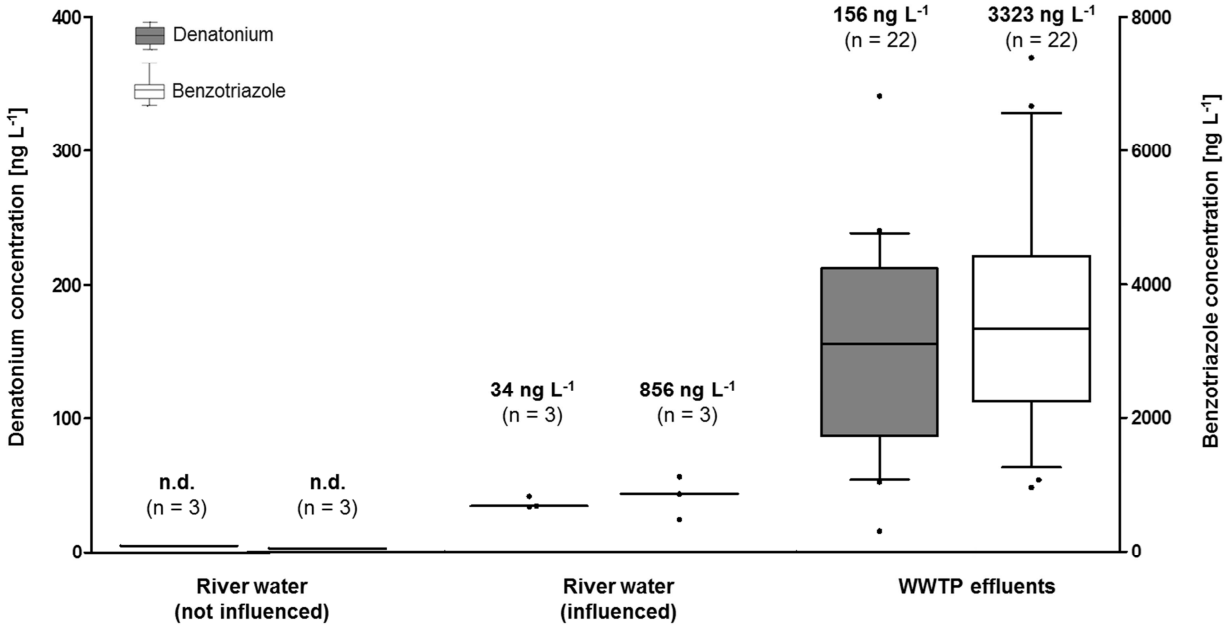


**Figure 4.4**: Denatonium (grey filled, left) and benzotriazole (not filled, right) concentrations in surface waters or WWTP effluents sampled in Baden-Württemberg, Germany, in 2015. Rivers were either influenced or not influenced by treated wastewater and median analyte concentrations are given above the boxplots (n.d. not detected).

The observed high concentration variability between the different WWTPs (Figure 4.4, Figure S4.6) might be explained by analyte fluctuations during grab sampling and the elimination efficiency of different water treatment processes. Pronounced intra- and interday variations of anthropogenic contaminants typically occur in WWTP effluents (Petrie et al., 2015) which cannot be accounted for by single grab samples.

Additionally, paracetamol was detected in 50% of the investigated WWTPs with a maximum concentration of 14 ng $L^{-1}$ (data not shown), which points towards reduced biological removal efficiencies in these plants. The lowest denatonium concentration was also observed in a WWTP using powdered activated carbon (PAC). Crosson et al. showed an efficient removal of denatonium by PAC in pure water, which might explain this observation (Crosson et al., 2014). However, a further evaluation of the effect of different treatment processes on denatonium removal was not subject of this investigation. Due to the coverage of a wide range of sizes and treatment processes of WWTPs considered, it is reasonable to assume that the data on denatonium occurrence in the federal state of Baden-Württemberg are representative for the whole country. A back-of-the-envelope calculation results in 1500 kg denatonium released via wastewater in Germany each year, taking into account a median denatonium concentration of 150 ng $L^{-1}$ in WWTP effluents and the annual wastewater volume discharged in Germany (i.e. about 10 billion $m^3$; Federal Statistical Office (Statistisches Bundesamt), 2013).

### 4.4.5 Occurrence of denatonium in two other European countries

Information from the database "Substances in Preparations in Nordic Countries" (SPIN, www.spin2000.net) confirmed that denatonium benzoate-containing products are also applied in other European countries. Assuming a similar disposal route compared to Germany, denatonium is expected to occur in the wastewater of other countries as well. Therefore, retrospective analysis of high-resolution mass spectrometry measurements was performed for WWTP effluents taken from Switzerland and Italy to support this hypothesis. Details about the measurements and samples are summarized in section 4.8.1 of the supporting information. Denatonium was unequivocally identified with a reference standard in samples of both countries (Figure S4.7). Rough concentration estimations were performed using a one-point calibration. Denatonium concentrations were in the range of 23 to 40 ng $L^{-1}$ in the two WWTPs from Switzerland and about 266 ng $L^{-1}$ in the Italian plant, which is in a similar range than in Germany (section 4.4.4). These results already point out the fact that the occurrence of denatonium is not only relevant for Germany but should be also in other countries where denatonium is used.

## 4.5 Conclusion

This is the first study describing denatonium as a water pollutant in Germany and two other European countries. The effect concentrations for denatonium are still several orders of magnitude higher than the detected environmental concentrations. However, if we take mixture toxicity into consideration, further knowledge on occurrence and fate of denatonium is required also in the context of the precautionary principle. Based on our results and the existing literature we identified the following research needs and knowledge gaps:

- Information about global production and application patterns
- Investigation of the occurrence in additional countries
- **(Eco-)toxicological studies** investigating potential (long-term) risks at environmentally relevant concentrations
- Elucidation of the **fate in the environment** including the identification of transformation products.

## 4.6 Acknowledgements

The German Federal Environmental Foundation (Deutsche Bundesstiftung Umwelt, DBU) is gratefully acknowledged for funding the Ph.D. scholarship of Sascha Lege. We thank Marc Schwientek and Hermann Rügner from the WESS Competence Cluster, as well as Thomas Glauner from Agilent Technologies, for providing WWTP effluent samples. Furthermore, we thank the three anonymous reviewers for their constructive and valuable comments.

## 4.7 References

Berning, C.K., Griffith, J.F., Wild, J.E., 1982. Research on the effectiveness of denatonium benzoate as a deterrent to liquid detergent ingestion by children. Fundamental and applied toxicology : official journal of the Society of Toxicology 2 (1), 44–48.

Björkner, B., 1980. Contact urticaria and asthma from denatonium benzoate (Bitrex®). Contact Dermatitis 6 (7), 466–471.

Corby, J.E., Doi, J., Conville, J.J., Murphy, S.R., McKenzie, D.A., 1993. Biodegradability of a Denatonium Bitterant. SAE Technical Paper 930587, 813–816.

Consumer Product Safety Commission United States of America, 1992. Final Report Study of Aversive Agents. Technical Report.

Cosmetic Ingredient Review Expert Panel, 2008. Final report of the safety assessment of Alcohol Denat., including SD Alcohol 3-A, SD Alcohol 30, SD Alcohol 39, SD Alcohol 39-B, SD Alcohol 39-C, SD Alcohol 40, SD Alcohol 40-B, and SD Alcohol 40-C, and the denaturants, Quassin, Brucine Sulfate/Brucine, and Denatonium Benzoate. International journal of toxicology 27 Suppl 1, 1–43.

Cowan-Ellsberry, C., Belanger, S., Dorn, P., Dyer, S., McAvoy, D., Sanderson, H., Versteeg, D., Ferrer, D., Stanton, K., 2014. Environmental Safety of the Use of Major Surfactant Classes in North America. Critical reviews in environmental science and technology 44 (17), 1893–1993.

Crosson, G., Crosson, K., Thorpe, S., MacPherson, L., Murdock, M., Smith, B., 2014. Activated carbon and clay minerals for the sorptive removal of denatonium ions from denatonium benzoate solutions. Journal of Water Resource and Protection 6 (8), 793–803.

ECHA, 2016. Registered dossier for denatonium benzoate (accessed June 12th, 2016). http://echa.europa.eu/registration-dossier/-/registered-dossier/16728.

European Commission, 2013. Commission Implementing Regulation (EU) No 162/2013 of 21 February 2013 amending the Annex to Regulation (EC) No 3199/93 on the mutual recognition of procedures for the complete denaturing of alcohol for the purposes of exemption from excise duty. OJ L 49, 55–61.

European Food Safety Authority, 2012. Conclusion on the peer review of the pesticide risk assessment of the active substance denatonium benzoate (approved as denathonium benzoate). EFSA Journal 10 (1), 2483–2517.

Federal Statistical Office (Statistisches Bundesamt), 2013. Öffentliche Wasserversorgung und öffentliche Abwasserentsorgung: Öffentliche Abwasserbehandlung und -entsorgung (accessed June 22nd, 2016). https://www.destatis.de/DE/Publikationen/Thematisch/UmweltstatistischeErhebungen/Wasserwirtschaft/AbwasserOeffentlich2190212139004.pdf?__blob=publicationFile.

Funke, J., Prasse, C., Lütke Eversloh, C., Ternes, T.A., 2015. Oxypurinol - A novel marker for wastewater contamination of the aquatic environment. Water research 74, 257–265.

Gao, P., Ding, Y., Li, H., Xagoraraki, I., 2012. Occurrence of pharmaceuticals in a municipal wastewater treatment plant: mass balance and removal processes. Chemosphere 88 (1), 17–24.

González-Mariño, I., Quintana, J.B., Rodríguez, I., Cela, R., 2011. Evaluation of the occurrence and biodegradation of parabens and halogenated by-products in wastewater by accurate-mass liquid chromatography-quadrupole-time-of-flight-mass spectrometry (LC-QTOF-MS). Water research 45 (20), 6770–6780.

Jonkers, N., Kohler, H.-P.E., Dammshäuser, A., Giger, W., 2009. Mass flows of endocrine disruptors in the Glatt River during varying weather conditions. Environmental pollution 157 (3), 714–723.

Kasprzyk-Hordern, B., Dinsdale, R.M., Guwy, A.J., 2009. The removal of pharmaceuticals, personal care products, endocrine disruptors and illicit drugs during wastewater treatment and its impact on the quality of receiving waters. Water research 43 (2), 363–380.

Kleinkauf, A., Macdonald, D.W., Tattersall, F.H., 1999. A bitter attempt to prevent non-target poisoning of small mammals. Mammal Review 29 (3), 201–204.

Klein-Schwartz, W., 1991. Denatonium benzoate: review of efficacy and safety. Veterinary and human toxicology 33 (6), 545–547.

Lange, C., Kuch, B., Metzger, J.W., 2015. Occurrence and fate of synthetic musk fragrances in a small German river. Journal of hazardous materials 282, 34–40.

Loos, R., Carvalho, R., António, D.C., Comero, S., Locoro, G., Tavazzi, S., Paracchini, B., Ghiani, M., Lettieri, T., Blaha, L., Jarosova, B., Voorspoels, S., Servaes, K., Haglund, P., Fick, J., Lindberg, R.H., Schwesig, D., Gawlik, B.M., 2013. EU-wide monitoring survey on emerging polar organic contaminants in wastewater treatment plant effluents. Water research 47 (17), 6475–6487.

Loos, R., Gawlik, B.M., Locoro, G., Rimaviciute, E., Contini, S., Bidoglio, G., 2009. EU-wide survey of polar organic persistent pollutants in European river waters. Environmental pollution 157 (2), 561–568.

Mullins, M.E., Zane Horowitz, B., 2004. Was it necessary to add Bitrex (denatonium benzoate) to automotive products? Veterinary and human toxicology 46 (3), 150–152.
Petrie, B., Barden, R., Kasprzyk-Hordern, B., 2015. A review on emerging contaminants in wastewaters and the environment: current knowledge, understudied areas and recommendations for future monitoring. Water research 72, 3–27.
Schiffman, S.S., Gatlin, L.A., Sattely-Miller, E.A., Graham, B.G., Heiman, S.A., Stagner, W.C., Erickson, R.P., 1994. The effect of sweeteners on bitter taste in young and elderly subjects. Brain Research Bulletin 35 (3), 189–204.
Schlüsener, M.P., Kunkel, U., Ternes, T.A., 2015. Quaternary Triphenylphosphonium Compounds: A New Class of Environmental Pollutants. Environmental science & technology 49 (24), 14282–14291.
Schwientek, M., Rügner, H., Beckingham, B., Kuch, B., Grathwohl, P., 2013. Integrated monitoring of particle associated transport of PAHs in contrasting catchments. Environmental pollution 172, 155–162.
Selle, B., Schwientek, M., Lischeid, G., 2013. Understanding processes governing water quality in catchments using principal component scores. Journal of Hydrology 486, 31–38.
Sibert, J.R., Frude, N., 1991. Bittering agents in the prevention of accidental poisoning: children's reactions to denatonium benzoate (Bitrex). Archives of emergency medicine 8 (1), 1–7.
Tran, N.H., Li, J., Hu, J., Ong, S.L., 2014. Occurrence and suitability of pharmaceuticals and personal care products as molecular markers for raw wastewater contamination in surface water and groundwater. Environmental science and pollution research international 21 (6), 4727–4740.
Velpandian, T., Nirmal, J., Arora, B., Ravi, A.K., Kotnala, A., 2012. Understanding the Charge Issues in Mono and di-Quaternary Ammonium Compounds for Their Determination by LC/ESI-MS/MS. Analytical Letters 45 (16), 2367–2376.
White, N.C., Litovitz, T., Benson, B.E., Horowitz, B.Z., Marr-Lyon, L., White, M.K., 2009. The impact of bittering agents on pediatric ingestions of antifreeze. Clinical pediatrics 48 (9), 913–921.

## 4.8 Supplementary information

### 4.8.1 Material and methods

***Sampling and sample preparation***

Surface water and WWTP effluent samples were collected during two sampling campaigns from an approximately 1300 km² large area in the federal state of Baden-Württemberg, Germany (Figure S4.1).

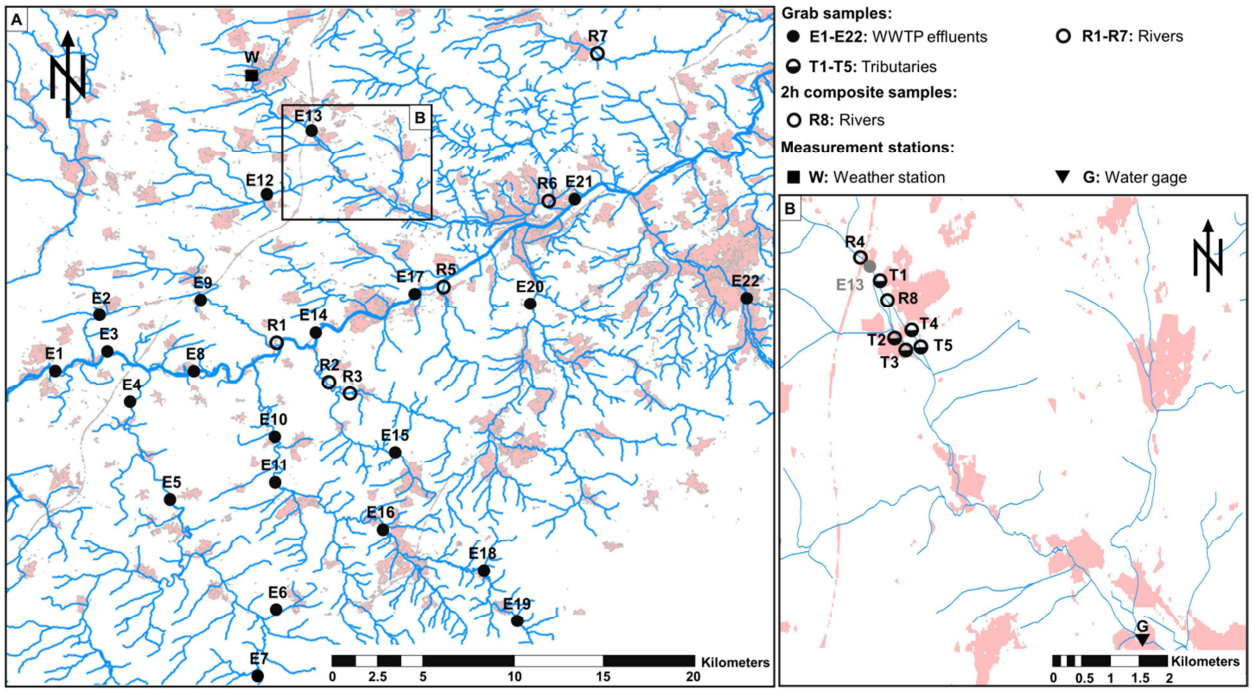


**Figure S4.1**: Location of surface water and WWTP sampling sites during the campaigns in April 2015 (A) and July – August 2014 (B) in the state of Baden-Württemberg, Germany.

The Ammer river, a tributary of the Neckar river, was sampled for seven consecutive days during the first campaign between July and August 2014. Background concentrations of trace pollutants, e.g. from combined sewer overflows (CSOs), were investigated by grab samples, which were taken three times per day approximately 100 m upstream of the WWTP (Figure S4.1B, R4). Composite samples were taken about 300 m downstream of the WWTP (Figure S4.1B, R8) and used to evaluate the impact of treated wastewater on the river water quality. For this purpose, 100 ml samples were taken each 15 min with a 3700 portable sampler (Teledyne Isco, USA) and combined for time periods of two hours.Additional grab samples were collected from tributaries of the Ammer river on the fifth day of the sampling campaign (Figure S4.1B, T1-T5), to investigate anthropogenic contaminants in small creeks (estimated flowrate ≤ 10 L $s^{-1}$) dominated by rain water and groundwater.

Due to the lack of a cooling system, composite samples were removed from the portable sampler three times per day, resulting in maximum exposure times to elevated temperatures of 6 h and 12 h during day and night sampling, respectively. All water samples were stored in amber glass bottles and transported on ice. Particle removal was performed immediately in the laboratory by centrifugation at 6000 g for 10 min and samples were stored afterwards in the dark at 4 °C for a maximum of 48 h until analysis. Precipitation data were obtained from the German Meteorological Service for the weather station in Herrenberg (Figure S4.1A, W). Water levels of the river Ammer (Figure S4.1B, G) were provided by the Baden-Württemberg State Institute for Environment, Metrology and Nature Conservation (LUBW). The widespread occurrence of Denatonium as water pollutant and the main sources of this compound in the environment were further investigated during a second sampling campaign in April 2015. Therefore, single grab samples were taken from a total of 22 WWTP effluents (Figure S4.1A, E1-E22), from three rivers influenced by treated wastewater (Figure S4.1A, R1, R2, R7), and from three rivers not influenced by WWTP effluents (Figure S4.1A, R3, R5, R6). The WWTPs represent a wide range of sizes (4000-124000 population equivalents) and treatment technologies (including powdered activated carbon PAC in addition to mechanical and biological treatment). Sample storage and transportation was similar to the first campaign from 2014, except for particle removal, which was performed with regenerated cellulose syringe filters (Captiva, pore size: 0.2 µm, Agilent Technologies, Germany).

Marc Schwientek and Hermann Rügner (WESS Competence Cluster, Tübingen, Germany) provided a WWTP effluent sample from the province Trentino in Italy. The sample was taken in May 2014, transported on ice to the laboratory and stored at 4 °C in the dark. Particles were removed with regenerated cellulose syringe filters (Captiva, pore size: 0.2 µm, Agilent Technologies, Germany) before sample analysis and the presented data were measured about one year after sampling. Despite this extended storage period, no significant changes in the denatonium concentration were expected, because previous studies suggested a high compound stability. Henderson *et al*. reported stable denatonium concentrations in consumer products stored for six months at room temperature (Henderson et al., 1998) and denatonium is considered as not biodegradable (Corby et al., 1993).

Thomas Glauner (Agilent Technologies, Germany) provided 14 d composite samples from two WWTP effluents in Switzerland. Samples were taken at two time periods in 2015, March 18$^{th}$ - 31$^{st}$ 2015 and June 16$^{th}$ - 23$^{rd}$, filtered immediately through a glass fiber filter and stored frozen at -20 °C.

Immediately before analysis, samples were thawed and particles were removed with regenerated cellulose syringe filters (Captiva, pore size: 0.2 µm, Agilent Technologies, Germany).

A total of 22 consumer products were bought from local supermarkets in Tübingen, Germany, in 2015. The majority of the investigated formulations were detergents, including 9 hard-surface cleaning products, 5 laundry detergents and 1 dishwashing liquid. Two shower gels for children, 2 bubble bath formulations, 1 nail polish remover and 1 skin cleansing product were classified as personal care products (PCPs). Additionally, 1 antifreeze windshield washer fluid was investigated. Denatonium benzoate was declared as ingredient in 20 out of the 22 products, except for the nail polish remover and skin cleansing formulation. Before measurement, all samples were diluted 1:1000 (w:w) with a isopropanol:water mixture (10%:90%, v:v), followed by an additional 1:100 (w:w) dilution with LC/MS grade water to give an overall dilution factor of $10^5$. No further sample treatment was applied and the dilutions were immediately analyzed after preparation.

***LC-ESI-QToF analysis***

High-resolution mass spectrometry based suspect screening was performed for the WWTP samples from Switzerland and Italy. Most conditions for the chromatographic separation of analytes were adopted from the targeted method for consumer products and a comparable HPLC system was used (chapter 4.3.3). However, no thermostat was available here and samples were kept therefore at room temperature (22 ± 2 °C). Furthermore, the injection volume was 100 µl and a modified gradient was applied: 0 min 95% A, 11 min 30% A, 11.1 min 0% A, 16 min 0% A, 16.1 min 95% A, 23 min 95% A.

Full scan mass analysis was performed with a 6550 quadrupole time of flight mass spectrometer (Agilent Technologies, Germany) operated in the extended dynamic mode (2 GHz) for small molecules (≤ 1700 m/z). MS spectra were recorded at a rate of 2 Hz between *m/z* 50-1000 and two reference compounds were continuously supplied to the ESI source for mass correction.

The observed mass deviation was usually ≤ 3 ppm and a resolution of 13000 (FWHM) was achieved at *m/z* 200. The ESI source was operated in the positive ionization mode and parameter settings were adopted from the targeted method (chapter 4.3.3), except for the capillary voltage which was set to 3500 V.

***Method validation and analytical quality control***

Matrix effects were investigated by three different techniques. A post column infusion setup, similar to the one described in Stahnke et al. (2009), was used for selected Ammer river water samples. Briefly, a mixed solution containing all analytes was introduced into the effluent stream before the mass spectrometer via a T-piece and a syringe pump, leading to constant analyte concentrations of 250 ng $L^{-1}$. The response of a single transition for each analyte was monitored over the complete chromatogram and signal intensities of blank (LC/MS grade water), as well as sample injections, were compared according to Stahnke et al. (2009) to estimate matrix effects. A smoothing factor of 0.6 was applied to the measured signals. Negative matrix effects stand generally for signal suppression and positive effects for signal enhancement. A WWTP effluent sample and a 1:100 diluted solid phase extract (200 fold enrichment) of a WWTP influent were available from different studies and investigated as complex matrices for which more pronounced matrix effects were expected. The injection volume for the blank and the individual samples was always 100 µl during post column infusion experiments. All WWTP effluent and surface water samples from the second sampling campaign in Baden-Württemberg in 2015 were analyzed twice, i.e. 1:20 diluted with tap water and non-diluted. Therefore, matrix effects could be estimated comparing the calculated concentrations of both measurements. In case of the diluted consumer products, matrix effects were evaluated for two products (1 shower gel and 1 hard-surface cleaner) by the standard addition approach. The experiment was performed in triplicates and the $1:10^5$ diluted samples were spiked with LC/MS grade water or four different denatonium concentrations. The maximum concentration considered for the standard addition approach was approximately twice the non-spiked sample.

### 4.8.2 Results and discussion

***Method validation for targeted analysis***

The median matrix effects observed for the six analytes in Ammer river water samples taken up- and downstream of the WWTP were usually less than ±20% (Figure S4.2), revealing no significant influence of the matrix on the quantification by external calibration.

In case of the more complex samples, pronounced ion suppression (up to 40%) was only observed for the diluted solid phase extracts of a WWTP influent sample, while the results for the WWTP effluent sample were similar to the river water samples.

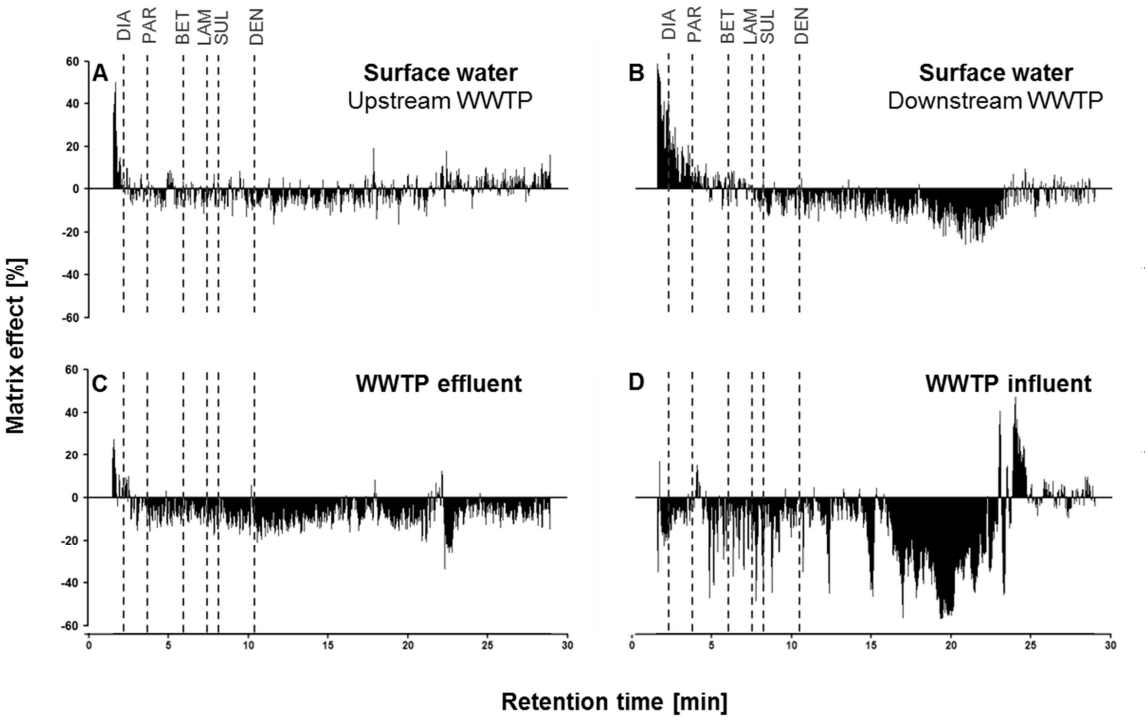


**Figure S4.2**: Median matrix effects observed for the six analytes in Ammer river water samples taken either upstream (A) or downstream (B) of the WWTP. Samples with higher contaminant loads, i.e. a WWTP effluent (C) and a diluted solid phase extract of a WWTP influent (D), were additionally investigated. The dashed lines are representing the retention times of diatrizoic acid (DIA), paracetamol (PAR), benzotriazole (BET), lamotrigine (LAM), sulfamethoxazole (SUL) and denatonium (DEN).

The observations from the post column infusion experiments were also supported by the dilution approach for the second set of samples, which was taken in Baden-Württemberg in 2015. Generally, the maximum observed difference between the concentration calculated for non-diluted and 1:20 diluted river water and WWTP effluent samples was less than 10% (data not shown).

In case of the diluted consumer products, matrix effects were exemplarily evaluated for one shower gel and one hard-surface cleaner with the standard addition approach. The concentrations retrieved from the linear regression of the spiked samples (Figure S4.3) were 66.1 ng $L^{-1}$ and 67.3 ng $L^{-1}$ for the shower gel and hard-surface cleaner, while the concentrations estimated with an external calibration were 65.8 ng $L^{-1}$ and 63.8 ng $L^{-1}$, respectively. The maximum observed signal enhancement of 5% for the hard-surface cleaner indicated no significant matrix effects.

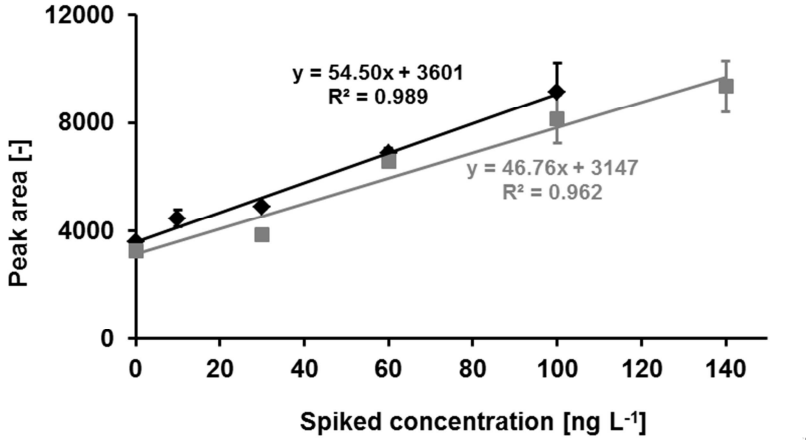


**Figure S4.3**: Linear regressions of the standard addition experiments for two diluted consumer products. The results in grey are for a hard-surface cleaner and the ones in black are for a shower gel.

**Table S4.1**: LC-ESI-QqQ method parameters for the environmental samples. Intra- and interday variation of the response of quality control (QC) samples are given as the relative standard deviation (RSD). Low, medium and high concentrations levels are equivalent to 16, 80 and 800 ng $L^{-1}$ of the respective analyte.

| Compound | LLOQ [ng $L^{-1}$] | $R^2$ (n = 7) | Regression type | Weight | Concentration level | Intraday variation of quantifier response [% RSD] (n = 3) | Interday variation of quantifier response [% RSD] (n = 7) |
|---|---|---|---|---|---|---|---|
| Benzotriazole | 7.5 | 0.997 ± 0.001 | Linear | 1/x | Low<br>Medium<br>High | 1<br>2<br>1 | 7<br>6<br>9 |
| Denatonium | 1 | 0.998 ± 0.001 | Linear | 1/x | Low<br>Medium<br>High | 5<br>2<br>3 | 6<br>6<br>7 |
| Diatrizoic acid | 25 | 0.996 ± 0.002 | Linear | 1/x | Medium<br>High | 2<br>2 | 8<br>7 |
| Lamotrigine | 2.5 | 0.997 ± 0.001 | Linear | 1/x | Low<br>Medium<br>High | 1<br>3<br>1 | 17<br>12<br>15 |
| Paracetamol | 2.5 | 0.997 ± 0.001 | Linear | 1/x | Low<br>Medium<br>High | 3<br>6<br>< 1 | 14<br>13<br>11 |
| Sulfamethoxazole | 2.5 | 0.998 ± 0.001 | Linear | 1/x | Low<br>Medium<br>High | 1<br>2<br>< 1 | 12<br>9<br>12 |

**Table S4.2**: LC-ESI-QqQ method parameters for the diluted consumer products. Intra- and interday variation of the response of quality control (QC) samples are given as the relative standard deviation (RSD). Low, medium and high concentrations levels are equivalent to 16, 80 and 800 ng $L^{-1}$ of denatonium.

| Compound | LLOQ [mg $kg^{-1}$] | $R^2$ | Regression type | Weight | Concentration level | Intraday variation of quantifier response [% RSD] (n = 4) | Interday variation of quantifier response [% RSD] |
|---|---|---|---|---|---|---|---|
| Denatonium | 0.1 | 0.997 | Linear | 1/x | Low | 7.0 | n.a. |
| | | | | | Medium | 3.2 | n.a. |
| | | | | | High | 2.9 | n.a. |

## *Sources and distribution of denatonium in a German river*

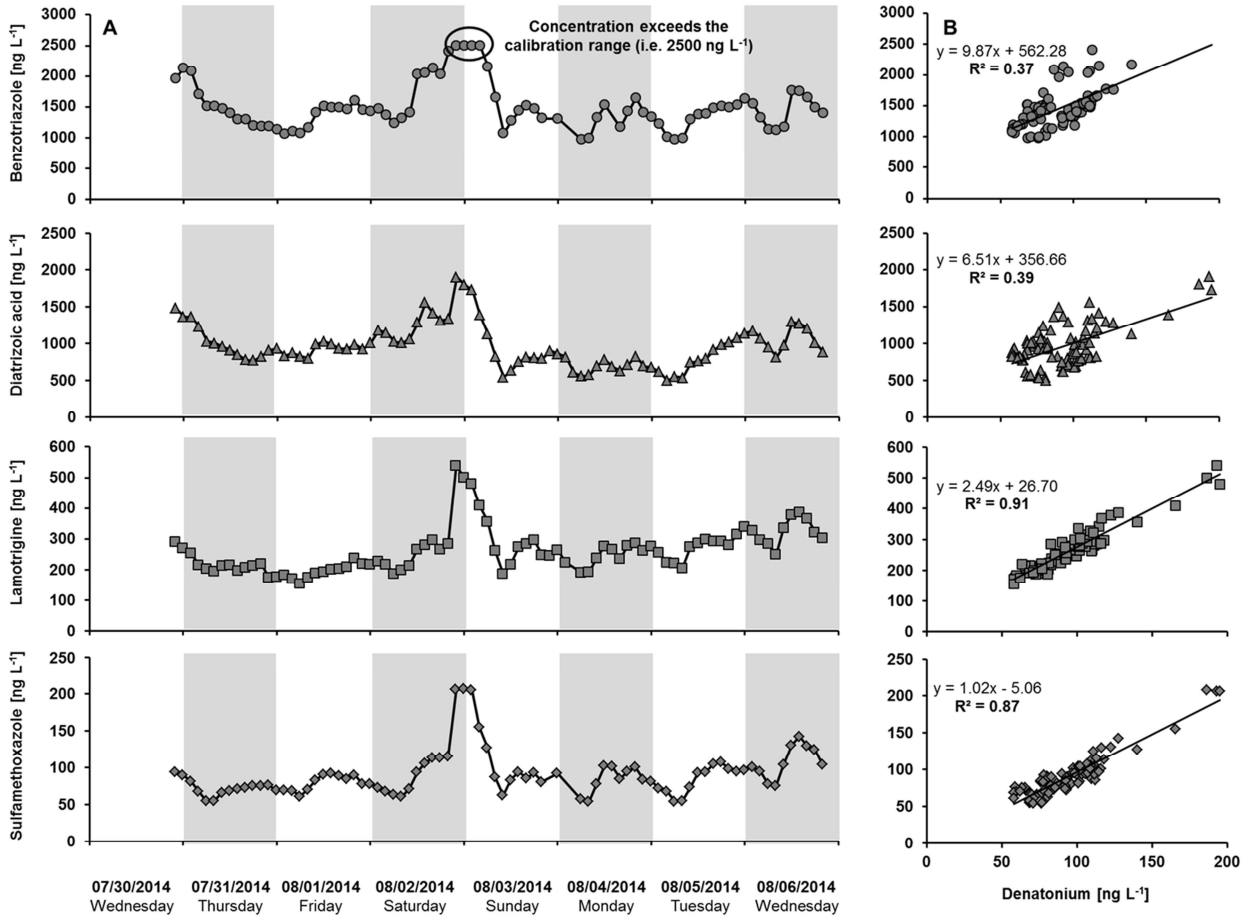


**Figure S4.4**: Absolute concentrations of benzotriazole, diatrizoic acid, lamotrigine, and sulfamethoxazole measured in the Ammer river downstream of the WWTP (A). A linear correlation between the concentrations measured for these compounds and for denatonium is shown in (B).

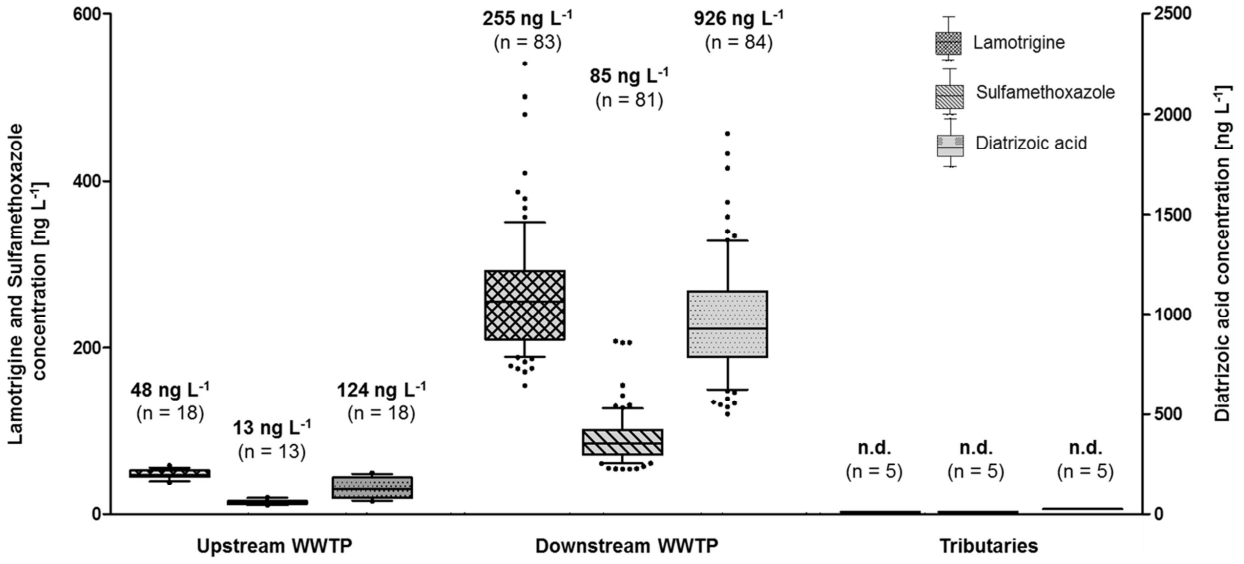


**Figure S4.5**: Lamotrigine (left), sulfamethoxazole (center) and diatrizoic acid (right) concentrations measured in the Ammer river up- and downstream of a WWTP and in five small creeks discharging into this river. Median analyte concentrations are indicated above the boxplots (n.d. not detected).

## *Screening of WWTP effluents in Baden-Württemberg, Germany*

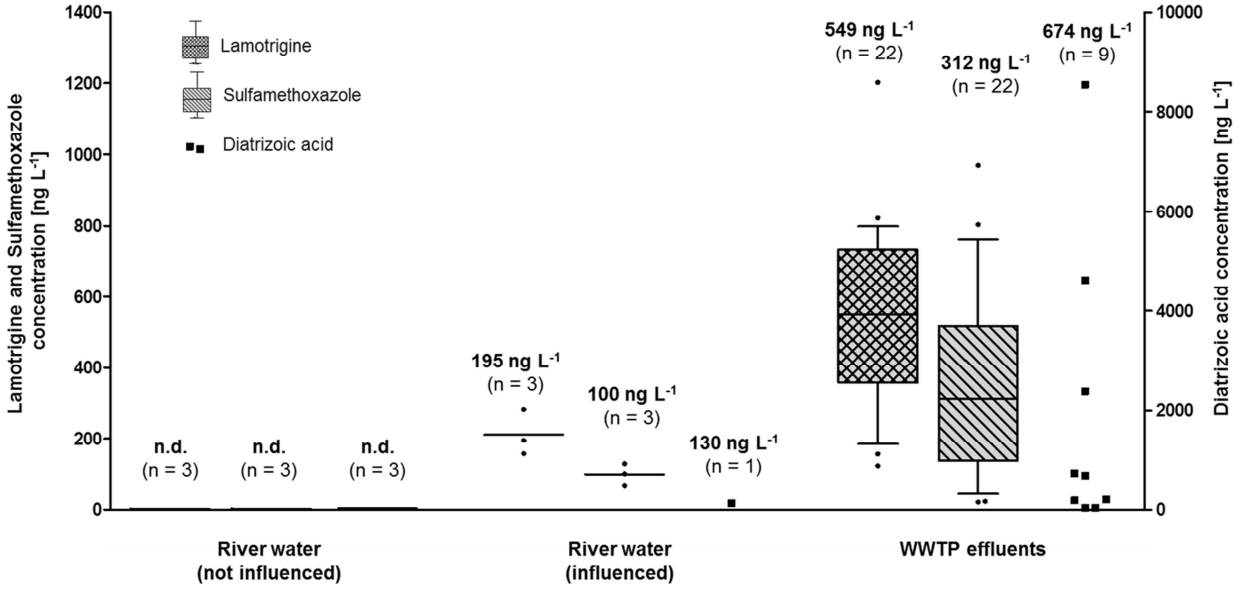


**Figure S4.6**: Lamotrigine (left), sulfamethoxazole (center), and diatrizoic acid (filled squares, right) concentrations in surface waters or WWTP effluents sampled in Baden-Württemberg, Germany, in 2015. Rivers were either influenced or not influenced by treated wastewater and median analyte concentrations are given above the datapoints or boxplots (n.d. not detected).

## *Occurrence of denatonium in two other European countries*

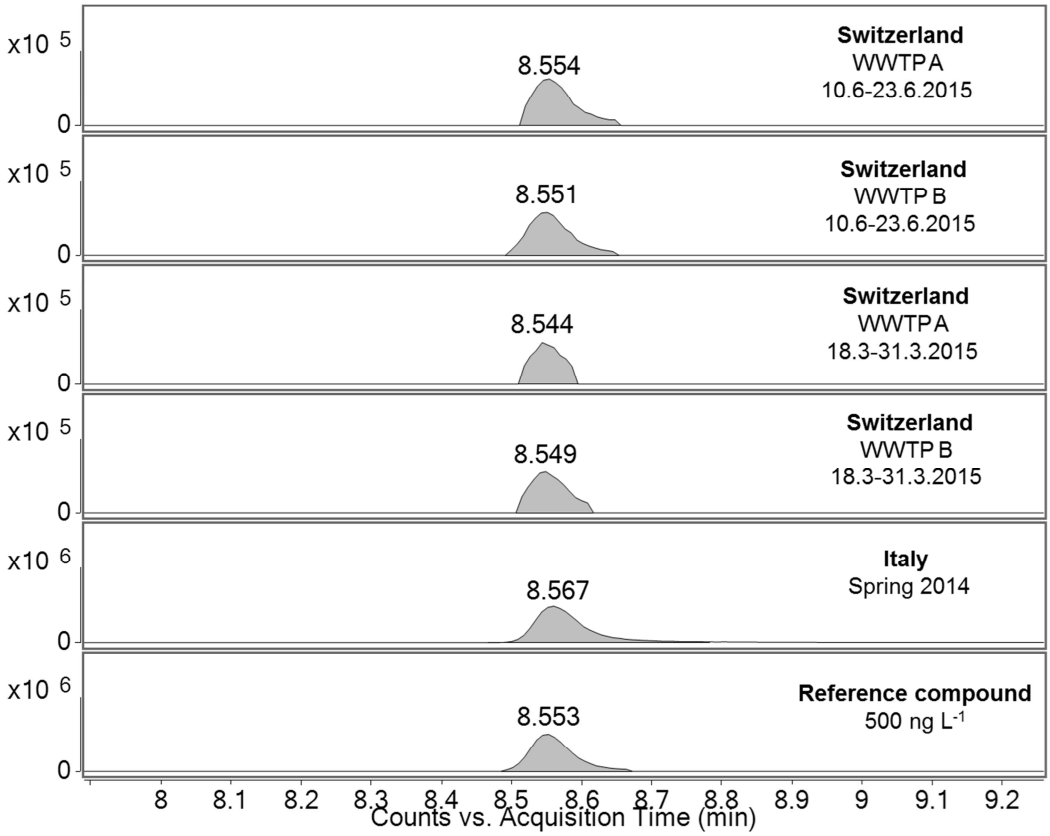


**Figure S4.7**: Extracted ion chromatograms for the denatonium ion (*m/z* 325.2274) in the WWTP effluent samples from Switzerland and Italy, as well as a reference solution containing 500 ng $L^{-1}$ denatonium. The extraction window was set to ± 10 ppm.

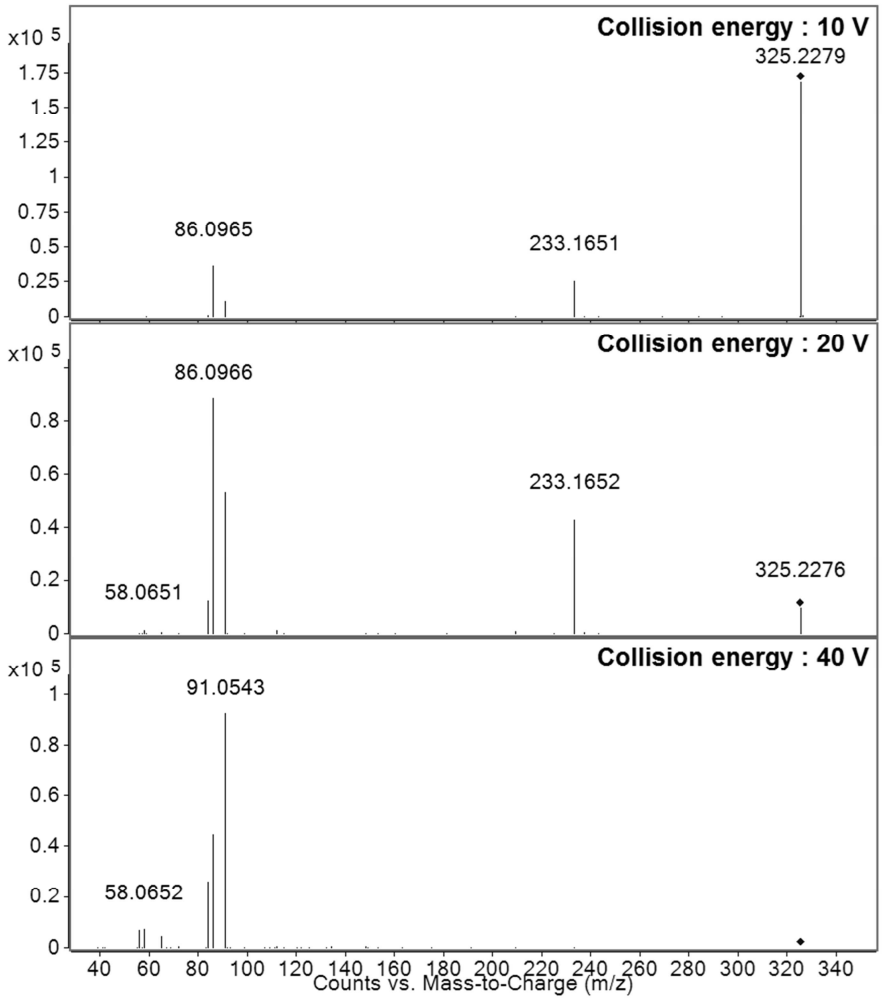


**Figure S4.8**: High-resolution MS/MS spectra for the $[M]^+$ ion (*m/z* 325.2275) of denatonium at three different collision energies (CE´s). The spectral information were also uploaded to the public repository MassBank (http://massbank.eu/MassBank) and can be found under the following accession numbers: TUE00281 (CE: 10 V), TUE00282 (CE: 20 V) and TUE00283 (CE: 40 V).

### 4.8.3 References

Corby, J.E., Doi, J., Conville, J.J., Murphy, S.R., McKenzie, D.A., 1993. Biodegradability of a Denatonium Bitterant. SAE Technical Paper 930587, 813–816.

Henderson, M.C., Neumann, C.M., Buhler, D.R., 1998. Analysis of denatonium benzoate in oregon consumer products by HPLC. Chemosphere 36 (1), 203–210.

Stahnke, H., Reemtsma, T., Alder, L., 2009. Compensation of matrix effects by postcolumn infusion of a monitor substance in multiresidue analysis with LC-MS/MS. Analytical Chemistry 81 (6), 2185–2192.

# 5 Identification of transformation products of denatonium – Occurrence in wastewater treatment plants and surface waters

**Authors**

Sascha Lege[a], Anna Eisenhofer[b], Jorge Eduardo Yanez Heras[a], Christian Zwiener[a]

[a] University of Tübingen, Environmental Analytical Chemistry, Hölderlinstraße 12, 72074 Tübingen, Germany

[b] Institute of Organic Chemistry, Faculty of Chemistry and Pharmacy, University of Regensburg, 93040 Regensburg, Germany

**Highlights**

- Indirect photodegradation and electrochemical oxidation resulted in overall ten TPs.
- Five products were identified with a confidence level of 2 or better.
- High persistence of denatonium in conventional wastewater treatment and in surface waters observed.
- Denatonium removal by ozonation is associated with the formation of polar TPs.

Published 2019 in the Elsevier journal *Science of The Total Environment*, vol. 686, pp. 140-150, DOI: 10.1016/j.scitotenv.2019.05.423. 

## 5.1 Abstract

Denatonium, one of the bitterest substances known to man, was recently identified as wastewater borne micropollutant in surface waters. Therefore, photodegradation experiments and electrochemical degradation were performed to identify abiotic and putative biotic transformation products (TPs). Indirect rather than direct photodegradation proved to be important for denatonium removal by solar irradiation and produced seven TPs. Amide hydrolysis, hydroxylation, N-dealkylation, and N-dearylation were revealed as the main mechanisms. Anodic oxidation of denatonium was related to the formation of overall ten products and despite considerable different yields, all TPs from indirect photodegradation were mimicked electrochemically. Among them, lidocaine was the only TP detected after conventional wastewater treatment and in surface waters. The occurrence of lidocaine was however associated with its application as local anesthetic rather than to a degradation of denatonium. The absence of additional products suggests that denatonium degradation is negligible under environmental conditions, supporting the previously described persistent nature of this compound. Advanced water treatment techniques however have the potential to degrade denatonium. About 74% of the initial denatonium load was removed from wastewater during pilot-scale ozonation. The degradation of denatonium was accompanied here with the formation of at least two polar products, which are passing unchanged through a sand filter after ozonation. Both substances have completely unknown (toxicological) properties and this study seems to be the first report about their structures in general, as none of them was found in any of the large compound libraries (e.g. PubChem).

## 5.2 Introduction

Denatonium benzoate (trade name Bitrex®), one of the bitterest compound known to man, is intentionally applied to a wide range of products (e.g. antifreeze, finger paints, and detergents) to prevent an intended or accidental consumption. Additionally, it ends up in numerous cosmetics and other personal care products due to the utilization of denatured alcohol (Cosmetic Ingredient Review Expert Panel, 2008). For example, the European Union requires a minimum concentration of 10 mg $L^{-1}$ denatonium benzoate as denaturing agent (European Commission, 2013). Although detailed information about the annual global production of this compound is missing, its recently updated registration dossier reveals that approximately 100-1000 tons are manufactured and/or imported each year in the European Economic Area (ECHA, 2019).

In agreement with its use pattern, denatonium was recently identified as a wastewater borne micropollutant in the environment (Lege et al., 2017), reaching concentrations up to 400 ng $L^{-1}$ in surface waters (Guillet et al., 2019). Acute toxic effects for aquatic species can be neglected at such low concentrations, because median lethal concentrations for selected invertebrates and rainbow trout are in the range of 400 to 1000 mg $L^{-1}$, respectively (European Food Safety Authority, 2012). Single compound toxicities however do not reflect the complexity of aquatic environments, where synergistic effects of chemical mixtures should not be neglected for a comprehensive risk assessment (Brian et al., 2005). Additionally, sub-lethal behavioral changes induced by environmentally relevant micropollutant concentrations have been demonstrated before (Painter et al., 2009). They might have an impact on the fitness and survival of aquatic species. Therefore, it is imperative to understand the fate of anthropogenic contaminants during wastewater treatment and to assess their fate in the environment.

In case of denatonium, information about the compounds stability are rather scarce, but the few sources available point generally towards a high persistence. Neither hydrolysis was observed in the pH range from 4 to 9, nor seems denatonium to be readily biodegradable (Consumer Product Safety Commission United States of America, 1992, Corby et al., 1993, ECHA, 2019). Although photodegradation in water can occur in more acidic environments ($DT_{50} \approx 15$ days at pH 5) , estimated half-lifes ranged from approximately 43 days to more than 235 days at pH 7 and pH 9, respectively (Health Canada, 2011). Unfortunately, details on the experimental procedures were usually not available from manufacturer data of the registration of denatonium. For example, it is not clear if only direct photolysis was investigated or if an indirect photodegradation mechanism was covered as well. In addition, the adaption and the composition of the microbial community (Horemans et al., 2014), as well as the predominant redox conditions (Falås et al., 2016), can have a significant effect on the biodegradation of a compound.

We decided therefore to use electrochemistry, a technique proven useful to mimic enzymatic transformation mechanisms (Johansson et al., 2007), as a culture-independent method to elucidate putative biodegradation products of denatonium.

Furthermore, direct and indirect phototransformation was studied under environmentally relevant conditions, exposing this compound to natural sunlight. Identified transformation products (TPs) were finally used as indicator compounds to assess the fate of denatonium primarily in conventional wastewater treatment plants (WWTPs) and surface waters.

Advanced oxidation techniques, like ozonation, are increasingly implemented as additional treatment step in WWTPs to reduce the micropollutant release into the environment (Eggen et al., 2014). The removal of those contaminants is however often related to the formation of unknown transformation products (Schollée et al., 2018). Electrochemistry has the potential to mimic processes leading to ozonation by-products (Faber et al., 2014) and we performed therefore retrospective data evaluation for the presence of denatonium and the here identified TPs in samples from pilot-scale wastewater ozonation as well.

## 5.3 Material and methods

### 5.3.1 Chemicals

Optima™ LC/MS grade acetonitrile (ACN), ammonium formate ($NH_4FA$), formic acid (FA), methanol (MeOH), and water were purchased from Fisher Chemical (Belgium). 4-methylbenzotriazole (≥ 98%), ammonium hydroxide (LC-MS grade), benzotriazole (≥ 98%), denatonium benzoate (≥ 98%), diclofenac (≥ 98%), monoethylglycinexylidide (syn. norlidocaine, ≥ 98%), paracetamol (≥ 99%), and trifluoroacetic acid (TFA, ≥ 99%) were obtained from Sigma-Aldrich (Germany), while 2,6-dimethylaniline (≥ 99%), 5-methylbenzotriazole (≥ 99%), lidocaine (≥ 99%), and N,N-diethylbenzylamine (≥ 98%) were purchased from TCI (Belgium). The transformation product N-benzyl-N-carboxymethyl-N,N-diethylammonium (TP 222) was synthesized based on previous work by Ziegler and Wittmann, 1985 and details about the two-step reaction from diethylbenzylamine are described in the supporting information (chapter 5.8.1). Individual stock solutions with analyte concentrations of 1 g $L^{-1}$ were usually prepared with ACN, except for norlidocaine and N-benzyl-N-carboxymethyl-N,N-diethylammonium which were dissolved in MeOH. A working solution containing all analytes was prepared in ACN with final concentrations of 10 mg $L^{-1}$ and subsequently diluted to 1 µg $L^{-1}$ using tap water. Stock and working solutions were stored in the freezer at -18 °C, while the dilutions in tap water were kept in the fridge at 8°C. Solutions stored in the freezer were renewed once per year, while dilutions in tap water were prepared freshly after a maximum storage duration of one week.

### 5.3.2 WWTP and surface water samples

Effluent grab samples of 22 different wastewater treatment plants from the federal state of Baden-Württemberg (Germany), one sample from a plant in Italy, as well as 14-day composite effluent samples from two Swiss WWTPs, were retrospectively evaluated for the presence of denatonium transformation products. Details about these samples and their treatment are given in Lege et al., 2017.

The fate of denatonium during conventional wastewater treatment was further investigated in 2016, taking 24-hour flow proportional composite samples from the influent and effluent of one of the previously monitored plants in Baden-Württemberg over a duration of five days. The plant treats about 28 000 $m^3$ wastewater $day^{-1}$ during dry weather conditions (about 100 000 population equivalents) and discharges finally into the river Neckar. Advanced wastewater treatment by ozonation and its impact on micropollutant removal in wastewater was studied in pilot-scale at the WWTP of a major city in Germany. Treatment plant characteristics, the ozonation process, and the samples are described in Merel et al., 2017. Briefly, an ozone dose of about 6 mg $L^{-1}$ ($O_3$/DOC ratio ≈ 0.5) was applied with a mean residence time of about 15 min in the ozone reactor. Time-proportional composite samples were taken after biological secondary treatment, after ozonation, as well as after flocculation and filtration through an anthracite/sand layer.

One of the additional goals of this study was to investigate the fate of denatonium once it is released into the environment. During a field study in summer 2014, grab samples were taken from the river Ammer upstream of a WWTP to assess background concentrations of micropollutants. In addition, 2-hour composite sampling was performed about 300 m and 3500 m downstream of the point where treated wastewater is discharged into this river (Lege et al., 2017). Analytes in selected samples were enriched 50 fold by solid phase extraction (SPE) on Oasis HLB cartridges and analyzed by LC-HRMS. Grab samples taken along the river Rhine, either enriched by SPE (details in Merel et al., 2018) or analyzed by large volume injection after centrifugation, were evaluated additionally for the presence of denatonium and its transformation products.

Sample treatment is described in the supporting information (chapter 5.8.2) and in the literature (Lege et al., 2017, Merel et al., 2017, Merel et al., 2018). LC-MS operating parameters are described in chapter 5.3.5 and in the supporting information (chapter 5.8.2).

The surface water matrix for the photodegradation experiment described in chapter 5.3.4 was sampled from the river Ammer (N48° 31' 26.5" E9° 03' 29.6"), about 15 km downstream of a discharging WWTP. Particles were removed by a Captiva syringe filter with a polyethersulfone membrane (15 mm diameter, 0.45 µm pore size, Agilent Technologies, Germany).

### 5.3.3 Electrochemical oxidation of denatonium benzoate

Electrochemical degradation of denatonium benzoate was performed in a 12 ml PEEK cell using either a boron-doped diamond (BDD) DIACHEM® electrode (here 10 µm diamond layer on Niobium substrate) from CONDIAS (Germany) or a SIGRADUR® glassy carbon (GC) electrode from HTW (Germany) as working electrode. The experiments were performed at room temperature (i.e. at about 22°C) and the active working area of the electrodes was about 3.2 $cm^{-2}$. The counter electrode was a platinum mesh (8 mm x 4 mm; Sigma-Aldrich, USA) and the reference a Ag/AgCl electrode (3M, BASi, USA).

Degradation experiments were performed with 20 mM $NH_4FA$ solutions containing 10 mg $L^{-1}$ denatonium adjusted to pH 4 and pH 7 with formic acid and ammonium hydroxide. The working electrode and the counter electrode were immersed in two different compartments of the PEEK cell, which were separated by a Vycor® porous glass frit. Adequate mixing of the solution in the oxidizing compartment with the working electrode was achieved by gentle magnetic stirring (300 rpm). The experiments were performed in triplicates for the different pH values and working electrodes, respectively.

Samples were taken from the oxidizing compartment of the cell before and after the application of a constant electrochemical potential +1.5 V vs. Ag/AgCl with an Autolab PGSTAT101 potentiostat (Metrohm, Germany) for 10 min. The samples were directly transferred to HPLC brown glass vials, which were sealed with Teflon lined caps, and stored at 8 °C. Analysis was performed with LC-HRMS on samples diluted 1:10 with tap water within a time frame of 48 h after the electrochemical degradation experiments.

GC working electrodes were cleaned after each experiment by the following procedure: 4 min polishing with a suspension of aluminum oxide (0.5 µm particles), followed by flushing with water; this procedure was repeated with 0.3 µm and 0.03 µm aluminum oxide and finally the electrode was sonicated for 10 min in LC-MS grade water.

In contrast, BDD electrodes were not polished manually but cleaned electrochemically in pH-adjusted ammonium formate buffer with square-wave pulses at voltages between -2 V and +2 V vs. Ag/AgCl alternately applied 150 times for 1 s each. Possible organic deposits on the counter electrode were removed daily by heating the platinum mesh with a Bunsen burner until it is red-hot.

### 5.3.4 Photodegradation of denatonium benzoate

Solutions for the photodegradation experiment were prepared by adding denatonium benzoate to a final concentration of 100 µg $L^{-1}$ denatonium either to LC/MS grade water (pH 8.4 at 20 °C, DOC = 0.5 mg $L^{-1}$, conductivity = 11 µS $cm^{-1}$, nitrate = not detected) or to river water (pH 8.2 at 20 °C, DOC = 2.2 mg $L^{-1}$, conductivity = 1180 µS $cm^{-1}$, nitrate = 30.1 mg $L^{-1}$). The pH of the LC/MS grade water was adjusted with $NH_4OH$ to match the value of the river water matrix. 50 ml of the denatonium solutions were either filled in 60 ml clear glass vials (light transmission typically about 50% at 300 nm and > 90% at wavelengths > 340 nm, details in Figure S5.6) or 60 ml amber glass vials (light transmission typically ≤ 5% at wavelengths ≤ 340 nm, more details in Figure S5.6), where the latter were additionally covered with aluminum foil to serve as dark controls. All vials were closed with PTFE covered screw caps and triplicate samples were generally prepared for each condition.

Outdoor experiments with natural sunlight exposure were performed at the field site of the Water & Earth System Science (WESS) institute (N48° 32' 23.91" E8° 57' 48.8") from June 15$^{th}$ to June 22$^{nd}$, 2015. The vials were installed here in a self-made sample holder facing south and the vials were inclined about 45° relative to the ground surface. Detailed meteorological information were available for the complete course of the experiment, as a NR01 net radiometer with a Pt100 temperature sensor (Hukseflux Thermal Sensors, Netherlands) and a rain gauge was installed at this site. 100 µl samples were withdrawn from the vials at the beginning of the experiment (t0), as well as after 68 h (t1) and 165 h (t2) of exposure, respectively. The samples were immediately diluted 1:10 with LC/MS grade water, transported on ice to the laboratory and stored there at 8 °C until analysis with LC-HRMS.

### 5.3.5 LC-ESI-Q-TOF analysis

Chromatographic separation of analytes was performed using a 1260 Infinity HPLC system (Agilent Technologies, Germany), consisting of a degasser (G4225A), a binary pump (G1312B), an autosampler (G1329B), and a column oven (G1316A).

Samples were kept in the autosampler at room temperature (23 ± 2 °C) and the injection volumes were typically in the range of 5 to 10 µl. However, up to 100 µl of the sample were injected in some cases to increase signal intensities of MS/MS measurements. Analytes were separated on a Poroshell EC-C18 column (2.1 x 100 mm, 2.7 µm, Agilent Technologies, Germany) coupled to a Poroshell EC-C18 guard column (2.1 x 5 mm, 2.7 µm, Agilent Technologies, Germany). The flowrate was always kept constant at 0.4 ml $min^{-1}$ and the column was held at 40 °C.

The mobile phases were usually water + 0.1% FA (A) and ACN + 0.1% FA (B), except for measurements to characterize quaternary ammonium compounds due to their ability to form TFA clusters (as demonstrated by Fisher et al., 1994). Water + 0.05% TFA (A) and ACN + 0.05% TFA (B) were used here as eluents. The following gradient program was used for separation of analytes in case of photodegradation or electrochemical oxidation: at 0 min 95% A, at 11 min 30% A, at 11.1 min 0% A, at 16 min 0% A, at 16.1 min 95% A, and at 23 min 95% A. The LC flow was diverted to the waste from 8.3 – 12 min for samples from electrochemical degradation experiments to prevent high denatonium concentrations from entering the mass spectrometer.

The HPLC system was connected to a 6550 iFunnel quadrupole time-of-flight (Q-TOF) mass spectrometer (Agilent Technologies, USA), equipped with an electrospray ionization (ESI) source and the Dual Spray Agilent Jet Stream technology. The Q-TOF was operated in the extended dynamic mode (2 GHz) for small molecules (≤ 1700 m/z). MS scans were performed at 2 Hz, while the acquisition rate was increased to 6 Hz in case of *All Ion* measurements or targeted MS/MS measurements for further structural characterization of the analytes. Data were always recorded for a mass range of *m/z* 50 – 1000. If not mentioned otherwise, ionization was performed in the positive mode and the ESI source was operated under the following conditions: drying gas temperature 150 °C, drying gas flow 16 L $min^{-1}$, sheath gas temperature 400 °C, sheath gas flow 12 L $min^{-1}$, and a nebulizer pressure of 35 psi. The capillary and nozzle voltages were kept at 3000 V and 300 V for both ionization modes, respectively. A reference solution, containing purine and hexakis(1H,1H,3H-tetrafluoropropoxy)phosphazine (HP-0921), was continuously supplied to the ESI source with the second sprayer and used for automatic mass correction. The observed mass error was typically ≤ 5 ppm and a resolution of 20000 (FWHM) was achieved for analytes at about *m/z* 1000.

Nitrogen, produced on-site with a nitrogen generator from Peak Scientific (Germany), was used as drying, sheath and nebulizing gas, while the collision cell was supplied with ultra-pure nitrogen (≥ 99.999%) from Westfalen AG (Germany).

### 5.3.6 Data processing

#### 5.3.6.1 Feature extraction

Centroid MS scan data obtained by LC-HRMS analysis were evaluated for the photodegradation and electrochemical transformation experiments separately in a typical non-targeted workflow. The batch recursive extraction algorithm for small molecules in the MassHunter Profinder software (Version B.06.00, Agilent Technologies, USA) was used for feature finding. Initially, this algorithm deconvolutes the chromatograms of the individual samples. A peak height filter of ≥ 1000 counts was applied. Neither retention time (RT) nor *m/z* filters were considered at this point. Individual peaks representing protonated species or sodium adducts of the same analyte, as well as their isotopologues, are grouped together as feature. The "common organic molecules" isotope model was used with a peak spacing tolerance of *m/z* 0.0025 + 7 ppm and a maximum charge state of 2 was allowed. Features with less than two ions were removed from further processing. Feature alignment with a retention time window of 0.15 min and a mass window of 10 ppm + 2 mDa was subsequently performed over all samples. Composite spectra were created for those features that exhibited an absolute height of ≥ 5000 counts and a MFE score of ≥ 70 in two out of three replicates. The so far performed data evaluation is the first step of the chosen algorithm, the so called recursive molecular feature extraction (rMFE). The next step, the find by ion process, is based on the composite data of all remaining features. The raw data of all samples are processed again by extracting ion chromatograms (*m/z* ± 20 ppm and RT ± 1.5 min) for the features on the consensus list, followed by an integration step to calculate peak areas. Only features that fulfilled abundance (height ≥ 5000 counts) and score (target score ≥ 80) requirements in all three replicates were finally exported in the compound exchange format (.cef files). Missing values were stated as zero abundance, median retention times and neutral masses were reported for all features. Generally, this two-step data processing with the recursive feature extraction improved the data quality by reducing the number of false negatives and the coefficient of variation for low abundant analytes, which might be missed by molecular feature extraction algorithm in single replicates.

#### 5.3.6.2 Statistical analysis and feature filtration

Peak filtering to extract putative transformation products was accomplished with the chemometric software package Mass Profiler Professional (MPP, version 14.9.1, Agilent Technologies, USA). Features were imported from .cef files and narrow windows (retention time window: 0.01 min and mass window: 0.01 mDa) were used for compound alignment over all samples, because median retention times and masses were previously exported from the Profinder software. Compounds with a coefficient of variation ≤ 25 % for their intensities over all replicates in one condition were subsequently filtered based on a volcano plot. Here, a moderated *t*-test, including the Benjamini Hochberg procedure to decrease the false positive rate for multiple testing, and a fold change (FC) analysis are combined comparing experimental samples with their respective blanks. The p-value cut-off ($p < 0.02$ for electrochemical degradation and $p < 0.05$ for photodegradation) was chosen so that the number of features expected by chance, a value calculated by MPP, is close to zero. Peaks were only considered as putative transformation products if signal intensities were at least three times higher than in the control samples. As the initial denatonium concentration for the photodegradation experiment was about 100 times lower, reduced product concentrations were generally expected compared to anodic oxidation. Therefore, an additional data filtration step based on the analyte abundance was only applied for samples obtained after electrochemical degradation. The threshold was set to a peak area of one million, which was equivalent to a product yield of about 0.01%, assuming a similar ionization efficiency of the products compared to denatonium.

#### 5.3.6.3 Identification of transformation products

Molecular formulas were initially assigned to putative TPs based on accurate masses and the observed isotope pattern using the MassHunter Qualitative Analysis software (version B.07.00, Agilent Technologies, USA). Subsequently, metabolites predicted *in-silico* with the BioTransformer tool (Djoumbou-Feunang et al., 2019) were assessed complementary to reported transformation mechanisms, e.g. for electrochemical degradation (Johansson et al., 2007, Jurva et al., 2003), to propose the most probable analyte structure matching the given elemental composition. In case the resulting molecule still contained the quaternary ammonium moiety, characteristic adduct formation, e.g. with sodium ions or TFA, was investigated additionally.

Mass spectral information obtained from collision-induced dissociation measurements were finally interpreted based on fragmentation rules reported in literature and in comparison to denatonium as parent compound.

The level of confidence for the compound identification was expressed in levels 1 to 5 according to Schymanski et al., 2014, where level 1 corresponds to structures confirmed with reference standards and level 2 to probable structures with either a library match (level 2a) or diagnostic evidence (level 2b). Tentative candidates are communicated as level 3, and the lowest confidence is assigned to unequivocal molecular formulas (level 4) or accurate mass detected (level 5).

## 5.4 Results and discussion

### 5.4.1 Direct and indirect photodegradation of denatonium

Denatonium benzoate solutions were exposed to natural sunlight during a field experiment over a duration of seven days. The observed shortwave radiation (285 – 3000 nm) varied during that time between 0 and 1284 W $m^{-2}$, with a daily average of 68 to 328 W $m^{-2}$. The average air temperature varied between 12.9 – 19.0 °C, with a minimum and maximum temperature of 9.3 °C and 23.3 °C, respectively. All recorded meteorological data are shown in Figure S5.7 along with indicators for the sampling time points. Generally, no significant change in the denatonium concentration was observed for the dark controls of both water matrices (Figure 5.1A and Figure S5.8). Hydrolysis of this compound, biodegradation, as well as sorption to the glass surface can therefore be ruled out as influencing factors for the given experimental conditions.

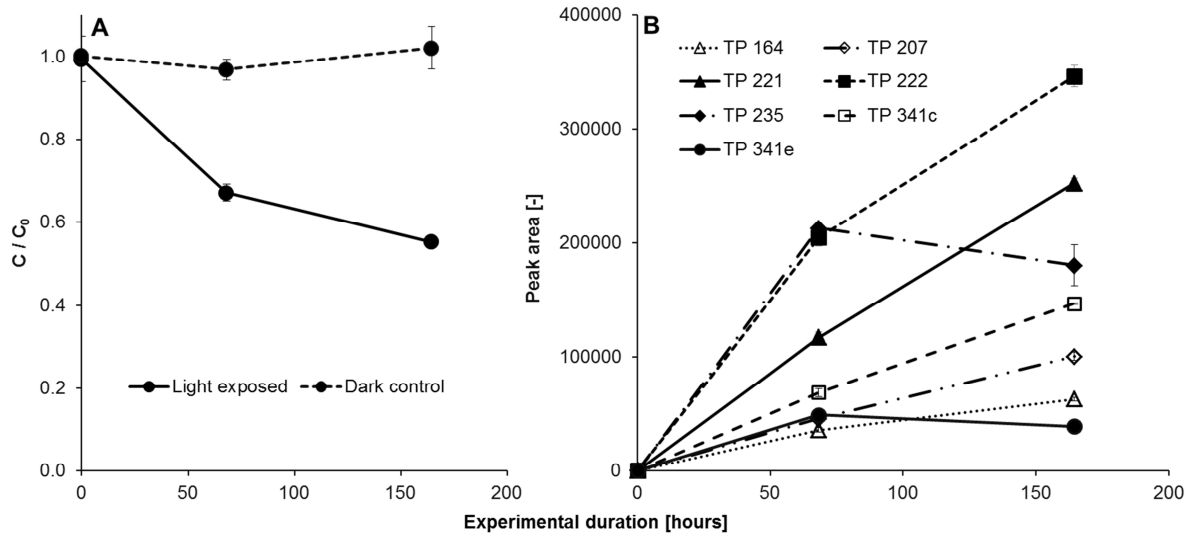


**Figure 5.1**: Time profile of the photodegradation of denatonium (A) and the formation of transformation products (B) in the river water matrix. Data from triplicate experiments (1s error bars, n=3).

For indirect photodegradation in river water matrix the denatonium concentration decreased by about 45 % within 165 hours (Figure 5.1), while no direct degradation was observed in the light exposed samples prepared with LC/MS grade water (Figure S5.8). The results can be explained by the low UV absorption of denatonium from the available UV irradiation of the sun at wavelengths above 290 nm (Figure S5.5), which is the precondition of any direct photolysis. Others found a half-life of ≥ 235 days for the photodegradation of denatonium in water at pH 9. However, no information on reaction parameters and the experimental setup were reported (Health Canada, 2011). The indirect attenuation of denatonium in the river water involved most likely reactive (oxygen) species. For example, hydroxyl radicals ($OH^{\bullet}$) are known as powerful oxidizing agents capable of the degradation of a wide range of organic compounds. Their formation in aquatic environments is well investigated and typically involves photosensitizing species (Gligorovski et al., 2015). Especially the mechanism via photo-activation of nitrate might be of great importance, as the concentration of this anion in the utilized surface water sample was rather high (about 30 mg $L^{-1}$). In contrast, chromophoric dissolved organic matter (here 2.2 mg $L^{-1}$ DOC) might play only a minor role in the formation of $OH^{\bullet}$, but it could affect the nitrate-induced photodegradation process due to inner filter effects and its radical scavenging properties. Scavenging also applies for the presence of equimolar amounts of benzoate, the predominant counter ion in commercially available denatonium products, as it is a known and widely applied $OH^{\bullet}$ trapping agent (Klein et al., 1975).

The occurrence of transformation products gives valuable hints on degradation processes and TPs have to be considered as environmental pollutants itself. In case of denatonium, the indirect photodegradation was associated with the formation of seven TPs (Figure 5.1B). Concentrations increased steadily for five of the seven compounds over the course of the experiment. Only the products TP 235 and TP 341e showed a typical behavior of intermediates which are further degraded with similar rates compared to their formation. The subsequent identification of the products revealed that TP 235 is transformed to TP 207 via N-dealkyation. Maxima for TP 235 and TP 341e occurred at about 68 hours.

### 5.4.2 Anodic oxidation of denatonium

Electrochemical degradation (EC) was investigated in addition to photodegradation, mimicking potential biotransformation processes of denatonium in the environment. Generally, two different working electrodes (i.e. BDD and GC), as well as acidic (pH 4) and neutral (pH 7) conditions, were tested and the influence of the experimental conditions on the TP formation is visualized in Figure 5.2. Overall, ten different products were observed after electrochemical oxidation using statistical analysis of high-resolution mass spectrometric (HRMS) data (as described in chapter 5.3.6.2) and seven of the identified TPs after EC also occurred as TPs from indirect photodegradation. The yield of electrochemical transformation products was strongly dependent on the experimental conditions and electrode materials and spans over more than three orders of magnitude (assuming similar ionization efficiencies). For example, the average observed peak area for TP 164 was about $3.5 \times 10^4$ with a BDD electrode at pH 7, while the average area of TP 221 was in the range of $4.8 \times 10^7$ under the same conditions.

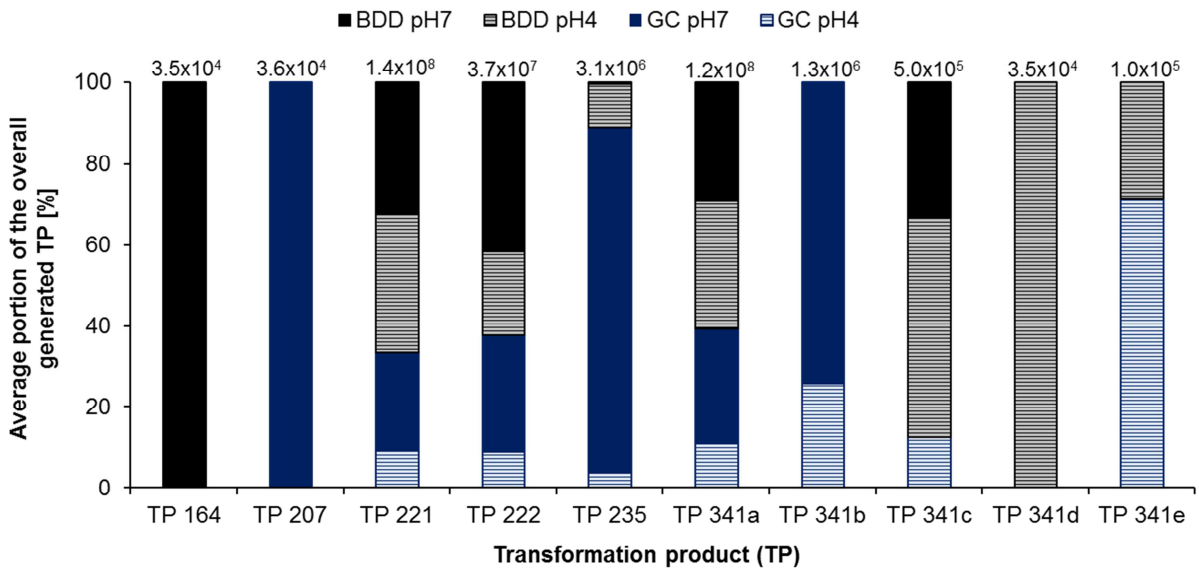


**Figure 5.2**: Average portion of the overall peak areas of ten transformation products (TPs) observed during anodic oxidation of denatonium. Two different working electrodes were tested: boron-doped diamond (BDD, shown in black); glassy carbon (GC, shown in blue) at pH 4 (striped) and pH 7 (solid). Numbers above the bars represent the sum of average peak areas observed for the respective TP under different conditions (n = 3; corrected by controls).

As expected, an influence of the applied working electrode and the pH of the solution on the TP formation could be observed, but it was not possible to identify a single most optimum working condition. Some products were for example only detected at a specific pH (e.g. TP 341e at pH 4) or for a single electrode material (e.g. TP 341b with glassy carbon), while other products were generated under all conditions but with varying yields (e.g. TP 221).

Although the use of boron-doped diamond is often considered as more advantageous compared to other electrode materials due to its corrosion stability and chemical inertness (Panizza and Cerisola, 2005). However, the presented results clearly point out that a wide range of working conditions should be evaluated to cover the broadest TP spectrum possible.

### 5.4.3 Identification of transformation products generated by photodegradation and electrochemical oxidation

Analyte structures were identified based on the approach described in chapter 5.3.6.3., including the assignment of molecular formulas and the consideration of *in-silico* predicted products. MS/MS spectra of the TPs were interpreted additionally by comparing them to fragmentation mechanisms described in literature and to MS/MS information obtained for their parent compound (Figure S5.9A).

The fragmentation spectrum of denatonium is characterized by the fragments at m/z 233.1653, 91.0544 and m/z 86.0966. Fragment m/z 233 is from the quaternary ammonium moiety, while the product ion m/z 91 originates from the benzyl moiety (Figure S5.9C). The azanium ion m/z 233 has a high structural similarity to the pharmaceutical lidocaine, which has an ethyl instead of an ethylidene moiety. Therefore, it is not surprising that denatonium and lidocaine share some common fragments (m/z 86.0964 and m/z 58.0651; reported for lidocaine in Shamai Yamin et al., 2018). MS/MS spectra recorded for m/z 233 (Figure S5.9B) enabled the identification of this ion as the precursor of two additional fragments, i.e. m/z 84.0808 and m/z 56.0495, formally being dehydrogenated species of the common ions shared by denatonium and lidocaine. The minor fragment m/z 65.0386 originates from the benzyl cation due to the loss of acetylene, which was already reported for this precursor before (Bijlsma et al., 2011). Although amides can typically undergo multiple fragmentation reactions (Weissberg and Dagan, 2011), no product ions were observed from this moiety of the analyte in case of denatonium and lidocaine, as the amide bond is stabilized due to resonance with the xylene ring (Joyce et al., 2004).The general identification procedure is exemplarily described below for the TP 164, while the process is summarized for the remaining nine products in chapter 5.8.5 of the supporting information:

***TP 164.*** An accurate mass of m/z 164.1431 was recorded for this TP, corresponding to an elemental composition of $C_{11}H_{17}N$ with an error of about -0.6 ppm. The MS/MS spectrum of this transformation product (Figure S5.10C) contains only three product ions, with m/z 91 ($C_7H_7^+$) and m/z 65 ($C_5H_5^+$) pointing towards the presence of a benzyl group in this compound. Considering the additional fragment m/z 72 ($C_4H_{10}N+$) and the structure of the parent molecule, N,N-diethylbenzylamine is the most plausible identity of this analyte. Retention time and MS/MS spectrum matching with a reference standard confirmed this finally, achieving identification level 1.

Extracted ion chromatograms of all detected products for the individual electrochemical conditions and photodegradation time points are shown together with their MS/MS spectra in Figure S5.10 to Figure S5.15. Table 5.1 summarizes all identified transformation products with their retention time, exact monoisotopic mass of the corresponding precursor ion, observed mass error, elemental composition, the degradation process by which they were formed, as well as the identification level. Structures of the TPs with an identification level between 1 and 3 are shown in Figure 5.3.

**Table 5.1**: Identified transformation products (TP) of denatonium ($C_{21}H_{29}N_2O$; $M^+$ *m/z* 325.228) from electrochemical and photo-induced degradation. Relative abundances of the TPs were estimated individually for the two degradation types and maximum observed peak areas for any condition (e.g. time point for photodegradation) were generally used. EC: electrochemical degradation, Photo: indirect photodegradation, n.d.: not detected.

| Transformation product | Retention time [min] | Ion species and monoisotopic mass [*m/z*] | Mass error [ppm] | Molecular formula | Relative abundance [%] | | Identification level |
|---|---|---|---|---|---|---|---|
| | | | | | EC | Photo | |
| TP 164 | 3.98 | $[M+H]^+$ 164.1434 | -0.63 | $C_{11}H_{17}N$ | < 1 | 14 | 1 |
| TP 207[a] | 4.70 | $[M+H]^+$ 207.1492 | -0.32 | $C_{12}H_{18}N_2O$ | < 1 | 25 | 1 |
| TP 221 | 3.68 | $M^+$ 221.1648 | -0.72 | $C_{13}H_{21}N_2O$ | 100 | 71 | 2b |
| TP 222 | 4.03 | $M^+$ 222.1489 | -0.20 | $C_{13}H_{20}NO_2$ | 34 | 100 | 1 |
| TP 235 | 5.45 | $[M+H]^+$ 235.1805 | -0.69 | $C_{14}H_{22}N_2O$ | 5 | 55 | 1 |
| TP 341a | 6.71 | $M^+$ 341.2224 | 0.45 | $C_{21}H_{29}N_2O_2$ | 71 | n.d. | 3 |
| TP 341b | 6.91 | $M^+$ 341.2224 | -0.59 | $C_{21}H_{29}N_2O_2$ | 3 | n.d. | 4 |
| TP 341c | 7.00 | $M^+$ 341.2224 | -0.69 | $C_{21}H_{29}N_2O_2$ | < 1 | 41 | 4 |
| TP 341d | 7.27 | $M^+$ 341.2224 | 0.53 | $C_{21}H_{29}N_2O_2$ | 1 | n.d. | 4 |
| TP 341e | 7.75 | $M^+$ 341.2224 | 0.52 | $C_{21}H_{29}N_2O_2$ | < 1 | 13 | 3 |

[a] secondary transformation product

### 5.4.4 Proposed transformation pathway of denatonium

Products observed for denatonium after electrochemical oxidation and photodegradation are summarized in a proposed transformation pathway (Figure 5.3). The reactions leading to their formation are discussed below.

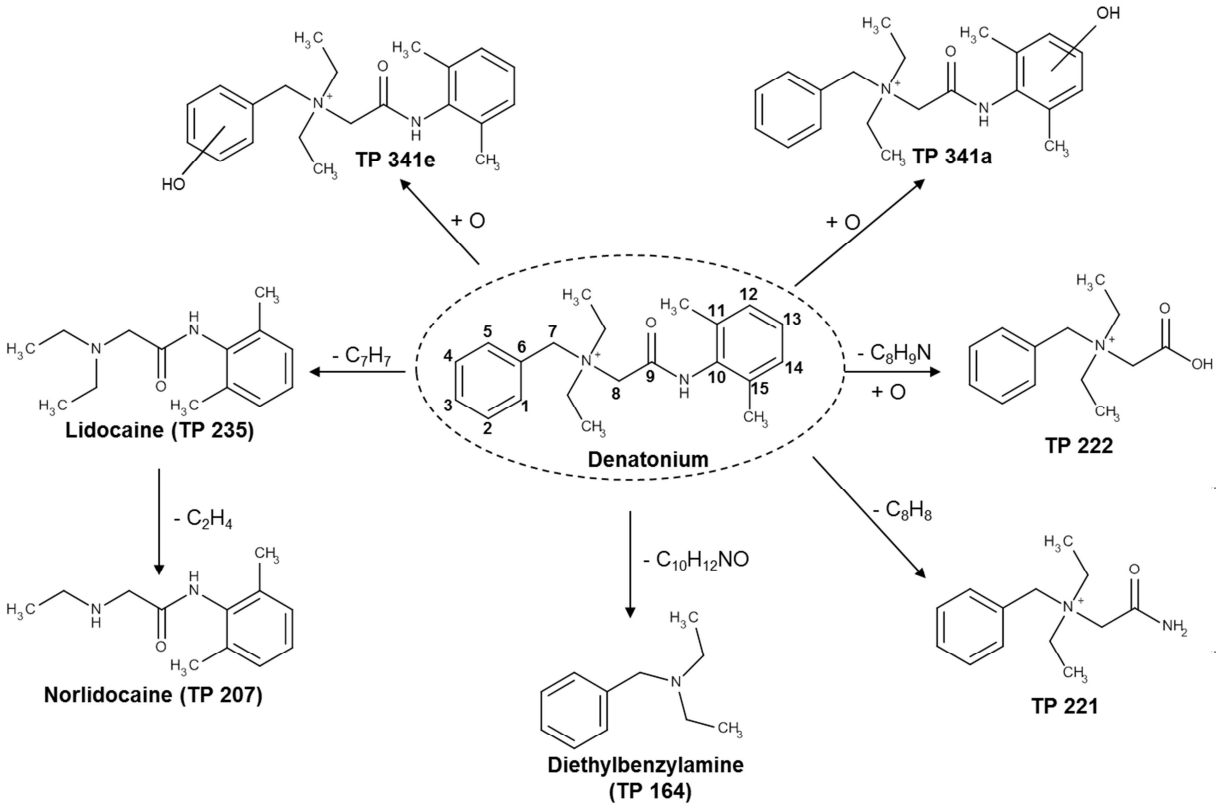


**Figure 5.3**: Proposed transformation pathway for denatonium due to anodic oxidation and indirect photodegradation. Only products with identification levels 1 to 3 have been considered here.

#### 5.4.4.1 N-dealkylation

The formation of diethylbenzylamine (TP 164) and lidocaine (TP 235) by indirect photodegradation revealed that dealkyation of the quaternary ammonium moiety could lead in principle to an attenuation of denatonium in surface waters. While no subsequent degradation of TP 164 occurred, lidocaine was further transformed into norlidocaine (TP 207) due to N-deethylation. Reactive oxygen species, like hydroxyl radicals, were most likely involved in the general transformation mechanism of denatonium, as was reported before for the indirect photolysis of perfluorochemicals (Plumlee et al., 2009).

Despite the fact that hydroxyl radicals can be generated by anodic oxidation on BDD working electrodes (Enache et al., 2009), dealkylation products were generally formed neither reproducibly nor in high yields by electrochemical treatment of denatonium. For example, only one out of three replicates showed significantly elevated lidocaine concentrations above the background level, using a GC working electrode at pH 7 (Figure S5.14A).

In contrast, diethylbenzylamine was generated on a BDD electrode at pH 7 in all replicates, but only in trace amounts (Figure S5.10A, Table 5.1). Therefore, it was assumed that the chosen potential of 1.5 V vs. Ag/AgCl was either too low for a significant formation of hydroxyl radicals or that they were trapped more efficiently by other species. Direct electron transfer could be the other mechanism involved in the formation of the majority of electrochemical denatonium products. In case of tertiary amines, electrochemical N-dealkylation follows this route (Mali'n et al., 2010, Nouri-Nigjeh et al., 2010), while a direct oxidation of the quaternary ammonium nitrogen is not feasible and electron transfer from an adjacent carbon atom was not observed (Nouri-Nigjeh et al., 2012). Due to the low reactivity towards electrochemical oxidation, quaternary ammonium compounds are frequently applied in industrial applications, e.g. as electrolytes, and are generally considered as one of the most electrochemically stable class of organic cations (Mousavi et al., 2015).

The biodegradation of denatonium could also lead to the formation of N-dealkylated products, which we observed for indirect photolysis. Aerobic microbial degradation of structurally related benzalkonium chlorides can proceed for example via a cleavage of the alkyl chain (Patrauchan and Oriel, 2003, Tezel et al., 2012). Additionally, the loss of the benzyl moiety of these compounds was observed under nitrate reducing conditions and traced back to a nucleophilic nitrite attack (Tezel and Pavlostathis, 2009).

#### 5.4.4.2 Hydroxylation

Overall, five different mono-hydroxylated products (TP 341a-e) were detected after photodegradation and anodic oxidation, but their yields differed significantly between both degradation experiments (Figure S5.15A and B, Table 5.1). The most abundant hydroxylated product after indirect photolysis was TP 341c (about 41 % relative abundance, Table 5.1), followed by TP 341e with a relative abundance of 13 %. While the MS/MS information of TP 341c was not conclusive to support a tentative structure of this analyte, the formation of TP 341e could be related to an aromatic hydroxylation of denatonium at the benzyl group.

However, both products were only formed to a minor extent during anodic oxidation. Independent of the working electrode and the pH, TP 341a was always the predominant hydroxylated species after electrochemical degradation of denatonium. Similar to TP 341e, an aromatic hydroxylation was postulated here, but the xylidine moiety was identified as the location of modification instead of the benzyl group. Hydroxylation of aromatic structures with electron donating substituents was achieved before, with the application of electrochemistry under neutral pH conditions without an EC-Fenton system (Johansson et al., 2007). Neither the electrochemically generated TP 341b nor the compound TP 341d were observed after indirect photodegradation of denatonium.

#### 5.4.4.3 Amide hydrolysis

The electrochemical bond-cleavage of structurally related amides of the type $Ph_2CHCONHAr$ was already discussed before (Golub and Becker, 2012) and the results were transferred to denatonium for the interpretation of its degradation. In contrast to Golub and Becker, 2012, who reported three sites for potential bond-cleavages, only two should apply here. The cleavage of the C8-C9 bond at the carbonyl group was not expected, because the intermediate species of the transformation process (i.e. a carbocation) would not be stabilized in case of denatonium, e.g. by charge delocalization. This hypothesis was finally supported by the product spectrum observed in electrochemically treated denatonium samples, as none of the putative products of the C8-C9 cleavage (e.g. a primary alcohol or an aldehyde as observed by Golub and Becker, 2012) could be detected. Amide cleavage occurred during anodic oxidation and indirect photodegradation and formed the carboxylic acid (TP 222). The complementary product of this process, i.e. 2,6-dimethylaniline (2,6-xylidine), was only observed in trace amounts for electrochemical oxidation with GC working electrodes (data not shown), but not in any other sample. Subsequent transformation of xylidine itself by electrochemically generated hydroxyl radicals was already investigated (Masomboon et al., 2010), but neither the reported nor any other TPs (e.g. from hydroxylation and further oxidation to quinoneimines) were observed here. The fate of this compound could therefore not be elucidated. Formation of TP 222 by amide cleavage could be a relevant biodegradation mechanism of denatonium in WWTPs or surface waters. Microbial degradation via this route was already reported for a wide range of amides (Helbling et al., 2010) and it was the only *in-silico* predicted microbial transformation process of denatonium.

Furthermore, amidases, the enzymes catalyzing amide hydrolysis and various other reactions, are present in numerous organisms, including bacteria, fungi, and plants (Sharma et al., 2009).

#### 5.4.4.4 N-dearylation

The product TP 221 was formed through a cleavage of the bond between the nitrogen atom in the amide moiety and the aryl group, which was also reported for structurally related compounds of the type $Ph_2CHCONHAr$ (Golub and Becker, 2012). Electron-donating substituents, i.e. here two methyl groups in *ortho*-position of the aryl group, generally enhance this bond-cleaving process. Therefore, it is not surprising that TP 221 was the most abundant transformation product observed after anodic oxidation and it was in addition an important product for indirect photodegradation of denatonium.

### 5.4.5 Fate of denatonium in WWTPs and surface waters, as well as occurrence of identified transformation products

Wastewater was already identified before as the main source of denatonium in the environment (Lege et al., 2017). Therefore, flow-proportional daily composite samples were taken from a WWTP over five days to investigate the potential denatonium attenuation during the treatment process. The highest daily-averaged denatonium concentrations were observed during dry weather conditions with 60 ng $L^{-1}$ and 58 ng $L^{-1}$ in the influent and effluent, respectively (Figure S5.16A). The measured concentrations varied with the weather conditions, with lowest concentrations being generally measured for the highest wastewater flowrates. This observation can be explained by a dilution of micropollutants with rainwater in the combined sewer system. Estimates of the total mass flux based on measured effluent concentrations and the wastewater flowrate revealed that the investigated WWTP released between 1.3 and 2.8 grams of denatonium per day into the receiving surface water. The efficiency of compound removal during wastewater treatment was estimated by comparing measured influent and effluent concentrations. In case of denatonium, observed removals varied between 16 % and -32 % over the course of the sampling campaign (Figure 5.4), which is in a low range and similar to other not-well removable micropollutants (Figure 5.4). Only the well-degradable pain reliever paracetamol showed complete removal, which is in agreement to previous findings (Margot et al., 2015). Negative removal typically occurred at highly variable flow conditions due to an improper sampling strategy, although flow-proportional composite samples were taken during this campaign.

Majewsky et al. used model simulations to demonstrate that the hydraulic retention time, as was considered in this study, is not the best parameter to determine the offset between the influent and effluent sampling periods. Errors in the estimated xenobiotic removal efficiencies have to be expected when mixing and the solute`s residence time distribution are neglected, especially under highly variable flow conditions (Majewsky et al., 2011).

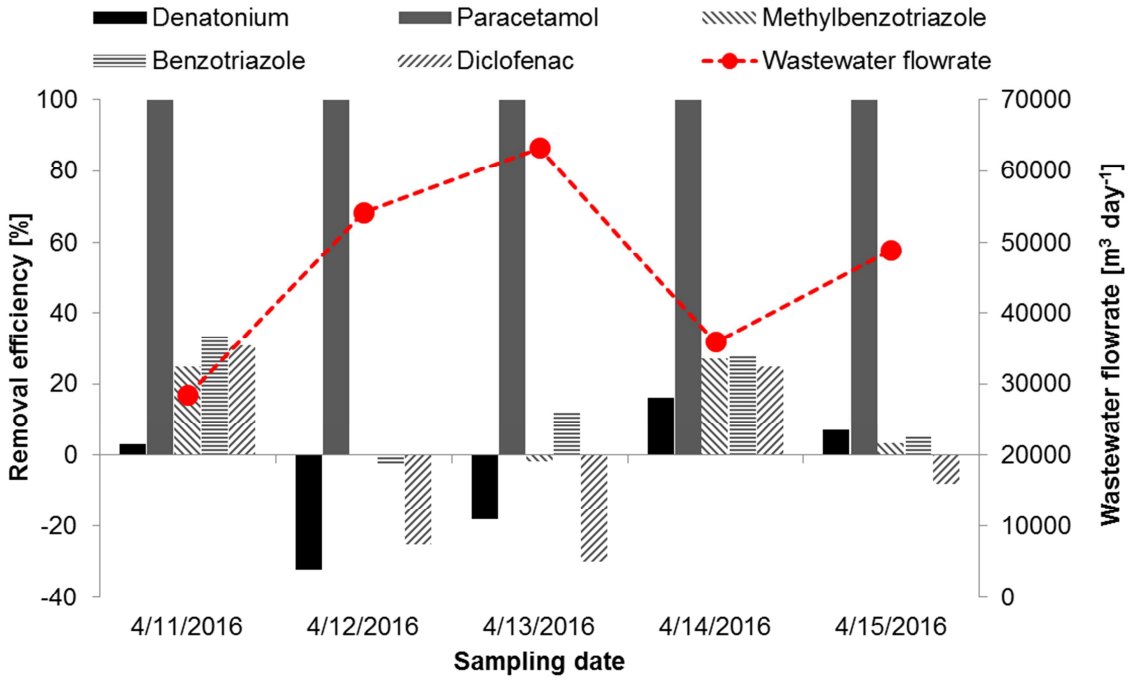


**Figure 5.4**: Removal efficiency of denatonium and four additional micropollutants estimated from 24 hour mixed samples of WWTP influents and effluents. Removal efficiencies are stated here for the sum of 4- and 5-methylbenzotriazole. The daily wastewater flowrate is shown for the duration of the sampling campaign. Relative standard deviations of triplicate sample analysis was always less than 2%.

Considering the sample on the first sampling day taken during dry weather, estimated removal efficiencies of additional micropollutants agreed well with those already reported in literature (Margot et al., 2015). No significant differences between the average daily influent and effluent concentrations of denatonium were observed on this day. This is in agreement with previous findings where denatonium was neither biodegraded nor removed by sorption when exposed to activated sludge (Corby et al., 1993). The presence of lidocaine in WWTP can be associated to its application as local anesthetic and to denatonium degradation. None of the additional transformation products described in the present study was generally observed in any effluent sample from overall 25 WWTPs (data not shown), covering three different countries and a wide range of treatment plant characteristics. Denatonium can be therefore considered as a persistent micropollutant in wastewater, which is not removed during conventional treatment.

Advanced wastewater treatment techniques have proven useful for the reduction of xenobiotic discharge to the environment and some countries plan or started already to upgrade existing WWTPs. For example, the Swiss government decided in 2014 to upgrade about 100 existing WWTPs either by ozonation or treatment with powdered activated carbon (PAC) (Eggen et al., 2014). While the sorption of denatonium to PAC has been investigated before (Crosson et al., 2014), no information was available so far about the compound´s fate during ozonation. Pilot-scale ozonation of secondary wastewater effluent, followed by flocculation and filtration through an anthracite/sand layer, was investigated at a treatment plant of a major city in Germany (details in Merel et al., 2017). Samples from this study were retrospectively investigated and the results point out that an ozone dose of about 6 mg $L^{-1}$ (corresponding to an O3/DOC ratio of 0.5) was sufficient to reduce the denatonium load in conventionally treated wastewater by about 74% (Figure S5.17). The attenuation of this compound was at least partially related to an N-dearylation or a hydrolysis of its amide moiety as the degradation products TP 221 and TP 222 were detected in the effluent of the ozone reactor. Lidocaine was observed here again in the conventionally treated wastewater. Its formation from denatonium due to ozonation could however not be elucidated as it was completely removed during the advanced oxidation step and transformed to at least some extent into its N-oxide (Merel et al., 2017). The final flocculation and filtration step did neither impact the abundance of denatonium nor of the two identified transformation products (Figure S5.17). Summarizing these results, an upgrade of WWTPs with ozonation would generally reduce the release of denatonium to the environment, but it is related to the formation of more polar TPs with so far unknown (toxicological) properties.

Similar to its behavior during conventional wastewater treatment, a rather high persistence of denatonium is expected once it is discharged into surface waters. Although photodegradation can theoretically take place here in addition, it is expected that denatonium undergoes rather slow transformation, if any at all. The reason is that the underlying process, being an indirect mechanism, requires favorable conditions (e.g. presence of photosensitizers) and no evidence was found so far that it actually takes place for denatonium in the environment. When reactive transport was recently assessed for a wide range of micropollutants in a wastewater-impacted river, the estimated attenuation of denatonium for a summer day was within the uncertainty of the analytical method and did not differ significantly from samples taken during the night (Guillet et al., 2019).

Furthermore, none of the characteristic phototransformation products of denatonium (e.g. TP 222) was found in any of the retrospectively analyzed surface water samples. The detection of lidocaine was again associated with its use pattern as pharmaceutical compound.

### 5.4.6 Risk of false-positive identification of TP 222 in WWTPs and surface waters

Whenever wastewater or river water was evaluated for the presence of the TPs of denatonium, an analyte with the monoisotopic mass *m/z* 222.1489 was detected in nearly all samples at a retention time (RT) of 3.0 min, which is different from the RT of TP 222 at 4.1 min (Figure 5.5B). The unknown shows also a very similar mass fragmentation pattern as TP 222 (Figure 5.5C and D). It didn´t occur in the least polluted surface waters, i.e. upstream of WWTPs and closest to the source of the river Rhine, suggesting that it is also a wastewater borne contaminant.

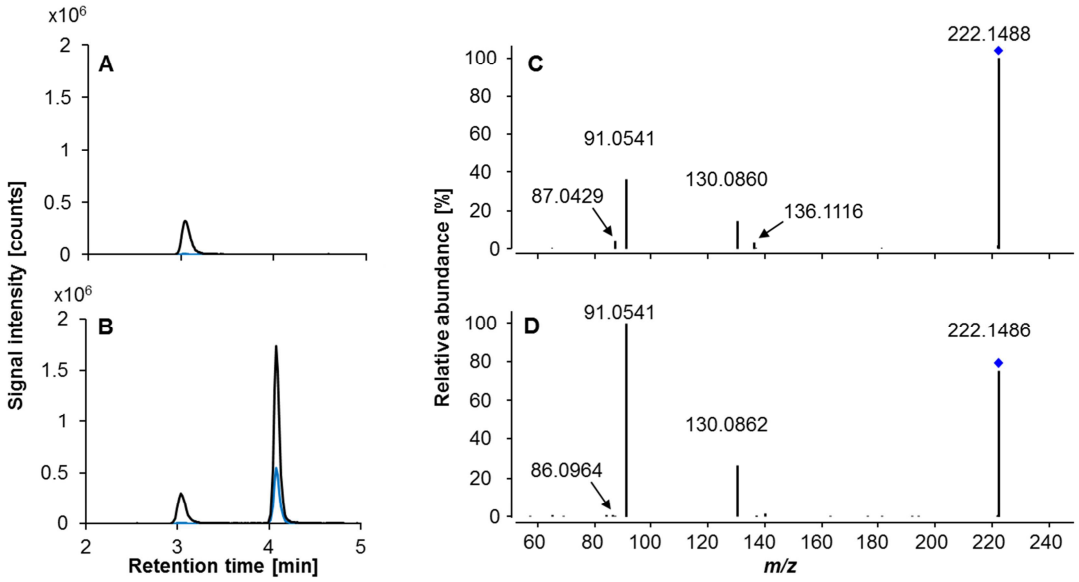


**Figure 5.5**: Extracted ion chromatograms of *m/z* 222.1489 (solid black line) and *m/z* 244.1308 (sodium adduct, solid blue line) for a WWTP effluent sample spiked (B) or not spiked (A) with TP 222. The extraction range was ±10 ppm. MS/MS spectra of the unknown analyte eluting at 3 min (C) and of TP 222 eluting around 4.1 min (D) were recorded at 10 V.

A false-positive identification of this degradation product is possible when using suspect screening approaches based on spectral libraries, since we shared the MS/MS spectra of TP 222 in the public repository MassBank (https://massbank.eu/, accession numbers TUE00851-TUE00853). Therefore we would like to highlight the RT difference and two less abundant product ions observed at low collision energies, which could help to distinguish between both analytes.

While the fragment *m/z* 136.1121 ($C_9H_{14}N^+$) was only generated by the unknown isobaric compound, no product ion with *m/z* 86.0964 ($C_5H_{12}N^+$) was observed for this compound after collision-induced activation. Furthermore, only TP 222 seems to form sodium adducts in the ESI source to a significant extent (Figure 5.5B). The web version of the *in-silico* fragmentation tool MetFrag (https://msbi.ipb-halle.de/MetFragBeta/; accessed on February 9th, 2019) was used in combination with the PubChem database to putatively identify the unknown compound. Assuming a permanently charged compound, 407 candidates were obtained for a mass based search for *m/z* 222.1489 ($M^+$) with a tolerated error of 5 ppm. Predicted fragments of 24 compounds matched all observed product ions for the unknown analyte with a relative abundance of more than 0.5%. The highest score was obtained for benzyl-(3-carboxypropyl)-dimethylazanium (PubChem ID 90655213) and benzyl-(1-carboxy-1-methyl-ethyl)-dimethyl-ammonium (PubChem ID 87520134). When the database search was extended to non-permanently charged analytes, more than 27000 candidates were obtained for *m/z* 222.1489 ($[M+H]^+$) with a tolerated mass deviation of 5 ppm. *In*-silico fragmentation of 1600 compounds matched the MS/MS spectrum of the unknown, and the best scores were obtained for methyl 3-[benzyl(ethyl)amino]propanoate (PubChem ID 28830360) and 4-(N-ethyl-2-methyl-anilino)butanoic acid (PubChem ID 11322478). Generally, PubChem did not contain literature references for any of the database matches, preventing further prioritization of the compounds as putative environmental pollutants via application information.

## 5.5 Conclusion

TPs of photodegradation and electrochemical oxidation of the recently described water contaminant denatonium were identified in this study. In combination with wastewater and river water analysis, we were able to gain more knowledge about its potential fate in WWTPs, as well as in the environment. Generally, the following conclusions were drawn from our observations:

- Denatonium is a persistent pollutant during conventional wastewater treatment, but it can be (partially) eliminated by ozonation. The removal via ozonation is however associated with the formation of polar transformation products with unknown (toxicological) properties.

- Overall, ten transformation products were observed for indirect photodegradation and anodic oxidation. Except for lidocaine, which originates most likely from its use as local anesthetic, none of these products was observed in environmental samples.
- No significant elimination of denatonium is expected once it is released into surface waters. Indirect photodegradation is considered to be very slow as the underlying mechanism requires favorable conditions and is impacted by compounds competing for reactive species.

## 5.6 Acknowledgements

The German Federal Environmental Foundation (Deutsche Bundesstiftung Umwelt, DBU) is gratefully acknowledged for funding the Ph.D. scholarships of Sascha Lege and Anna Eisenhofer. The German Research Foundation (DFG) is gratefully acknowledged for funding the project ZW 73/14. Technical support by Bernice Nisch (University of Tübingen) with the DOC and ion determination and execution of the photodegradation experiments by Julian Sorwat (University of Tübingen) are highly appreciated.

## 5.7 References

Bijlsma, L., Sancho, J.V., Hernández, F., Niessen, Wilfried M A, 2011. Fragmentation pathways of drugs of abuse and their metabolites based on QTOF MS/MS and MS(E) accurate-mass spectra. Journal of mass spectrometry 46 (9), 865–875.

Brian, J.V., Harris, C.A., Scholze, M., Backhaus, T., Booy, P., Lamoree, M., Pojana, G., Jonkers, N., Runnalls, T., Bonfà, A., Marcomini, A., Sumpter, J.P., 2005. Accurate prediction of the response of freshwater fish to a mixture of estrogenic chemicals. Environmental health perspectives 113 (6), 721–728.

Consumer Product Safety Commission United States of America, 1992. Final Report Study of Aversive Agents. Technical Report.

Corby, J.E., Doi, J., Conville, J.J., Murphy, S.R., McKenzie, D.A., 1993. Biodegradability of a Denatonium Bitterant. SAE Technical Paper 930587, 813–816.

Cosmetic Ingredient Review Expert Panel, 2008. Final report of the safety assessment of Alcohol Denat., including SD Alcohol 3-A, SD Alcohol 30, SD Alcohol 39, SD Alcohol 39-B, SD Alcohol 39-C, SD Alcohol 40, SD Alcohol 40-B, and SD Alcohol 40-C, and the denaturants, Quassin, Brucine Sulfate/Brucine, and Denatonium Benzoate. International journal of toxicology 27 Suppl 1, 1–43.

Crosson, G., Crosson, K., Thorpe, S., MacPherson, L., Murdock, M., Smith, B., 2014. Activated carbon and clay minerals for the sorptive removal of denatonium ions from denatonium benzoate solutions. Journal of Water Resource and Protection 6 (8), 793–803.

Djoumbou-Feunang, Y., Fiamoncini, J., Gil-de-la-Fuente, A., Greiner, R., Manach, C., Wishart, D.S., 2019. BioTransformer: a comprehensive computational tool for small molecule metabolism prediction and metabolite identification. Journal of cheminformatics 11 (1), 2.

ECHA, 2019. Registered dossier for denatonium benzoate (accessed January 16th, 2019). https://echa.europa.eu/registration-dossier/-/registered-dossier/16728.

Eggen, Rik I L, Hollender, J., Joss, A., Schärer, M., Stamm, C., 2014. Reducing the discharge of micropollutants in the aquatic environment: the benefits of upgrading wastewater treatment plants. Environmental science & technology 48 (14), 7683–7689.

Enache, T.A., Chiorcea-Paquim, A.-M., Fatibello-Filho, O., Oliveira-Brett, A.M., 2009. Hydroxyl radicals electrochemically generated in situ on a boron-doped diamond electrode. Electrochemistry Communications 11 (7), 1342–1345.

European Commission, 2013. Commission Implementing Regulation (EU) No 162/2013 of 21 February 2013 amending the Annex to Regulation (EC) No 3199/93 on the mutual recognition of procedures for the complete denaturing of alcohol for the purposes of exemption from excise duty. OJ L 49, 55–61.

European Food Safety Authority, 2012. Conclusion on the peer review of the pesticide risk assessment of the active substance denatonium benzoate (approved as denathonium benzoate). EFSA Journal 10 (1), 2483–2517.

Faber, H., Lutze, H., Lareo, P.L., Frensemeier, L., Vogel, M., Schmidt, T.C., Karst, U., 2014. Liquid chromatography/mass spectrometry to study oxidative degradation of environmentally relevant pharmaceuticals by electrochemistry and ozonation. Journal of chromatography. A 1343, 152–159.Falås, P., Wick, A., Castronovo, S., Habermacher, J., Ternes, T.A., Joss, A., 2016. Tracing the limits of organic micropollutant removal in biological wastewater treatment. Water research 95, 240–249.

Fisher, D.L., Arthur Moseley, M., Mullis, J.O., Norwood, D.L., Baillie, T.A., 1994. Recognition of quaternary ammonium compounds using mass spectrometry. Rapid Commun. Mass Spectrom. 8 (1), 65–70.

Gligorovski, S., Strekowski, R., Barbati, S., Vione, D., 2015. Environmental Implications of Hydroxyl Radicals ((•)OH). Chemical reviews 115 (24), 13051–13092.

Golub, T., Becker, J.Y., 2012. Electrochemical oxidation of amides of type Ph2CHCONHAr. Organic & biomolecular chemistry 10 (19), 3906–3912.

Guillet, G., Knapp, J.L., Merel, S., Cirpka, O.A., Grathwohl, P., Zwiener, C., Schwientek, M., 2019. Fate of wastewater contaminants in rivers: Using conservative-tracer based transfer functions to assess reactive transport. Science of The Total Environment 656, 1250–1260.

Health Canada, 2011. Proposed Re-evaluation Decision PRVD2011-15: Denatonium Benzoate. Health Canada Pest Management Regulatory Agency (accessed January, 17th 2019). http://publications.gc.ca/collections/collection_2011/sc-hc/H113-27-2011-15-eng.pdf.

Helbling, D.E., Hollender, J., Kohler, H.-P.E., Fenner, K., 2010. Structure-based interpretation of biotransformation pathways of amide-containing compounds in sludge-seeded bioreactors. Environmental science & technology 44 (17), 6628–6635.

Holcapek, M., Jirásko, R., Lísa, M., 2010. Basic rules for the interpretation of atmospheric pressure ionization mass spectra of small molecules. Journal of chromatography. A 1217 (25), 3908–3921.

Horemans, B., Hofkens, J., Smolders, E., Springael, D., 2014. Biofilm formation of a bacterial consortium on linuron at micropollutant concentrations in continuous flow chambers and the impact of dissolved organic matter. FEMS microbiology ecology 88 (1), 184–194.

Johansson, T., Weidolf, L., Jurva, U., 2007. Mimicry of phase I drug metabolism,-novel methods for metabolite characterization and synthesis. Rapid communications in mass spectrometry 21 (14), 2323–2331.

Joyce, C., Smyth, W.F., Ramachandran, V.N., O'Kane, E., Coulter, D.J., 2004. The characterisation of selected drugs with amine-containing side chains using electrospray ionisation and ion trap mass spectrometry and their determination by HPLC-ESI-MS. Journal of pharmaceutical and biomedical analysis 36 (3), 465–476.

Jurva, U., Wikström, H.V., Weidolf, L., Bruins, A.P., 2003. Comparison between electrochemistry/mass spectrometry and cytochrome P450 catalyzed oxidation reactions. Rapid communications in mass spectrometry 17 (8), 800–810.

Klein, G.W., Bhatia, K., Madhavan, V., Schuler, R.H., 1975. Reaction of hydroxyl radicals with benzoic acid. Isomer distribution in the radical intermediates. J. Phys. Chem. 79 (17), 1767–1774.

Lege, S., Guillet, G., Merel, S., Yanez Heras, Jorge Eduardo, Zwiener, C., 2017. Denatonium - A so far unrecognized but ubiquitous water contaminant? Water research 112, 254–260.

Majewsky, M., Gallé, T., Bayerle, M., Goel, R., Fischer, K., Vanrolleghem, P.A., 2011. Xenobiotic removal efficiencies in wastewater treatment plants: residence time distributions as a guiding principle for sampling strategies. Water research 45 (18), 6152–6162.

Mali'n, T.J., Weidolf, L., Castagnoli, N., Jurva, U., 2010. P450-catalyzed vs. electrochemical oxidation of haloperidol studied by ultra-performance liquid chromatography/electrospray ionization mass spectrometry. Rapid communications in mass spectrometry 24 (9), 1231–1240.

Margot, J., Rossi, L., Barry, D.A., Holliger, C., 2015. A review of the fate of micropollutants in wastewater treatment plants. WIREs Water 2 (5), 457–487.

Masomboon, N., Ratanatamskul, C., Lu, M.-C., 2010. Chemical oxidation of 2,6-dimethylaniline by electrochemically generated Fenton's reagent. Journal of hazardous materials 176 (1-3), 92–98.

Merel, S., Benzing, S., Gleiser, C., Di Napoli-Davis, G., Zwiener, C., 2018. Occurrence and overlooked sources of the biocide carbendazim in wastewater and surface water. Environmental pollution 239, 512–521.

Merel, S., Lege, S., Yanez Heras, Jorge E, Zwiener, C., 2017. Assessment of N-Oxide Formation during Wastewater Ozonation. Environmental science & technology 51 (1), 410–417.

Mousavi, Maral P. S., Kashefolgheta, S., Stein, A., Bühlmann, P., 2015. Electrochemical Stability of Quaternary Ammonium Cations: An Experimental and Computational Study. J. Electrochem. Soc. 163 (2), H74.

Nouri-Nigjeh, E., de Vries, Marcel P., Bruins, A.P., Bischoff, R., Permentier, H.P., 2012. Electrochemical oxidation of quaternary ammonium electrolytes: Unexpected side reactions in organic electrochemistry. Electrochemistry Communications 21, 54–57.

Nouri-Nigjeh, E., Permentier, H.P., Bischoff, R., Bruins, A.P., 2010. Lidocaine oxidation by electrogenerated reactive oxygen species in the light of oxidative drug metabolism. Analytical chemistry 82 (18), 7625–7633.

Painter, M.M., Buerkley, M.A., Julius, M.L., Vajda, A.M., Norris, D.O., Barber, L.B., Furlong, E.T., Schultz, M.M., Schoenfuss, H.L., 2009. Antidepressants at environmentally relevant concentrations affect predator avoidance behavior of larval fathead minnows (Pimephales promelas). Environmental toxicology and chemistry 28 (12), 2677–2684.

Panizza, M., Cerisola,G., 2005. Application of diamond electrodes to electrochemical processes. Electrochimica Acta 51(2), 191-199.

Patrauchan, M.A., Oriel, P.J., 2003. Degradation of benzyldimethylalkylammonium chloride by Aeromonas hydrophila sp. K. J Appl Microbiol 94 (2), 266–272.

Plumlee, M.H., McNeill, K., Reinhard, M., 2009. Indirect Photolysis of Perfluorochemicals: Hydroxyl Radical-Initiated Oxidation of N -Ethyl Perfluorooctane Sulfonamido Acetate (N -EtFOSAA) and Other Perfluoroalkanesulfonamides. Environmental science & technology 43 (10), 3662–3668.

Schollée, J.E., Bourgin, M., Gunten, U. von, McArdell, C.S., Hollender, J., 2018. Non-target screening to trace ozonation transformation products in a wastewater treatment train including different post-treatments. Water research 142, 267–278.

Schymanski, E.L., Jeon, J., Gulde, R., Fenner, K., Ruff, M., Singer, H.P., Hollender, J., 2014. Identifying small molecules via high resolution mass spectrometry: communicating confidence. Environmental science & technology 48 (4), 2097–2098.

Shamai Yamin, T., Prihed, H., Shifrovitch, A., Dagan, S., Weissberg, A., 2018. Oxidation-assisted structural elucidation of compounds containing a tertiary amine side chain using liquid chromatography mass spectrometry. Journal of mass spectrometry JMS 53 (6), 518–524.

Sharma, M., Sharma, N.N., Bhalla, T.C., 2009. Amidases: versatile enzymes in nature. Rev Environ Sci Biotechnol 8 (4), 343–366.

Tezel, U., Pavlostathis, S.G., 2009. Transformation of Benzalkonium Chloride under Nitrate Reducing Conditions. Environmental science & technology 43 (5), 1342–1348.

Tezel, U., Tandukar, M., Martinez, R.J., Sobecky, P.A., Pavlostathis, S.G., 2012. Aerobic biotransformation of n-tetradecylbenzyldimethylammonium chloride by an enriched Pseudomonas spp. community. Environmental science & technology 46 (16), 8714–8722.

Weissberg, A., Dagan, S., 2011. Interpretation of ESI(+)-MS-MS spectra—Towards the identification of “unknowns”. International Journal of Mass Spectrometry 299 (2-3), 158–168.

Ziegler, E., Wittmann, H., 1985. Über Reaktionen mit Betainen, 19. Mitt. Über den Einfluß der Substituenten am kationischen Zentrum von Betainen auf die Bildungstendenz der Di-trifluoracetyl-N-Ylide. Monatshefte für Chemie – Chemical Monthly 116 (6-7), 821–829.

## 5.8 Supplementary information

### 5.8.1 Synthesis of the transformation product N-Benzyl-N-carboxymethyl-N,N-diethylammonium in a two-step reaction

Commercial reagents and starting materials were purchased from commercial suppliers and used without further purification. Solvents were used in p.a. quality and dried according to common procedures, if necessary. Dry nitrogen was used as inert gas atmosphere. NMR-spectra were recorded on a Bruker Avance 400 (1H: 400 MHz, 13C: 101 MHz, T = 300 K) or a Bruker Avance 300 (1H: 300 MHz, 13C: 75 MHz, T = 295 K) using the solvent residual peak as internal reference (CDCl3: δ H 7.26; δ C 77.0; D2O: δ H 4.79). Abbreviations used for signal multiplicity: 1H-NMR: s (singlet), d (doublet), t (triplet), q (quartet), quint (quintet), sept (septet), m (multiplet)); coupling constants (J) are in Hertz (Hz). 13C-NMR: (+) = primary/tertiary, (−) = secondary, (q) = quaternary carbon. Reactions were monitored by thin-layer chromatography using silica gel plates ALUGRAM Xtra SIL G/UV254 from Macherey-Nagel; visualization was accomplished with UV light (254 nm or 366 nm). Flash column chromatography was performed on a Biotage Isolera Spektra One automated flash purification system with UV-Vis detector. As stationary phase Merck silica gel 60 M (0.040-0.063 mm, 230-440 mesh) was used. Mass spectra were recorded on Finnigan MAT95 (EI-MS), Agilent Q-TOF 6540 UHD (ESI-MS, APCI-MS), Finnigan MAT SSQ 710 A (EI-MS, CI-MS) or ThermoQuest Finnigan TSQ 7000 (ES-MS, APCI-MS) spectrometer. Melting points were determined using a Stanford Research Systems OptiMelt MPA 100 and are uncorrected. IR spectra were measured on Cary630 from Agilent technologies.

The synthesis follows a procedure reported for similar compounds (Ziegler and Wittmann, 1985).

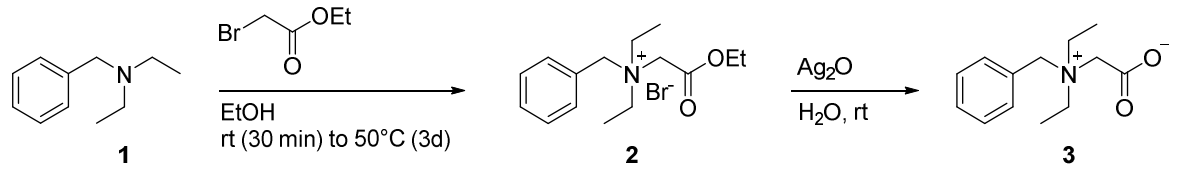


**1** **2** **3**

**Step 1:** Synthesis and characterization of the intermediate N-Benzyl-N-(ethoxycarbonylmethyl)-N,N-diethylammonium bromide (Compound 2, Babayan et al., 1976)

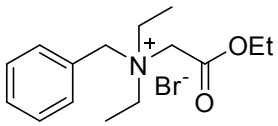


Chemical Formula: $C_{15}H_{24}BrNO_2$
Molecular Weight: 330,27

A mixture of *N*,*N*-diethylbenzylamine (2.75 mL, 15.0 mmol) and ethyl bromoacetate (2.00 mL, 18.0 mmol) in ethanol (6 mL) was stirred for 30 min at room temperature, then 3 d at 50°C until complete crystallization was achieved. The solvent was evaporated and the crude product was purified by automated flash column chromatography (dichloromethane/methanol: 3% → 10% methanol) and subsequent recrystallization from isopropanol. Compound **2** was obtained as white solid (3.51 g, 10.6 mmol, 71 %).

**Mp:** 131 °C

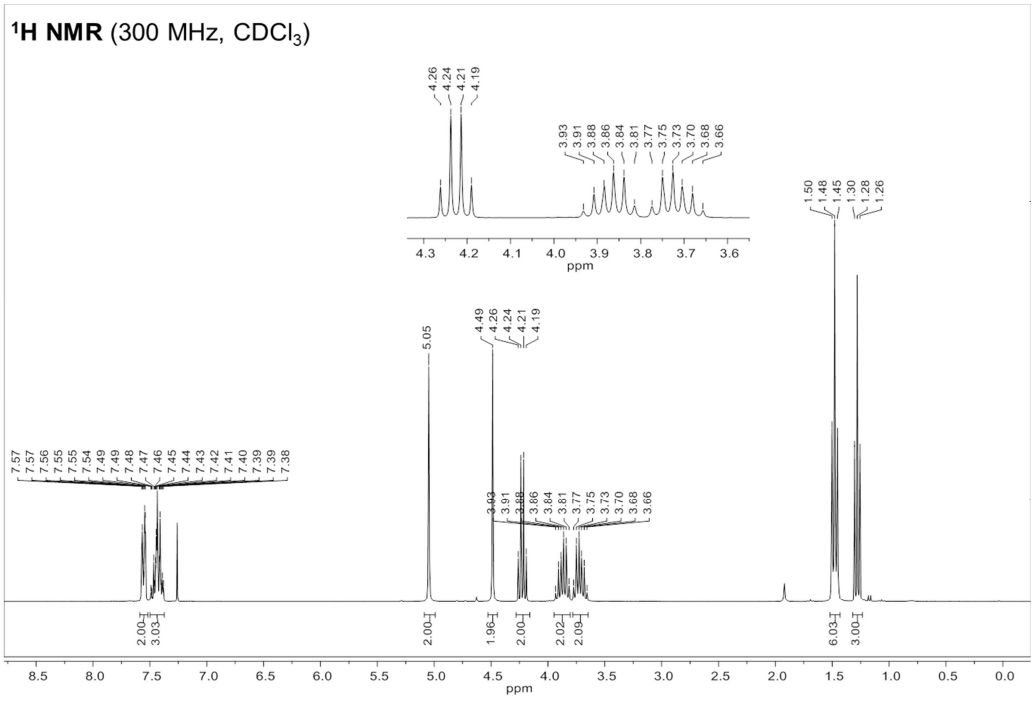


**Figure S5.1**: $^1$H NMR spectrum of N-Benzyl-N-(ethoxycarbonylmethyl)-N,N-diethyl-ammonium bromide. 300 MHz, $CDCl_3$: δ = 7.59 – 7.52 (m, 2H), 7.51 – 7.36 (m, 3H), 5.05 (s, 2H), 4.49 (s, 2H), 4.23 (q, J = 7.1 Hz, 2H), 3.87 (dq, J = 14.5, 7.3 Hz, 2H), 3.72 (dq, J = 14.3, 7.2 Hz, 2H), 1.48 (t, J = 7.3 Hz, 6H), 1.28 (t, J = 7.1 Hz, 3H).

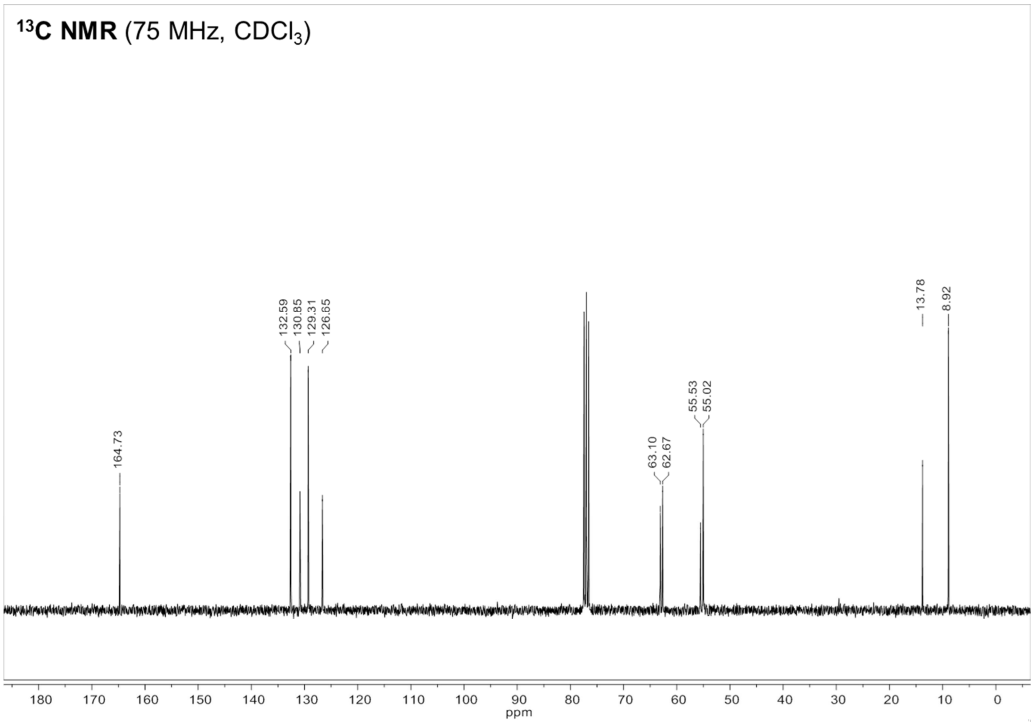


**Figure S5.2**: $^{13}C$ NMR spectrum of N-Benzyl-N-(ethoxycarbonylmethyl)-N,N-diethyl-ammonium bromide. 75 MHz, $CDCl_3$: δ = 164.73 (q), 132.59 (+), 130.85 (+), 129.31 (+), 126.65 (q), 63.10 (-), 62.67 (-), 55.53 (-), 55.02 (-), 13.78 (+), 8.92 (+).

**IR ν [$cm^{-1}$]:** 3038 (w), 2978 (m), 2941 (w), 1756 (s), 1461 (m), 1252 (w), 1204 (s), 1055 (m), 999 (m), 857 (m), 798 (m), 757 (s), 701 (s).

**MS (ESI):** m/z (%) = 250.2 (100, $M^+$).

**HRMS (ESI):** calcd. for $C_{15}H_{24}NO_2$ ($M^+$), m/z = 250.1802; found 250.1806.

**Step 2:** Synthesis and characterization of the final product N-Benzyl-N-carboxymethyl-N,N-diethylammonium (Compound 3) from the intermediate N-Benzyl-N-(ethoxycarbonylmethyl)-N,N-diethylammonium bromide (Compound 2)

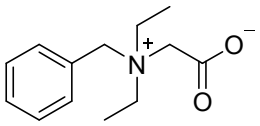

Chemical Formula: $C_{13}H_{19}NO_2$
Molecular Weight: 221,30

Compound **2** (3.04 g, 9.20 mmol) was dissolved in water (34 mL), and 1.05 equiv. of silver(I) oxide (2.24 g, 9.66 mmol) was added. The suspension was stirred for 20 h in the dark. The precipitate was filtered off. The solvent was removed by lyophilisation. The remaining off-white solid was purified by automated flash column chromatography (dichloromethane/methanol: 3% → 10% methanol). Betaine **3** was obtained as hygroscopic crystalline, white solid (1.76 g, 7.95 mmol, 86 %).

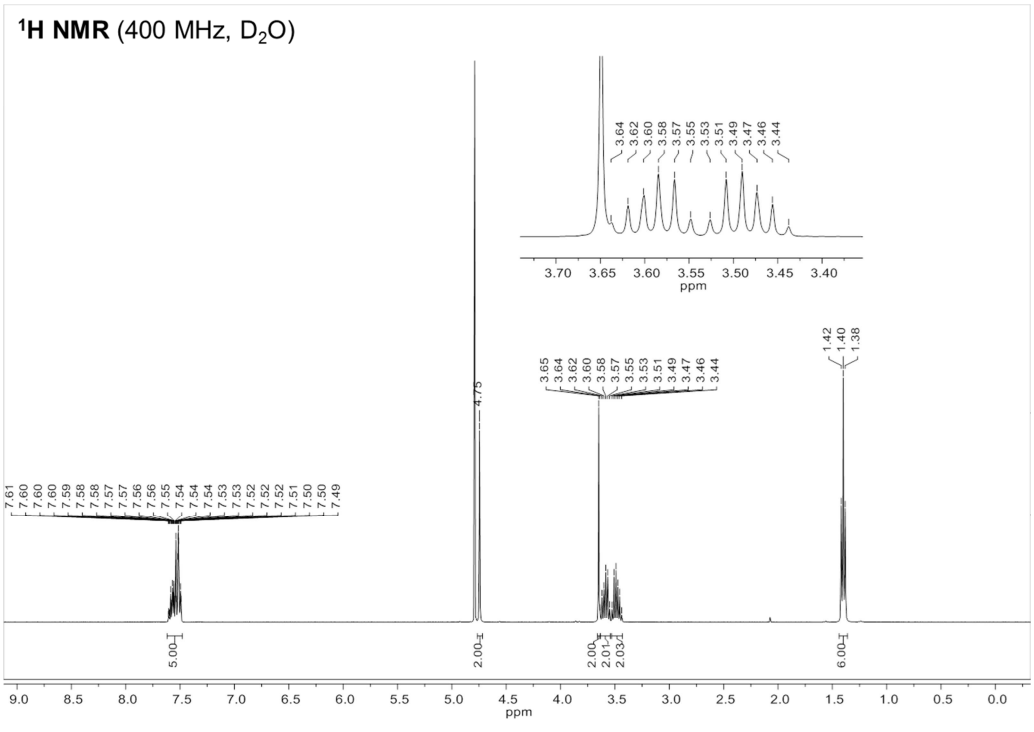


**Figure S5.3**: $^1$H NMR spectrum of N-Benzyl-N-carboxymethyl-N,N-diethylammonium. 400 MHz, $D_2O$: δ [ppm] = 7.61 – 7.48 (m, 5H), 4.75 (s, 2H), 3.65 (s, 2H), 3.59 (dq, J = 14.5, 7.5 Hz, 2H), 3.48 (dq, J = 14.2, 7.3 Hz, 2H), 1.40 (t, J = 7.3 Hz, 6H).

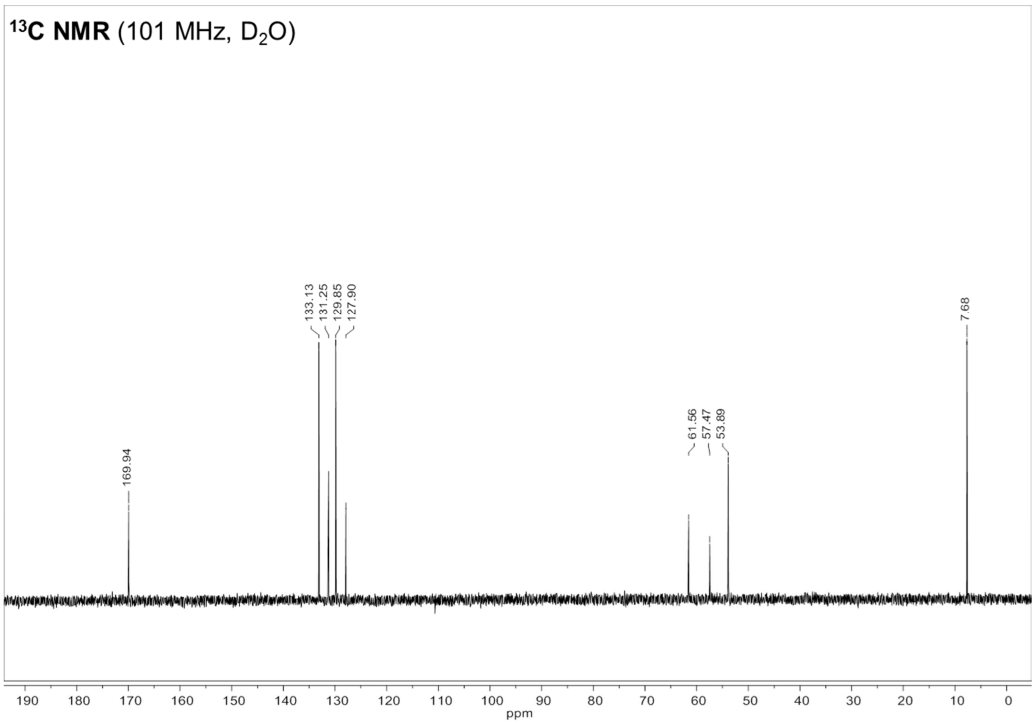


**Figure S5.4**: $^{13}$C NMR spectrum of N-Benzyl-N-carboxymethyl-N,N-diethylammonium. 101 MHz, $D_2O$: δ [ppm] = 169.94 (q), 133.13 (+), 131.25 (+), 129.85 (+), 127.90 (q), 61.56 (-), 57.47 (-), 53.89 (-), 7.68 (+).

**IR ν [cm$^{-1}$]:** 3392[a] (w), 3034 (w), 2989 (w), 1625 (s), 1461 (m), 1405 (m), 1375 (m), 1215 (w), 1156 (w), 1118 (w), 1036 (m), 992 (m), 924 (w), 898 (w), 865 (m), 798 (m), 760 (s), 716 (s).

**MS (ESI):** m/z (%) = 222.1 (100, $MH^+$), 443.3 (3, $2MH^+$).

**HRMS (ESI):** calcd. for $C_{13}H_{20}NO_2$ $(M+H)^+$, m/z 222.1489; found 222.1496.

[a] traces of water due to hygroscopic properties

### 5.8.2 Sample treatment and sample analysis

***Samples from WWTPs***

Effluent grab samples from 22 different WWTPs taken in the federal state of Baden-Württemberg (Germany) in 2015, as well as two samples from Swiss and one sample from an Italian treatment plant (sampling details in Lege et al., 2017), were filtered through regenerated cellulose syringe filters (Captiva RC, 0.2 µm pore size, Agilent Technologies) prior to analysis with an LC-HRMS method similar to the one described in chapter 5.3.5. Large-volume injection (i.e. 100 µl) was always performed and a slightly different gradient was applied for the chromatography of the German WWTP effluent samples: at 0 min 95% A, at 17 min 10% A, at 17.1 min 0% A, at 22 min 0% A, at 22.1 min 95% A, and at 29 min 95% A. Samples from pilot-scale ozonation of conventionally treated wastewater were evaluated in a different context before (Merel et al., 2017), but served here again for the investigation of denatonium removal. 100 µl of filtered samples were analyzed by the method described in chapter 5.3.5, with only the following adjustment to the LC gradient: at 0 min 95% A, at 1 min 95% A, at 15 min 10% A, at 15.1 min 0% A, at 23 min 0% A, followed by re-equilibration to 95% A for 7 min. *All Ion* measurements were generally performed for these WWTP samples at an acquisition rate of 6 Hz, gaining alternately information about parent ions (at 0 V collision energy), as well as collision induced fragments (at 20 V and 40 V collision energy).

The 24-hour flow proportional composite influent and effluent samples, taken from a single WWTP over the duration of five days, were analyzed by UHPLC-HRMS. Chromatographic separation of analytes was performed using a 1290 Infinity II system (Agilent Technologies, Germany), consisting of a binary pump (G7120A), a multisampler (G7167B), and a column oven (G7116B). Analog to the other WWTP samples, particles were removed also here with a regenerated cellulose syringe filter, but a 1:5 dilution with tap water was applied as an additional treatment step. The required dilution ratio for the minimization of matrix effects was previously determined by recovery experiments with spiked reference standards. Diluted samples were kept in the multisampler at 8 °C and 50 µl was used as injection volume.

Analytes were separated on an Eclipse Plus C18 RRHD column (2.1 x 100 mm, 1.8 µm, Agilent Technologies, Germany) and the flowrate, as well as the column temperature, were always kept constant at 0.4 ml $min^{-1}$ and 30 °C, respectively.

Water + 0.1% FA (A) and methanol + 0.1% FA (B) were used here as eluents and the following gradient program was applied: at 0 min 95% A, at 18 min 0% A, at 22 min 0% A, at 22.1 min 95% A, and at 26 min 95%. Slightly different source conditions were used here for electrospray ionization in the 6550 Q-TOF: drying gas temperature 130 °C, drying gas flow 14 L $min^{-1}$, sheath gas temperature 400 °C, sheath gas flow 12 L $min^{-1}$, and a nebulizer pressure of 25 psi. The capillary and nozzle voltages were kept at 3500 V and 0 V for the here applied positive ionization mode, respectively. The reference solution was supplied here to the second nebulizer with an isocratic pump (G1310B, Agilent Technologies), delivering a constant flow of 100 µl $min^{-1}$ for a set flow of 1 ml $min^{-1}$ and a 1:10 split. Data were recorded here also in the *All Ion* mode, with the same settings as described before.

***River water samples***

Grab and 2-hour composite samples taken from the river Ammer in the summer 2014 were initially adjusted with 1 M HCl to pH 7 ± 0.1. Particles were removed subsequently by filtration with a bottle-top vacuum filtration unit through a glass microfiber filter (Whatman® GF/F,0.7 µm average pore size). Oasis® HLB cartridges (60 mg sorbent, Waters) were conditioned by passing 3 ml of a 1:1 (v/v) ethyl acetate (EtAc, HPLC grade, Acros, Belgium) - methanol (MeOH, Optima LC/MS grade, Fisher Scientific) mixture and 3 ml MeOH through each cartridge. Equilibration of the sorbent was performed with 3 ml 5 mM ammonium acetate ($NH_4Ac$, Optima LC/MS grade, Fisher Scientific) adjusted to pH 7, prior to the loading of 50 ml surface water samples at a flowrate of about 2 ml $min^{-1}$. Generally, all surface water samples were kept on ice for the complete extraction procedure to reduce any bias by potential degradation reactions. The bed was washed after sample loading with 2 ml of the 5 mM, pH-adjusted $NH_4Ac$ solution, followed by a drying step with nitrogen for 5 min. Elution of analytes was performed twice with 2 ml EtAc:MeOH (1:1,v/v) each time and the extraction solvent was collected in a single vial. The solvent was added here with a flowrate of 1 ml $min^{-1}$, equilibrated with the sorbent for 1 min, followed by a 1 ml air push to improve solvent recovery. Extracts were evaporated to dryness at 40 °C with a gentle stream of nitrogen and analyte reconstitution was finally performed in 1 ml of a water-acetonitrile (ACN, Optima LC/MS grade, Fisher Scientific) mixture (95:5, v/v). The extracts were transferred to HPLC vials, sealed with Teflon lined caps, and stored in the fridge at about 8 °C.

In 2014, 26 grab samples were taken along the complete length of the river Rhine. Large volume injection of 100 µl onto the HPLC column was performed for these samples, independent if they were treated by centrifugation (6000 rpm for 10 min) or by solid phase extraction. The latter was described in Merel et al., 2018, enriching analytes 100 fold on Bond Elut Plexa cartridges (Agilent Technologies). In contrast, injection volumes were reduced to 10 µl for extracts of Ammer river water samples, as higher micropollutant concentrations were expected here. However, the same LC-MS method was applied to all samples. Analyte separation was performed on a HSS T3 column (C18, 2.1 x 75 mm, 2.5 µm, Waters) using a constant flowrate of 0.4 ml $min^{-1}$ and a column temperature of 40 °C. Water + 0.1% FA (A) and ACN + 0.1% FA (B) were used here as eluents and the following gradient program was used: at 0 min 95% A, at 1 min 95% A, at 15 min 10% A, at 15.1 min 0% A, at 23 min 0% A, followed by re-equilibration to 95% A for 7 min. The Q-TOF mass spectrometer was operated under the same conditions as described in chapter 5.3.5. *All Ion* measurements were performed here at an acquisition rate of 3 Hz, gaining alternately information about parent ions (at 0 V collision energy), as well as collision induced fragments (at 20 V and 40 V collision energy).

### 5.8.3 Additional information for the photodegradation experiment

UV/visible absorption spectra of 10 mg $L^{-1}$ denatonium benzoate in 20 mM $NH_4FA$ buffer were recorded with a photoLab® 6600 UV-VIS spectrophotometer (WTF, Germany) and are shown in Figure S5.5. The buffer was either adjusted to pH3, pH7 or pH11, respectively, and solutions without the target compound were used for blank subtraction.

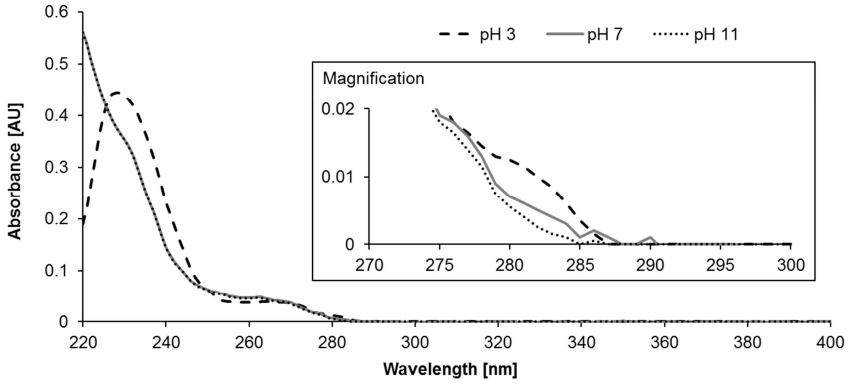


**Figure S5.5**: UV-Vis absorbance spectra between 220 nm and 400 nm for 10 mg $L^{-1}$ denatonium benzoate in $NH_4FA$ buffer.

The influence of the pH on the absorbance spectra can be traced back to benzoic acid, which is the predominant counterion in commercial denatonium products. Benzoic acid has a pKa value of 4.2 (https://pubchem.ncbi.nlm.nih.gov/, PubChem) and a predicted one of 4.08 (https://chemicalize.com/, ChemAxon). Denatonium in contrast has a predicted pKa value of 12.1 for the hydrogen atom in the amide moiety. However, neither denatonium nor benzoic acid absorb light with wavelengths ≥ 290 nm at any investigated pH, which would be the relevant range for direct photodegradation.

The two water matrices, i.e. the filtered river water and the pH-adjusted LC/MS grade water, were evaluated with respect to their dissolved organic carbon (DOC) content and to the present ions. The results are summarized in Table S5.1.

**Table S5.1**: Properties of the two water matrices used for the photodegradation experiments. Ions marked with an asterisk were detected below the limit of quantification, while n.d. indicates they were not detected.

| | LC/MS grade water (pH adjusted) | River water | Limit of quantification (LOQ) |
|---|---|---|---|
| pH | 8.4 | 8.2 | |
| conductivity [µS $cm^{-1}$] | 11 | 1180 | |
| DOC [mg $L^{-1}$] | 0.5 | 2.2 | |
| **Anions [mg $L^{-1}$]** | | | |
| $F^-$ | < 0.1* | 0.2 | 0.1 |
| $Cl^-$ | 0.8 | 56.2 | 0.1 |
| $NO_2^-$ | n.d. | n.d. | 0.1 |
| $Br^-$ | n.d. | n.d. | 0.1 |
| $NO_3^-$ | n.d. | 30.1 | 0.1 |
| $PO_3^{2-}$ | n.d. | n.d. | 0.3 |
| $SO_4^{2-}$ | n.d. | 320.6 | 0.3 |
| **Cations [mg $L^{-1}$]** | | | |
| $Na^+$ | < 0.1* | 26.9 | 0.1 |
| $NH_4^+$ | 0.4 | n.d. | 0.4 |
| $K^+$ | 1.0 | 5.3 | 0.1 |
| $Mg^{2+}$ | < 0.2* | 45.8 | 0.2 |
| $Ca^{2+}$ | 0.7 | 174.5 | 0.5 |

The light transmission curves for the two types of glassware used for the photodegradation experiment were provided by the manufacturing company La-Pha-Pack (Germany) and are shown in Figure S5.6.

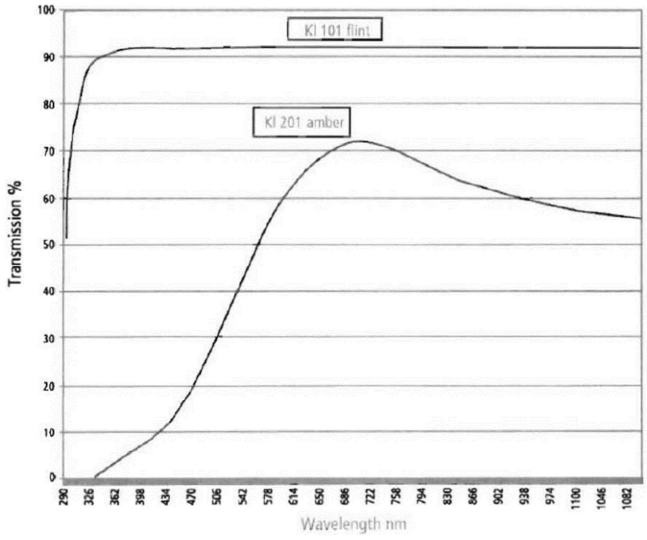


**Figure S5.6**: Typical light transmission curves of the glass vials used for the photodegradation experiments.

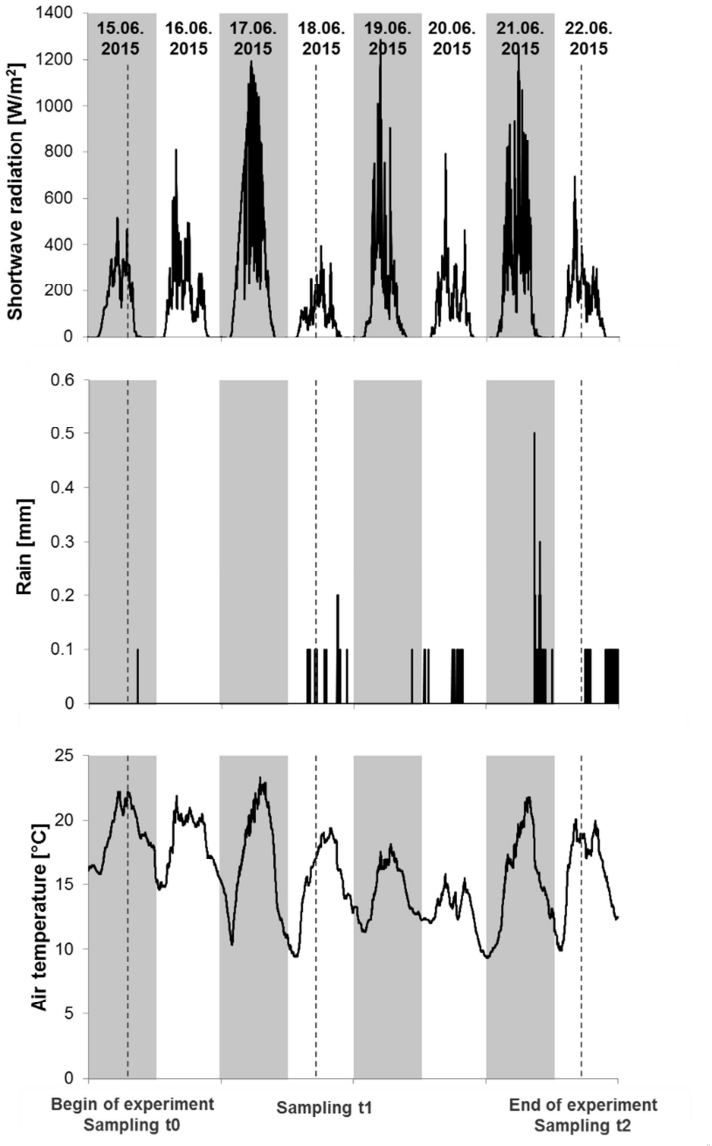


**Figure S5.7**: Detailed meteorological data recorded for the time course of the photodegradation experiment

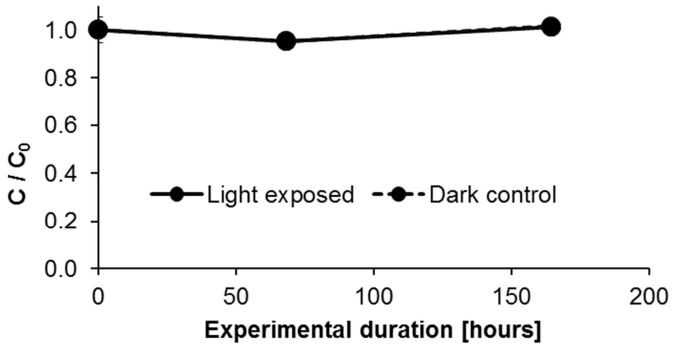


**Figure S5.8**: Time profile of the photodegradation of denatonium in the LC/MS grade water matrix. Data from the triplicate experiments were averaged here and the observed relative standard deviation was ≤ 0.05. No difference was observed between dark controls and light exposed samples.

### 5.8.4 Proposed collision induced dissociation pathway of denatonium

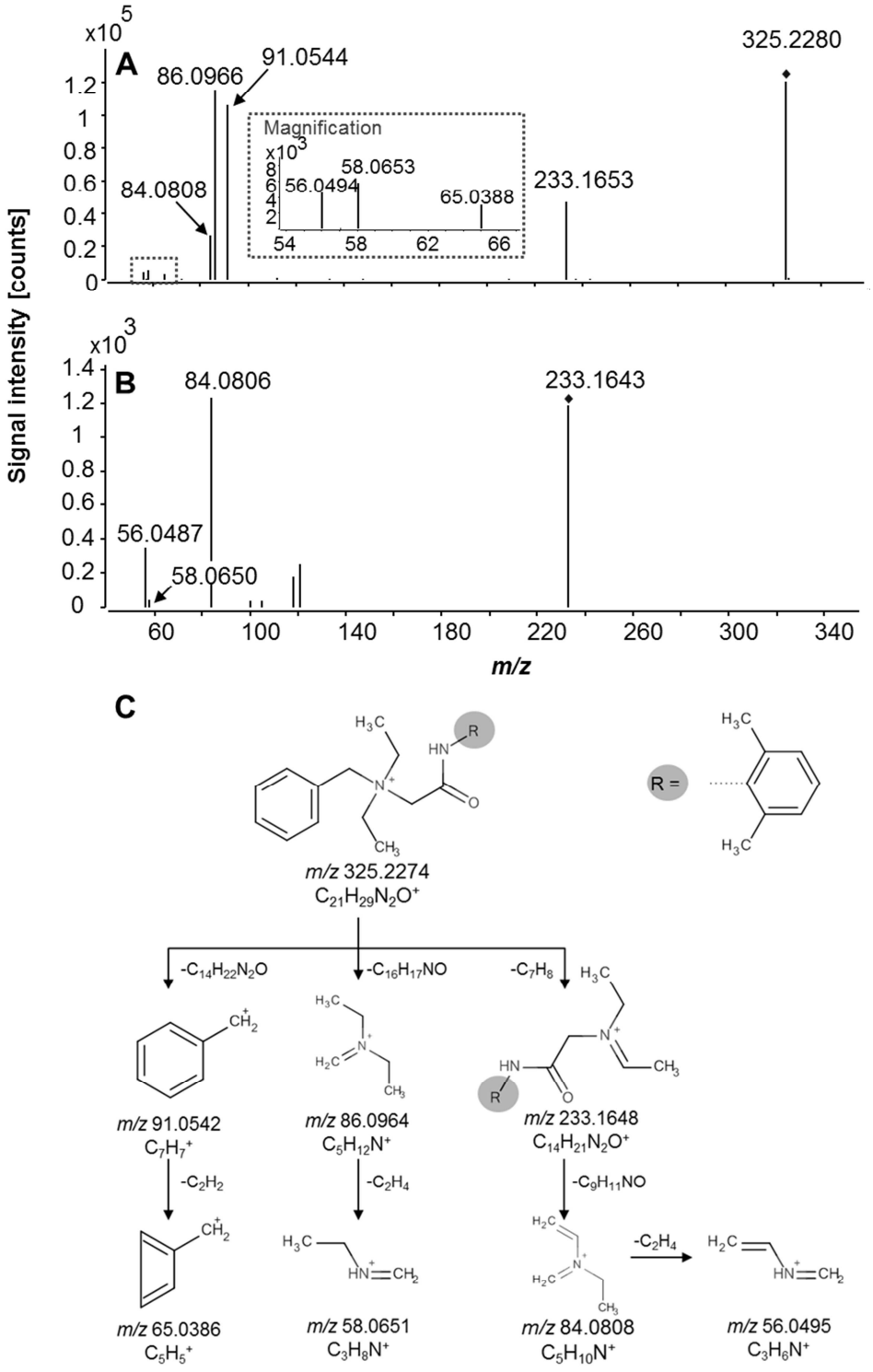


**Figure S5.9**: Merged MS/MS spectra of denatonium (A) and its in-source fragment *m/z* 233 (B) for three collision energies (10 V, 20 V, 40 V). Additionally, the proposed fragmentation pathway is shown including exact masses of the product ions (C). Non-averaged spectra of denatonium for the individual collision energies can be found in MassBank (https://massbank.eu) under the accession numbers TUE00281-TUE00283.

### 5.8.5 Identification of denatonium products observed after electrochemical oxidation and photodegradation

***TP 164***

An accurate mass of m/z 164.1431 was recorded for this TP, corresponding to an elemental composition of $C_{11}H_{17}N$ with an error of about -0.6 ppm. The MS/MS spectrum of this transformation product (Figure S5.10C) contains only three product ions, with m/z 91 ($C_7H_7^+$) and m/z 65 ($C_5H_5^+$) pointing towards the presence of a benzyl group in this compound. Considering the additional fragment m/z 72 ($C_4H_{10}N^+$) and the structure of the parent molecule, N,N-diethylbenzylamine is the most plausible identity of this analyte. Retention time and MS/MS spectrum matching with a reference standard confirmed this finally, achieving identification level 1.

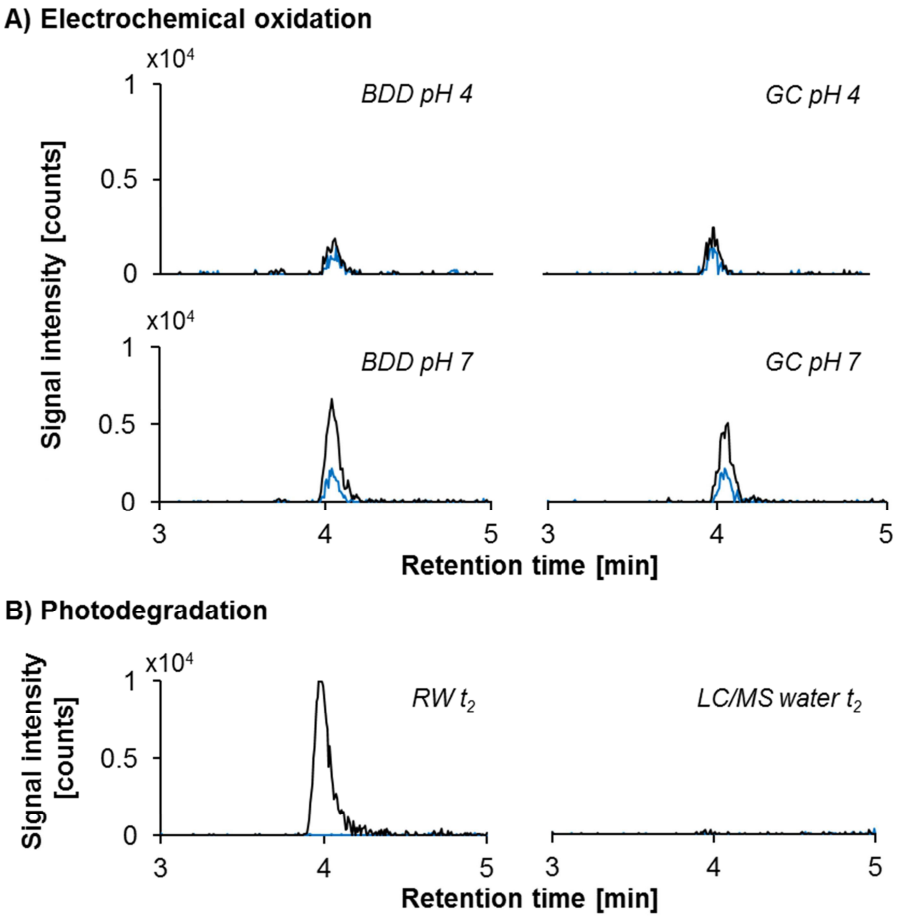


**Figure S5.10:** Extracted ion chromatograms for TP 164 ($C_{11}H_{17}N$, rt = 3.98 min) in samples from electrochemical oxidation (A) and photodegradation (B). The *m/z* 164.1434 was extracted with a mass tolerance of ± 10 ppm. Data are averaged for the triplicate samples, either from negative controls (solid blue line) or from degraded samples (solid black line).

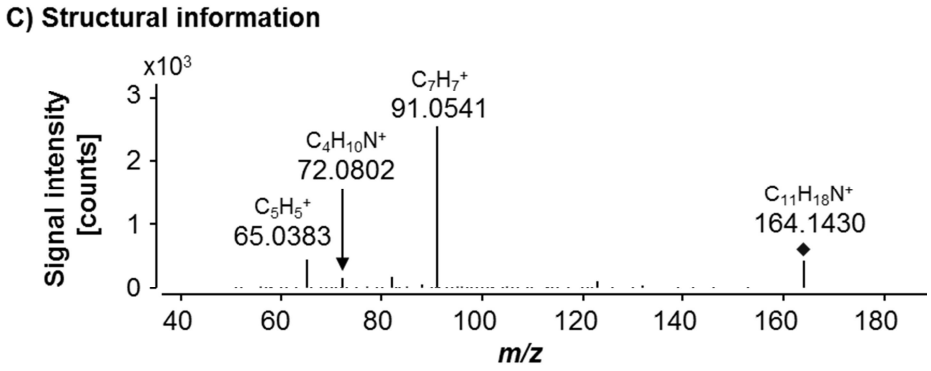


**Continuation of Figure S5.10**: The merged MS/MS spectrum for product ions recorded at 10 V, 20 V, and 40 V is shown in (C) and data were obtained for a reference standard. MS/MS spectra for a reference standard were also uploaded to the MassBank under the accession numbers TUE00831-TUE00833.

***TP 207***

Only a single major product ion (*m/z* 58, $C_3H_8N^+$) was observed for the analyte with the unequivocal molecular formula corresponding to $C_{12}H_{18}N_2O$ (Figure S5.11C). The absence of additional characteristic fragments suggested the loss of the benzyl moiety during the degradation process of denatonium, explaining an elemental difference of seven carbon and seven hydrogen atoms. The cleavage of the remaining two carbon atoms and four hydrogen atoms could be explained by an additional N-dealkylation step leading to the loss of an ethyl group. Performing a database search in PubChem (https://pubchem.ncbi.nlm.nih.gov/search/) for the proposed structure putatively identified this compound as norlidocaine, a known metabolite of lidocaine, which was finally confirmed with a commercial standard (level 1).

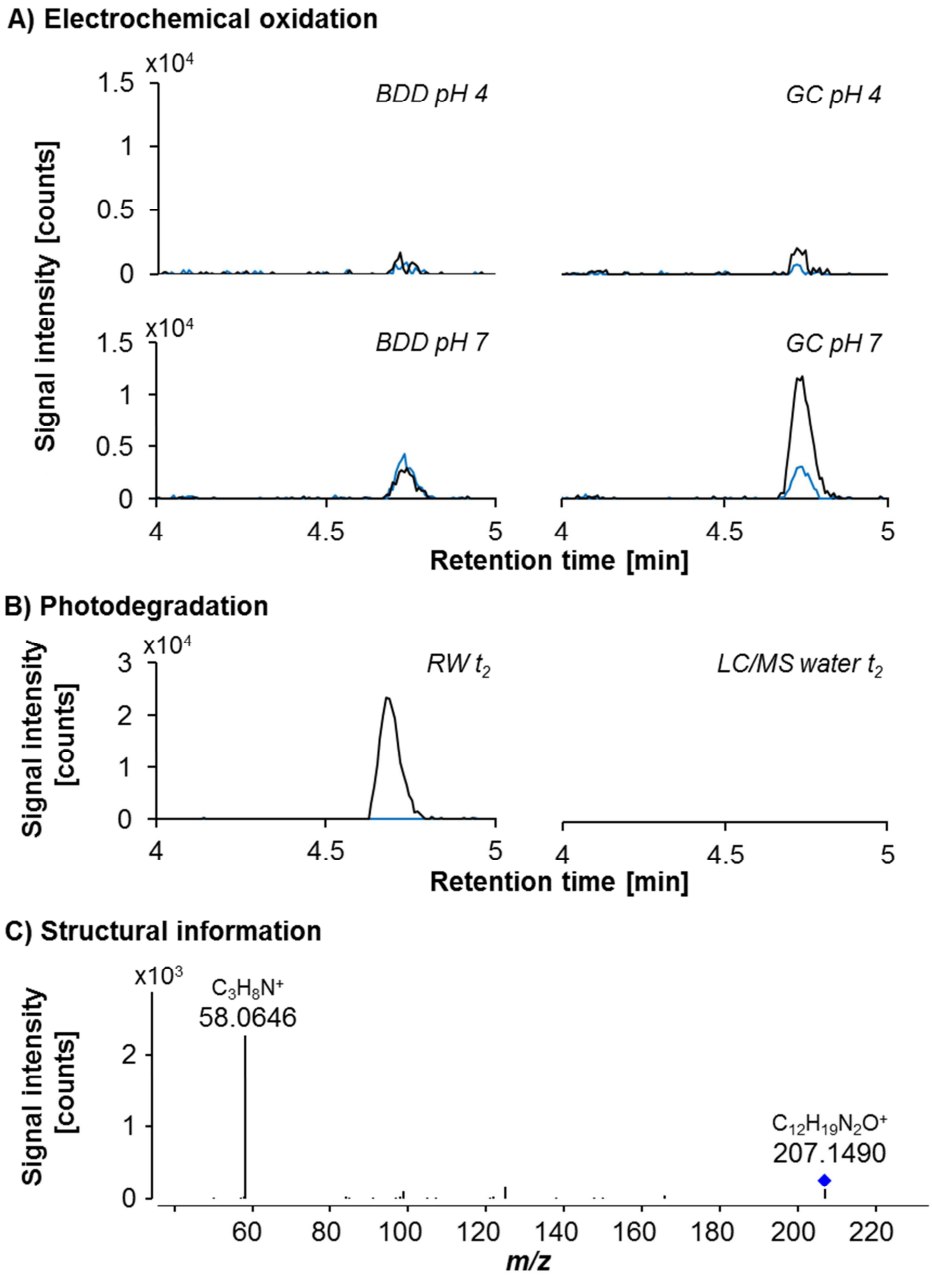


**Figure S5.11**: Extracted ion chromatograms for TP 207 ($C_{12}H_{18}N_2O$, rt = 4.70 min) in samples from electrochemical oxidation (A) and photodegradation (B). The *m/z* 207.1492 was extracted with a mass tolerance of ± 10 ppm. Data are averaged for the triplicate samples, either from negative controls (solid blue line) or from degraded samples (solid black line). The merged MS/MS spectrum for product ions recorded at 10 V, 20 V, and 40 V is shown in (C) and data were obtained for the photodegradation sample in the river water matrix at $t_2$. MS/MS spectra for a reference standard were uploaded to the MassBank under the accession numbers TUE00841-TUE00843.

***TP 221***

The elemental composition of $C_{13}H_{21}N_2O$ was assigned with a mass error of about -0.7 ppm to the most polar degradation product observed in this study. Characteristic product ions for the benzyl group (e.g. *m/z* 91), as well as the diethylamine moiety (e.g. *m/z* 86), were observed in the MS/MS spectrum (Figure S5.12C), suggesting that the quaternary ammonium structure of denatonium is conserved. In addition, a neutral loss of $NH_3$ (*m/z* 129 → *m/z* 112) points towards a primary amide group (Holcapek et al., 2010). The only plausible mechanism left therefore was the loss of the xylene group. TP 221 was putatively identified as benzyl(carbamoylmethyl)diethylazanium (level 2b), a compound which seems to be completely unknown so far, as it was not found in any of the large substance databases like PubChem or ChemSpider (http://www.chemspider.com/).

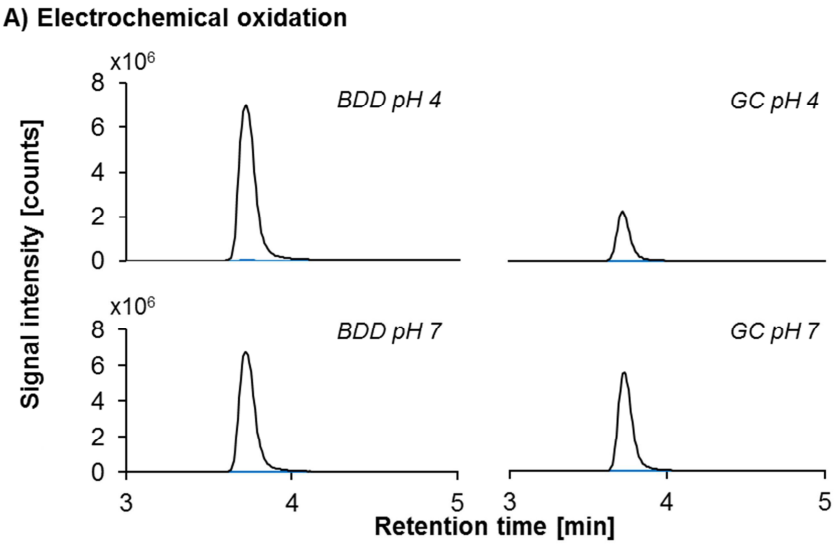


**Figure S5.12:** Extracted ion chromatograms for TP 221 ($C_{13}H_{21}N_2O$, rt = 3.68 min) in samples from electrochemical oxidation (A).

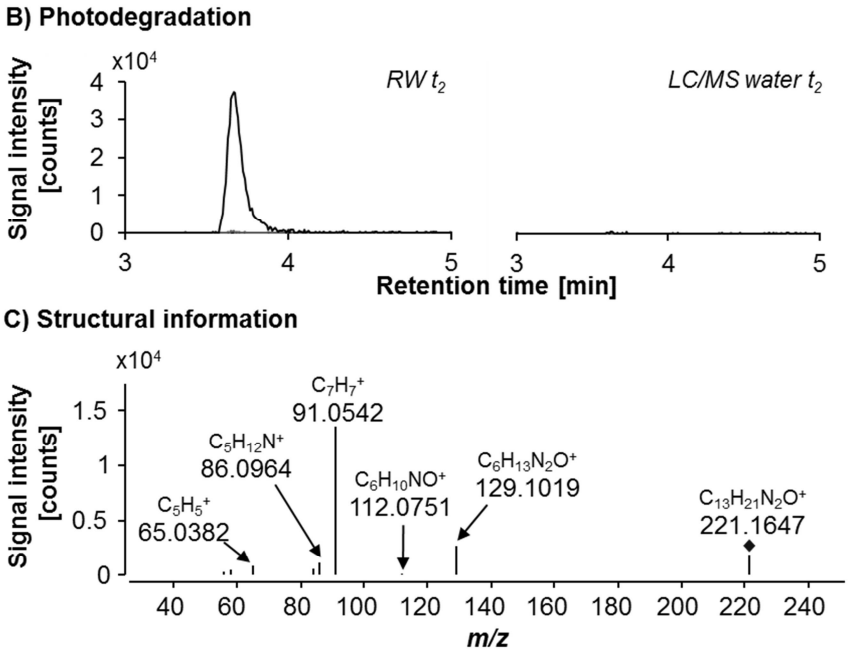


**Continuation of Figure S5.12**: Extracted ion chromatograms for TP 221 ($C_{13}H_{21}N_2O$, rt = 3.68 min) in samples from photodegradation (B). The *m/z* 221.1648 was extracted with a mass tolerance of ± 10 ppm. Data are averaged for the triplicate samples, either from negative controls (solid blue line) or from degraded samples (solid black line). The merged MS/MS spectrum for product ions recorded at 10 V, 20 V, and 40 V is shown in (C) and data were obtained for the sample taken after anodic oxidation with a BDD electrode at pH 4. Individual MS/MS spectra were uploaded to the MassBank under the accession numbers TUE00871-TUE00873.

***TP 222***

A formula of $C_{13}H_{20}NO_2$ could be assigned to this analyte. Fragmentation of this compound (Figure S5.13C) is rather similar to TP 221, suggesting that the benzyl and the quaternary ammonium moieties are also unchanged. The most probable suggestion to explain TP 222 with a formal loss of $C_8H_9N$ and a gain of O is an amide hydrolysis of denatonium, generating a carboxylic acid product, which is also predicted *in-silico* as putative microbial transformation product with the BioTransformer tool. The proposed structure was additionally supported by the characteristic behavior of TP 222 in the ionization source (compare to Fisher et al., 1994), as this analyte was the only quaternary ammonium compound in this study generating sodium or trifluoroacetic acid adducts in positive ($[M^+ - H + Na^+]^+$, *m/z* 244.1308) or negative ionization mode ($[M^+ - H + TFA^-]^-$, *m/z* 334.1272), respectively. Neither was a match found in any compound database for the proposed structure nor a commercial standard was available. Therefore, N-benzyl-N-carboxymethyl-N,N-diethylammonium was synthesized in a two-step reaction from diethylbenzylamine, verifying the proposed structure of TP 222 and achieving identification level 1.

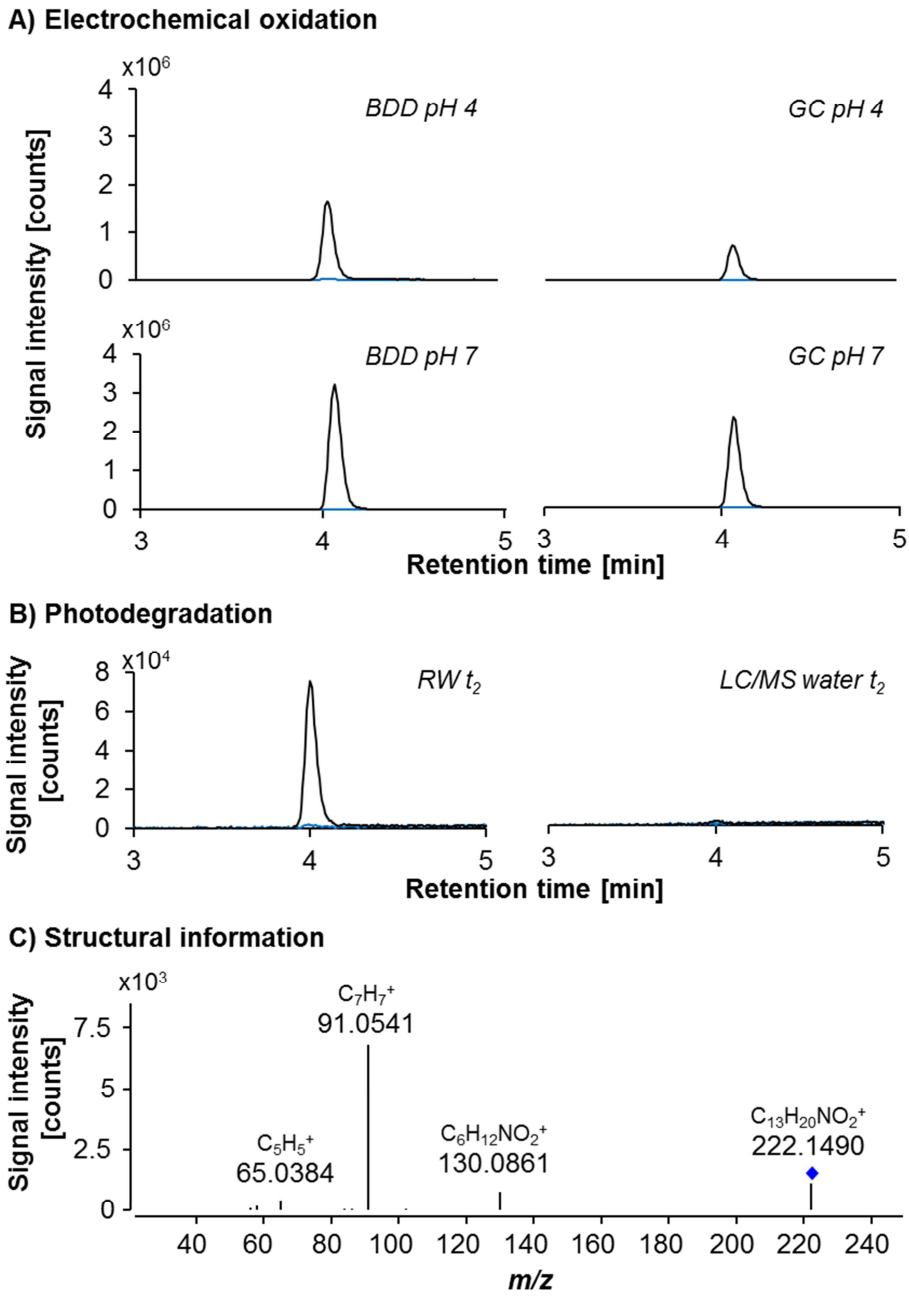


**Figure S5.13**: Extracted ion chromatograms for TP 222 ($C_{13}H_{20}NO_2$, rt = 4.03 min) in samples from electrochemical oxidation (A) and photodegradation (B). The *m/z* 222.1489 was extracted with a mass tolerance of ± 10 ppm. Data are averaged for the triplicate samples, either from negative controls (solid blue line) or from degraded samples (solid black line). The merged MS/MS spectrum for product ions recorded at 10 V, 20 V, and 40 V is shown in (C) and data were obtained for the sample taken after anodic oxidation with a BDD electrode at pH 7. MS/MS spectra for a reference standard were uploaded to the MassBank under the accession numbers TUE00851-TUE00853.

***TP 235***

The chemical formula $C_{14}H_{22}N_2O$ could be assigned with an error of 0.7 ppm and only two major product ions (*m/z* 58 and *m/z* 86) occurred (Figure S5.14C). The formal loss of $C_7H_7$ and the absence of the tropylium ion as fragment points to lidocaine, which was finally verified based on retention time and spectral matching with a reference standard (level 1).

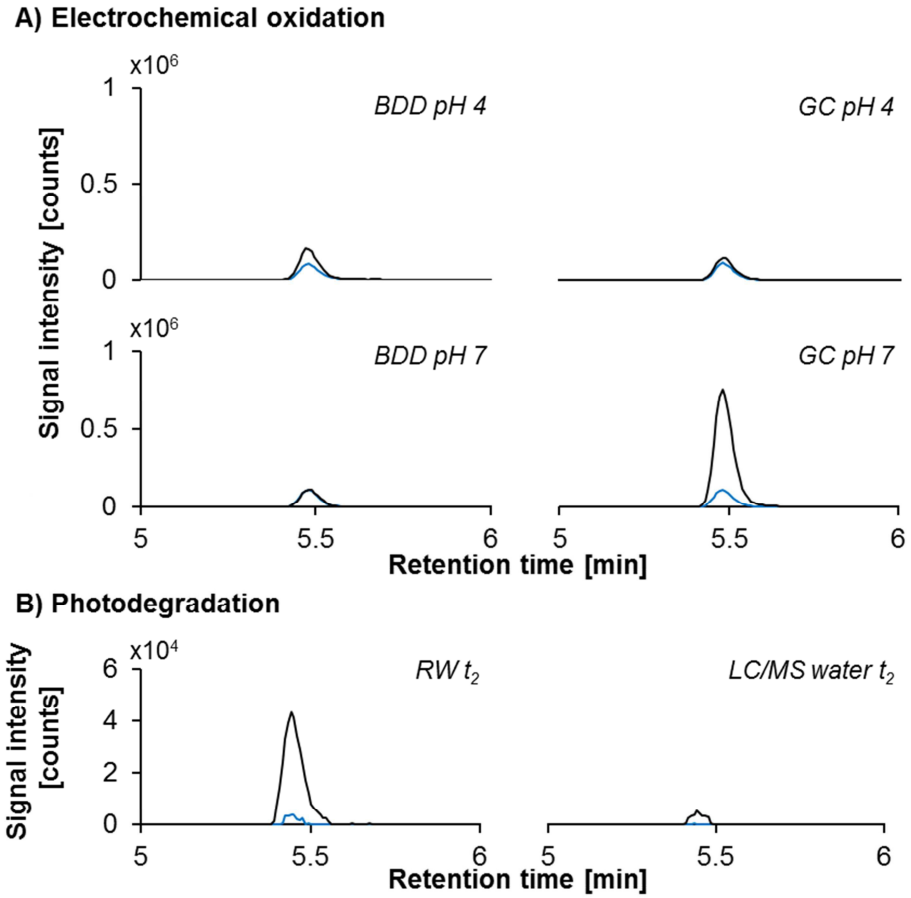


**Figure S5.14**: Extracted ion chromatograms for TP 235 ($C_{14}H_{22}N_2O$, rt = 5.45 min) in samples from electrochemical oxidation (A) and photodegradation (B). The *m/z* 235.1805 was extracted with a mass tolerance of ± 10 ppm. Data are averaged for the triplicate samples, either from negative controls (solid blue line) or from degraded samples (solid black line).

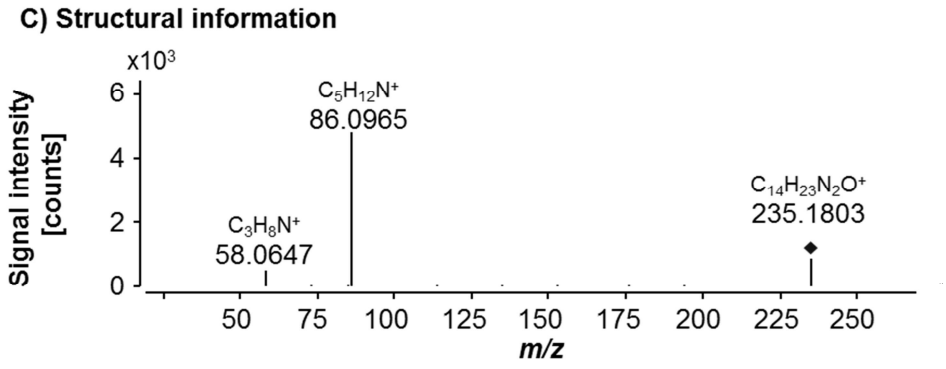


**Continuation of Figure S5.14**: The merged MS/MS spectrum for product ions recorded at 10 V, 20 V, and 40 V is shown in (C) and data were obtained for a reference standard. MS/MS spectra for a reference standard were also uploaded to the MassBank under the accession numbers TUE00461-TUE00463.

### *TP 341a-e*

Overall, five isomers were observed after anodic oxidation and indirect photodegradation, to which the molecular formula $C_{21}H_{29}N_2O_2$ could be assigned with a mass error of less than 1 ppm. The elemental composition of the analytes differed by a single oxygen atom to the parent compound, suggesting a mono-hydroxylation of denatonium. MS/MS spectra could be only recorded for TP 341a (Figure S5.15C), TP 341c (Figure S5.15D), and TP 341e (Figure S5.15E), as neither the chromatographic resolution nor the abundance of the two additional isomers promised high-quality structural information. Generally, all fragmentation patterns for the three isomers exhibited characteristic fragments for the diethylamine moiety (e.g. *m/z* 86), suggesting that no aliphatic hydroxylation at the ethyl groups took place. Furthermore, the characteristic tropylium cation (*m/z* 91) was observed for the products TP 341a and TP 341c, revealing an unchanged benzyl moiety for those analytes. In contrast, a product ion with *m/z* 107 ($C_7H_7O^+$) instead of *m/*z 91 was observed for TP 341e, which dissociated further into *m/z* 77 ($C_6H_5^+$). The formation of TP 341e was therefore related to an aromatic hydroxylation of the benzyl moiety. As the exact location of the hydroxylation could not be determined, the proposed structure was identified with a confidence level of 3. The fragmentation pattern of TP 341a generally resembled the one of denatonium itself and the only difference was observed for the azanium ion. The mass of this fragment was shifted in case of the transformation product by 16 Da to *m/z* 249, reflecting the incorporation of an additional oxygen atom.

As the hydroxylation of aromatic moieties containing electron donating substituents can be easily performed electrochemically (Johansson et al., 2007), it was concluded that the xylidine group was most likely modified in case of TP 341a.

However, it could not be determined which of the two possible positions, i.e. either in *para* or *meta* position to the amide moiety, was modified here (identification level 3). TP 341c was the only analyte for which a neutral loss of water was observed from the parent ion (*m/z* 341 → *m/z* 323). This initial dehydration process was most likely followed by the cleavage of the benzyl moiety, leading to the unmodified azanium ion with *m/z* 233. Direct loss of the benzyl group from the parent ion seemed to be of minor importance, as only traces of the hydroxylated species (*m/z* 249) could be observed here. In contrast to the other hydroxylated transformation products, an additional fragment was observed for TP 341c, i.e. *m/z* 146 ($C_{10}H_{12}N^+$). This product ion might originate from a cleavage of the quaternary ammonium moiety at the C8 atom (for numbering scheme see Figure 5.3) and a loss of oxygen from the carbonyl group. However, it was not possible to propose a structure that satisfied all those observations and the identification of TP 341c was therefore stopped at an unequivocal molecular formula (identification level 4). The same confidence level was achieved for the two additional isomers, TP 341b and TP 341d, as no further structural information were available for these analytes.

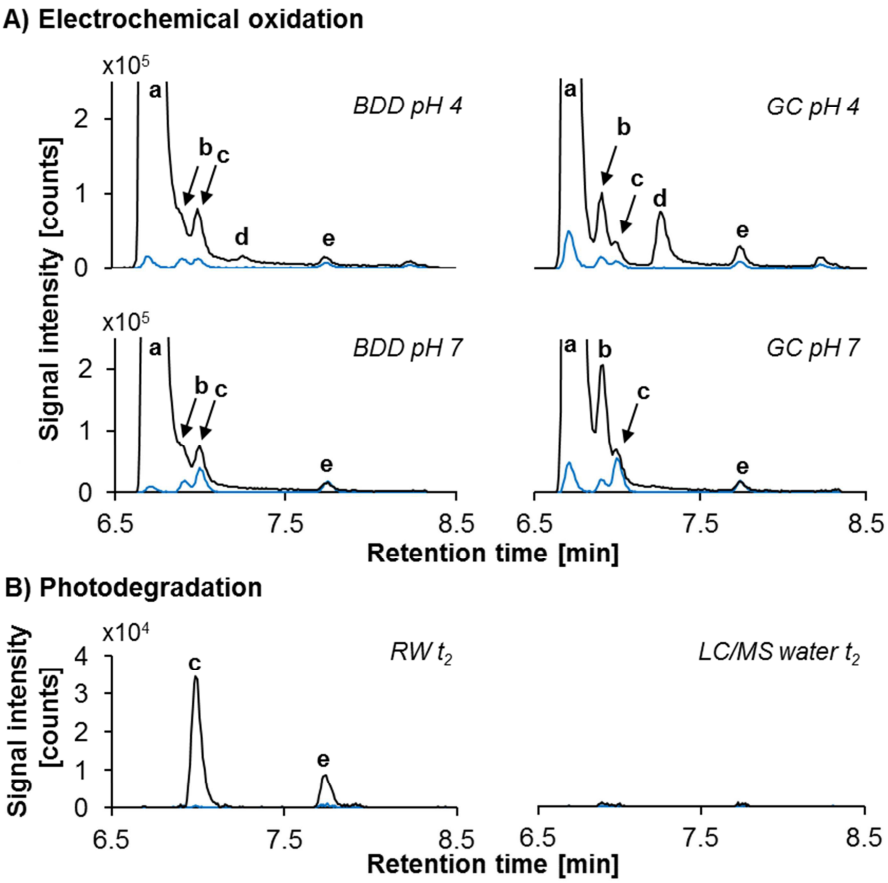


**Figure S5.15**: Extracted ion chromatograms for TP 341a-e ($C_{21}H_{29}N_2O_2$, retention times ranging from 6.71 min to 7.75 min for the five isomers) in samples from electrochemical oxidation (A) and photodegradation (B). The *m/z* 341.2224 was extracted with a mass tolerance of ± 10 ppm. Data are averaged for the triplicates, either from blanks (solid blue line) or from samples after treatment (solid black line).

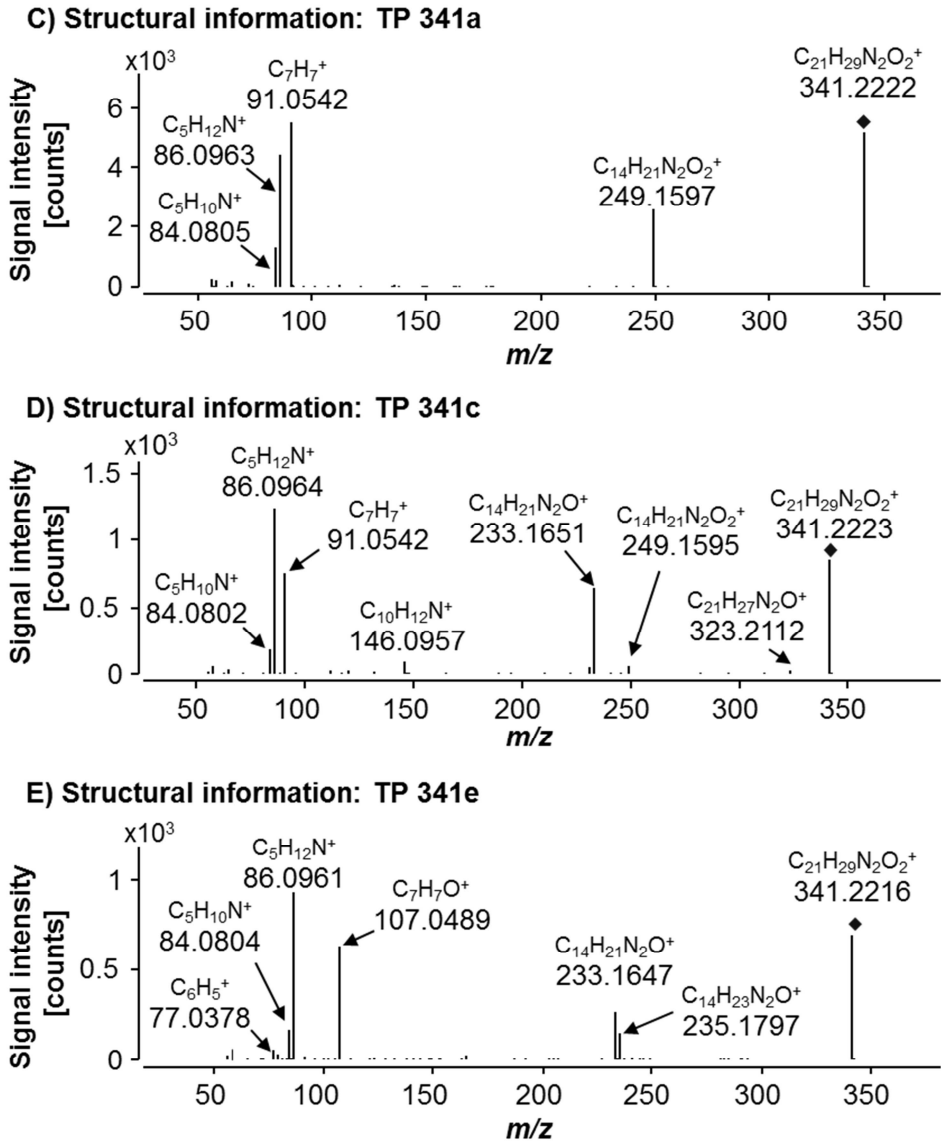


**Continuation of Figure S5.15**: The merged MS/MS spectra for product ions recorded at 10 V, 20 V, and 40 V are shown in (C) for TP 341a, in (D) for TP 341c, and in (E) for TP 341e. In case of TP 341a, data were obtained for the sample taken after anodic oxidation with a BDD electrode at pH 7. MS/MS spectra of TP 341c and TP 341e were recorded for the photodegradation sample in the river water matrix at $t_2$. MS/MS spectra were uploaded to the MassBank under the following accession numbers: TUE00881-TUE00883 (TP 341a), TUE00891-TUE00893 (TP 341c), and TUE00901-TUE00903 (TP 341e).

### 5.8.6 Screening for denatonium and its transformation products in WWTP samples

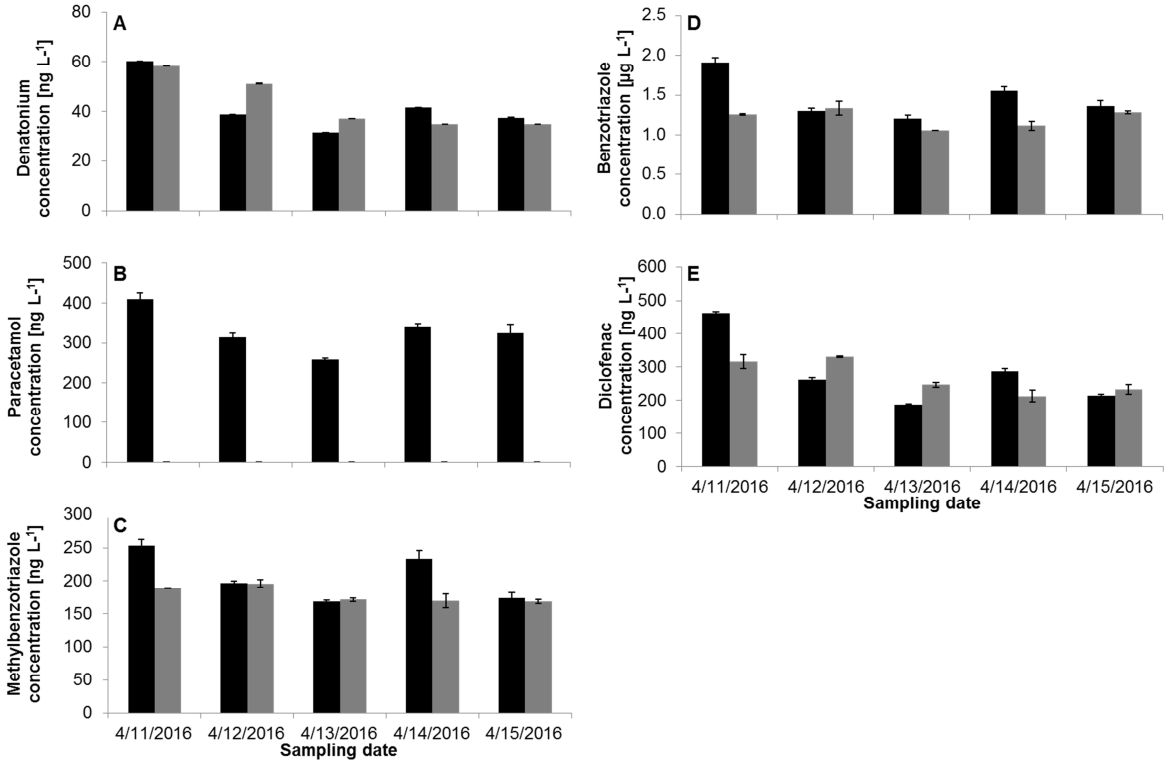


**Figure S5.16**: Measured concentrations of denatonium (A), paracetamol (B), 4- and 5-methylbenzotriazole (C), benzotriazole (D), and diclofenac (E) in 24 hour composite samples of a WWTP influent (black bars) and effluent (grey bars). Error bars represent the observed standard deviations for triplicate sample analysis.

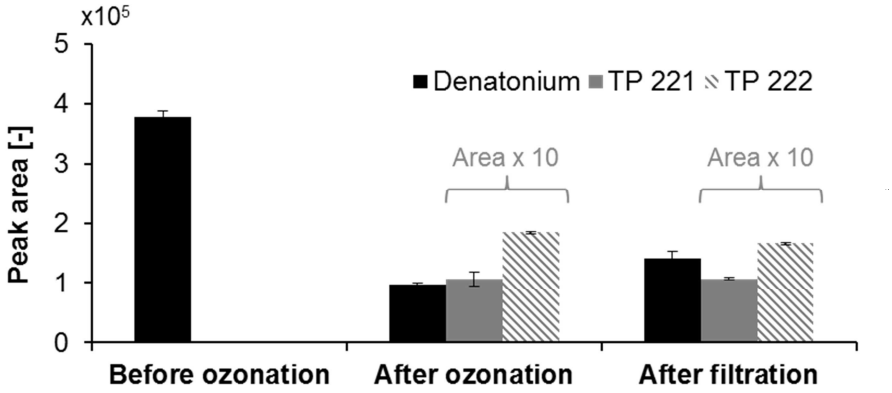


**Figure S5.17**: Peak areas of denatonium and its two transformation products TP 221 and TP 222 observed during a study applying pilot-scale ozonation to conventionally treated wastewater. Samples were taken before the ozone reactor, after the ozone reactor and from the effluent of a anthracite/sand filter. Data were average over triplicate injections of each sample and the error bars represent the standard deviation.

### 5.8.7 References

Babayan, A.T., Kocharyan, S. T., Ogandzhanyan, S. M., 1976. Investigations in the field of amines and ammonium compounds.: CXX. Synthesis of α-dialkylarylaminocarboxylates. Armyanskii Khimicheskii Zhurnal 29 (5), 403–408.

Lege, S., Guillet, G., Merel, S., Yanez Heras, Jorge Eduardo, Zwiener, C., 2017. Denatonium - A so far unrecognized but ubiquitous water contaminant? Water Research 112, 254–260.

Merel, S., Benzing, S., Gleiser, C., Di Napoli-Davis, G., Zwiener, C., 2018. Occurrence and overlooked sources of the biocide carbendazim in wastewater and surface water. Environmental Pollution 239, 512–521.

Merel, S., Lege, S., Yanez Heras, Jorge E, Zwiener, C., 2017. Assessment of N-Oxide Formation during Wastewater Ozonation. Environmental Science & Technology 51 (1), 410–417.

Ziegler, E., Wittmann, H., 1985. Über Reaktionen mit Betainen, 19. Mitt. Über den Einfluß der Substituenten am kationischen Zentrum von Betainen auf die Bildungstendenz der Di-trifluoracetyl-N-Ylide. Monatshefte für Chemie – Chemical Monthly 116 (6-7), 821–829.

# 6 Abiotic and biotic transformation of torasemide - Occurrence of degradation products in the aquatic environment

**Authors**

Sascha Lege, Julian Sorwat, Jorge Eduardo Yanez Heras, Christian Zwiener

University of Tübingen, Environmental Analytical Chemistry at the Center for Applied Geoscience, Hölderlinstraße 12, 72074 Tübingen, Germany

**Highlights**

- Overall sixteen abiotic and biotic products identified for torasemide.
- Formation of reactive products proven with trapping experiments using reduced glutathione.
- Torasemide and carboxytorasemide detected in all WWTPs and wastewater-impacted surface waters.

Submitted to the Elsevier journal *Water Research*.

## 6.1 Abstract

The pharmaceutical torasemide is an important loop diuretic and was 2017 one of the ten most prescribed drugs in Germany. Despite its detection in different compartments of the urban water cycle including drinking water, no studies were so far performed to elucidate its fate in the environment and the occurrence of transformation products (TPs). Therefore, we investigated the phototransformation, microbial degradation, transformation with human liver microsomes and anodic oxidation of torasemide to obtain good coverage of environmentally relevant degradation products. Overall sixteen products were identified, covering the following reaction mechanisms: aromatic and aliphatic hydroxylation, including further oxidation to carboxylic acids and quinone imines, amide cleavage, N-dealkylation, N-dearylation, and sulfonamide hydrolysis to sulfonic acids. Especially the formation of quinone imines could be of concern as they are highly reactive electrophiles. Torasemide itself was observed in all investigated wastewater treatment plant (WWTP) samples and wastewater-impacted surface waters. The maximum detected concentration was about 350 ng $L^{-1}$. Only three of the sixteen transformation products were generally observed in at least one of the samples and the most frequently detected TPs were the human metabolites hydroxytorasemide (TP 364a) and carboxytorasemide (TP 378a). The complete removal of TP 364a during wastewater treatment was in agreement with the results of microbial degradation experiments. TP 364a was most likely transformed into TP 378a, which was microbially less degraded in lab experiments. Based on estimated concentrations, TP 378a could reach about 1 µg $L^{-1}$ in the investigated wastewater matrices.

## 6.2 Introduction

Pharmaceuticals are generally considered an important group of anthropogenic micropollutants in aquatic environments, as they are designed to cause effects and often exhibit a rather high stability. After excretion from the human body or due to improper disposal, pharmaceuticals typically end up in sewer systems. However, many micropollutants are only insufficiently removed from sewage in wastewater treatment plants (WWTPs) (Margot et al., 2015), and therefore introduced by these point sources into the environment. Selected pharmaceuticals, e.g. carbamazepine, were already frequently detected in European surface waters (Loos et al., 2009) and low concentrations of human drugs could be sporadically observed in ground water (Loos et al., 2010) or even tap water (Jones et al., 2005).

Torasemide (or torsemide) is an important loop diuretic for the treatment of hypertension and edema. The compounds prescriptions increased continuously over the last decade in Germany, from almost 546 million defined daily doses (DDDs) in 2008 (Schwabe and Paffrath, 2009) to 876 million DDDs in 2017 (Schwabe et al., 2018). In 2017, torasemide was also one of the ten most prescribed drugs in Germany (Schwabe et al., 2018), with a prescribed amount of about 13 tons[a] for that year. Generally, the compounds gain in popularity can be linked to studies suggesting improved pharmacokinetics and further potential benefits of torasemide compared to other loop diuretics, like furosemide (Herchuelz et al., 1988, Buggey et al., 2015).

Several studies have already shown the presence of torasemide in the urban water cycle, even if is subjected to an extensive human phase I metabolism and only 20% of the drug are excreted unchanged via urine by healthy patients (Knauf and Mutschler, 1998). Measured concentrations varied from about 10 to 195 ng $L^{-1}$ for samples taken from WWTPs or surface waters receiving treated wastewater (Gros et al., 2012,Gurke et al., 2015,Singer et al., 2016,Ternes et al., 2019). In addition, the presence of this drug was proven in groundwater from a former wastewater infiltration site (Wode et al., 2015) and trace amounts (i.e. 1 ng $L^{-1}$) were even detected in drinking water (Gros et al., 2012).

The most important human transformation products are formed by aliphatic hydroxylation (TP 364a, for TP structures see Figure 6.2) and subsequent oxidation of the intermediate TP 364a into a carboxylic acid (TP 378a). These two metabolites actually account for more than 50% of an administered torasemide dose that can be recovered in urine patients, while less than 2% of torasemide are excreted via urine as the aromatic hydroxylation product TP 364b (Knauf and Mutschler, 1998). A recent study putatively identified carboxy torasemide in environmental samples by suspect screening (Ternes et al., 2019). The authors reported that higher signal intensities were observed for M5 compared to torasemide itself, which is in agreement with the excreted amounts of torasemide and its metabolites. In contrast hydroxytorasemide (TP 364a), another abundant metabolite, could not be detected above the limit of quantification, even in samples from a WWTP with the highest torasemide concentrations measured (Ternes et al., 2019).

[a] The amount of torasemide was estimated based on the prescribed DDDs in 2017 and the information from the WHO Collaborating Centre for Drug Statistics Methodology that one DDD is equivalent to 15 mg (WHO Collaborating Centre for Drug Statistics Methodology, December 13th, 2018).

Currently, there is no information available about the fate of torasemide once released into wastewater and ultimately into the environment. Therefore, the aim of this study is to provide a comprehensive overview on the possible formation of biotic and abiotic transformation products and their occurrence in WWTPs and surface waters.

## 6.3 Material and methods

### 6.3.1 Chemicals

Optima™ LC/MS grade acetic acid (HAc), acetonitrile (ACN), ammonium acetate ($NH_4Ac$), ammonium formate ($NH_4FA$), formic acid (FA), methanol (MeOH), and water were purchased from Fisher Chemical (Belgium). Ammonium hydroxide (LC-MS grade), reduced nicotinamide adenine dinucleotide phosphate (NADPH) tetrasodium salt (≥ 97%), and diclofenac (≥ 98%) were obtained from Sigma-Aldrich (Germany), while torasemide (≥ 98%) was purchased from TCI (Belgium), hydroxytorasemide (CAS 99300-68-2, ≥ 98%) from Toronto Research Chemicals (TRC, Canada). Reduced L-glutathione for biochemistry (≥ 98%) was supplied by Carl Roth (Germany). Anhydrous $K_2HPO_4$ (≥ 99%) and $KH_2PO_4$ (≥ 99%) for the phosphate buffer were obtained from Acros Organics (Belgium) and Merck (Germany), respectively. Human liver microsomes (HLMs) pooled from 50 different adult donors with mixed gender were purchased from ThermoFisher Scientific. The microsomal protein concentration of the obtained lot was 20 mg $ml^{-1}$ and the cytochrome P450 content was about 0.344 nmol P450 per mg protein.

Individual stock solutions of diclofenac, torasemide, and hydroxytorasemide were prepared in MeOH with an analyte concentration of 1 g $L^{-1}$. A working solution containing all analytes was also prepared in MeOH with a final concentration of 10 mg $L^{-1}$ and all subsequent dilutions were prepared using tap water. Stock and working solutions were stored in the freezer at -18 °C, while the dilutions in tap water were kept in the fridge at 8 °C. Solutions stored in the freezer were renewed once per year, while dilutions in tap water were prepared freshly after a maximum storage duration of one week.

### 6.3.2 WWTP and surface water samples

In April 2015, grab samples were taken from the effluents of 22 different wastewater treatment plants (E1-E22) and six surface waters in the federal state of Baden-Württemberg (Germany). Three of the samples were taken from rivers impacted with treated wastewater (R1, R2, and R7) and three additional samples were taken from rivers not influenced by WWTP effluents (R3, R5, and R6).

Details about the sampling locations are provided in the supporting information of (Lege et al., 2017). LC-ESI-QqQ mass spectrometry was applied for the quantification of torasemide in these samples. Method details are summarized in section 6.3.7 of this publication.

Retrospective analysis of high-resolution mass spectrometric (HRMS) data of samples taken from WWTPs and wastewater impacted rivers was performed additionally to evaluate the occurrence of here identified transformation products of torasemide in the environment. The grab samples taken from effluents of the WWTPs E1-E22 in 2015 were investigated for this purpose, as well as additional samples that were taken from the plant E21 in April 2016. At WWTP E21 24-hour flow proportional composite samples were taken from the influent and effluent over the duration of five days. The river Ammer in the federal state of Baden-Württemberg (Germany) was chosen as an example to represent surface waters significantly impacted by treated wastewater. Therefore, 2-hour composite samples were taken from this river about 300 m downstream of a WWTP in summer 2014. The acquisition methods for HRMS measurements of these samples with LC-ESI-QTOF-MS are summarized in (Lege et al., 2019) and differed slightly from the method applied for the evaluation of transformation products of torasemide as described in section 6.3.8.

The WWTP and surface water samples were typically treated by filtration (regenerated cellulose, pore size: 0.2 µm, Captiva, Agilent Technologies, Germany) prior to analysis, except the ones taken from the river Ammer in 2014. Analytes in the Ammer river water samples were enriched 50 fold by solid phase extraction (SPE) on Oasis HLB® cartridges (Waters, USA). Details for the SPE method are given elsewhere (supporting information of Lege et al., 2019).

### 6.3.3 Electrochemical oxidation

Electrochemical degradation of torasemide was performed in a 12 ml PEEK cell using a boron-doped diamond electrode (BDD, DIACHEM® with a 10 µm diamond layer on Niobium substrate) from CONDIAS (Germany) as working electrode. The experiment was performed at about 22 °C and an active electrode area of about 3.2 $cm^2$. The counter electrode was an 8 mm x 4 mm platinum mesh (Sigma-Aldrich, USA). A Ag/AgCl electrode (3M, BASi, USA) served as reference. Degradation experiments were performed with 20 mM $NH_4FA$ solutions containing 10 mg $L^{-1}$ torasemide adjusted either to pH 3 or pH 7 with formic acid and ammonium hydroxide.

The working electrode and the counter electrode were immersed in two different compartments of the PEEK cell, which were separated by a Vycor® porous glass frit. Adequate mixing of the solution in the oxidizing compartment, i.e. with the working electrode, was achieved by gentle magnetic stirring (300 rpm). Experiments were performed in triplicates at different pH values. Control samples were taken from the oxidizing compartment of the cell before and treated samples after the application of +1.5 V vs. Ag/AgCl with an Autolab PGSTAT101 potentiostat (Metrohm, Germany) for 10 min. The samples were directly transferred to HPLC brown glass vials and either kept unmodified, diluted with tap water as control for the addition of reduced glutathione (GSH), or spiked with a freshly prepared aqueous solution of GSH at a final concentration of 10 mg $L^{-1}$. The vials were sealed with Teflon lined caps, and stored at 8 °C. Analysis was performed with LC-HRMS within 48 h after the electrochemical degradation. The BDD electrode was cleaned electrochemically in pH-adjusted ammonium formate buffer without torasemide. For this cleaning 150 square-wave pulses between -2 V and +2 V vs. Ag/AgCl were alternately applied for 1 s each. Possible organic deposits on the counter electrode were removed after the last electrochemical experiment of a day by heating up the platinum mesh with a Bunsen burner until it is red-hot.

### 6.3.4 Photodegradation with natural sunlight

Solutions for the photodegradation experiment were prepared by adding torasemide to a final concentration of 100 µg $L^{-1}$ either to LC/MS grade water (pH 8.4 at 20 °C, DOC = 0.5 mg $L^{-1}$, conductivity = 11 µS $cm^{-1}$, nitrate ≤ 0.1 mg $L^{-1}$) or to pH-adjusted river water (final pH 8.2 at 20 °C, DOC = 2.2 mg $L^{-1}$, conductivity = 1180 µS $cm^{-1}$, nitrate = 30.1 mg $L^{-1}$). In addition, the same concentration of diclofenac was spiked separately to LC/MS grade water, serving as positive control for direct photodegradation. Generally, 50 ml of the solutions were filled either to 60 ml clear glass vials (light exposed samples) or to 60 ml amber glass vials wrapped with aluminum foil (dark controls). All vials were closed with PTFE covered screw caps. Duplicate samples were generally prepared for each condition. An outdoor experiment was performed in summer 2015, exposing the solutions for about 7 days to natural sunlight. 100 µl samples were withdrawn from the vials at the beginning of the experiment (t0), as well as after 20 h (t1), 44 h (t2), 68 h (t3), 92 h (t4), and 165 h (t5) of exposure to sunlight, respectively.

After the experiment the samples were immediately diluted 1:10 with LC/MS grade water, transported on ice to the laboratory and stored there at 8 °C until LC-HRMS analysis. Further details about the experiment, including meteorological data, are summarized in a previous publication (Lege et al., 2019).

### 6.3.5 Liver microsomal incubations

A mixture of microsomal protein and torasemide, dissolved in 100 mM phosphate buffer (prepared from $KH_2PO_4$ and $K_2HPO_4$ and adjusted to pH 7.4 with 1 M phosphoric acid), was pre-incubated for 2 min at 37 °C. After the addition of NADPH, the mixture was further incubated for 60 min at 37 °C. Every 10 min, tubes were taken briefly out of the water bath and shaken manually. The total volume of the incubation mixture was 200 µl with the following final concentrations: 0.5 mg $ml^{-1}$ microsomal protein, either 1 µM or 10 µM torasemide, and 10 mM NADPH. The incubation was terminated by the addition of 400 µl ice-cold acetonitrile for the precipitation of proteins. After centrifugation (at 10000 g for 5 min), the supernatant was diluted 1:10 (v/v) with tap water and analyzed by LC-ESI-MS. All incubations were performed in triplicates and two torasemide concentrations were investigated to identify putative substrate inhibition. Negative control incubations were carried out without the cofactor NADPH and samples for the zero time point were obtained by terminating the reaction immediately after the addition of NADPH.

### 6.3.6 Aerobic microbial degradation with sewage sludge

The microbial transformation experiment was initiated by adding 544 µg torasemide to 400 g activated sludge in glass flasks (giving an initial concentration of about 1.36 µg torasemide per gram aqueous sludge). The experiment was performed in duplicates for three weeks in a dark room, which was air-conditioned to 22 °C. The reactors were continuously stirred with magnetic stirrers and aerated with aquarium pumps to guarantee aerobic conditions. Evaporative water loss was balanced by refilling the flasks to their initial weight, minus the previously taken sample volume. This was always performed before new 2 ml samples were withdrawn. Sampling started 10 min after the addition of torasemide and was performed subsequently on a daily basis. The samples were filtered through cellulose acetate syringe filters (0.45 µm pore size, Agilent Technologies) and stored frozen at -20 °C before analysis. Limitation of nutrients was avoided by adding 1 ml of a complex substrate mixture (20 g $L^{-1}$ NaCl, 2 g $L^{-1}$ $MgCl_2 \cdot 6\ H_2O$, 0.3 g $L^{-1}$ KCl, 5 g $L^{-1}$ yeast extract, 5 g $L^{-1}$ trypton, and 3 g $L^{-1}$ glycerol) every two days to the reactors containing activated sludge.

Control samples were taken from reactors with activated sludge without torasemide, and from others with only water and torasemide, to elucidate background contaminants and abiotic hydrolysis.

### 6.3.7 Target analysis using LC-ESI-QqQ mass spectrometry

The separation of analytes was performed using a 1260 Infinity I HPLC system (Agilent Technologies, Germany), consisting of a degasser, a binary pump, an autosampler, a thermostat, and a column oven. Samples were kept in the autosampler at 10 °C. Direct aqueous injection of 100 µl of filtered surface water and WWTP samples were used for analysis. A Poroshell EC-C18 column (2.1 x 100 mm, 2.7 µm, Agilent Technologies, Germany) coupled to a Poroshell EC-C18 guard column (2.1 x 5 mm, 2.7 µm, Agilent Technologies, Germany) was used as stationary phase, which was kept at a constant temperature of 40 °C. The mobile phases used were (A) water + 0.1% HAc + 0.1 mM $NH_4Ac$ and (B) ACN + 0.1% HAc. The following gradient program was used for separation: at 0 min 98% A, a linear decrease to 20% A within 17 min, at 17.1 min 0% A, at 23 min 0% A, at 23.1 min 98% A, and at 32 min 98% A. The flowrate was always kept constant at 0.4 ml $min^{-1}$.

Determination of analytes was achieved after LC separation with a 6490 triple quadrupole mass spectrometer (Agilent Technologies, Germany) using the positive ionization mode. The ESI source was operated under the following conditions: drying gas temperature 150 °C, drying gas flow 16 L $min^{-1}$, sheath gas temperature 400 °C, sheath gas flow 12 L $min^{-1}$, and a nebulizer pressure of 35 psi. The capillary and nozzle voltages were kept at 2500 V and 300 V, respectively. Nitrogen, produced on-site with a nitrogen generator from Peak Scientific (Germany), was used as drying, sheath and nebulizing gas, while the collision cell was supplied with ultra-pure nitrogen (≥ 99.999%) from Westfalen AG (Germany).

Two MRM transitions were monitored for torasemide in a window ± 0.6 min around the compounds retention time of 9.3 min. The transition from the protonated parent ion *m/z* 349.1 to the fragment *m/z* 264.1 was recorded for a collision energy of 16 eV and used as quantifier. The analytes identity was additionally verified by the second transition from the protonated parent ion *m/z* 349.1 to the product ion *m/z* 168.1. A collision energy of 48 eV was applied for this qualifier. Dwell times were automatically adjusted by the acquisition software at a constant scan rate of 3 Hz for each transition and were always ≥ 10 ms.

### 6.3.8 Suspect and non-target screening applying high-resolution mass spectrometry

#### 6.3.8.1 LC-ESI-QTOF analysis

Chromatographic separation of analytes was performed using a 1260 Infinity HPLC system (Agilent Technologies, Germany). Samples were kept in the autosampler at room temperature (23 ± 2 °C) and the injection volume was typically 10 µl. Analytes were separated on a Poroshell EC-C18 column (2.1 x 100 mm, 2.7 µm, Agilent Technologies, Germany) coupled to a Poroshell EC-C18 guard column (2.1 x 5 mm, 2.7 µm, Agilent Technologies, Germany). The flowrate was always kept constant at 0.4 ml $min^{-1}$ and the column was held at 40 °C. The mobile phases were (A) water + 0.1% FA and (B) ACN + 0.1% FA. The following gradient program was used for separation of analytes: at 0 min 95% A, linear increase to 30% A within 11 min, at 11.1 min 0% A, at 16 min 0% A, at 16.1 min 95% A, and at 23 min 95% A. The LC flow was diverted to the waste from 7.7 – 12 min for samples from electrochemical degradation experiments to prevent high torasemide concentrations from entering the mass spectrometer.

The HPLC system was connected to a 6550 iFunnel quadrupole time-of-flight (Q-TOF) mass spectrometer (Agilent Technologies, USA), equipped with an electrospray ionization (ESI) source and the Dual Spray Agilent Jet Stream technology. The Q-TOF was operated in the extended dynamic mode (2 GHz) for small molecules (≤ 1700 m/z). MS scans were performed at 2 Hz, while the acquisition rate was increased to 6 Hz for targeted MS/MS measurements for further structural characterization of the analytes. A narrow isolation width (~ 1.3 amu) was chosen for precursor ion selection and MS/MS spectra were recorded for collision energies of 10 eV, 20 eV, and 40 eV, respectively. Data were always recorded for a mass range of *m/z* 50 – 1000. The ESI source was operated under the following conditions: drying gas temperature 150 °C, drying gas flow 16 L $min^{-1}$, sheath gas temperature 400 °C, sheath gas flow 12 L $min^{-1}$, and a nebulizer pressure of 35 psi. The capillary and nozzle voltages were kept at 3500 V and 300 V for both ionization modes, respectively. A reference solution, containing purine and hexakis(1H,1H,3H-tetrafluoropropoxy)phosphazine (HP-0921), was continuously supplied to the ESI source with the second sprayer and used for automatic mass correction. The observed mass error was typically ≤ 5 ppm and a resolution of 20000 (FWHM) was achieved for analytes at about *m/z* 1000.

Nitrogen, produced on-site with a nitrogen generator from Peak Scientific (Germany), was used as drying, sheath and nebulizing gas, while the collision cell was supplied with ultra-pure nitrogen (≥ 99.999%) from Westfalen AG (Germany).

#### 6.3.8.2 Data processing and compound identification

The initial step of data evaluation was performed with the batch recursive extraction algorithm for small molecules in the MassHunter Profinder software (Version B.06.00, Agilent Technologies, USA). All information belonging to the same analyte, e.g. ion species and respective isotopologues, are gathered over multiple runs and combined in this tool as a single feature. Generally, a retention time window of 0.15 min and a mass window of 10 ppm + 2 mDa were applied here for feature alignment. Features that fulfilled abundance (height ≥ 5000 counts) and score (target score ≥ 80) requirements in all three replicates were finally exported for further statistical analysis.

Putative transformation products were extracted from the feature list based on the chemometric software package Mass Profiler Professional (MPP, version 14.9.1, Agilent Technologies, USA). Only compounds with a coefficient of variation ≤ 25 % for their intensities over all replicates were considered for subsequent filtration based on a volcano plot. Here, a moderated t-test, including the Benjamini Hochberg procedure to decrease the false positive rate for multiple testing, and a fold change (FC) analysis are combined, comparing experimental samples with their respective blanks. The p-value cut-off ($p < 0.02$) was chosen so that the number of features expected by chance, a value calculated by MPP, is close to zero. Peaks were only considered as putative transformation products if signal intensities were at least two times higher than in the control samples.

The features left after filtration with the MPP software were imported into the MassHunter Qualitative Analysis software (version B.07.00, Agilent Technologies, USA), where molecular formulas were assigned to them based on accurate masses and the observed isotope pattern. Shifts in the elemental composition between a putative transformation product and torasemide itself were compared to those listed for typical phase I reactions (Holcapek et al., 2008).

Additionally, literature was reviewed for transformation process already reported for other drugs, e.g. for anodic oxidation, and *in-silico* prediction of putative microbial degradation products of torasemide was performed with the EAWAG pathway prediction system (EAWAG-PPS, http://eawag-bbd.ethz.ch/predict/; accessed on November 24$^{th}$, 2019).

Product ion spectra from collision-induced dissociation were comprehensively interpreted when available to support or reject the proposed analyte structure, especially in comparison to the fragmentation pathway of the parent compound torasemide and its forced degradation products (Kurmi et al., 2017). The level of confidence for the compound identification was generally expressed in levels 1 to 5 according to (Schymanski et al., 2014), where level 1 corresponds to structures confirmed with reference standards and level 2 to probable structures with a library match or additional diagnostic evidence. Tentative candidates are communicated as level 3, and the lowest confidence is assigned to unequivocal molecular formulas (level 4) or accurate mass detected (level 5).

## 6.4 Results and discussion

### 6.4.1 Abiotic and biotic degradation of torasemide

Different degradation experiments were performed to obtain the best coverage of potential environmentally relevant transformation products (TPs) of torasemide. Incubations with liver microsomes should mimic the human phase I metabolism, while photolysis and microbial degradation experiments were performed to investigate the fate of this compound once released to wastewater and surface waters. Putative enzymatic reactions were additionally simulated by anodic oxidation. Trapping experiments with reduced glutathione were performed to reveal reactive TPs. The identification process of the products, as well as a discussion of their formation and potential toxicity in the context of available literature, is summarized in the following subchapters.

#### 6.4.1.1 Identification of transformation products

Post-acquisition data evaluation using suspect and non-target screening approaches revealed the formation of overall sixteen different transformation products by the investigated degradation processes. Torasemide and most TPs can be generally detected in the positive and negative ionization mode, and MS/MS spectra were usually recorded for both ESI modes to facilitate the structure elucidation.

Analyte identification was based on the initial assignment of the most plausible structures to unequivocal molecular formulas, applying biotransformation rules from *in-silico* tools or transformation mechanisms previously reported in literature. Furthermore, product ion spectra from collision-induced dissociation were comprehensively interpreted, especially in comparison to the fragmentation pathway of the parent compound torasemide (Kurmi et al., 2017). The complete identification procedure is exemplarily demonstrated below for the product TP 378a.

The unequivocal molecular formula of $C_{16}H_{18}N_4O_5S$ was assigned with a mass error of about -0.2 ppm to the transformation product TP 378a, which was only observed during biodegradation with activated sludge. *In-silico* prediction of microbial transformation with the EAWAG-PPS suggested 13 putative structures, which would explain the formal loss of two hydrogen atoms and the addition of two oxygen atoms compared to the parent compound. However, transformation processes modifying the isopropyl group (8 out of 13 products) could be rejected based on MS/MS information (Figure 6.1A), as the two dominant product ions *m/z* 294 and *m/z* 320 were generated through the loss of the unmodified N-isopropylformamide and isopropylamine moieties, respectively (Figure 6.1B).

The remaining *in-silico* products were all formed via oxidation of the methyl moiety of the tolyl group to an aldehyde, but involved either an additional aromatic hydroxylation or the subsequent oxidation of the aldehyde to a carboxylic acid. The latter species was already reported as the major human metabolite (Knauf and Mutschler, 1998) and was here the only structure where the most abundant product ions agreed with the previously reported dissociation pathway of torasemide (Figure 6.1B).

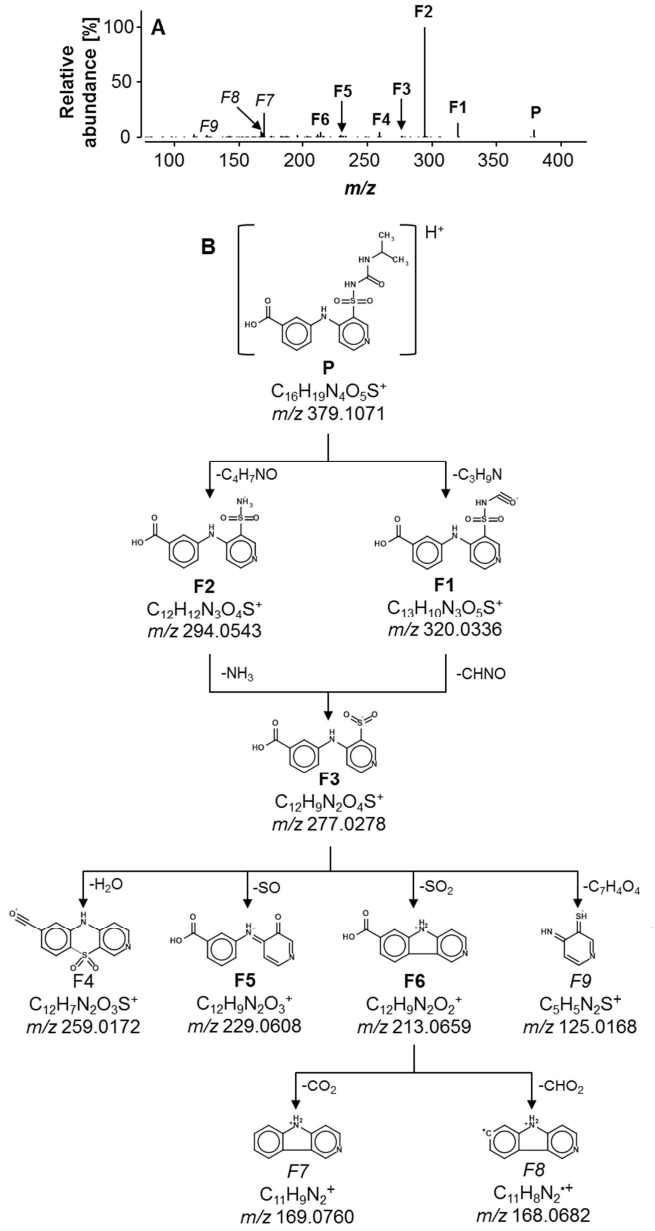


**Figure 6.1**:Product ion spectrum for the [M+H]+ of TP 378a, averaged over collision energies of 10 V, 20 V, and 40 V (A), as well as the proposed fragmentation pathway of this analyte (B). MS/MS information were recorded for a biodegradation sample after about 21 days. The pathway was mainly derived based on the previously described fragmentation behavior of torasemide (Kurmi et al., 2017) and structures of the parent ion (P) and the most characteristic fragments (F1-F9) are shown here. Only the proposed structure for F4 differs from the previously described torasemide fragmentation pathway. Indices highlighted in bold represent product ions including the carboxyl group, while this moiety is absent in ions highlighted in italic.

Similar to the positive ionization mode, the loss of N-isopropylformamide from the parent ion was also observed as a dominant fragmentation process in the ESI(-) mode (Figure S 6.16B in the supporting information). The resulting product ion with *m/z* 292 ($C_{12}H_{10}N_3O_4S^-$) fragmented further into *m/z* 248 ($C_{11}H_{10}N_3O_4S^-$) via the neutral loss of $CO_2$, a characteristic process for carboxylic acids (Holcapek et al., 2010).

Simple retention time models based on predicted logD values were already applied in the context of compound identification (Stanstrup et al., 2013) and this relationship was also qualitatively assessed here. The retention times and calculated logD values of TP 378a, torasemide and hydroxytorasemide correlated well (calculated for pH 4 with the partitioning plugin in MarvinSketch from ChemAxon, version 6.3.1): hydroxytorasemide (TP 364a) (rt = 5.98 min, logD = 0.33) < TP 378a (rt = 6.22 min, logD = 0.69) < Torasemide (rt = 7.99 min, logD = 1.61). Sufficient diagnostic evidence, based on MS/MS information and the elution behavior, was therefore collected to support the identification of TP 378a as the previously reported human metabolite with confidence level 2.

Available MS/MS spectra of additional products are documented in chapter 6.8.1 of the supporting information. Table 6.1 summarizes all products along with their retention times, monoisotopic mass of the protonated species, the observed mass error, and the chemical formulae. Furthermore, the confidence level according to (Schymanski et al., 2014), as well as the degradation experiments for which the respective TPs were observed, are shown here. Proposed analyte structures for TPs with a confidence level of 1 and 2 are shown in Figure 6.2. Reference standards were not available for the quantification of most TPs and it was therefore not possible to obtain complete mass balances for the degradation experiments. Although the investigation of multiple degradation processes suggests generally a good coverage of the most important transformation products, neither the formation of additional minor TPs nor a mineralization can be completely ruled out.

**Table 6.1**: Identified transformation products (TP) of torasemide ($C_{16}H_{20}N_4O_3S$, rt = 7.96 min, $[M+H]^+$ *m/z* 349.1329) observed after microbial degradation (Bio), anodic oxidation (EC), photolysis (Photo), and incubation with human liver microsomes (HLM). Peak intensities were normalized to the TP with the highest intensity within one treatment type (e.g. Bio or EC); mass error is calculated for the measured mass compared to the exact mass.

| **Transformation product** | **Retention time** [min] | **Exact monoisotopic mass of $[M+H]^+$** [*m/z*] | **Mass error** [ppm] | **Molecular formula** | **Relative abundance** [%] | | | | **Identification level** |
|---|---|---|---|---|---|---|---|---|---|
| | | | | | **Bio** | **EC** | **HLM** | **Photo** | |
| TP 102 | 1.46 | 103.0866 | 0.97 | $C_4H_{10}N_2O$ | n.d. | 17 | n.d. | n.d. | 2 |
| TP 173 | 0.84 | 174.0332 | 0.86 | $C_5H_7N_3O_2S$ | 6 | 5 | n.d. | n.d. | 2 |
| TP 258 | 1.95 | 259.0859 | 1.14 | $C_9H_{14}N_4O_3S$ | 13 | 84 | n.d. | 35 | 2 |
| TP 264 | 6.12 | 265.0641 | -0.64 | $C_{12}H_{12}N_2O_3S$ | n.d. | 1 | n.d. | n.d. | 2 |
| TP 278 | 2.12 | 279.0434 | 0.34 | $C_{12}H_{10}N_2O_4S$ | n.d. | 2 | n.d. | n.d. | 2 |
| TP 280 | 4.11 | 281.0591 | -0.59 | $C_{12}H_{12}N_2O_4S$ | n.d. | 1 | n.d. | n.d. | 2 |
| TP 306 | 6.16 | 307.0859 | -0.30 | $C_{13}H_{14}N_4O_3S$ | 14 | n.d. | 3 | n.d. | 2 |
| TP 320 | 5.57 | 321.0652 | -2.01 | $C_{13}H_{12}N_4O_4S$ | n.d. | 4 | n.d. | n.d. | 2 |
| TP 322 | 4.95 | 323.0809 | 0.57 | $C_{13}H_{14}N_4O_4S$ | n.d. | 2 | n.d. | n.d. | 2 |
| TP 362 | 7.63 | 363.1122 | 0.53 | $C_{16}H_{18}N_4O_4S$ | 8 | 100 | n.d. | 84 | 2 |
| TP 364a | 5.98 | 365.1278 | 0.78 | $C_{16}H_{20}N_4O_4S$ | n.d. | n.d. | 100 | n.d. | 1 |
| TP 364b | 6.64 | 365.1278 | 0.26 | $C_{16}H_{20}N_4O_4S$ | 12 | 68 | 6 | 100 | 2 |
| TP 364c | 7.45 | 365.1278 | 0.35 | $C_{16}H_{20}N_4O_4S$ | n.d. | 6 | n.d. | n.d. | 3 |
| TP 378a | 6.22 | 379.1071 | -0.20 | $C_{16}H_{18}N_4O_5S$ | 100 | n.d. | n.d. | n.d. | 2 |
| TP 378b | 6.91 | 379.1071 | 0.55 | $C_{16}H_{18}N_4O_5S$ | n.d. | 1 | n.d. | n.d. | 4 |
| TP 393 | 7.83 | 394.1180 | 0.13 | $C_{16}H_{19}N_5O_5S$ | n.d. | n.d. | n.d. | 99 | 4 |

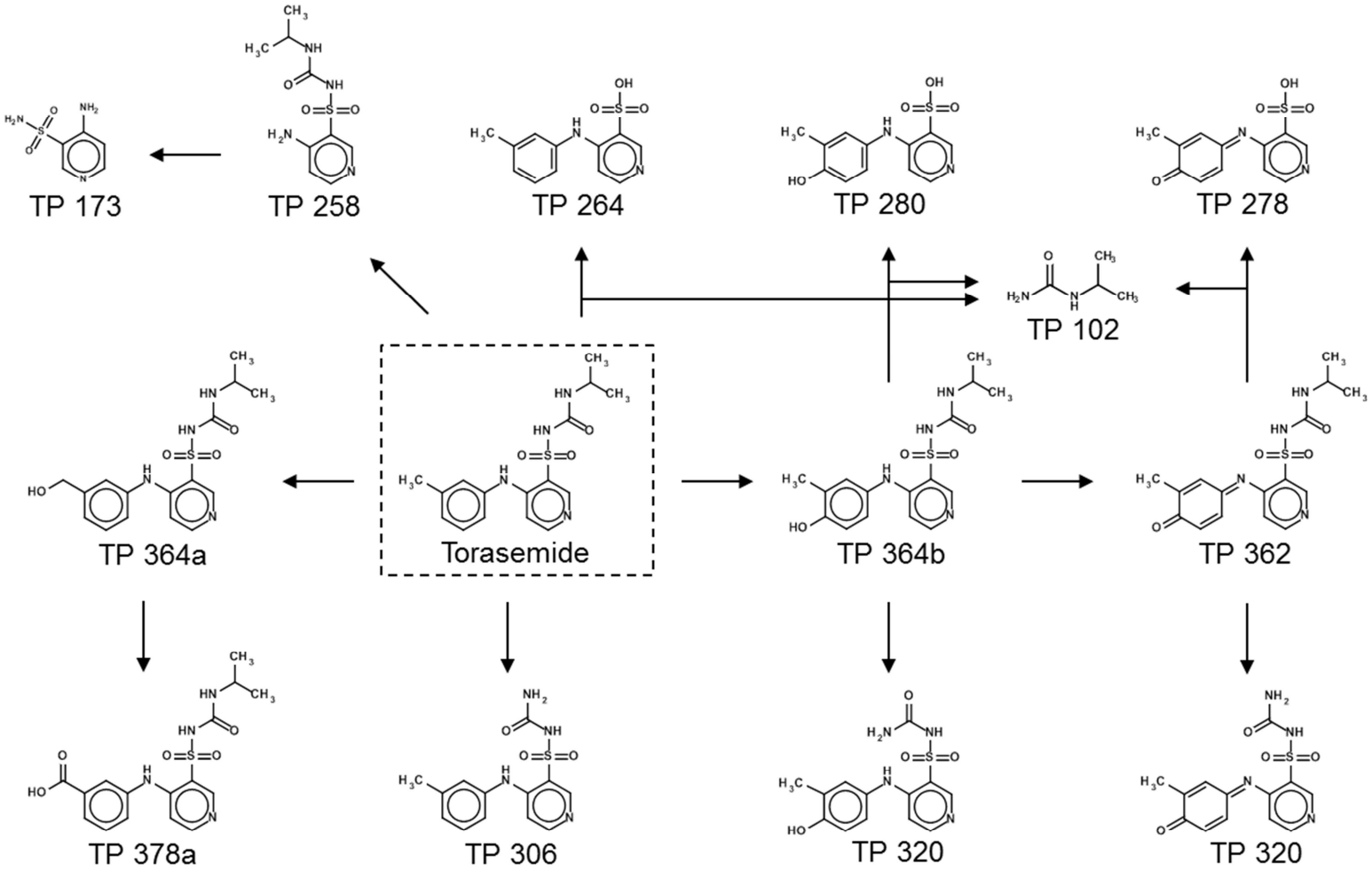


**Figure 6.2**: Proposed analyte structures of putatively identified transformation products with an identification level of 1 and 2.

### 6.4.1.2 Incubation with HLMs

When incubated with HLMs for 60 min in the presence of NADPH, torasemide concentrations decreased by 23% and 33% for initial drug concentrations of 10 µM and 1 µM, respectively (Figure 6.3). Concentration changes were generally not observed in control samples without the cofactor. The degradation of torasemide was accompanied with the formation of TP 364a, TP 364b and TP 306. The highest relative TP abundance was observed for the lowest dose of 1 µM torasemide. A concentration depended inhibition of the enzymatic process by the substrate was therefore assumed. TP 364a was by far the most abundant TP and appeared at a relative peak area of up to 11% of torasemide (Figure 6.3). TP 364b and TP 306 were with 6% and 3% of TP 364a much less abundant. These findings agreed only partially with the reported product spectrum for human metabolism (Barroso et al., 2001) with torasemide carboxylic acid (TP 378a) as the main metabolite. The hydroxylated tolyl species TP 364a found in the HLM experiments can be considered as a precursor of the human metabolite. The TPs 306 and 364b formed by N-dealkylation and aromatic hydroxylation, respectively, play only a negligible role in the excretion of torasemide. Reasons for incomplete oxidation by HLM could be a limitation of the cofactor NADPH and a different function of cytochrome P450 isoforms in the HLMs. For example, it is known that the formation of TP 364a is catalyzed predominantly by CYP2C9 (Miners et al., 1995).

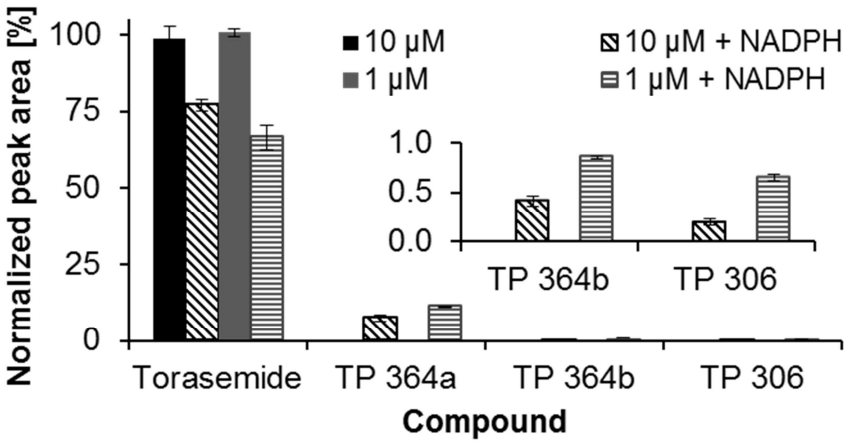


**Figure 6.3**: Remaining fraction of torasemide and normalized peak areas of generated transformation products after incubation with human liver microsomes for 60 min. Experimental conditions with and without NADPH are represented by striped and solid bars, respectively. Normalization was performed to the average peak area of torasemide determined in the control samples (i.e. without the cofactor NADPH) at the time zero (1 s error bars, n = 3).

#### 6.4.1.3 Anodic oxidation and identification of reactive metabolites

The successful mimicry of phase I metabolism by electrochemical techniques was already demonstrated before and investigated here as well for the simulation of putative enzymatic transformation processes. Independent of the pH, about 10% of the initial torasemide concentration was degraded applying a potential of 1.5 V vs. Ag/AgCl for 10 min (data not shown). EC treatment of torasemide produced 12 TPs. The most abundant TPs are the aromatic hydroxylation product TP 364b and its oxidation product TP 362 (quinone imine), and the N-dearylation product TP 258 (loss of the tolyl moiety). Electrochemical formation of transformation products was generally favored at a neutral pH, except for TP 258 in which case the product yield was increased almost 40-fold under acidic conditions (data not shown).

The minor human metabolite 4'-hydroxytorasemide (TP 364b) was the third most abundant degradation product after anodic oxidation of torasemide and accumulated to a relative amount of 68%. Aromatic hydroxylation via electrochemical degradation was already reported for other molecules before (Johansson et al., 2007) and the presence of electron-donating substituents, here the methyl group of the tolyl moiety, is generally considered beneficial for this process. In addition to TP 364b, another isobaric species (TP 364c) of significantly lower abundance (6%) was detected after electrochemical degradation of torasemide, eluting at a retention time of about 7.5 min. N-oxide formation was already demonstrated for torasemide in the presence of hydrogen peroxide (Kurmi et al., 2017). However, N-oxides elute typically later than their respective parent compound (Merel et al., 2017), a principle which held true also for torasemide on a reversed phase column (Kurmi et al., 2017). Due to an earlier elution of TP 364c compared to its parent molecule, the putative identification of this analyte as N-oxide was rejected. Aromatic hydroxylation was therefore left here as well as the most plausible mechanism of formation for this product. In contrast to incubations with liver microsomes, the hydroxylation of the methyl group generating TP 364a was not observed during anodic oxidation. This is generally owed to the high oxidation potential of hydrocarbons, preventing a direct electrochemical oxidation of aliphatic carbons (Jurva et al., 2003). This mechanism could however be simulated in principle by EC-Fenton systems involving reactive hydroxyl radicals (Johansson et al., 2007), but a similar setup was not evaluated here.

The quinone imine TP 362, a dehydrogenation product of TP 364b, was the most abundant transformation product observed after electrochemical degradation of torasemide. This product is of specific importance since the electrophilic compound is highly reactive and can directly react with a wide range of cell nucleophiles, e.g. DNA or proteins, or can generate reactive oxygen species through redox cycling (Klopčič and Sollner Dolenc, 2018). Deleterious effects, like hepatotoxicity, were associated with the formation of these reactive metabolites and were responsible for example for the market withdrawal of the antimalarial drug amodiaquine (Naisbitt et al., 1998). Also the anodic oxidation of paracetamol led to the formation of N-acetyl-p-benzoquinone-imine (NAPQI, Nematollahi et al., 2009). The identification of reactive TPs is often performed by trapping with nucleophiles and especially the reaction with reduced glutathione (GSH) has been applied in the context of an electrochemical simulation of phase I metabolism (Madsen et al., 2007). When GSH was added to the torasemide solution after anodic oxidation at pH 7, the concentration of the TP 362 decreased by more than 99% and three isobaric GSH-conjugates with an elemental composition of $C_{26}H_{35}N_7O_{10}S_2$ (TP 363, $C_{16}H_{18}N_4O_4S$, plus one GSH, $C_{10}H_{17}N_3O_6S$) could be observed (Figure 6.4).

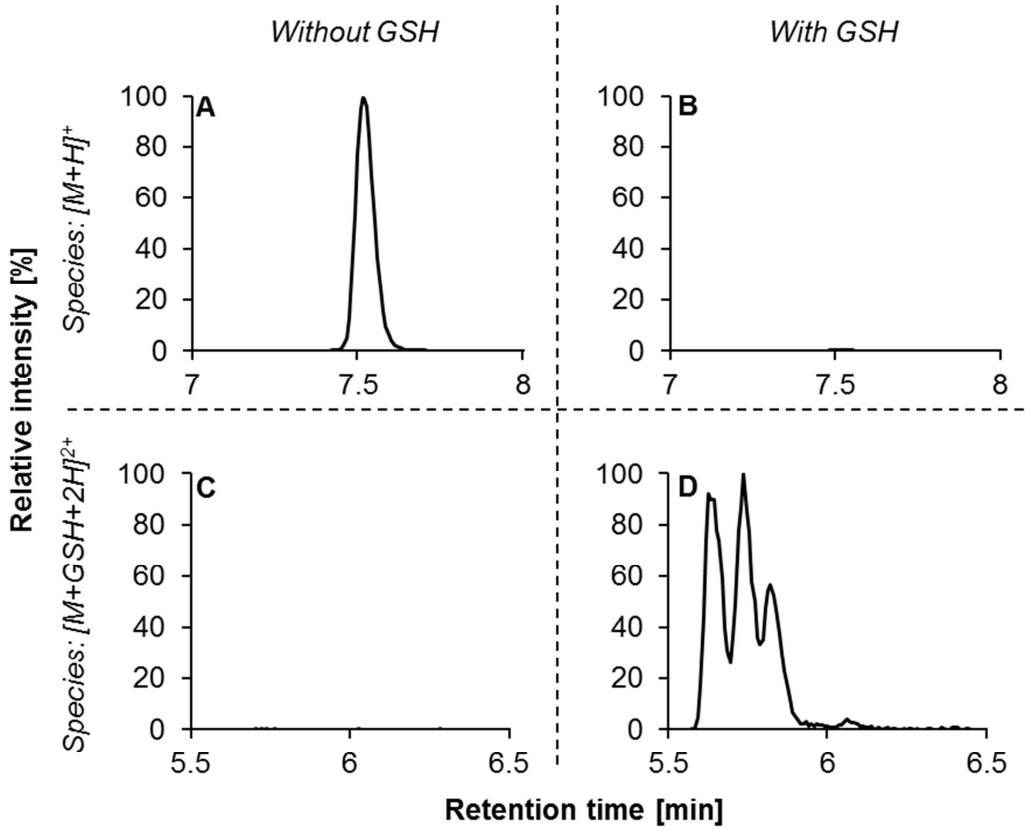


**Figure 6.4**: Extracted ion chromatograms for TP 362 ($[M+H]^+$; *m/z* 363.1122, A and B) and the glutathione (GSH) conjugate of TP 362 ($[M+GSH+2H]^{2+}$; *m/z* 335.6017, C and D) in a sample obtained after anodic oxidation of torasemide at pH 7. The extraction window for the chromatograms was ± 10 ppm and normalization of the signal intensities was performed in relation to the maximum intensity observed for each species, respectively. The doubly charged GSH conjugate showed significantly higher signal intensity compared to the singly charged ion.

The GSH conjugates of TP 362 eluted between 5.6 min and 5.9 min and the maximum observed mass error for the most abundant ionic species $[M+2H]^{2+}$ (*m/z* 335.6016) was 1.2 ppm. The results strongly support the proposed structure of TP 362 as quinone imine and its reactive nature. After EC degradation of torasemide also TP 278, TP 320, and TP 378b were revealed as reactive metabolites based on their reaction with glutathione (section 6.8.1 of the supporting information).

While TP 378b is potentially a hydroxylated species of TP 362, the products TP 320 and TP 278 could be formed from TP 362 via N-dealkylation (loss of the isopropyl group) and sulfonamide hydrolysis to a sulfonic acid, respectively. In general, N-dealkylation was reported for the electrochemical transformation of other molecules before (Johansson et al., 2007), while the formation of sulfonic acids from sulfonamides was specifically demonstrated for BDD electrodes (Fabiańska et al., 2014).

The hydrogenated species of both TPs, i.e. TP 280 and TP 322, were also detected after anodic oxidation, but with relative abundances about half of their quinone imine precursors.

Generally, activation by hydroxylation and further dehydrogenation seemed to be required before dealkylation could take place, as this degradation mechanism was only observed for TP 364b (leading to TP 322) and TP 362 (leading to TP 320). The direct N-dealkylation of torasemide itself leading towards TP 306 could not be mimicked electrochemically. In contrast, sulfonamide hydrolysis to a sulfonic acid took place for torasemide itself, leading towards the formation of TP 264. The additional cleavage product for all sulfonamide hydrolysis reactions, which is here isopropylurea (TP 102), was observed after anodic oxidation as well and this compound accumulated to a relative abundance of 17%.

The second most abundant product TP 258 was formed via N-dearylation, cleaving of the tolyl group. Due to the loss of this moiety it was however not possible to elucidate if an activation, similar to the hydroxylation in case of N-dealkylation, was required prior to the N-dearylation taking place. Subsequent degradation of TP 258 via amide cleavage at the urea moiety led to the formation of the primary sulfonamide TP 173, which was detected with a relative abundance of 5%.

#### 6.4.1.4 Microbial degradation with activated sludge

An improved understanding of torasemide TPs formed during conventional wastewater treatment was expected from aerobic biodegradation experiments. The time courses of relative concentrations for the parent compound and putative TP´s are shown in Figure 6.5. The spiked torasemide concentration remained constant over the first three days (Figure 6.5A), indicating that sorption onto sludge and abiotic hydrolysis can be ruled out under the given experimental conditions. This hypothesis was also supported by control samples with torasemide spiked to water, as the initial and final torasemide concentrations did not differ here (Figure 6.5A). An initial lag-phase was observed prior to the initiation of torasemide degradation, which occurred three to seven days into the experiment. An acclimation of the microbial community or a suppressed degradation of torasemide due to competition with more readily degradable nutrients are potential explanations for the observed lag-phase. Once biodegradation began, the torasemide concentration dropped on average to 88% of the initially spiked amount after one week and decreased continuously to 59% within two additional weeks (Figure 6.5A).

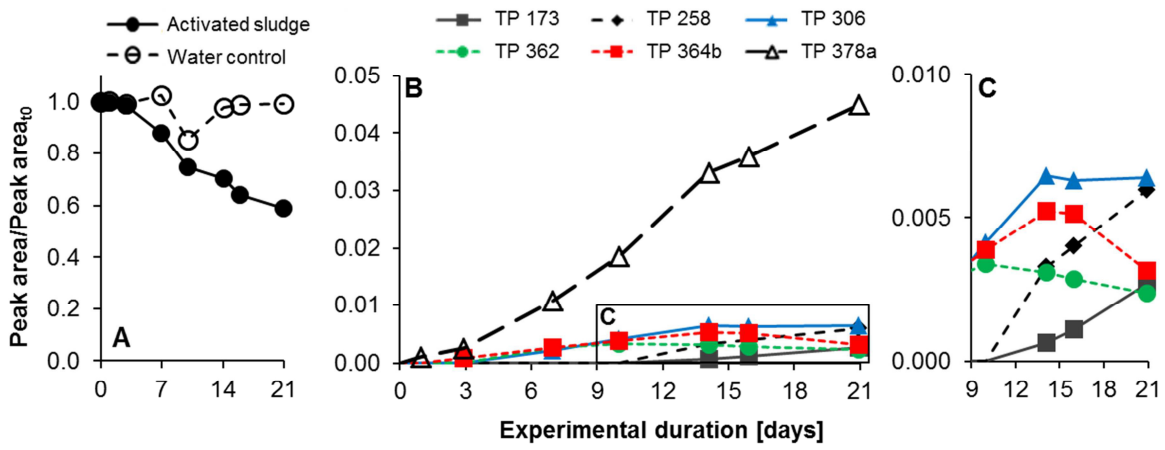


**Figure 6.5**: Time course of the relative torasemide concentration spiked to activated sludge (A) and the relative abundances of biotransformation products observed (B). A zoomed-in view of TP concentrations between day 9 and 21 is shown in C. Average values of duplicate samples are generally presented; the range of single samples was typically ≤ 0.02. Normalization was always performed to the average torasemide peak area measured in samples taken 20 min after spiking.

The decrease in the torasemide concentration was generally related to the formation of six metabolites. Most TPs were detected after the initial lag-phase and in case of the carboxylic acid TP 378a the concentration increased steadily over the complete experimental duration. Assuming comparable ionization efficiencies, this product was the most abundant TP, exceeding the other metabolites more than 5-fold, and about 5% of the initially spiked torasemide was finally recovered as TP 378a (Figure 6.5B). TP 378a is already known as the main human metabolite torasemide carboxylic acid (Knauf and Mutschler, 1998)). It is noteworthy that TP 364a, the main degradation product with HLMs (section 6.4.1.2) and the reported intermediate of TP 378a, was not detected during the microbial degradation study. It was therefore assumed that microorganisms oxidizing torasemide to TP 378a either do not release the intermediate TP 364a or that the transformation of TP 364a occurs so fast that it does not accumulate to significant amounts in the medium.

Similar to TP 378a, the concentrations of TP 173 and TP 258 were also steadily increasing until the end of the experiment, but in contrast to all other products, they were only detected in samples taken after 14 days. The reactions leading to their formation, e.g. a N-dearylation in case of TP 258, might require a previous activation of torasemide and it is very likely that these compounds are secondary metabolites. The stagnant (TP 306) or decreasing (TP 362 and TP 364b) concentrations of some metabolites towards the end of the experiment could generally support this hypothesis (Figure 6.5C). Except for TP 306 and TP 378a, all additional metabolites were also generated by anodic oxidation of torasemide.

#### 6.4.1.5 Direct and indirect photodegradation

Photodegradation of torasemide by natural sunlight was studied in deionized water (direct photolysis) and in surface water (indirect photodegradation) over seven days. Generally, there was no direct photodegradation observed for torasemide within this time frame (Figure 6.6A), although this compound shows a UV-Vis absorption spectrum similar to diclofenac (Figure S 6.18 in supporting information). Diclofenac is known for its rapid and direct degradation (Salgado et al., 2013) and was almost completely removed within one day under the same conditions (Figure 6.6B). Compared to torasemide, diclofenac contains however two photolabile C-Cl bonds where direct photolysis is suggested to start (Poiger et al., 2001). As torasemide does not undergo direct photolysis, this process is not influencing the fate of this compound in the environment and does not lead to a formation of degradation products.

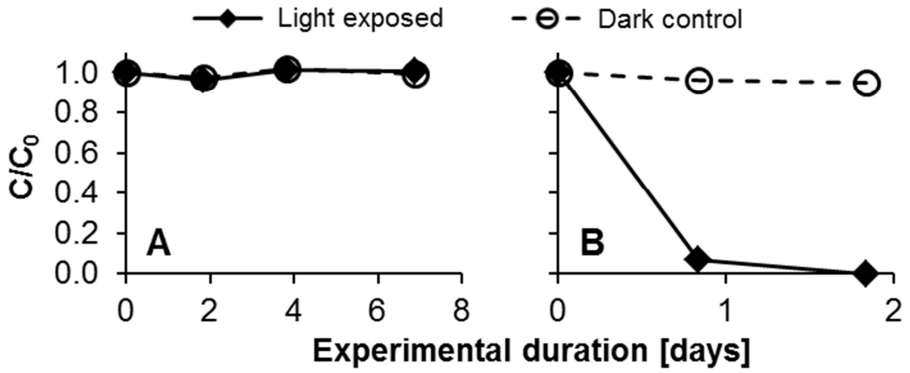


**Figure 6.6**: Concentration profiles of torasemide (A) and diclofenac (B) during direct photodegradation in the LC/MS grade water matrix investigated over one week. Average values from duplicate experiments are shown.

In contrast, indirect photodegradation in surface water removed torasemide by 77% within one week, while no degradation was observed in dark controls (Figure 6.7A). It produced 4 TPs, mainly the aromatic hydroxylation TP 364b and its oxidation product TP 362 (quinone imine), TP 393 (nitro toresamide) and TP 258. TP 364b and TP 362 were already detected in samples taken after 24 hours and their concentrations increased steadily until the third or fourth day, respectively (Figure 6.7B). Towards the end of the experiment, the concentrations decreased slightly, suggesting subsequent transformation. The TP 258, which was putatively formed by N-dearylation of torasemide, was detected the first time after about two days and its concentration increased until the end of the field study. Assuming similar ionization efficiencies, TP 258 was the least abundant phototransformation product of torasemide. In contrast to these three products, which were already observed after anodic oxidation or during microbial degradation, TP 393 was solely observed for indirect photodegradation.

The elemental composition of this analyte points towards a nitration of torasemide, a phototransformation process already reported for the herbicide monuron (Nélieu et al., 2008). Generally, the mechanism could be induced by nitrite or nitrate in the presence of oxygen, but the water analysis supports the route via nitrate. While about 30 mg $L^{-1}$ of nitrate were detected in the surface water utilized for the field study, nitrite was not detected (detailed analysis results in the supporting information of Lege et al., 2019). The general importance of nitrate for the indirect photodegradation under these conditions was also highlighted in the context of denatonium (Lege et al., 2019). Nitrate is known as a photosensitizing species that influences the formation of reactive oxygen species in aquatic environments (Gligorovski et al., 2015) and can therefore ultimately impact the fate of organic micropollutants in the environment (Wang et al., 2017).

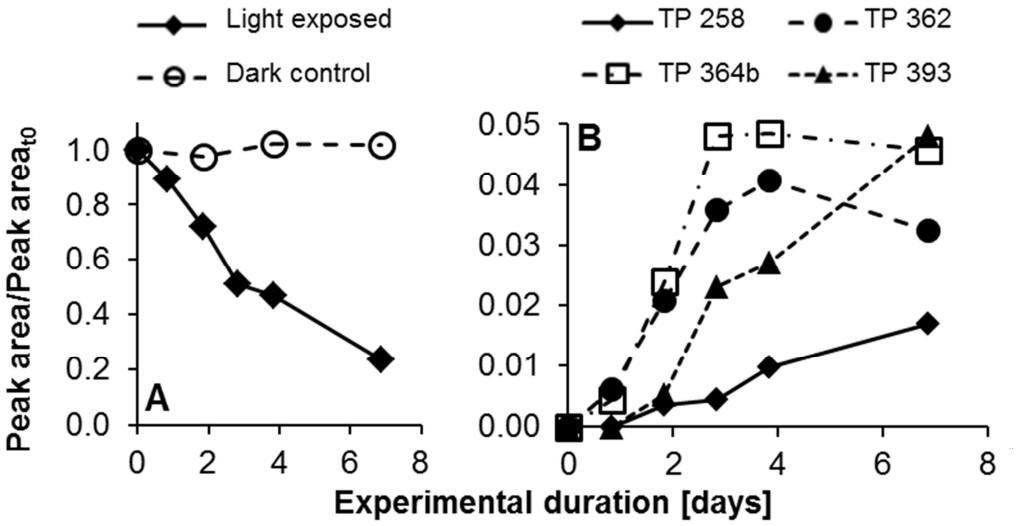


**Figure 6.7**: Concentration profiles of torasemide (A) and four transformation products (B) during indirect photodegradation in the river water matrix investigated over one week. Torasemide concentrations in (A) are shown for light exposed and dark control conditions, while the concentration profiles for the TPs (B) represent only light exposed conditions. Average values from duplicate experiments are presented. Normalization was always performed to the average torasemide peak area measured in samples taken at the beginning of the experiment.

### 6.4.2 Occurrence of torasemide and its TPs in aqueous samples

In 2015, grab samples were taken from 22 effluents of WWTPs and 3 rivers in Baden-Württemberg, Germany, and torasemide concentrations were determined by target analysis with LC-ESI-QqQ mass spectrometry. Torasemide was detected in rivers downstream of WWTPs in the range from 34 ng $L^{-1}$ to 67 ng $L^{-1}$ (Figure 6.8). Concentrations in the WWTP effluents were between 31 ng $L^{-1}$ and 348 ng $L^{-1}$ with a median concentration of 181 ng $L^{-1}$ and hence in the same range as previously reported (Gros et al., 2012,Gurke et al., 2015,Singer et al., 2016,Ternes et al., 2019).

High concentration variability between different WWTP effluents was also observed before and the authors of previous studies generally suggested differences in micropollutant removal efficiency or differences in the wastewater composition (e.g. by dilution with industrial wastewater) as potential reasons (Singer et al., 2016).

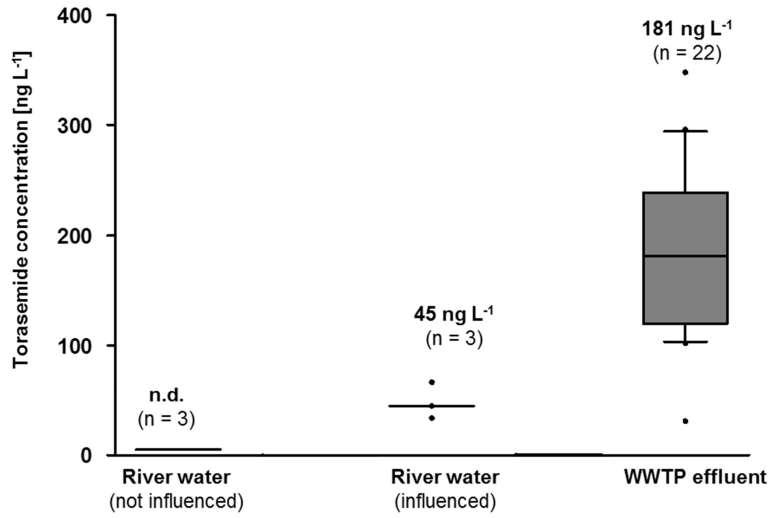


**Figure 6.8**: Torasemide concentrations in surface waters or effluents from the WWTPs E1-E22 sampled in Baden-Württemberg, Germany, in 2015. Rivers were either influenced or not influenced by treated wastewater and median analyte concentrations are given above the boxplots (n.d. not detected). The concentrations were determined with a targeted approach applying LC-ESI-QqQ MS.

In addition to the quantification of the parent compound torasemide itself, retrospective suspect screening was also performed for samples analyzed with high-resolution mass spectrometry (LC-ESI-QTOF-MS) to shed light on the occurrence of its transformation products. Overall, only three of the sixteen (putatively) identified TPs were detected in at least one of the WWTP or surface water samples (Table 6.2).

**Table 6.2**: Detection of torasemide and its transformation products in samples from WWTP influents, WWTP effluents and the Ammer river. The detection frequencies are given as the number of detections per total number of samples investigated from each sampling campaign. Furthermore, the average ratios of the peak areas of the TPs over the peak areas of torasemide in the respective sample are given in brackets. If a TP was detected more than once, the standard deviation is given as well.

| Compound | WWTP E21 (April 2016) | | WWTPs E1-E22 (April 2015) | Ammer river (July-August 2014) |
|---|---|---|---|---|
| | Influent | Effluent | Effluent | |
| Torasemide | 5 / 5 | 5 / 5 | 22 / 22 | 7 / 7 |
| TP 258 | 0 / 5 | 0 / 5 | 1 / 22 (0.38) | 0 / 7 |
| TP 364a | 5 / 5 (0.52 ± 0.07) | 0 / 5 | 1 / 22 (0.20) | 0 / 7 |
| TP 378a | 5 / 5 (2.83 ± 0.29) | 5 / 5 (3.38 ± 0.11) | 22 / 22 (2.38 ± 0.72) | 7 / 7 (1.91 ± 0.15) |

The TP 258, the product generated by N-dearylation, was generally the least frequently detected torasemide product and it was present only in a single WWTP effluent sample. The human metabolite hydroxytorasemide (TP 364a) seemed to be of similar low environmental relevance. Although it was detected in all influent samples of the treatment plant E21, this metabolite was completely removed during wastewater treatment in this plant. This observation was in agreement with the microbial degradation experiments performed for torasemide using activated sludge. While the final product carboxytorasemide (TP 378a) accumulated over time, the precursor TP 364a was never detected in these experiments, which suggests a high biodegradability (chapter 6.4.1.4). The fact that this compound was observed in one of the additional 22 analyzed effluent samples might be related to differences in the microbial community or the present nutrient conditions. The here suggested low persistence of the human metabolite TP 364a generally agrees with previous findings by Ternes et al., who did not detect this analyte in any of their investigated surface water or WWTP effluent samples (Ternes et al., 2019). These authors already identified carboxytorasemide (TP 378a) putatively in their samples and reported higher peak areas for this metabolite compared to torasemide itself. The same trend was also observed in our data and the average ratio of the signal intensities for TP 378a compared to torasemide were about 3.4, 2.5 and 1.9 for the five WWTP influent samples, all 27 WWTP effluent samples combined and the seven surface water samples, respectively (Table 6.2). The increase in the signal ratios for the metabolite compared to the parent compound during wastewater treatment in the plant E21 support the biodegradation of TP 364a and potentially torasemide itself, leading towards the generation of carboxytorasemide.

As already suggested by the microbial degradation experiments, TP 378a seemed to be more persistent and it is therefore not surprising that it was detected in all samples taken from WWTPs and wastewater-impacted surface waters. Assuming similar ionization efficiencies for TP 378a and torasemide an estimated concentration level at about 1 µg $L^{-1}$ of carboxytorasemide could be postulated in WWTP effluents.

## 6.5 Conclusions

Overall sixteen biotic and abiotic degradation products of the loop diuretic torasemide were identified in this study. The presence of these TPs and their parent compound was investigated in wastewater treatment plants and receiving surface waters to shed more light on the occurrence and the potential fate of these analytes in the environment. Generally, the following conclusions were drawn by us:

- Torasemide is susceptible to microbial degradation and indirect photodegradation.
- Biotransformation and indirect photodegradation produced the quinone imine TP 362, a reactive intermediate which can directly react with a wide range of cell nucleophiles, e.g. DNA or proteins and is therefore of toxicological relevance.
- The human metabolite TP 364a is not environmentally relevant as it is usually removed by microbial degradation during wastewater treatment.
- The metabolite carboxytorasemide (TP 378a) in contrast exhibits an increased persistence and is frequently detected in treated wastewater and surface waters.
- Rough concentration estimates for TP 378a suggest amounts up to 1 µg $L^{-1}$ in treated wastewater. Additional measurements are however required using reference standards for accurate quantification.

## 6.6 Acknowledgements

The German Federal Environmental Foundation (Deutsche Bundesstiftung Umwelt, DBU) is gratefully acknowledged for funding the Ph.D. scholarships of Sascha Lege. The German Research Foundation (DFG) is gratefully acknowledged for funding the project ZW 73/14. We thank Marius Majewsky (formerly at the Engler-Bunte-Institute at the Karlsruhe Institue of Technology, Germany) for performing the microbial degradation experiments.

## 6.7 References


Barroso, M.B., Alonso, R.M., Jiménez, R.M., 2001. Simultaneous determination of torasemide and its major metabolite M5 in human urine by high-performance liquid chromatography-electrochemical detection. Journal of chromatographic science 39 (11), 491–496.

Buggey, J., Mentz, R.J., Pitt, B., Eisenstein, E.L., Anstrom, K.J., Velazquez, E.J., O'Connor, C.M., 2015. A reappraisal of loop diuretic choice in heart failure patients. American heart journal 169 (3), 323–333.

Fabiańska, A., Białk-Bielińska, A., Stepnowski, P., Stolte, S., Siedlecka, E.M., 2014. Electrochemical degradation of sulfonamides at BDD electrode: kinetics, reaction pathway and eco-toxicity evaluation. Journal of hazardous materials 280, 579–587.

Gligorovski, S., Strekowski, R., Barbati, S., Vione, D., 2015. Environmental Implications of Hydroxyl Radicals ((•)OH). Chemical reviews 115 (24), 13051–13092.

Gros, M., Rodríguez-Mozaz, S., Barceló, D., 2012. Fast and comprehensive multi-residue analysis of a broad range of human and veterinary pharmaceuticals and some of their metabolites in surface and treated waters by ultra-high-performance liquid chromatography coupled to quadrupole-linear ion trap tandem mass spectrometry. Journal of chromatography. A 1248, 104–121.

Gurke, R., Rößler, M., Marx, C., Diamond, S., Schubert, S., Oertel, R., Fauler, J., 2015. Occurrence and removal of frequently prescribed pharmaceuticals and corresponding metabolites in wastewater of a sewage treatment plant. The Science of the total environment 532, 762–770.

Herchuelz, A., Deger, F., Douchamps, J., Ducarne, H., Broekhuysen, J., 1988. Comparative pharmacodynamics of torasemide and furosemide in patients with oedema. Arzneimittel-Forschung 38 (1A), 180–183.

Holcapek, M., Jirásko, R., Lísa, M., 2010. Basic rules for the interpretation of atmospheric pressure ionization mass spectra of small molecules. Journal of chromatography. A 1217 (25), 3908–3921.

Holcapek, M., Kolárová, L., Nobilis, M., 2008. High-performance liquid chromatography-tandem mass spectrometry in the identification and determination of phase I and phase II drug metabolites. Analytical and bioanalytical chemistry 391 (1), 59–78.

Johansson, T., Weidolf, L., Jurva, U., 2007. Mimicry of phase I drug metabolism--novel methods for metabolite characterization and synthesis. Rapid communications in mass spectrometry : RCM 21 (14), 2323–2331.

Jones, O.A., Lester, J.N., Voulvoulis, N., 2005. Pharmaceuticals: a threat to drinking water? Trends in biotechnology 23 (4), 163–167.

Jurva, U., Wikström, H.V., Weidolf, L., Bruins, A.P., 2003. Comparison between electrochemistry/mass spectrometry and cytochrome P450 catalyzed oxidation reactions. Rapid communications in mass spectrometry : RCM 17 (8), 800–810.

Klopčič, I., Sollner Dolenc, M., 2018. Chemicals and Drugs Forming Reactive Quinone and Quinone Imine Metabolites. Chemical research in toxicology.

Knauf, H., Mutschler, E., 1998. Clinical pharmacokinetics and pharmacodynamics of torasemide. Clinical pharmacokinetics 34 (1), 1–24.

Kurmi, M., Patel, N., Jhajra, S., Bharatam, P.V., Singh, S., 2017. Characterization of forced degradation products of torasemide through MS tools and explanation of unusual losses observed during mass fragmentation of drug and degradation products through density functional theory. Journal of pharmaceutical and biomedical analysis 145, 209–218.

Lege, S., Eisenhofer, A., Yanez Heras, Jorge Eduardo, Zwiener, C., 2019. Identification of transformation products of denatonium – Occurrence in wastewater treatment plants and surface waters. Science of The Total Environment 686, 140–150.

Lege, S., Guillet, G., Merel, S., Yanez Heras, Jorge Eduardo, Zwiener, C., 2017. Denatonium - A so far unrecognized but ubiquitous water contaminant? Water research 112, 254–260.

Loos, R., Gawlik, B.M., Locoro, G., Rimaviciute, E., Contini, S., Bidoglio, G., 2009. EU-wide survey of polar organic persistent pollutants in European river waters. Environmental pollution (Barking, Essex : 1987) 157 (2), 561–568.

Loos, R., Locoro, G., Comero, S., Contini, S., Schwesig, D., Werres, F., Balsaa, P., Gans, O., Weiss, S., Blaha, L., Bolchi, M., Gawlik, B.M., 2010. Pan-European survey on the occurrence of selected polar organic persistent pollutants in ground water. Water research 44 (14), 4115–4126.

Madsen, K.G., Olsen, J., Skonberg, C., Hansen, S.H., Jurva, U., 2007. Development and evaluation of an electrochemical method for studying reactive phase-I metabolites: correlation to in vitro drug metabolism. Chemical research in toxicology 20 (5), 821–831.

Margot, J., Rossi, L., Barry, D.A., Holliger, C., 2015. A review of the fate of micropollutants in wastewater treatment plants. WIREs Water 2 (5), 457–487.

Merel, S., Lege, S., Yanez Heras, Jorge E, Zwiener, C., 2017. Assessment of N-Oxide Formation during Wastewater Ozonation. Environmental science & technology 51 (1), 410–417.

Miners, J.O., Rees, D.L., Valente, L., Veronese, M.E., Birkett, D.J., 1995. Human hepatic cytochrome P450 2C9 catalyzes the rate-limiting pathway of torsemide metabolism. The Journal of pharmacology and experimental therapeutics 272 (3), 1076–1081.

Naisbitt, D.J., Williams, D.P., O'Neill, P.M., Maggs, J.L., Willock, D.J., Pirmohamed, M., Park, B.K., 1998. Metabolism-dependent neutrophil cytotoxicity of amodiaquine: A comparison with pyronaridine and related antimalarial drugs. Chemical research in toxicology 11 (12), 1586–1595.

Nélieu, S., Shankar, M.V., Kerhoas, L., Einhorn, J., 2008. Phototransformation of monuron induced by nitrate and nitrite ions in water: Contribution of photonitration. Journal of Photochemistry and Photobiology A: Chemistry 193 (1), 1–9.

Nematollahi, D., Shayani-Jam, H., Alimoradi, M., Niroomand, S., 2009. Electrochemical oxidation of acetaminophen in aqueous solutions: Kinetic evaluation of hydrolysis, hydroxylation and dimerization processes. Electrochimica Acta 54 (28), 7407–7415.

Poiger, T., Buser, H.R., Müller, M.D., 2001. Photodegradation of the pharmaceutical drug diclofenac in a lake: pathway, field measurements, and mathematical modeling. Environmental toxicology and chemistry 20 (2), 256–263.

Salgado, R., Pereira, V.J., Carvalho, G., Soeiro, R., Gaffney, V., Almeida, C., Vale Cardoso, V., Ferreira, E., Benoliel, M.J., Ternes, T.A., Oehmen, A., Reis, M A M, Noronha, J.P., 2013. Photodegradation kinetics and transformation products of ketoprofen, diclofenac and atenolol in pure water and treated wastewater. Journal of hazardous materials 244-245, 516–527.

Schwabe, U., Paffrath, D., 2009. Arzneiverordnungs-Report 2009. Springer Berlin Heidelberg, Berlin, Heidelberg.

Schwabe, U., Paffrath, D., Ludwig, W.-D., Klauber, J., 2018. Arzneiverordnungs-Report 2018. Springer Berlin Heidelberg, Berlin, Heidelberg.

Schymanski, E.L., Jeon, J., Gulde, R., Fenner, K., Ruff, M., Singer, H.P., Hollender, J., 2014. Identifying small molecules via high resolution mass spectrometry: communicating confidence. Environmental science & technology 48 (4), 2097–2098.

Singer, H.P., Wössner, A.E., McArdell, C.S., Fenner, K., 2016. Rapid Screening for Exposure to "Non-Target" Pharmaceuticals from Wastewater Effluents by Combining HRMS-Based Suspect Screening and Exposure Modeling. Environmental science & technology 50 (13), 6698–6707.

Stanstrup, J., Gerlich, M., Dragsted, L.O., Neumann, S., 2013. Metabolite profiling and beyond: approaches for the rapid processing and annotation of human blood serum mass spectrometry data. Analytical and bioanalytical chemistry 405 (15), 5037–5048.

Ternes, T., Dierkes, G., Boulard, L., Weizel, A., 2019. Method development for analysis of pharmaceuticals in environmental samples. Texte 42/2019. Umweltbundesamt, Dessau-Roßlau.

Wang, Y., Roddick, F.A., Fan, L., 2017. Direct and indirect photolysis of seven micropollutants in secondary effluent from a wastewater lagoon. Chemosphere 185, 297–308.

WHO Collaborating Centre for Drug Statistics Methodology, December 13th, 2018. ATC/DDD Index (accessed September 14th, 2019). https://www.whocc.no/atc_ddd_index/.

Wode, F., van Baar, P., Dünnbier, U., Hecht, F., Taute, T., Jekel, M., Reemtsma, T., 2015. Search for over 2000 current and legacy micropollutants on a wastewater infiltration site with a UPLC-high resolution MS target screening method. Water research 69, 274–283.

## 6.8 Supplementary information

### 6.8.1 Identification of torasemide transformation products

The structure elucidation of the TPs performed in this study began typically with the comparison of the products elemental composition to the one of the parent compound itself. The most probable reaction mechanisms were assumed based on the elemental differences leading to initial hypotheses about the compounds structure. If available, these initial assumptions about analyte structures were compared to structural information obtained from MS/MS experiments. Previously reported fragmentation pathways for torasemide and forced degradation products (Kurmi et al., 2017) were also reviewed in this context. Finally, trapping experiments with reduced glutathione were evaluated for electrochemical transformation products to support assumptions about a reactive nature of the analyte and the occurrence of specific moieties, e.g. a quinone imine. Generally, no data are presented in the context of trapping experiments for those products which did not react with glutathione.

**TP 102**

The elemental composition of $C_4H_{10}N_2O$ was assigned with a mass error of about 1 ppm to the transformation product eluting at 1.46 min. TP 102 was only detected after anodic oxidation of torasemide, with a relative abundance of almost 20 % compared to the most dominant electrochemical product. Considering the structure of the parent molecule itself, the cleavage of the sulfonamide bond was the most plausible transformation mechanism, which could explain the formal loss of $C_{12}H_{10}N_2O_2S$ from torasemide. TP 102 was therefore putatively identified as isopropylurea, an identity which was further supported by MS/MS information (Figure S 6.1). The neutral loss of $NH_3$ from the parent ion (*m/z* 103 → *m/z* 86), as well as from a fragment with $CH_5N_2O$ (*m/z* 61 → *m/z* 44), points towards the presence of a primary amide moiety (Holcapek et al., 2010). The formation of the product ion *m/z* 61 can be explained by the neutral loss of an isopropyl group from the protonated TP 102. Further evidence for the isopropyl group was observed with the fragment *m/z* 43, to which the elemental composition $C_3H_7^+$ was assigned. This product ion represents most likely the isopropyl carbocation itself, a species which is generally stabilized due to the inductive effect of the two methyl moieties. Due to the MS/MS information and the absence of more plausible analyte structures, TP 102 was identified with the confidence level 2.

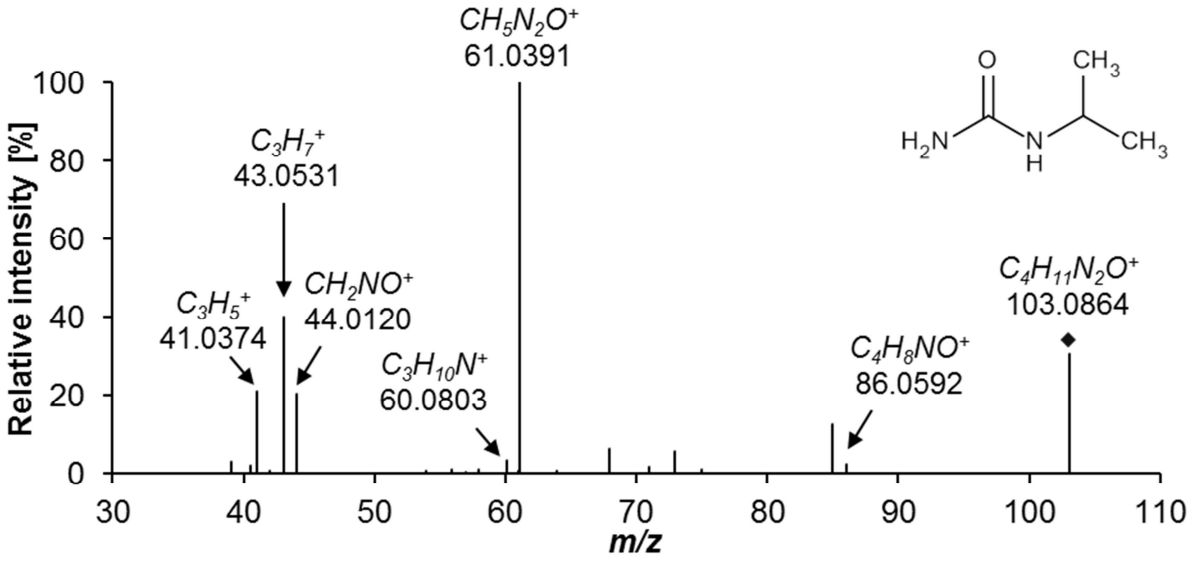


**Figure S 6.1**: Merged MS/MS spectrum for TP 102 (*m/z* 103.0866, $[M+H]^+$, rt = 1.46 min). Product ions were recorded individually at 10 V, 20 V, and 40 V and combined to a single spectrum. Data were recorded for a sample taken after anodic oxidation with a BDD electrode at pH 7.

**TP 173**

The most polar transformation product of torasemide observed during this study was detected after microbial degradation and anodic oxidation, respectively. The elemental composition of $C_5H_7N_3O_2S$ was assigned with a mass error of about 0.9 ppm to this compound. The loss of the tolyl group via N-dearylation combined with the cleavage of the urea moiety are suggested as the most plausible mechanisms which lead towards a primary sulfonamide with the assigned elemental composition. MS/MS information recorded for this analyte (Figure S 6.2) generally support this hypothesis. The neutral loss of ammonia (*m/z* 174 → *m/z* 157) is the result of the direct bond cleavage at the sulfonamide moiety and the product ions *m/z* 93 and *m/z* 94 represent the aminopyridine structure. Based on this evidence, the analyte was putatively identified with the level 2.

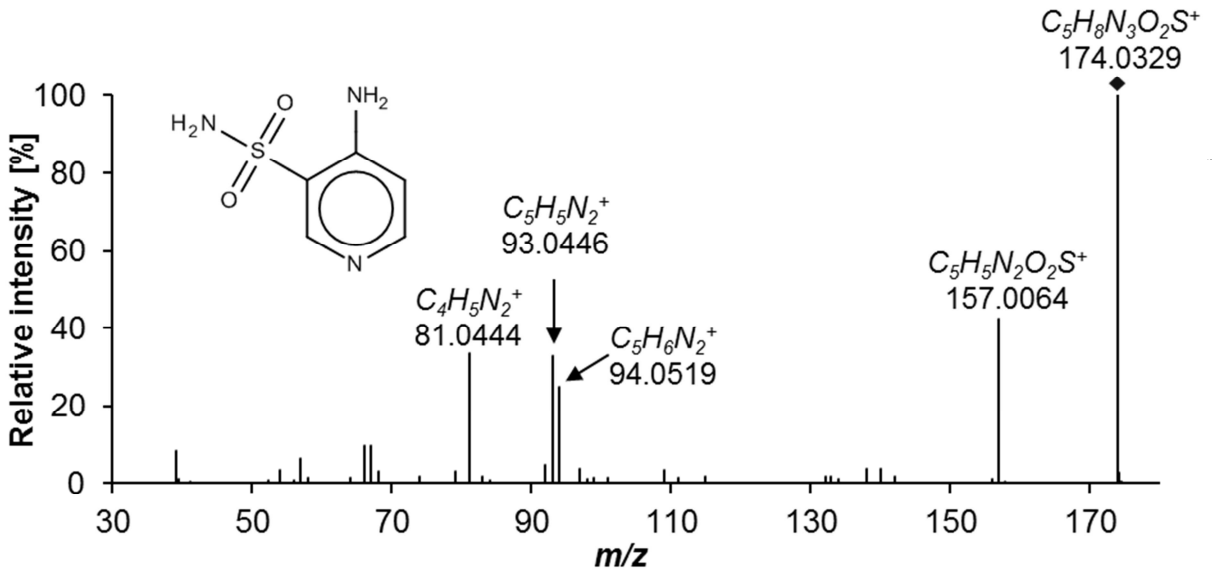


**Figure S 6.2**: Merged MS/MS spectrum for TP 173 (*m/z* 174.0332, $[M+H]^+$, rt = 0.84 min). Product ions were recorded individually at 10 V, 20 V, and 40 V and combined to a single spectrum. Data were recorded for a sample taken after anodic oxidation with a BDD electrode at pH 3.

**TP 258**

TP 258 was the second most abundant product observed after anodic oxidation and it was additionally present in samples from microbial degradation and phototransformation studies. Accurate mass measurements were used to assign the molecular formula $C_9H_{14}N_4O_3S$ to this compound with an error of about 1.1 ppm. This composition of TP 258 differs by seven carbon atoms and six hydrogen atoms to torasemide itself, pointing towards the loss of the tolyl group as formation mechanism.

In principle, TP 258 can be transformed into TP 173 due to cleavage of the analyte at the urea moiety. The similarity of both structures becomes also obvious when comparing their MS/MS spectra in the positive ionization mode (Figure S 6.2 and Figure S 6.3A), as the most dominant product ions of TP 173 (i.e. *m/z* 157, *m/z* 94, *m/z* 93, and *m/z 81*) and the protonated species of TP 173 itself are also important fragments in the spectrum of TP 258 (Figure S 6.3A). In addition, the nature of the two additional product ions for TP 258, i.e. *m/z 200* and *m/z* 109, support the proposed structure. The cleavage of isopropylamine at the urea moiety can lead towards the fragment *m/z* 200, a process which is covered also by one of the general dissociation mechanisms reported for ureas (Weissberg and Dagan, 2011).

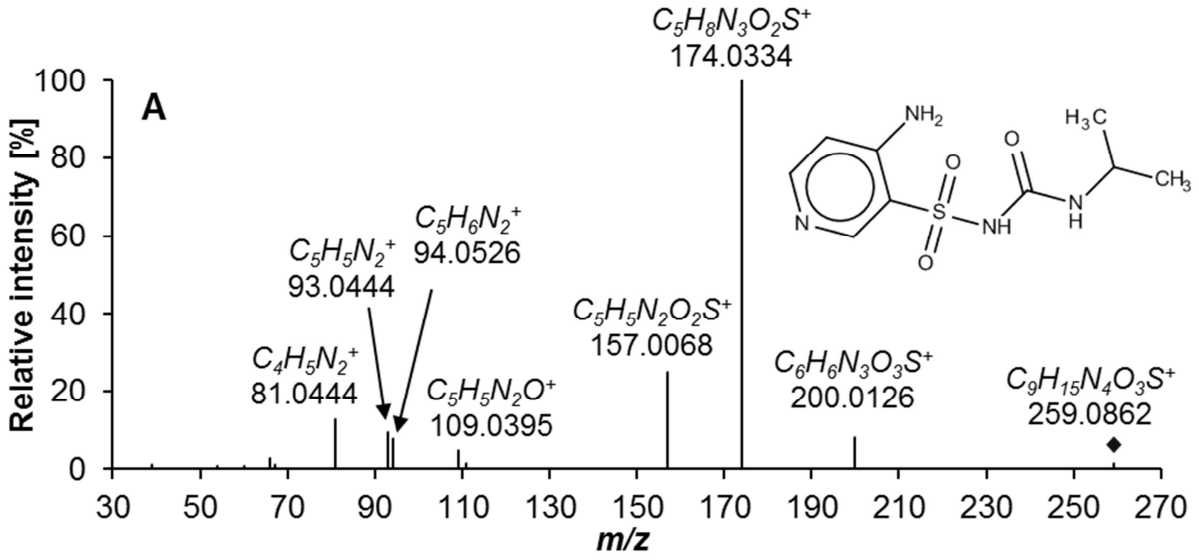


**Figure S 6.3A**: Merged MS/MS spectrum for TP 258 recorded in the positive ionization mode (*m/z* 259.0859, $[M+H]^+$, rt = 1.95 min). Product ions were recorded individually at 10 V, 20 V, and 40 V and combined to a single spectrum. Data were recorded for a sample taken after anodic oxidation with a BDD electrode at pH 3.

In contrast, the formation of the product ion *m/z* 109 ($C_5H_5N_2O^+$) cannot be linked to a direct bond cleavage as an oxygen atom seems to be bound to the aminopyridine moiety. However, Song et al. described a rearrangement process for sulfonamides (leading to a fragment ion **B** in their publication, Song et al., 2014), which can explain the observation of the fragment *m/z* 109 in our case. Following their explanation, the fragment *m/z* 157 is most likely the precursor for a "stepwise rearrangement reaction including heterolytic C–S bond cleavage and intramolecular nucleophilic substitution" (Song et al., 2014), ultimately leading to the product ion *m/z* 109 in case of TP 258.

As the analyte TP 258 was also ionizable in the ESI- mode, structural information were also recorded for the $[M-H]^-$ species for the sake of completeness (Figure S 6.3B). However, this spectrum was not interpreted in addition as the spectral information from the positive mode (Figure S 6.3A) were considered sufficient to support the structural identification of TP 258 with a confidence level 2.

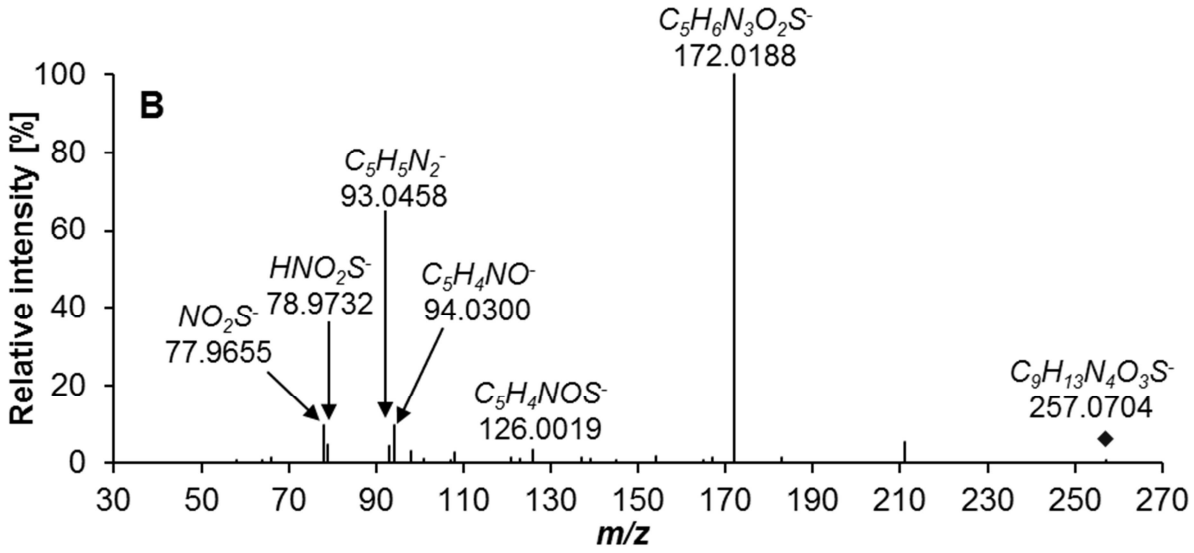


**Figure S 6.3**B: Merged MS/MS spectrum for TP 258 recorded in the negative ionization mode (*m/z* 257.0714, $[M-H]^-$, rt = 1.95 min). Product ions were recorded individually at 10 V, 20 V, and 40 V and combined to a single spectrum. Data were recorded for a sample taken after anodic oxidation with a BDD electrode at pH 3.

**TP 264**

The transformation product TP 264 was generally of low abundance in the samples from the degradation studies and could be only observed after anodic oxidation at pH 7. Based on accurate mass measurements and isotope information, the elemental composition $C_{12}H_{12}N_2O_3S$ was assigned to this analyte with a mass error of – 0.6 ppm. Kurmi et al. reported a species with the same elemental composition (i.e. **DP 1**) for the forced degradation of torasemide in the presence of hydrogen peroxide and identified it as 4-[(3-methylphenyl)amino]pyridine-3-sulfonic acid (Kurmi et al., 2017). All seven product ions from *m/z* 125 to *m/z* 247 reported by these authors for **DP 1** were also observed for the protonated species of TP 264 in our study (Figure S 6.4A).

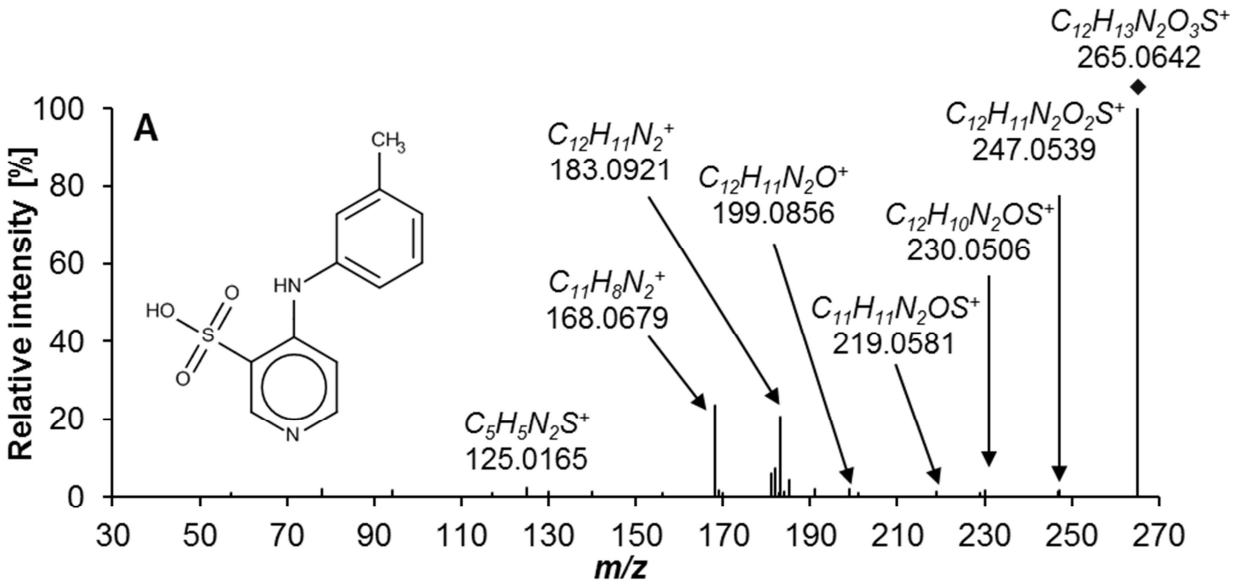


**Figure S 6.4A**: Merged MS/MS spectrum for TP 264 recorded positive ionization mode (*m/z* 265.0641, $[M+H]^+$, rt = 6.12 min). Product ions were recorded individually at 10 V, 20 V, and 40 V and combined to a single spectrum. Data were recorded for a sample taken after anodic oxidation with a BDD electrode at pH 7.

In addition, the dissociation pattern in the ESI- mode (Figure S 6.4B) supports the analytes nature as a sulfonic acid in accordance with (Holcapek et al., 2010), as the neutral loss of $SO_3$ from the parent ion (*m/z* 263 → 183) and the presence of the characteristic $SO_3^-$ radical (*m/z* 80) can be observed.

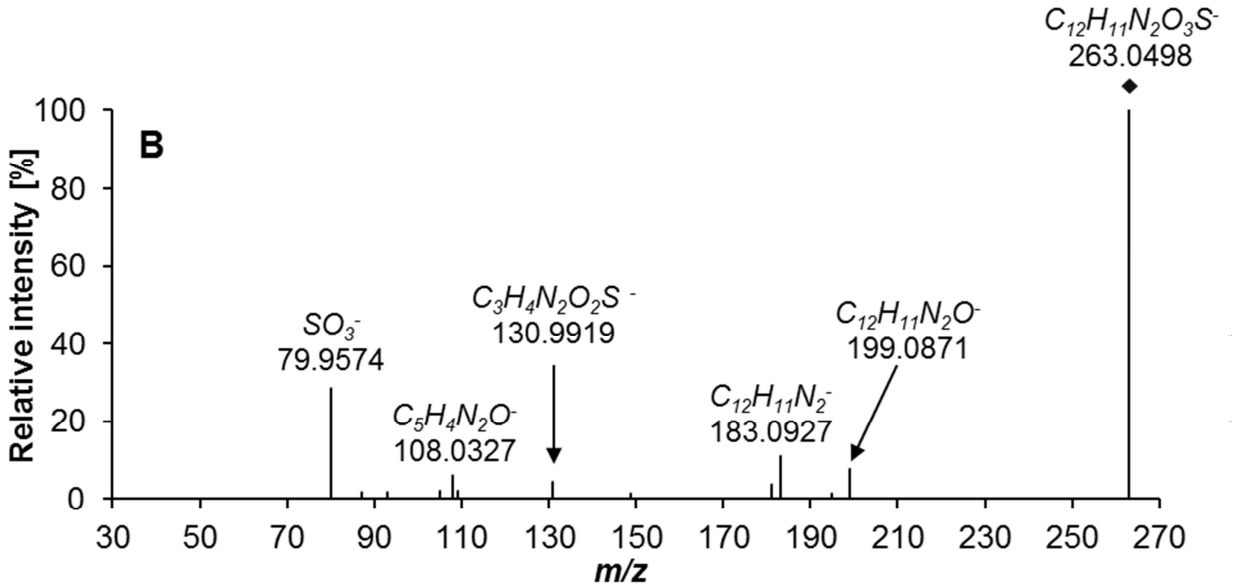


**Figure S 6.4B**: Merged MS/MS spectrum for TP 264 recorded in the negative ionization mode (*m/z* 263.0496, $[M-H]^-$, rt = 6.12 min). Product ions were recorded individually at 10 V, 20 V, and 40 V and combined to a single spectrum. Data were recorded for a sample taken after anodic oxidation with a BDD electrode at pH 7.

The anodic oxidation of sulfonamides to sulfonic acids with boron doped diamond working electrodes was also already demonstrated before (Fabiańska et al., 2014), additionally supporting the plausibility of our tentative identification of TP 258. Based on the diagnostic evidence we assigned the putative structure to this analyte with the confidence level 2.

**TP 278**

The product TP 278 was only observed after anodic oxidation at pH 7 and it was also of low abundance compared to other transformation products under these conditions. The molecular formula $C_{12}H_{10}N_2O_4S$ was assigned to this analyte with a mass error of 0.34 ppm. Based on the characteristic MS/MS information in the negative ionization mode (Figure S 6.5B), including the neutral loss of SO3 from the parent ion (m/z 277 → m/z 197) and the $SO_3^-$ radical (*m/z* 80) (characteristic behavior according to Holcapek et al., 2010), the analyte was putatively identified as sulfonic acid. In comparison to TP 264, which was also tentatively identified as sulfonic acid, TP 278 has one additional oxygen atom but two fewer hydrogen atoms. It is likely that the additional oxygen atom of TP 278 is the result of a hydroxylation reaction and this species underwent additional oxidation, e.g. to a quinone imine, which would explain the difference by two hydrogen atoms. Based on the MS/MS information recorded in the ESI+ mode (Figure S 6.5A), it was excluded that the aminopyridine moiety is actually the location for this modification. Characteristic product ions previously assigned to the unmodified aminopyridine moiety in case of the products TP 173 and TP 258 (i.e. *m/z* 81, *m/z* 93 and *m/z* 157), could be also observed here.

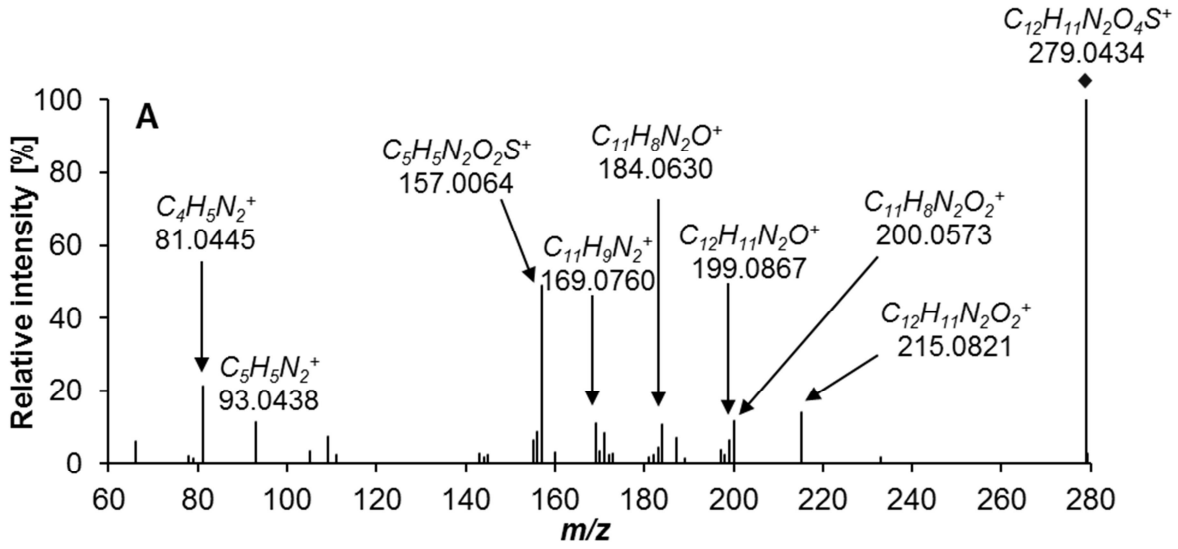


**Figure S 6.5**A: Merged MS/MS spectrum for TP 278 recorded in the positive ionization mode (*m/z* 279.0434, $[M+H]^+$, rt = 2.12 min). Product ions were recorded individually at 10 V, 20 V, and 40 V and combined to a single spectrum. Data were recorded for a sample taken after anodic oxidation with a BDD electrode at pH 7.

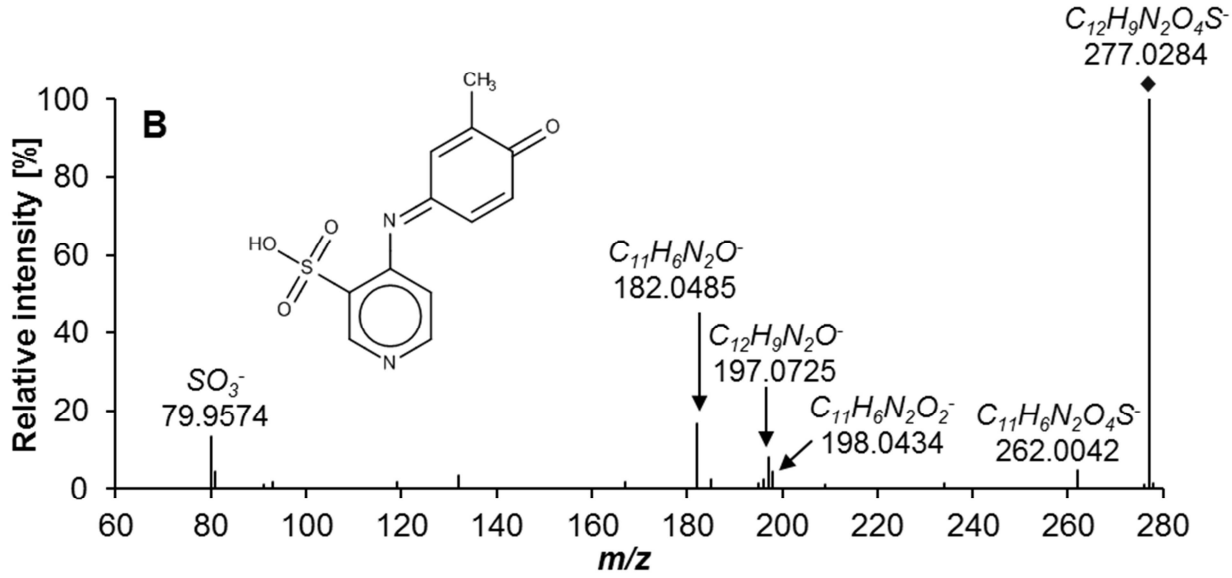


**Figure S 6.5B**: Merged MS/MS spectrum for TP 278 recorded in the negative ionization mode (*m/z* 277.0289, $[M-H]^-$, rt = 2.12 min). Product ions were recorded individually at 10 V, 20 V, and 40 V and combined to a single spectrum. Data were recorded for a sample taken after anodic oxidation with a BDD electrode at pH 7.

Most product ions reported for torasemide and its forced degradation products are actually related to the [(3-methylphenyl)amino]pyridine moiety (Kurmi et al., 2017). As we excluded the aminopyridine structure as location for the modification, any mass shift in those product ions previously reported for this moiety is therefore pointing towards the tolyl group as location of modification.

And at least the following mass shifts comparing the reported product ions the the fragments of TP 279 in ESI+ mode could be observed:

*m/z* 199.0866 ($C_{12}H_{11}N_2O^+$) → *m/z* 215.0821 ($C_{12}H_{11}N_2O_2^+$)

*m/z* 183.0917 ($C_{12}H_{11}N_2^+$) → *m/z* 199.0867 ($C_{12}H_{11}N_2O^+$)

*m/z* 168.0682 ($C_{11}H_8N_2^+$) → *m/z* 184.0630 ($C_{11}H_8N_2O^+$)

Therefore we concluded that the tolyl group is most likely impacted by the modification. This hypothesis is also supported by the activation of the tolyl group due to an inductive effect of the methyl moiety and a mesomeric effect of the amine group. The transformation products TP 320 or TP 362 are potential parent compounds of TP 278 and we tentatively identified TP 278 with a confidence level 2.

The reactive nature of the transformation product was also verified based on the conjugation with reduced glutathione (Figure S 6.6). The absence of the TP 278 in samples to which GSH was added (Figure S 6.6B) could be linked to the presence of two GSH conjugates, eluting around 4 minutes (Figure S 6.6D).

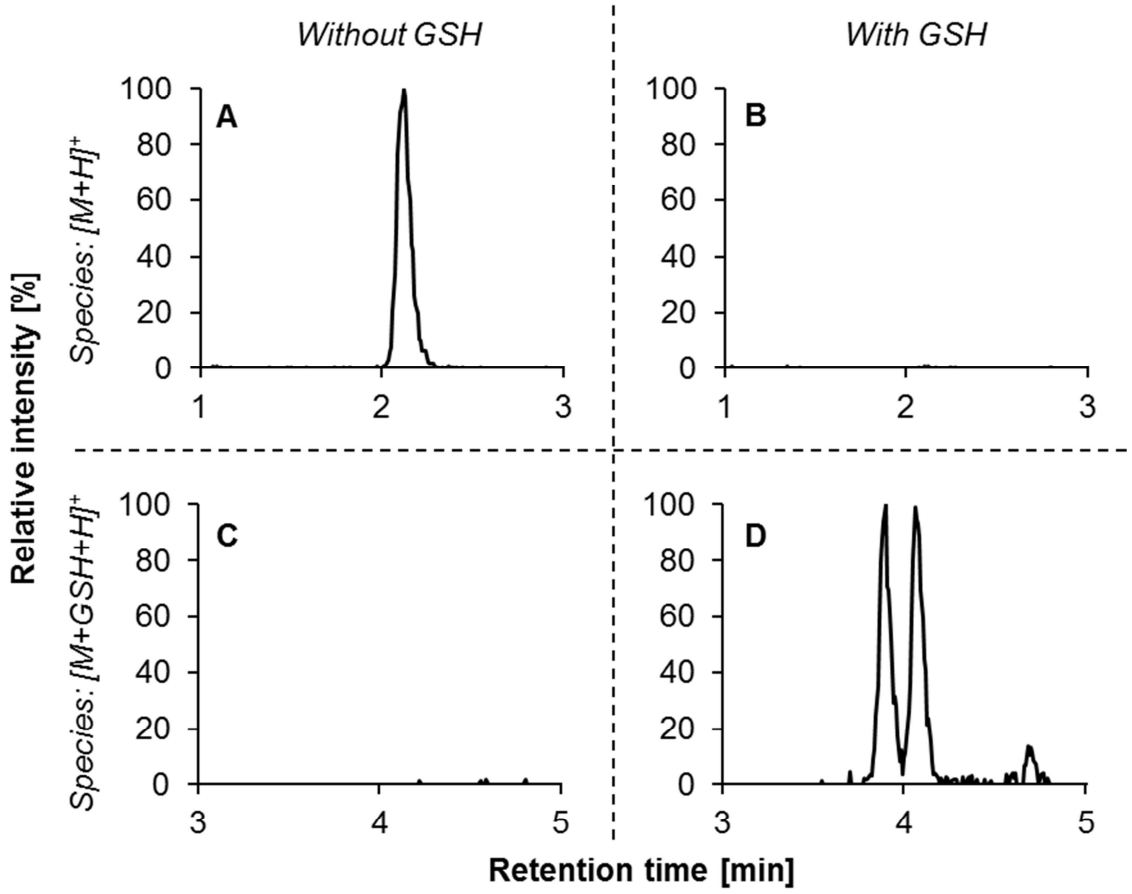


**Figure S 6.6**: Extracted ion chromatograms for the $[M+H]^+$ (*m/z* 279.0434, A and B) and $[M+GSH+H]^+$ (*m/z* 586.1272, C and D) of the TP 278 in a sample obtained after anodic oxidation of torasemide at pH7 that was either diluted with tap water (A and C) or an equal volume of a reduced glutathione (GSH) solution (B and D). The extraction window for the chromatograms was ± 10 ppm and normalization of the signal intensities was performed in relation to the maximum intensity observed for each species, respectively.

**TP 280**

The product TP 280 was observed only in samples taken after anodic oxidation of torasemide at pH7 and this analyte eluted at a retention time of about 4.1 minutes. The molecular formula $C_{12}H_{12}N_2O_4S$ was assigned to this compound with an error of -0.6 ppm. As the TP 280 differs only by two additional hydrogen atoms from the TP 278 we concluded that TP 280 is the reduced form of the reactive species TP 278. MS/MS information recorded in the negative ionization mode were again pointing towards the presence of a sulfonic acid moiety as was already discussed for the products TP 264 and TP 278 before. In addition, the fragment information supported a hydroxylation of the tolyl group as a product ion with the composition $C_7H_7O^-$ (*m/z* 107) could be observed.

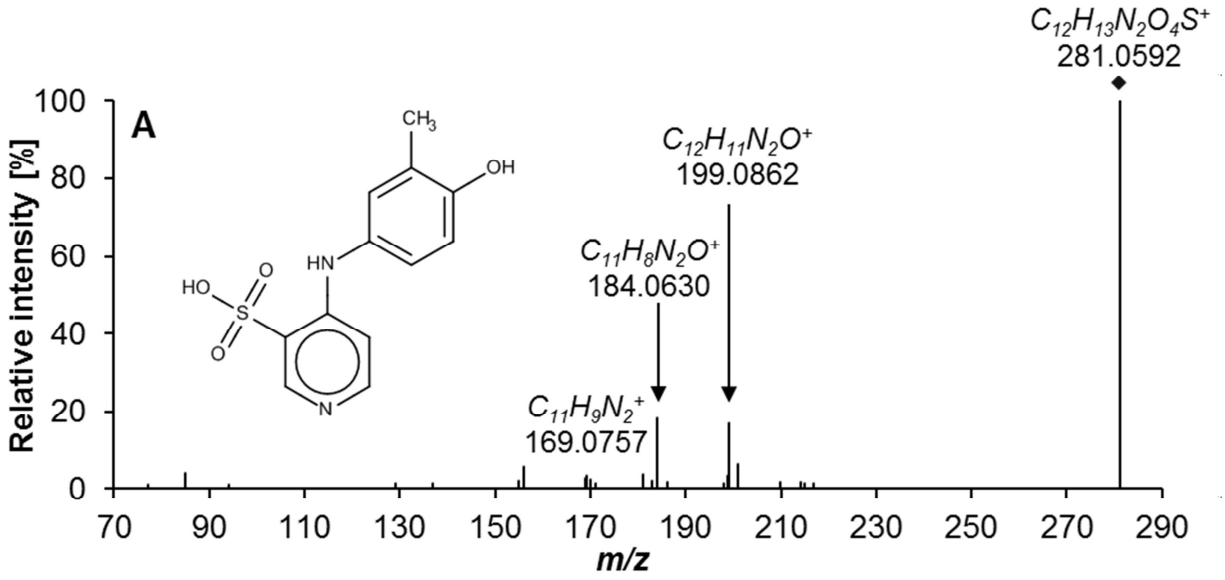


**Figure S 6.7A**: Merged MS/MS spectrum for TP 280 recorded in the positive ionization mode (*m/z* 281.0591, $[M+H]^+$, rt = 4.11 min). Product ions were recorded individually at 10 V, 20 V, and 40 V and combined to a single spectrum. Data were recorded for a sample taken after anodic oxidation with a BDD electrode at pH 7.

Assuming that the transformation products TP 322 and TP 364b are potential precursors of TP 280, the location of hydroxylation would be in *para* position to the amine of the toluidine group. Based on the available information we tentatively identified TP 280 with the confidence level 2.

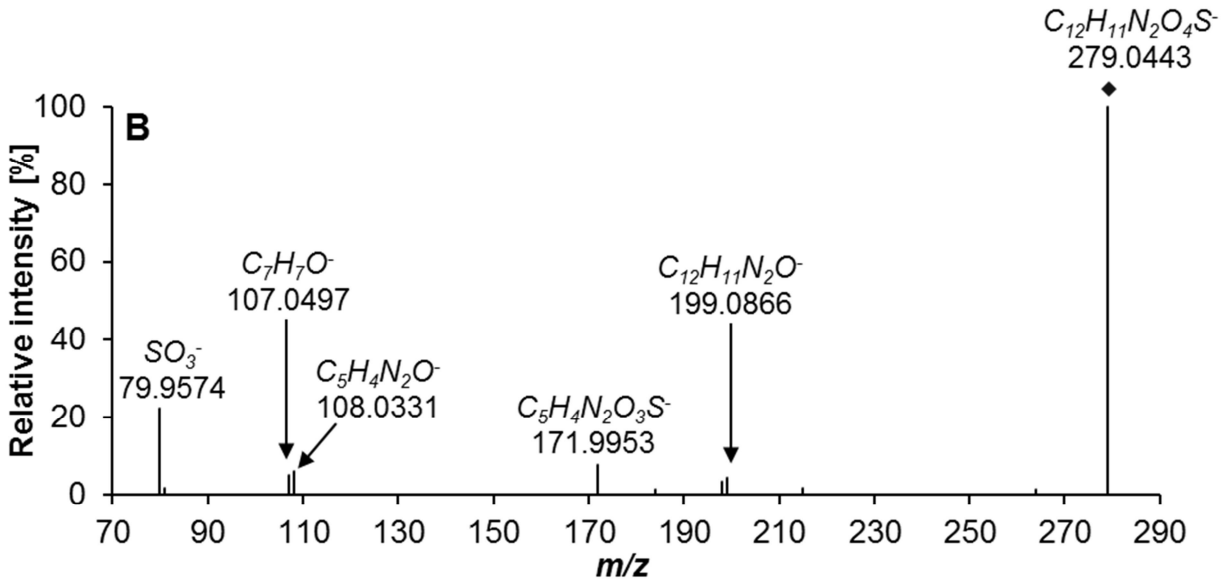


**Figure S 6.7B**: Merged MS/MS spectrum for TP 280 recorded in the negative ionization mode (*m/z* 279.0445, $[M-H]^-$, rt = 4.11 min). Product ions were recorded individually at 10 V, 20 V, and 40 V and combined to a single spectrum. Data were recorded for a sample taken after anodic oxidation with a BDD electrode at pH 7.

**TP 306**

The product TP 306 was observed only for the enzyme-based degradation processes, i.e. microbial degradation and incubation with human liver microsomes. Generally, an elemental composition of $C_{13}H_{14}N_4O_3S$ was assigned to this analyte with a mass error of about -0.3 ppm, which differs by $-C_3H_6$ from the parent compound torasemide itself. Depropylation is generally a known phase I degradation mechanism (Holcapek et al., 2008) and cleavage of the isopropyl group was already reported for the human metabolism of torasemide before (Barroso et al., 2001). The relative retention time shift for TP 306 (rt = 6.16 min) compared to torasemide (rt = 7.96 min) itself is about 0.77, which is close to the relative shift of 0.73 reported for the loss of an isopropyl group before (Holcapek et al., 2008 refers to Kamata et al., 2006 which we could however not access). As the loss of the isopropyl group is the only plausible reaction mechanism for torasemide that could explain the observed elemental composition shift, we tentatively identified the TP 306 with a confidence level of 2.

**TP 320**

Like most of the here described transformation products, TP 320 was also only observed after anodic oxidation of torasemide at pH7. The elemental composition of $C_{13}H_{12}N_4O_4S$ was assigned to this analyte with a mass error of -2.0 ppm. In comparison to torasemide itself, TP 320 differs by $–C_3H_8$ and +O. The easiest way to cleave three carbon atoms from torasemide itself is via N-deisopropylation ($-C_3H_6$), which is also the underlying mechanism in the formation of TP 306. Generally, the MS/MS information recorded for the positive ionization mode support the loss of the isopropyl group (Figure S 6.8A). The formation of the product ion *m/z* 304 can be explained by the loss of the primary amine from the urea moiety (→neutral loss of $NH_3$), while a cleavage of the carbonyl-C and the secondary amine of the urea moiety leads to a primary sulfonamide with *m/z* 278.

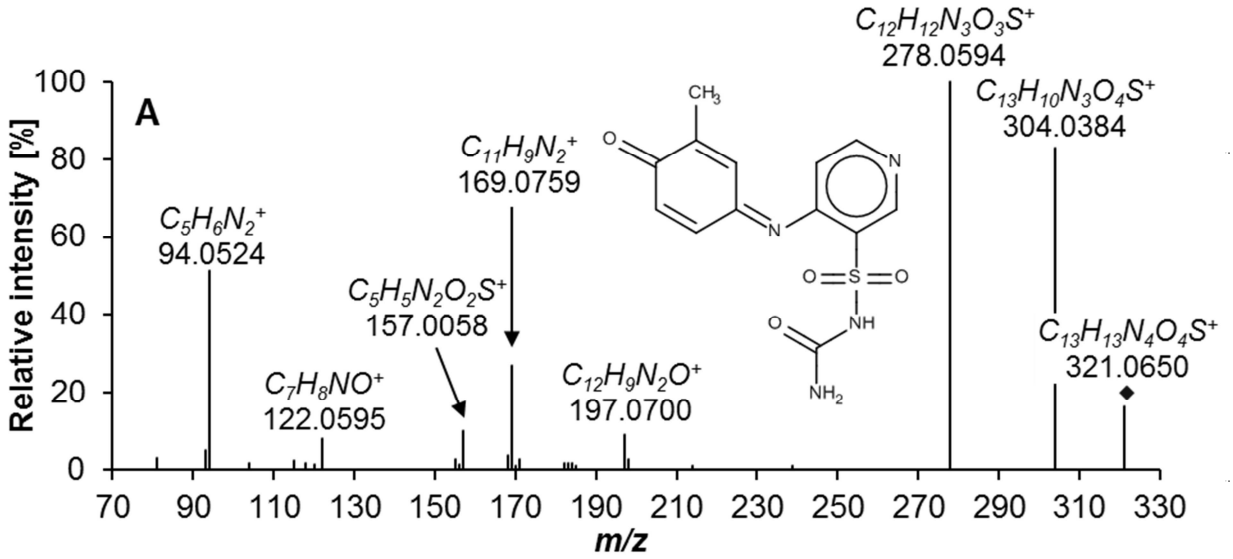


**Figure S 6.8A**: Merged MS/MS spectrum for TP 320 recorded in the positive ionization mode (*m/z* 321.0652, $[M+H]^+$, rt = 5.57 min). Product ions were recorded individually at 10 V, 20 V, and 40 V and combined to a single spectrum. Data were recorded for a sample taken after anodic oxidation with a BDD electrode at pH 7.

The same collision induced dissociation pathways were also observed in the ESI- mode, leading towards the fragments *m/z* 302 and *m/z* 276 (Figure S 6.8B).

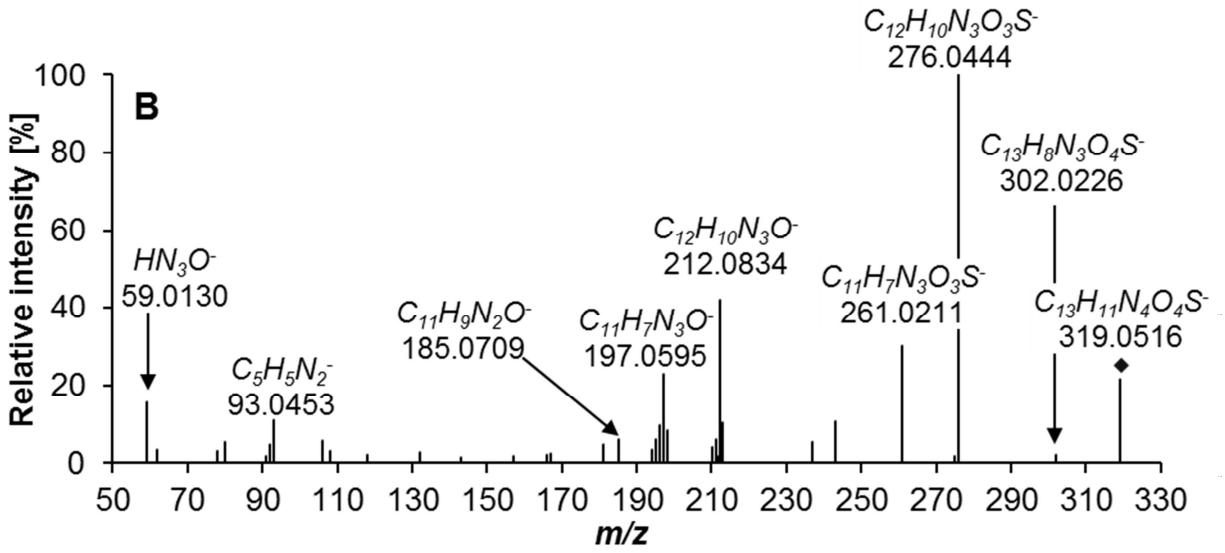


**Figure S 6.8B**: Merged MS/MS spectrum for TP 320 recorded in the negative ionization mode (*m/z* 319.0506, $[M-H]^-$, rt = 5.57 min). Product ions were recorded individually at 10 V, 20 V, and 40 V and combined to a single spectrum. Data were recorded for a sample taken after anodic oxidation with a BDD electrode at pH 7.

Similar to TP 278, the remaining elemental composition difference of $-H_2$ and +O is most likely related to a hydroxylation step followed by an additional oxidation. The tolyl group is also in case of TP 320 the most probable structure where this modification takes place (especially due to the activation of this group as described for TP 278 before) and some product ions support this hypothesis as well. For example, the fragment *m/z* 94 in the ESI+ mode (Figure S 6.8A) represents most likely the unmodified aminopyridine moiety and the fragment $C_7H_8NO^+$ (*m/z* 122) reflects in contrast the modified toly group including a nitrogen atom from the aminopyridine moiety. Assuming that the transformation product TP 364b is the parent compound of TP 320, the location of hydroxylation would be in *para* position to the amine of the toluidine group. Based on the available information we tentatively identified TP 320 with the confidence level 2.

Similar to TP 278, the reactive nature of TP 320 was demonstrated with a trapping experiment (Figure S 6.9). The transformation product itself was only detected in the absence of glutathione (Figure S 6.9A), while two GSH conjugates of TP 320 were observed in a retention time window from 4 min to 5 min for a sample where glutathione was added (Figure S 6.9D).

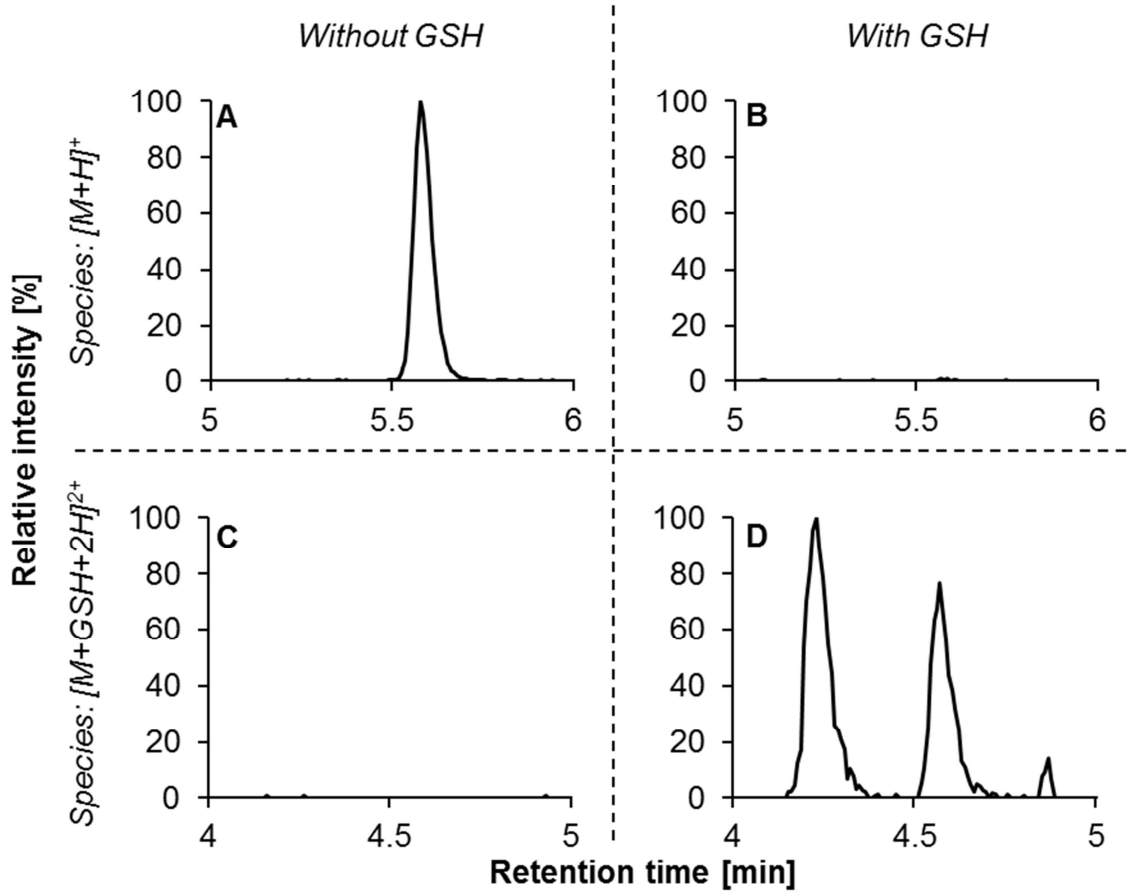


**Figure S 6.9**: Extracted ion chromatograms for the $[M+H]^+$ (*m/z* 321.0652, A and B) and $[M+GSH+2H]^{2+}$ (*m/z* 314.57815, C and D) of the TP 320 in a sample obtained after anodic oxidation of torasemide at pH7 that was either diluted with tap water (A and C) or an equal volume of a reduced glutathione (GSH) solution (B and D). The extraction window for the chromatograms was ± 10 ppm and normalization of the signal intensities was performed in relation to the maximum intensity observed for each species, respectively. The doubly charged GSH conjugate was extracted here as it showed significantly higher signal intensity compared to the singly charged species.

**TP 322**

The transformation product TP 322 was only observed with a low abundance in samples taken after anodic oxidation at pH 7. The elemental composition of $C_{13}H_{14}N_4O_4S$ could be assigned to this analyte with a mass error of about 0.6 ppm. This analyte differs only by two additional hydrogen atoms compared to TP 320. Analogous to TP 278 and TP 280, it was therefore assumed that TP 322 is the reduced species of the reactive transformation product TP 320 and that this analyte was formed from torasemide via hydroxylation of the tolyl group and N-deisopropylation. Assuming that the transformation product TP 364b is the precursor of TP 322, the location of hydroxylation would be in *para* position to the amine of the toluidine group. The MS/MS information recorded for this analyte are shown in Figure S 6.10A and Figure S 6.10B for the positive and negative ionization mode, respectively. Based on the available information we tentatively identified TP 322 with the confidence level 2.

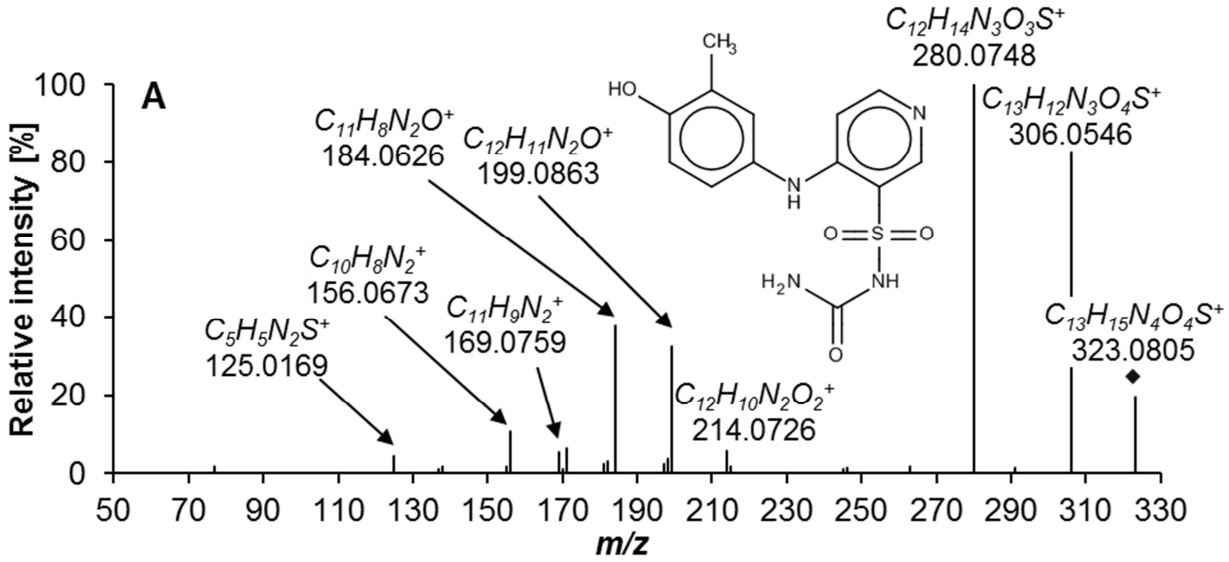


**Figure S 6.10A**: Merged MS/MS spectrum for TP 322 recorded in the positive ionization mode (*m/z* 323.0809, $[M+H]^+$, rt = 4.95 min). Product ions were recorded individually at 10 V, 20 V, and 40 V and combined to a single spectrum. Data were recorded for a sample taken after anodic oxidation with a BDD electrode at pH 7.

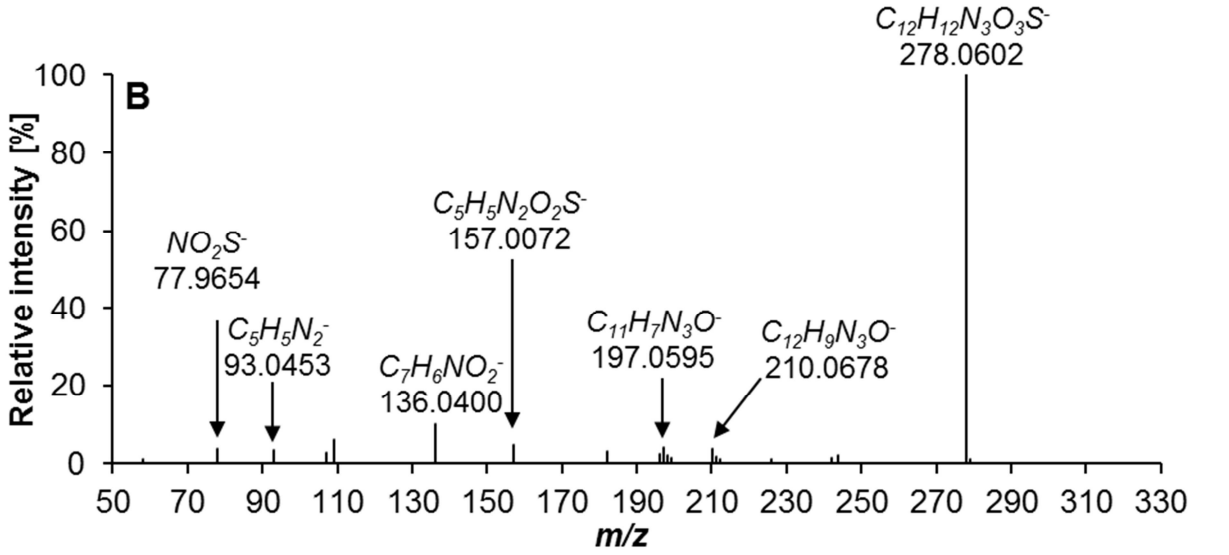


**Figure S 6.10B**: Merged MS/MS spectrum for TP 322 recorded in the negative ionization mode (*m/z* 321.0663, $[M-H]^-$, rt = 4.95 min). Product ions were recorded individually at 10 V, 20 V, and 40 V and combined to a single spectrum. Data were recorded for a sample taken after anodic oxidation with a BDD electrode at pH 7. The deprotonated species $[M-H]^-$ itself was not present in the merged spectra.

**TP 362**

The transformation product TP 362 is the most dominant electrochemical transformation product of torasemide and also an important phototransformation and microbial degradation product. Based on accurate mass measurements and isotope information, the molecular formula $C_{16}H_{18}N_4O_4S$ was assigned to this compound with an error of 0.5 ppm. This composition differs by $–H_2$ and +O from torasemide itself and we assumed therefore that TP 362 is the result of a hydroxylation step followed by an additional oxidation. The MS/MS spectra for this analyte recorded in the positive and negative ionization mode are shown in Figure S 6.11A and Figure S 6.11B, respectively. As the products TP 362 and TP 320 differ only in the isopropyl group, which is cleaved off initially during collision induced dissociation of torasemide and its forced degradation products (Kurmi et al., 2017), it is not surprising that the MS/MS spectra for those two transformation products have a high similarity (Figure S 6.8A and Figure S 6.11A for ESI+ and Figure S 6.8B and Figure S 6.11B for ESI-).

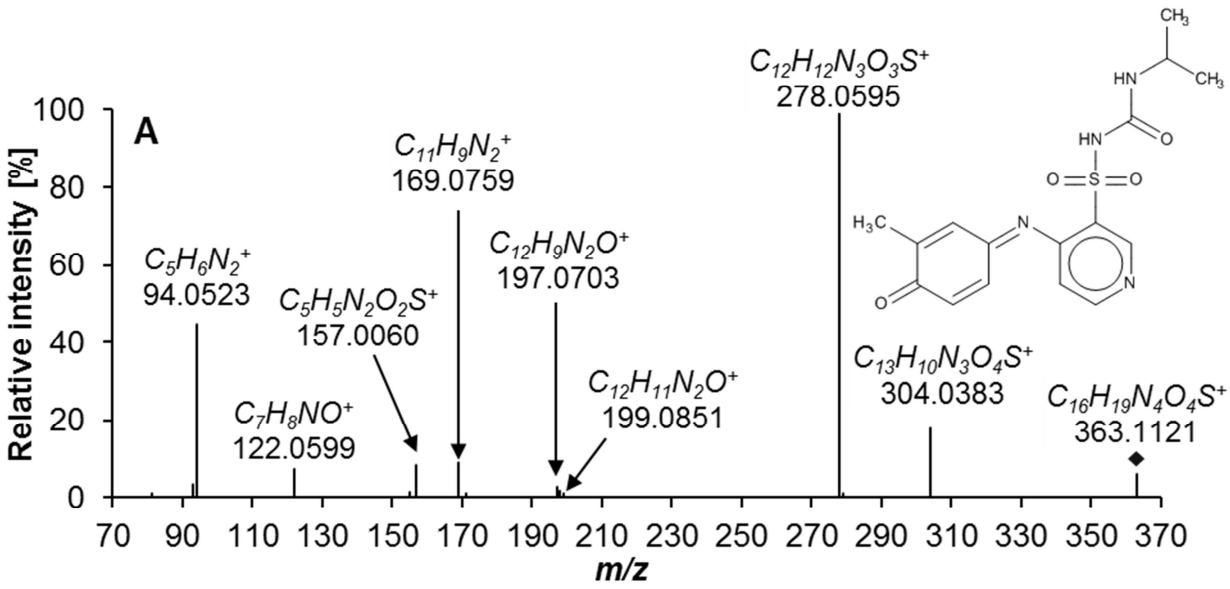


**Figure S 6.11A**: Merged MS/MS spectrum for TP 362 recorded in the positive ionization mode (*m/z* 363.1122, $[M+H]^+$, rt = 7.63 min). Product ions were recorded individually at 10 V, 20 V, and 40 V and combined to a single spectrum. Data were recorded for a sample taken after anodic oxidation with a BDD electrode at pH 7.

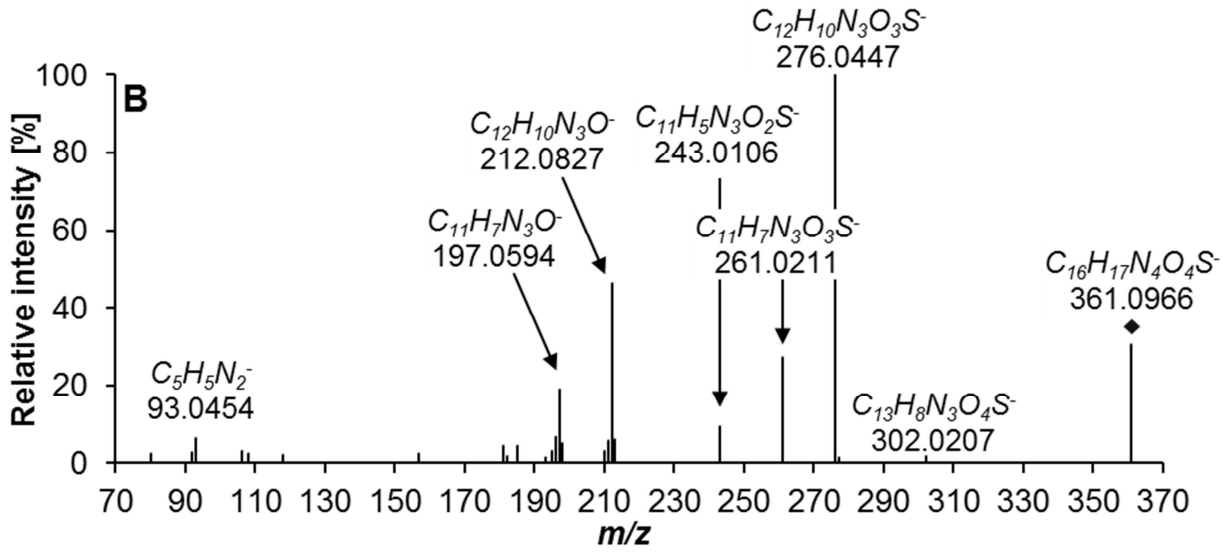


**Figure S 6.11B**: Merged MS/MS spectrum for TP 362 recorded in the negative ionization mode (*m/z* 361.0976, $[M-H]^-$, rt = 7.63 min). Product ions were recorded individually at 10 V, 20 V, and 40 V and combined to a single spectrum. Data were recorded for a sample taken after anodic oxidation with a BDD electrode at pH 7.

The suggested analyte structure of TP 362 was additionally supported by its reactive nature that was demonstrated based on trapping experiments with glutathione (Figure 6.4in the manuscript). The peak are of this analyte was reduced by about 99% in the presence of GSH compared to the control sample and TP 362 formed three conjugates in the presence of GSH. Assuming that TP 364b is the parent compound undergoing oxidation to TP 362, we tentatively identified the structure of TP 362 with the confidence level 2.

**The products TP 364a – TP 364c**

Overall, three isobaric compounds with the exact mass *m/z* 365.1278 for their protonated species ($[M+H]^+$) were detected in samples from the four different degradation studies. The elemental composition $C_{16}H_{20}N_4O_4S$ was assigned to these analytes with mass errors ranging from 0.2 ppm to 0.8 ppm. The molecular formulas of those products differ only by a single oxygen atom compared to torasemide itself, suggesting a hydroxylation of torasemide during the degradation experiments.

***TP364a*** is the most polar of the three isobaric analytes, eluting at a retention time of about 5.9 min. This transformation product was only detected after the incubation of torasemide with human liver microsomes (HLM) and it was the most abundant product for this type of degradation. TP 364a was not detected for any of the other three degradation experiments.

In contrast to all other transformation products, TP 364a could be identified with a confidence level 1 due to the availability of a reference standard of the human metabolite hydroxytorasemide (CAS 99300-68-2). Identification was based on comparing retention times and MS/MS spectra of the analyte obtained from torasemide incubation with HLM and the reference standard as shown in Figure S 6.12 and Figure S 6.13, respectively.

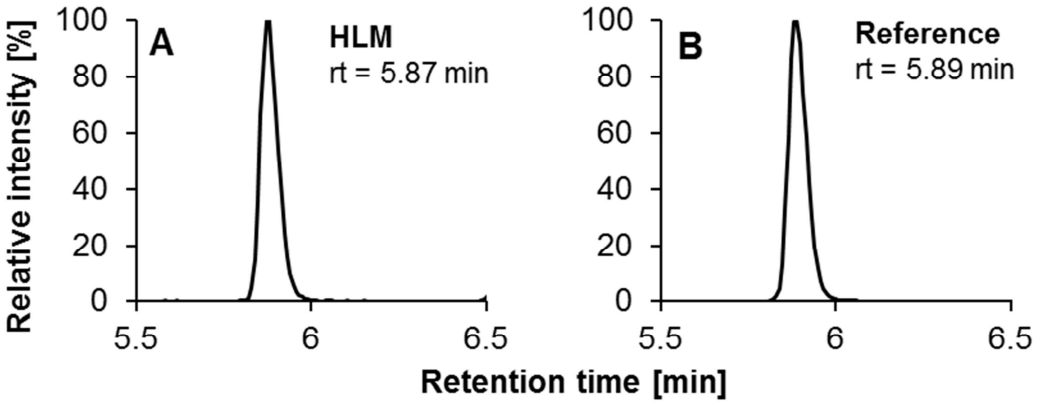


**Figure S 6.12**: Extracted ion chromatograms for the $[M+H]^+$ species of $C_{16}H_{20}N_4O_4S$ (*m/z* 365.1278) for a sample taken after degradation of torasemide in the presence of human liver microsomes (A) and for a reference standard of the human metabolite hydroxytorasemide (B). The extraction window for the chromatograms was ± 10 ppm.

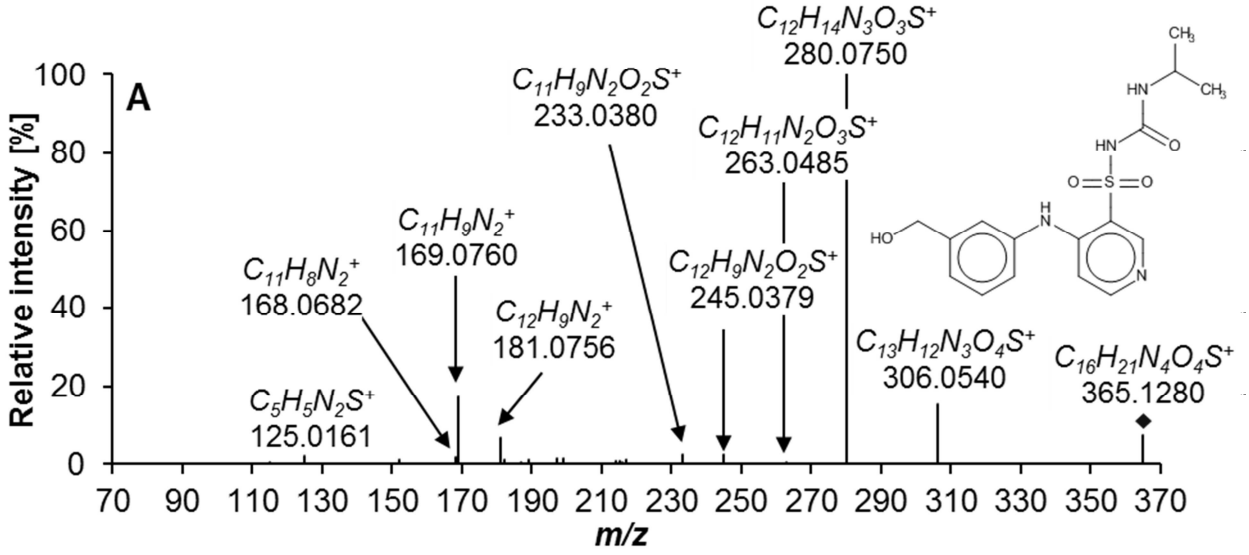


**Figure S 6.13A**: Merged MS/MS spectrum for TP 364a recorded in the positive ionization mode (*m/z* 365.1278, $[M+H]^+$, rt = 5.89 min). Product ions were recorded individually at 10 V, 20 V, and 40 V and combined to a single spectrum. Data were recorded for a reference standard of the human metabolite hydroxytorasemide.

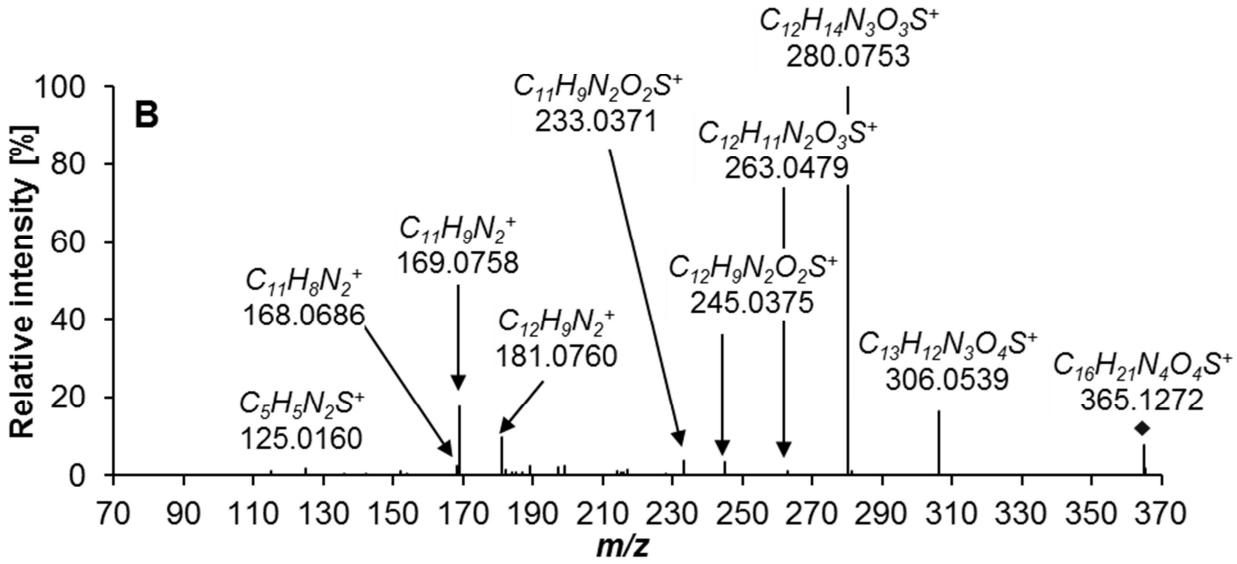


**Figure S 6.13B**: Merged MS/MS spectrum for TP 364a recorded in the positive ionization mode (*m/z* 365.1278, $[M+H]^+$, rt = 5.87 min). Product ions were recorded individually at 10 V, 20 V, and 40 V and combined to a single spectrum. Data were recorded for a sample taken after incubation of torasemide with human liver microsomes for 60 min.

***TP364b*** was eluting at a retention time of about 6.6 min and it was the only transformation product that was detected in samples from all four degradation experiments. The relative abundance of this product ranged from 6% after incubation of torasemide with liver microsomes to 100% in samples from phototransformation experiments. From previous reports about the human metabolism it was known, that torasemide cannot only undergo hydroxylation of the methyl group leading to TP 364a. The aromatic hydroxylation of the tolyl moiety in *para* position to the secondary amine can take place as well (Knauf and Mutschler, 1998). As TP 364b was also observed for incubations with human liver microsomes we assumed that TP 364b is actually the known human metabolite 4'-hydroxytorasemide (CAS 99300-67-1). Aromatic hydroxylation during anodic oxidation is also a well-known process mimicking phase I metabolism (Johansson et al., 2007). MS/MS spectra recorded for TP 364b in the positive mode are shown in Figure S 6.14 and based on the diagnostic data we identified the analyte with a confidence level of 2.

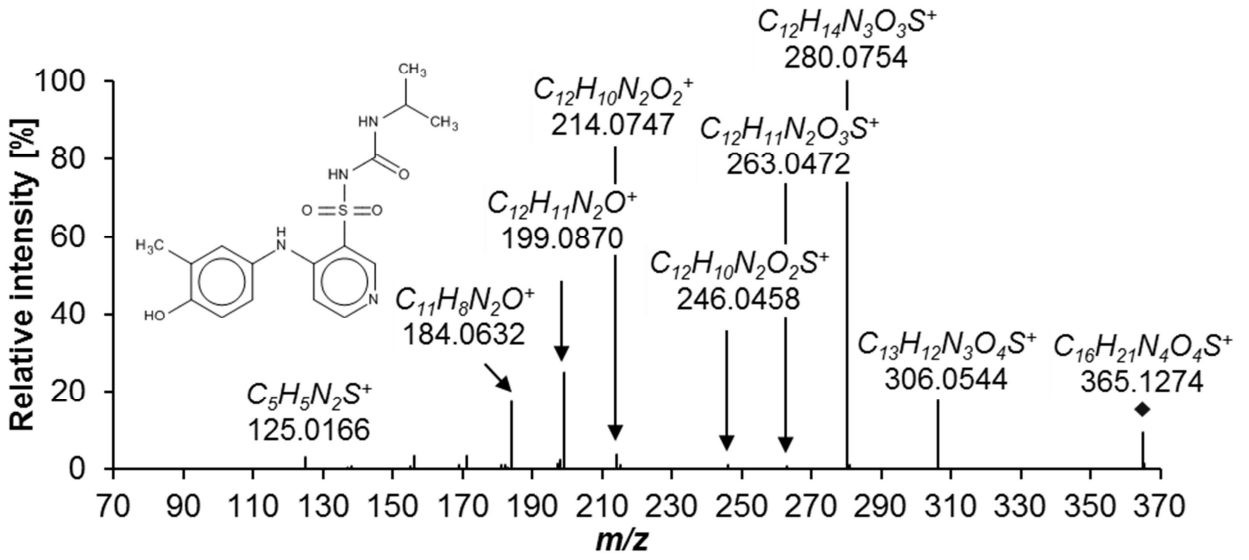


**Figure S 6.14**: Merged MS/MS spectrum for TP 364b recorded in the positive ionization mode (*m/z* 365.1278, $[M+H]^+$, rt = 6.64 min). Product ions were recorded individually at 10 V, 20 V, and 40 V and combined to a single spectrum. Data were recorded for a sample taken after anodic oxidation with a BDD electrode at pH 3.

***TP364c*** was the latest eluting of the three isobaric analytes with a retention time of 7.5 min. Similar to many other transformation products, TP 364c was only detected after anodic oxidation of torasemide at pH 7 and this analyte accumulated to a relative abundance of 6%. The formation of torasemide N-oxide in the presence of hydrogen peroxide was already demonstrated (Kurmi et al., 2017). However, as already discussed in the main manuscript (section 6.4.1.3) it is unlikely that TP 364c is actually an N-oxide as these products tend to elute later than their parent compounds (Merel et al., 2017). Similar to TP 364b, TP 364c is most likely the result of an aromatic oxidation because this mechanism can be easily performed electrochemically, in contrast to an aliphatic hydroxylation (Jurva et al., 2003). The hydroxylation could take place again at the tolyl group as the methyl moiety and the bound amine are ortho-/para-directing substituents. In case of TP 364b, the hydroxylation took place in para position to the amine moiety, leaving the carbon atom in para position of the methyl group for the hydroxylation in case of TP 364c. A hydroxylation between the methyl and the amine group, i.e. in ortho position of both substituents, would be unlikely.

Unfortunately, the recorded MS/MS information (Figure S 6.15) were not conclusive. Therefore, we could not propose a location of the hydroxylation and putatively identified TP 364c only with the confidence level 3.

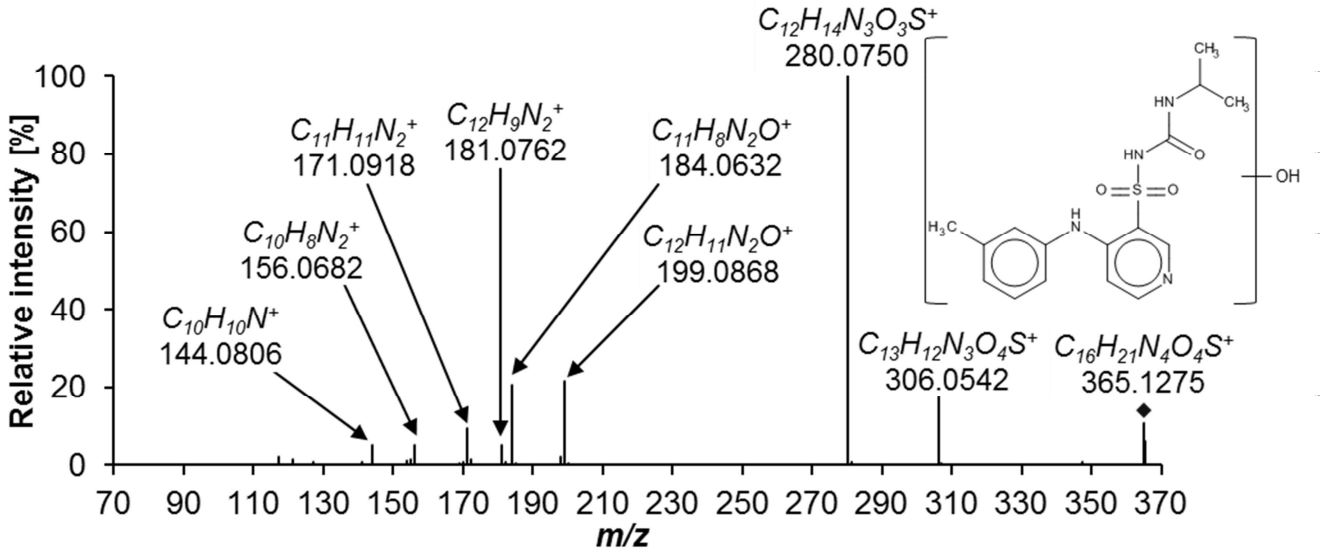


**Figure S 6.15**: Merged MS/MS spectrum for TP 364c recorded in the positive ionization mode (*m/z* 365.1278, $[M+H]^+$, rt = 7.63 min). Product ions were recorded individually at 10 V, 20 V, and 40 V and combined to a single spectrum. Data were recorded for a sample taken after anodic oxidation with a BDD electrode at pH 7.

**The products TP 378a and TP 378b**

Two isobaric transformation products with the exact mass m/z 379.1071 for their protonated species ($[M+H]^+$) were observed for torasemide. TP 378a was only observed after microbial degradation with activated sludge and was here the most dominant degradation product. In contrast, TP 378b was a product of low abundance that was only observed after anodic oxidation of torasemide at pH7. Generally, the elemental composition $C_{16}H_{18}N_4O_5S$ was assigned to both analytes with mass errors of -0.2 and 0.6 ppm, respectively.

The identification of ***TP 378a*** was exemplarily performed in depth in the manuscript (section 6.4.1.1) and is therefore not repeated here in the supporting information. However, the MS/MS information recorded in the positive, as well as negative ionization mode, are summarized in more detail in Figure S 6.16.

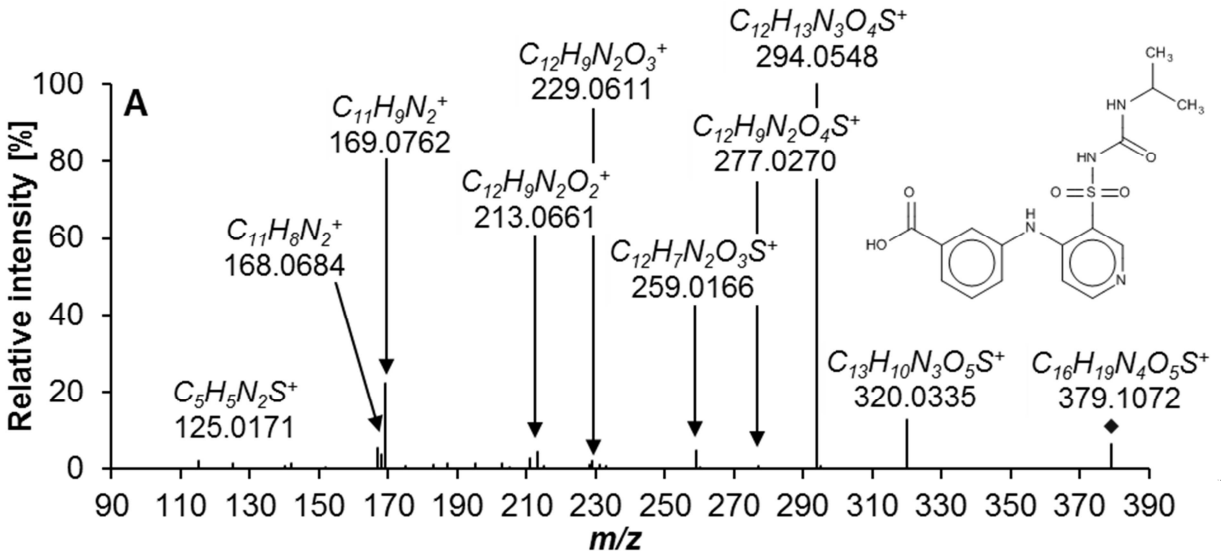


**Figure S 6.16A**: Merged MS/MS spectrum for TP 378a recorded in the positive ionization mode (*m/z* 379.1071, $[M+H]^+$, rt = 6.22 min). Product ions were recorded individually at 10 V, 20 V, and 40 V and combined to a single spectrum. Data were recorded for a sample taken after microbial degradation with activated sludge.

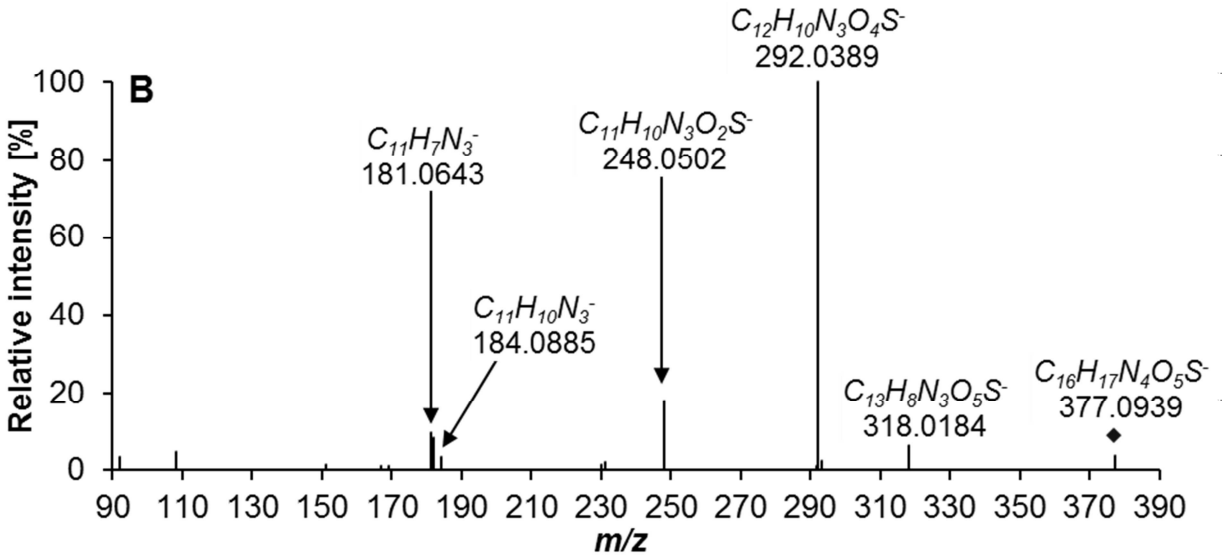


**Figure S 6.16B**: Merged MS/MS spectrum for TP 378a recorded in the negative ionization mode (*m/z* 377.0925, $[M-H]^-$, rt = 6.22 min). Product ions were recorded individually at 10 V, 20 V, and 40 V and combined to a single spectrum. Data were recorded for a sample taken after microbial degradation with activated sludge.

Carboxytorasemide is the only transformation product with the elemental composition $C_{16}H_{18}N_4O_5S$ that was reported in literature so far. Therefore, it was surprising to detect in addition to TP 378a also the low abundant degradation product ***TP 378b***. The elemental difference for example compared to torasemide itself by $-H_2$ and $+O_2$ could be explained by di-hydroxylation were an additional oxidation, e.g. to a quinone imine, takes place. Trapping experiments performed for this analyte in the presence of glutathione verified also the reactive nature of TP 378b (Figure S 6.17), suggesting a similarity to other electrophiles (e.g. TP 362) that were identified in this study.

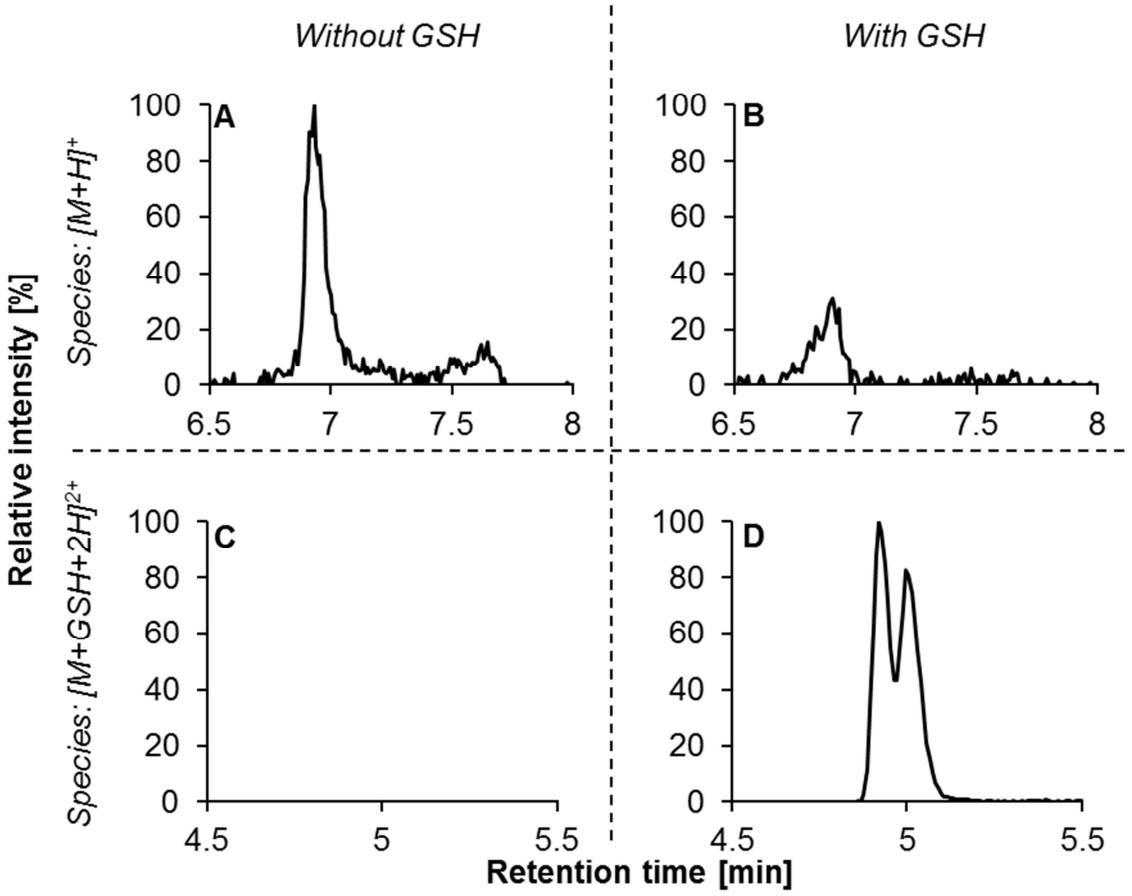


**Figure S 6.17**: Extracted ion chromatograms for the [M+H]+ (m/z 379.1071, A and B) and [M+GSH+2H]2+ (m/z 343.5991, C and D) of the TP 378b in a sample obtained after anodic oxidation of torasemide at pH7 that was either diluted with tap water (A and C) or an equal volume of a reduced glutathione (GSH) solution (B and D). The extraction window for the chromatograms was ± 10 ppm and normalization of the signal intensities was performed in relation to the maximum intensity observed for each species, respectively. The doubly charged GSH conjugate was extracted here as it showed significantly higher signal intensity compared to the singly charged species.

Unfortunately, we were not able to record MS/MS spectra with a sufficient quality due to the low abundance of the analyte in the sample. Therefore, we could identify the analyte only with a confidence level of 4.

**TP 393**

The transformation product TP 393 was only observed during the photodegradation of torasemide and it accumulated to almost the same level as TP 364b, the most abundant TP for this type of degradation. Based on accurate mass information, the elemental composition $C_{16}H_{19}N_5O_5S$ could be assigned to this analyte with an error of 0.13 ppm. The elemental composition in comparison to torasemide differs therefore by –H + $NO_2$ and we assumed therefore that TP 393 was formed via nitration from the parent compound. The discussion of the plausibility of this hypothesis was included in the main manuscript (section 6.4.1.5).

Unfortunately, the analyte intensity was too low to record MS/MS information with a sufficient quality. Due to the absence of further structural information, we tentatively identified TP 393 only with the confidence level 4.

### 6.8.2 Additional information for photodegradation

UV/visible absorption spectra of 10 mg $L^{-1}$ torasemide or diclofenac were recorded with a photoLab® 6600 UV-VIS spectrophotometer (WTF, Germany) and are shown in Figure S 6.18. Spectra were recorded for pure, as well as acidified (10% 1M HCl) and basic (10% 1M NaOH) methanol and solutions without the target compound were used for blank subtraction.

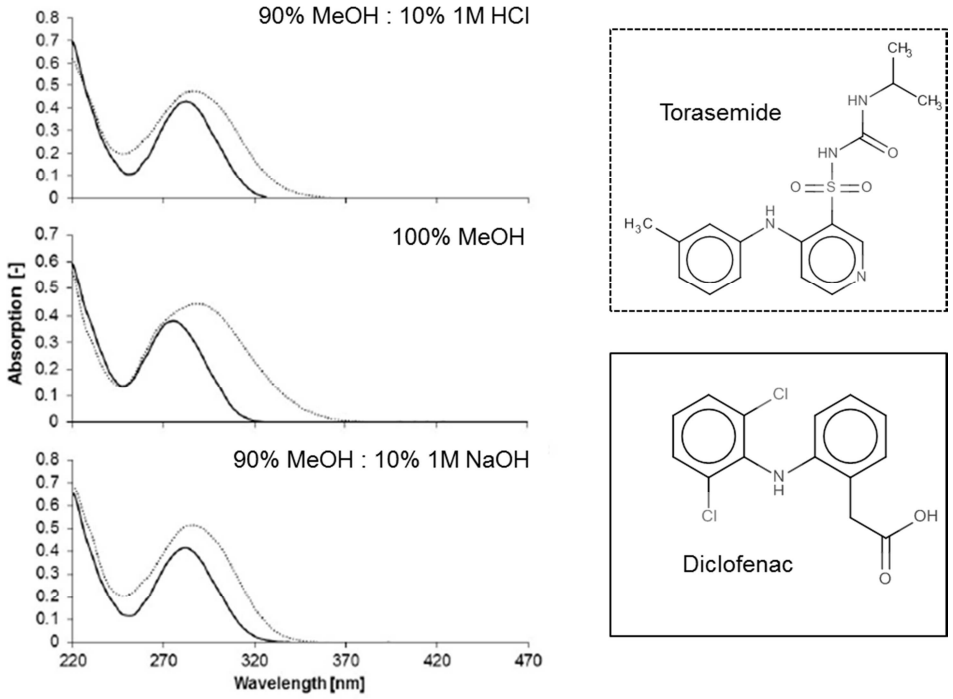


**Figure S 6.18**: UV-Vis absorption spectra of 10 mg $L^{-1}$ torasemide (dotted line) and 10 mg $L^{-1}$ diclofenac (solid line). Acidified methanol (90% MeOH + 10% 1M HCl, A), pure methanol (B), or basic methanol (90% MeOH + 10% 1M NaOH, C) were used as solvents.

### 6.8.3 References


Barroso, M.B., Alonso, R.M., Jiménez, R.M., 2001. Simultaneous determination of torasemide and its major metabolite M5 in human urine by high-performance liquid chromatography-electrochemical detection. Journal of chromatographic science 39 (11), 491–496.

Fabiańska, A., Białk-Bielińska, A., Stepnowski, P., Stolte, S., Siedlecka, E.M., 2014. Electrochemical degradation of sulfonamides at BDD electrode: kinetics, reaction pathway and eco-toxicity evaluation. Journal of hazardous materials 280, 579–587.

Holcapek, M., Jirásko, R., Lísa, M., 2010. Basic rules for the interpretation of atmospheric pressure ionization mass spectra of small molecules. Journal of chromatography. A 1217 (25), 3908–3921.

Holcapek, M., Kolárová, L., Nobilis, M., 2008. High-performance liquid chromatography-tandem mass spectrometry in the identification and determination of phase I and phase II drug metabolites. Analytical and bioanalytical chemistry 391 (1), 59–78.

Johansson, T., Weidolf, L., Jurva, U., 2007. Mimicry of phase I drug metabolism--novel methods for metabolite characterization and synthesis. Rapid communications in mass spectrometry : RCM 21 (14), 2323–2331.

Jurva, U., Wikström, H.V., Weidolf, L., Bruins, A.P., 2003. Comparison between electrochemistry/mass spectrometry and cytochrome P450 catalyzed oxidation reactions. Rapid communications in mass spectrometry : RCM 17 (8), 800–810.

Kamata, T., Katagi, M., Kamata, H.T., Miki, A., Shima, N., Zaitsu, K., Nishikawa, M., Tanaka, E., Honda, K., Tsuchihashi, H., 2006. Metabolism of the psychotomimetic tryptamine derivative 5-methoxy-N,N-diisopropyltryptamine in humans: identification and quantification of its urinary metabolites. Drug metabolism and disposition: the biological fate of chemicals 34 (2), 281–287.

Knauf, H., Mutschler, E., 1998. Clinical pharmacokinetics and pharmacodynamics of torasemide. Clinical pharmacokinetics 34 (1), 1–24.

Kurmi, M., Patel, N., Jhajra, S., Bharatam, P.V., Singh, S., 2017. Characterization of forced degradation products of torasemide through MS tools and explanation of unusual losses observed during mass fragmentation of drug and degradation products through density functional theory. Journal of pharmaceutical and biomedical analysis 145, 209–218.

Merel, S., Lege, S., Yanez Heras, Jorge E, Zwiener, C., 2017. Assessment of N-Oxide Formation during Wastewater Ozonation. Environmental science & technology 51 (1), 410–417.

Song, D., Liu, H., Zhang, A., Qu, J., 2014. Fragmentation of typical sulfonamide drugs via heterolytic bond cleavage and stepwise rearrangement. RSC Adv 4 (89), 48426–48432.

Weissberg, A., Dagan, S., 2011. Interpretation of ESI(+)-MS-MS spectra—Towards the identification of “unknowns”. International Journal of Mass Spectrometry 299 (2-3), 158–168.

# 7 Summary and conclusions

Anthropogenic compounds and their transformation products are a potential threat to drinking water resources and aqueous habitats. However, prior to a risk assessment and prioritization of micropollutants, knowledge about their occurrence and fate in the environment is required. The goal of this study was to expand the picture about compounds of emerging concern, focusing on the previously unknown micropollutant denatonium and the pharmaceutical torasemide. In addition to their concentration ranges in surface waters and WWTPs, abiotic and biotic degradation studies were performed to gain an overview of transformation products. Finally, water samples were screened for the presence of these TPs assessing the environmental relevance of these degradation products. The most important results for the two compounds are summarized in the following:

**Denatonium**

- Household and personal care products released to sewer systems are the main source of denatonium in wastewater. Even if it is not declared as an ingredient, denatonium is most likely present in products containing denatured alcohol, as denatonium is an important denaturing agent.
- Denatonium enters the environment usually via the discharge of (un-)treated wastewater into receiving surface waters. Based on a rough back-of-the-envelope calculation about 1.5 tons of this compound are released into the environment in Germany each year.
- In principle, denatonium can undergo indirect photodegradation in surface waters and seven TPs were identified. Except for lidocaine, none of these TPs seems to be of environmental relevance. Even the occurrence of lidocaine was associated rather with its application as local anesthetic than being a product of denatonium degradation.
- The here presented results and literature data generally point towards a high persistence of denatonium. No significant compound removal can be observed during conventional wastewater treatment and the majority of denatonium released to the surface water might therefore end up and accumulate in the environment.

- Advanced water treatment techniques can be beneficial for micropollutant removal and data presented in this thesis reveal almost 75% removal of an initial denatonium load during pilot-scale ozonation of a conventionally treated wastewater. However, denatonium removal was related here to the formation of at least two polar TPs with unknown (toxicological) properties.

**Torasemide**

- Similar to denatonium, the release of (un-)treated wastewater is the main source of torasemide in the environment. Torasemide was generally detected in all investigated WWTPs with a median concentration of about 180 ng $L^{-1}$ in effluent samples.
- Overall sixteen TPs could be putatively identified in abiotic and biotic degradation experiments, but only three of them were detected in at least one WWTP or surface water sample.
- The data suggest a low persistence and therefore low environmental relevance of the human metabolite hydroxytorasemide (TP 364a), as this compound seems to be rapidly transformed in the sewer system or during wastewater treatment into the final product carboxytorasemide (TP 378a).
- Carboxytorasemide was observed in WWTP or river water samples as frequently as torasemide itself, but at significantly higher abundances (factor 2-3 higher when comparing peak areas; however, no reference standard was available for TP 378a). Due to higher concentrations and a potentially increased persistence (as suggested by biodegradation studies), the monitoring and evaluation of TP 378a as micropollutant might be even more important compared to torasemide itself.

Generally, electrochemical degradation has proven useful here as a cheap, simple, and fast technique to generate degradation products of potential environmental relevance. Especially mimicking abiotic processes worked very well and, except for the nitration of torasemide, all indirect photodegradation products of denatonium and torasemide were covered electrochemically. However, neither hydroxytorasemide nor carboxytorasemide, two important products of enzymatic torasemide degradation, could be generated by direct anodic oxidation. Therefore, it is recommended to perform at least one biotic transformation experiment (e.g. microbial degradation with activated sludge) in addition to electrochemical degradation for the best coverage of environmentally relevant TPs.

# 8 Outlook and further needs

The work presented in this thesis generally increases the knowledge on the occurrence and fate of denatonium and torasemide as micropollutants. Environmentally relevant transformation products of these substances were identified as well. The following tasks are proposed now as a continuation of this work, ultimately enabling an assessment of denatonium, torasemide, and their TPs as compounds of emerging concern:

- Water samples investigated during the studies were preliminary taken from WWTPs and surface waters in Baden-Württemberg, Germany. It is recommended to extend screening approaches to more areas in Germany and additional countries, to gain a better understanding of the occurrence and therefore relevance of the studied micropollutants. The sharing of MS/MS information in the publicly available MassBank repository will most likely facilitate this screening, as other analytical scientists are now enabled to putatively identify those compounds in their own environmental samples.
- Carboxytorasemide was the most frequently detected TP and its estimated surface water concentrations exceeded those of all other investigated analytes in this study. However, quantification based on a reference standard is still required to verify this hypothesis. As this TP is potentially less biodegradable as its parent compound, abiotic and biotic degradation studies should be performed for carboxytorasemide to elucidate its fate in the environment.
- Investigation of sediment interactions, as well as uptake and accumulation in biota, to better understand the behavior of these micropollutants is necessary. The impact of changing pollutant mixtures should be considered in the context of sediments as well. For example, sodium and chloride ion concentrations can be significantly higher during winter time, when road salt is released to surface waters. Under these conditions, for example the quaternary ammonium compound denatonium might be released from negatively charged mineral surfaces leading to an increase in the aqueous concentration.
- Adverse effects of environmentally relevant concentrations (typically $< 1$ µg $L^{-1}$) on aquatic flora and fauna should be investigated to support a potential risk assessment. Long-term experiments, accounting also for potential mixture-effects, should be included to mimic the continuous exposure to a complex pollutant mixture with concentrations far below levels of acute toxicity in surface waters.

The measurement data initially evaluated for the selection of denatonium and torasemide as study compounds (see chapter 2), were retrospectively evaluated for the presence of TPs identified in this work. Two previously unknown analytes could be now identified as lidocaine and carboxytorasemide (Figure 8.1). However, more than 98% of the analytes extracted by a non-targeted data evaluation approach still remain unknown.

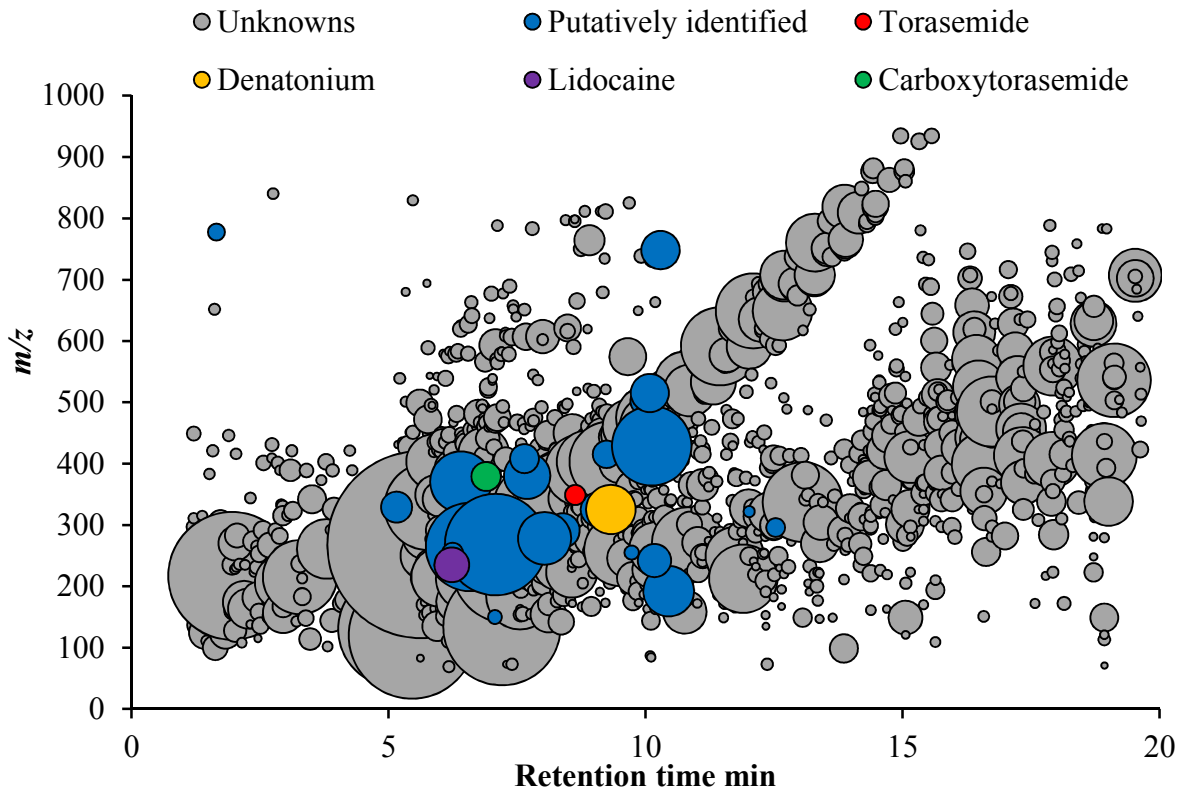


**Figure 8.1:** Overview of unknown (grey), putatively identified (generally blue; green: carboxytorasemide) and unequivocally identified (red:torasemide, orange:denatonium, purple: lidocaine) analytes in a solid phase extract of a wastewater impacted surface water sample. Putative identification was generally performed by comparing All Ion spectra to a spectral library and at least two fragments from the library had to be present for identification. Carboxytorasemide was also counted as putatively identified, as no reference standard was available. The bubble size represents the analytes peak area.

The fact that after time consuming degradation studies and challenging and mostly manual data interpretation for the identification of TPs, only a few additional candidates could be finally identified, reveals the need for an acceleration of the analytical workflow in the context of environmental micropollutants. Generally, community-driven approaches and automatization are considered as most promising for the challenging task of unknown compound identification and some requirements or improvements for existing processes are summarized in the following:

- **Comprehensive database of globally manufactured chemicals including important compound information**

  A single source of truth for globally produced chemicals would be beneficial in the context of micropollutant identification and prioritization. Especially production information, countries where compounds are used and authorized, physico-chemical, and toxicological data, as well as information about the compounds fate (including known TPs) would be helpful. Information required for a putative compound identification (i.e. MS/MS spectra and retention times) could be provided by the manufacturers in the context of compound registration or by analytical scientists and stored in this database as well.

- **Exchange and storage of analytical data**

  Sample analysis performed with high-resolution mass spectrometric (HRMS) data, especially when data-independent MS/MS information are simultaneously recorded, has the advantage of retrospective data evaluation. Therefore, it is possible to evaluate samples analyzed at any location and point in time for the presence of analytes of interest. This idea was recently realized with the NORMAN digital sample freezing platform (DSFP) (Alygizakis et al., 2019), where geo-referenced HRMS data are stored and provided for evaluation. This platform is currently focusing on data from Europe and its use is disclosed to members of the NORMAN association that contributed HRMS data. However, the authors plan to make it publicly available after thorough testing. This can be a valuable tool to underpin the widespread occurrence of substances. Additionally, the data can be used to prioritize the identification of transformation products obtained from laboratory studies (e.g. applying anodic oxidation), focusing mainly on analytes that are detected in at least some of the digitally "frozen" samples. Compounds of lower or no environmental relevance are therefore neglected, increasing the overall efficiency of the analytical work.

- **Automation of transformation studies and high-throughput screening capabilities**

  The low throughput of typical degradation studies is one of the major difficulties in investigating the transformation products for thousands of parent compounds. Experiments are usually performed off-line in batch reactors, from which samples are manually taken and the subsequent analysis is triggered by a user.

Applying strategies for process analytical technology could be therefore beneficial for the overall throughput, including automated sampling from reactors and the immediate analysis by LC-HRMS without any user input. Furthermore, performing transformation reactions in flow, rather than batch reactors, could additionally enable process automation. For example, electrochemical flow cells are commercially available and immobilized enzyme reactors were used already in combination with liquid chromatography.

While the measurement itself is performed completely autonomously, the subsequent evaluation of the data is typically done by the analytical scientist. Efficiency is lost here for example when sample analysis finishes overnight and the scientist starts working a few hours later. Furthermore, data evaluation strategies include usually repetitive tasks and often do not differ significantly between studies. Therefore, a single workflow could be designed and automatically executed once sample analysis finishes. In the context of putative compound identification and suspect screening, software tools are nowadays publicly available to predict transformation products and MS/MS spectra for a given molecular structure applying rules obtained from training data. Therefore, TPs could be predicted for a given parent compound, samples can be screened for them and the identity additionally verified comparing recorded and predicted MS/MS spectra. False-positive and false-negative predictions by these *in-silico* methods are nowadays an issue preventing the routine application. However, an increase of available training data will most likely improve the prediction quality or better algorithms will be found so that the combination of *in-silico* prediction techniques with automated data evaluation is a promising strategy.

## Reference

Alygizakis, N.A., Oswald, P., Thomaidis, N.S., Schymanski, E.L., Aalizadeh, R., Schulze, T., Oswaldova, M., Slobodnik, J., 2019. NORMAN digital sample freezing platform: A European virtual platform to exchange liquid chromatography high resolution-mass spectrometry data and screen suspects in “digitally frozen” environmental samples. Trends in Analytical Chemistry 115, 129–137.

## Danksagung

Mein erster und ganz besonderer Dank gilt meinem Doktorvater, Prof. Dr. Christian Zwiener, der mich schon als Masterstudent mit der faszinierenden Welt des Non-Target Screenings in Kontakt brachte und es mir ermöglichte diese Entdeckungsreise als Promotionsstudent in seiner Arbeitsgruppe fortzuführen. Seine Unterstützung und die fachlichen Diskussionen haben diese Arbeit geformt und ich danke ihm ausdrücklich für die Freiheiten bei der Wahl meiner Forschungsschwerpunkte und das Vertrauen in mich und meine Arbeit.

Prof. Dr. Stefan B. Haderlein danke ich ganz herzlich für die Übernahme des Zweitgutachtens.

Ausgesprochener Dank gilt der Deutschen Bundesstiftung Umwelt für die finanzielle Unterstützung in Form eines Promotionsstipendiums.

Mein weiterer Dank geht an meine Freunde, sowie Kolleginnen und Kollegen aus der Arbeitsgruppe Umweltanalytik an der Universität Tübingen. Besonders danken möchte ich dabei Stephanie Nowak, die durch ihre Unterstützung im Labor und ihre positive Art ein wichtiger Stützpfeiler im Arbeitsalltag war. Dr. Jorge E. Yanez Heras danke ich vor allem für seine Freundschaft, aber auch für das Teilen seines Wissens rund um die Elektrochemie. Dr. Sylvain Merel, Dr. Selina Tisler und Zi Wang danke ich für das tolle Arbeitsklima. Boris Bugsel, Ulf Lüder, Klaus Röhler und Julian Sorwat danke ich für ihre Unterstützung meiner Forschung durch Abschlussarbeiten und Praktika.

Schließlich möchte ich meiner Familie für ihre immerwährende Unterstützung danken. Meiner Ehefrau Barbara gebührt dabei mein allergrößter Dank für ihre Geduld, ihr Verständnis und ihre Unterstützung. Nur ihrer Bereitschaft mir den Rücken für die Dissertation frei zu halten habe ich es zu verdanken, dass aus dieser Arbeit doch mehr wurde als nur eine „unendliche Geschichte“.